Feasibility study P18 (final report)

Prepared by: V. Vandeweijer,
R. Groenenberg,
R. Donselaar,
M. Pluymaekers,
D. Loeve,
C. Hofstee,
M. Nepveu,
B. Orlic,
O. Akemu,
U. Miersemann,
T. Benedictus,
R. Arts,
F. Neele,
W. Meindertsma,
M. Dillen

Reviewed by: C. Hofstee

Approved by: J.Brouwer
(CATO-2 Director)

Table of Content

3. Reservoir geology and petrophysics study

Executive Summary

This chapter describes the reservoir geology, overburden and petrophysics of the P18 gas field, which is operated by TAQA Energy B.V. It is located in the offshore part of the Dutch sector, 20km off the coast of the “2e Maasvlakte”, the latest extension to the port of Rotterdam. Here, E.On is building a coal-fired power plant, of which the emitted CO_2 should be captured, transported, and injected into the (almost) depleted gas reservoirs of the P18 field. Aims of this report are to review the current state of knowledge on the reservoir geology and petrophysics of the reservoirs, estimate their potential storage volume based on GIIP, discuss the properties and sealing quality of the caprock and overburden, and indicate the level of uncertainty in the information provided. The subsurface data on the P18 reservoirs used to compile this report come from four sources: TAQA Energy B.V., the NLOG website (oil- and gas information portal of the Netherlands), the “DINO Loket” database operated by TNO, and TNO itself.

High-caloric gas is being produced from the P18 field since 1993. It is trapped in Triassic-aged sandstones of mixed fluvial/aeolian origin below impermeable layers of clay. The P18 field consists of three blocks that are bound by a system of NW-SE oriented normal faults, which are sealing because of juxtaposition of permeable reservoir intervals with impermeable intervals in the overburden. Block P18-2 has three compartments, whereas blocks P18-4 and P18-6 each have one compartment. The top of the compartments lies at depths between 3175 m and 3455 m below sea level. Production data suggests that most faults between the compartments are sealing, except for the one between compartments P18-02I and P18-02II, which is not sealing in the current situation.

Average gross reservoir thickness in the production wells is 200m. Average NTG of the four individual production zones identified in the reservoir (0.62-0.96) increases from base to top over the reservoir interval. Average porosity is highest in the upper zone (7-13%), is slightly lower in the middle two zones (5-9%), and lowest in the lower zone (3-5%). Permeabilities were calculated based on a porosity-permeability relation, i.e., they follow the same trend. They are highest in the upper zone (2-207mD), lower in the middle two zones (0.1-0.8mD), and lowest in the lower zone (< 0.1mD). Combined thickness of the upper and middle two zones is approx. 100m, as is the thickness of the lower zone. Average water saturations are lowest in the upper (0.24-0.47) and lower of the middle two zones (0.32-0.42), and highest in the lower zone (0.78-0.92).

The primary seal to the P18 reservoirs is 150m thick, and consists of impermeable siltstones, claystones, evaporites and dolostones that directly overlie the reservoir. Closure along the reservoir-bounding faults is obtained by juxtaposition of permeable reservoir intervals with impermeable intervals in the overburden. Most of the bounding faults do not continue further upward into the overburden than the shales of the Altena group, the secondary seal, which is approx. 500m thick. Faults that do penetrate the primary and secondary seal are rare. It is unlikely that their sealing capacity has been compromised, since higher up in the overburden additional seals with substantial thickness are located.

Dynamic GIIP of the P18 field, estimated based on production data, is 17.22BCM. GIIP estimates obtained from the reservoir model are substantially lower: 15.39BCM. For block P18-02, the discrepancy between static and dynamic GIIP is only about 7%, which can easily be attributed to differences in porosity and average water saturation between the wells and the property model. For block P18-04 and P18-06, the discrepancy is much higher, and likely attributed to a combination of under- and overestimated property values (porosity, water saturation) and

structural uncertainty, i.e., reservoir-bounding faults that are slightly off in lateral position and dip compared to the 3D seismic.

3.1. Introduction

This chapter describes in detail the reservoir geology, overburden and petrophysics of the P18 gas field that is selected for CO_2-storage. It forms part of the geological research that is carried out by TU Delft and TNO in work package 3.1 of the CATO-2 project. The P18 field, which is operated by TAQA Energy B.V., is located in the offshore part of the Dutch sector, about 20km off the coast of the “2e Maasvlakte”, the latest extension to the port of Rotterdam (Fig. 1). Here, E.On is building a coal-fired power plant, of which the emitted CO_2 should be captured, transported, and injected into the (almost) depleted gas reservoirs of the P18 field. Aims of this report are to review in detail the current state of knowledge on the reservoir geology and petrophysics of the reservoirs, estimate their potential storage volume based on GIIP, discuss the properties and sealing quality of the caprock and overburden, and indicate the level of uncertainty in the information provided. A potential migration pathway study is described in a separate report by TNO. The information in this report forms the basis for the work in WP3.02 (reservoir simulation), WP3.03 (geomechanical modelling), and WP3.04 (well integrity) of the CATO-2 project.

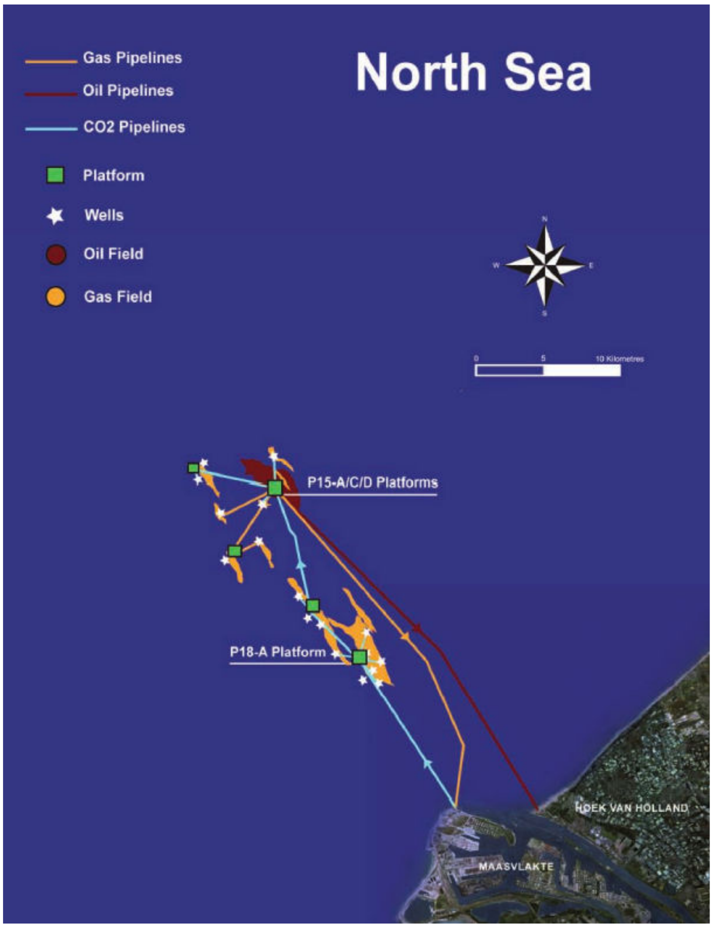

Figure 3.1: P18 gas fields and existing infrastructure (TAQA Energy B.V. 2008)

3.2. Background on P18

Rotterdam (Figure 3.1). High-caloric gas is being produced from these reservoirs since 1993. The gas reservoirs consist of sandstones of Triassic age (249-245 Ma; Geluk, 2005), and are sealed by impermeable layers of clay at a depth of 3.5km below the surface. The gas is produced through the P18-A satellite platform, and the P15-ACD processing and accommodations facilities in the adjacent P15 block, from where it is transported to the coast by a 40-km-long gas pipeline.

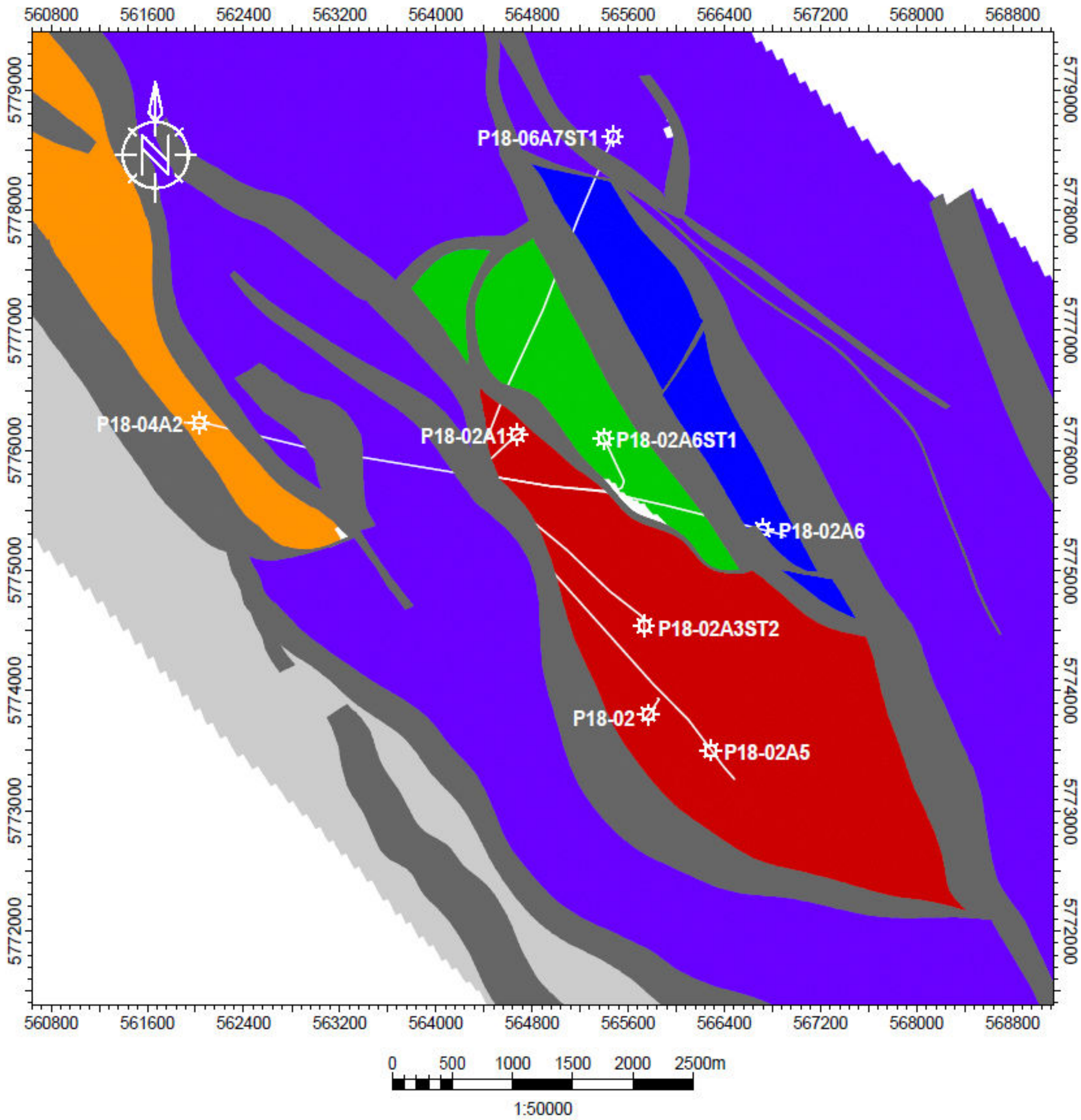

Figure 3.2: Layout of the P18 field, with position of wells at the top of the reservoir interval (top Bunter). Orange: P18-4 block; Red: P18-2, compartment I; Green: P18-2, compartment II; Blue: P18-2, compartment III; P18-6: purple block drilled by P18-06A7ST1.

The P18 field consists of three blocks, the P18-2, P18-4 and P18-6 blocks (Figure 3.2). P18-2 was discovered in 1989 with the exploration well P18-02. It consists of three compartments, P18-2I, P18-2II, and P18-2III.

P18-2I came on stream first, in 1993. It contains three production wells: P18-02-A1, P18-02-A3ST2, P18-02-A5ST1, and the exploration well P18-02. Compartment P18-2III contains one production well, P18-02-A6, and came on stream in 1997. Compartment P18-2II came on stream in 2003, and also contains one production well, P18-02-A6ST1. Since then, this production well produces simultaneously from the P18-02II and P18-02III compartments. Block P18-04 was discovered in 1991, and production started from well P18-04-A2 in 1993. Block P18-6 was discovered in 2003, and production started from well P18-06-A7ST1 in 2003.

Peak production was established in 1998, with a cumulative year production of 2.2 Bcm. At the end of 2009, the total cumulative production of all P18 blocks was 17.3 Bcm. The current depletion status is approx. 95% (with respect to the abandonment pressure). Abandonment of the different blocks is expected in the period 2014-2018.

3.3. Data and methods

3.3.1. Sources of data

The subsurface data on the P18 reservoirs come from four sources (Table 1): TAQA Energy B.V., the NLOG website (oil- and gas information portal of the Netherlands), the "DINO Loket" database operated by TNO, and TNO itself.

Table 1: Sources of data

TAQA	DINO-Loket & NLOG site	TNO in-house/TU Delft
• Reservoir model, both in RESCUE, and in RMS format, incl. relevant properties • Fault surfaces, as point data, in depth • Horizons of the reservoir intervals, in time and depth • Well data of the reservoir interval • Formation tops • Completion diagrams • 3D seismic cube <u>in two-way-travel time</u> • Production data	• P18 gas extraction plan • 3D seismic cubes of surrounding blocks • Formation water composition • Mineral composition • Gas composition • Core samples	• Regional interpretations of horizons at group level, and faults • Composite well logs • Outcrop samples

3.3.2. Methods

Static reservoir modelling

Static reservoir modelling was done in Petrel™, Schlumberger's reservoir modelling suite, which is selected as the tool to use for this purpose within CATO-2. Because of the different scales the various disciplines within CATO-2 work in, two static geological models were constructed that differ in horizontal and vertical resolution:

1. A <u>reservoir-scale</u> geological model with high resolution (region of interest 18x9km; cell size 50mx50m; 38 equally-spaced layers in the reservoir interval). It is used for the GIIP estimates (see Chapter 7), flow simulation studies and geochemical modelling studies. It focuses on the reservoirs of the P18 field, and forms the basis for the facies-based property modelling that is planned for early 2011. It was completely rebuilt in Petrel because of import problems with the original static reservoir model from TAQA that was

built in RMS, the reservoir-modelling suite from Roxar. In particular, uncorrectable artefacts arose during the import process into Petrel (reservoir modelling software) and MORES (reservoir simulator used for history matching), particularly in relation to the numerous faults, which were not correctly reproduced. Therefore, a new static model was built in Petrel from the original subsurface data from TAQA (Table 1, left column). It has exactly the same resolution as the RMS model, which allowed import of the Gaussian-based property distribution of the RMS model into the Petrel model. Quality control was done by comparing the location of the horizons and faults, the properties, and the GIIP of the different compartments, in the new CATO-2 model to those of the original TAQA model. It was concluded that the differences are negligible (see Chapter 3.7 on uncertainties).

2. A regional-scale model at lower resolution (region of interest 40kmx30km; cell size 250mx250m; layering added in the geomechanical model). This model is larger in size than the reservoir-scale model, and is used in the geomechanical modelling study. It contains the main stratigraphical units of the reservoir and overburden, and the main faults in the reservoir and the overburden. Bounding surfaces that define the stratigraphical units are based on regional interpretations made by TNO. Using well data, 3D and 2D seismic, these interpretations were verified, and adapted when deemed appropriate. For the top and base of the reservoir only (top and base of the Main Buntsandstein Subgroup), the horizons from the higher-resolution reservoir-scale model were inserted to maximize the compatibility between the two models.

Quality control

Quality control of the reservoir-scale model was done by comparing the depth of the horizons and the location of faults with the 3D seismic data cube supplied by TAQA. The seismic data were supplied in two-way travel times, so a time to depth conversion was needed to compare model with the seismic data. The data on seismic interval velocities provided by TAQA proved to be unusable for the purpose of time-depth conversion because of well-tying of the horizons in the depth domain. Therefore, it was decided to build a new velocity model based on regional-scale velocity modelling work performed in-house at TNO, newly interpreted seismic, and well tops in combination with additional velocity log data from wells. The regional velocity model was built on the basis of velocity information of 22 wells in the area (40 x 30 km) covered by the regional model. Wells were used mainly from the P15, P18, Q13, and Q16 blocks, supplemented by wells KDZ-02-S1, MON-02-S1, and MSG-01. The velocity model is based on a so-called “V_{int}-Z_{mid}” relation of the main lithostratigraphic layers. Per layer, a linear velocity function was used:

$$V(z) = V_0 + K * z$$

where V stands for velocity (ms^{-1}) and z represents depth (m). The estimate of V_0 and K was made by taking the least squares approximation of V_{int} as function of Z_{mid}. Values of V_0 and K thus obtained are given in Table 2.

The new velocity model was used for time-depth conversion of the reinterpreted stratigraphic horizons that were used for the regional-scale model. Quality control of the reservoir-scale model was done by comparing the position of the marker horizons and the position and dip of the faults to the 3D seismic cube provided by TAQA that was depth-converted using our new velocity model. It was concluded that there are small differences, mainly in lateral position and dip of faults, which are not negligible. Differences in fault dip can be attributed to differences in time-depth conversion due to the use of different velocity models. However, differences in the lateral position of faults in the order of 50-100m (1-2 voxels in the reservoir-scale model) can only be traced back to the original seismic interpretation. This has implications for GIIP estimates, as will be illustrated in Chapter 9.

Table 2: values of V_0 and K used in the time-depth conversion

Unit ID	Stratigraphic name	$V_0(ms^{-1})$	$K(s^{-1})$
N	North Sea Group	1692.6	0.51
CK	Chalk Group	2324.1	0.75
KN	Rijnland Group	1708	0.9
S+AT	Schieland Group and Altena Group	2772.7	0.33
RN	Upper Germanic Trias Group	2788.9	0.45
RB	Lower Germanic Trias Group	2080.4	0.34

Core and outcrop sampling

In order to facilitate work in other work packages of CATO-2, two core workshops were organized, one at the TNO core facility in Zeist, and one at the core facility of the Nederlandse Aardolie Maatschappij (NAM) in Assen. Purpose of these workshops was to assess the influence of sedimentation processes and diagenesis on the flow properties of the P18 reservoirs. Furthermore, plug samples were taken from the reservoir interval in the core of the P18-02 exploration well, and from the core of well P18-A-01 in the P18-01 field nearby. Plug samples of the caprock, taken from wells Q16-4 and Q16-FA-101, were provided by NAM. Furthermore, rock samples of the reservoir and seal rocks were collected from outcrops in quarries in Germany. Plug and outcrop samples were handed-over to members of WP3.02 and WP3.03 for further study.

3.4. Geological setting

3.4.1. Structural history

The reservoir rocks of the P18 field are of Triassic age (249-245 Ma; Geluk, 2005), and belong to the Main Buntsandstein Subgroup. The Triassic rocks in the Netherlands represent part of the post-Variscan sedimentary mega-cycle. Its deposition was strongly controlled by a sequence of rift pulses that started in the Late Triassic, and lasted until the Middle Jurassic. It can be subdivided into a pre-rift, syn-rift and post-rift stage.

Pre-rift stage

The Early Triassic was characterised by regional, thermal subsidence. During the Early Triassic, sedimentation continued in a gentle northwards dipping basin (Southern Permian Basin) but under semi-arid continental conditions. At the southern margin of this basin, the area of deposition of the rocks of the P18 reservoirs (Figure 3.3), fine-grained lacustrine sediments were laid down initially, followed by a sandy fluvial and aeolian succession: the Main Buntsandstein Subgroup.

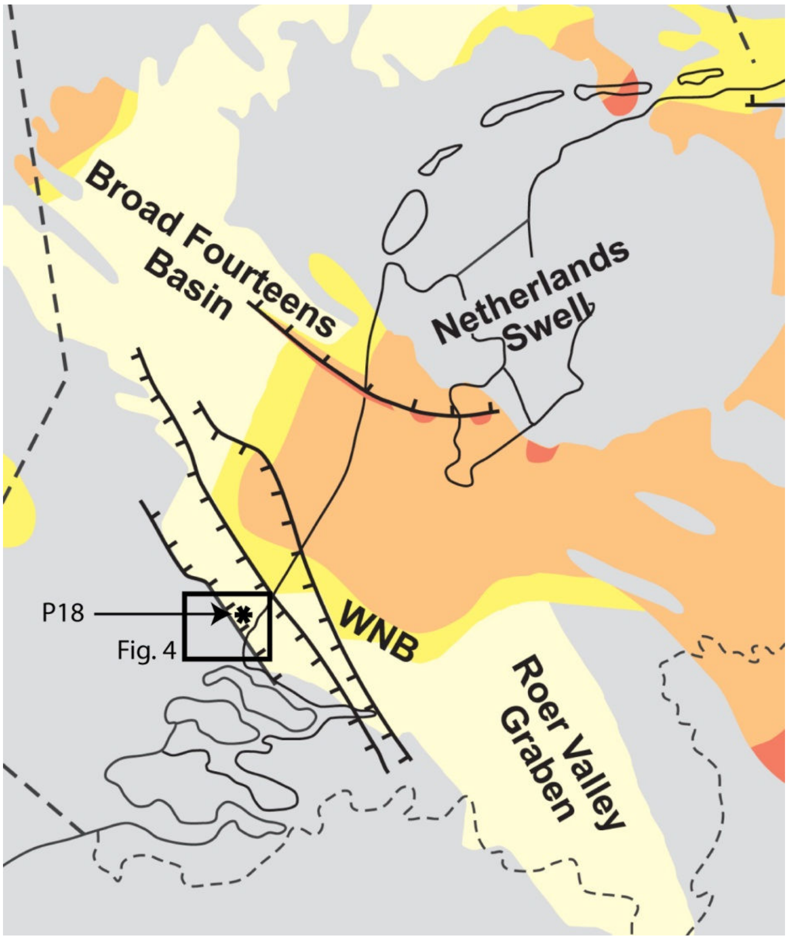

Figure 3.3: (Geluk 2007, after Geluk & Röhling 1997, 1999): Subcrop map of the Hardegsen Unconformity (= top reservoirs P18). Colours indicate formation; red: Lower Buntsandstein Fm., orange: Volpriehausen Fm., yellow: Detfurth Fm., white: Hardegsen Fm., grey: platform areas. WNB: West-Netherlands Basin.

These sediments were derived from the nearby London-Brabant Massif to the south, and the Rhenish massif to the southeast, which formed part of the northern rim of the Variscan orogenic belt (Geluk et al., 1996, Van Balen et al., 2000).

Rift stage

Active rifting started in the Middle Triassic. Several rift pulses broke up the large basin into a number of NW-SE trending fault-bounded sub-basins (Figure 3.4; De Jager, 2007). One of the sub-basins formed was the West Netherlands Basin (WNB; Figure 3.3), a well-known oil- and gas province in the Netherlands that also contains the P18 gas field. From Middle to Late Triassic, during the *Early Kimmerian* rift phase, the WNB was formed, a structurally rather simple large-scale half-graben, bounded to the north by a major fault zone (Geluk, 1999b). During the Late Triassic to Early Cretaceous, rifting intensified, and faulting caused differential subsidence of the various subunits of the basin (van Balen et al., 2000).

The strongest rifting occurred during the Late Jurassic to Early Cretaceous (Van Wijhe, 1987; De Jager et al., 1996; Racero-Baena & Drake, 1996). This caused the breaking-up of the basin into various sub-units, and large thickness variations in the Late Jurassic basin infill, i.e., thick in the basins and thin or absent on the highs.

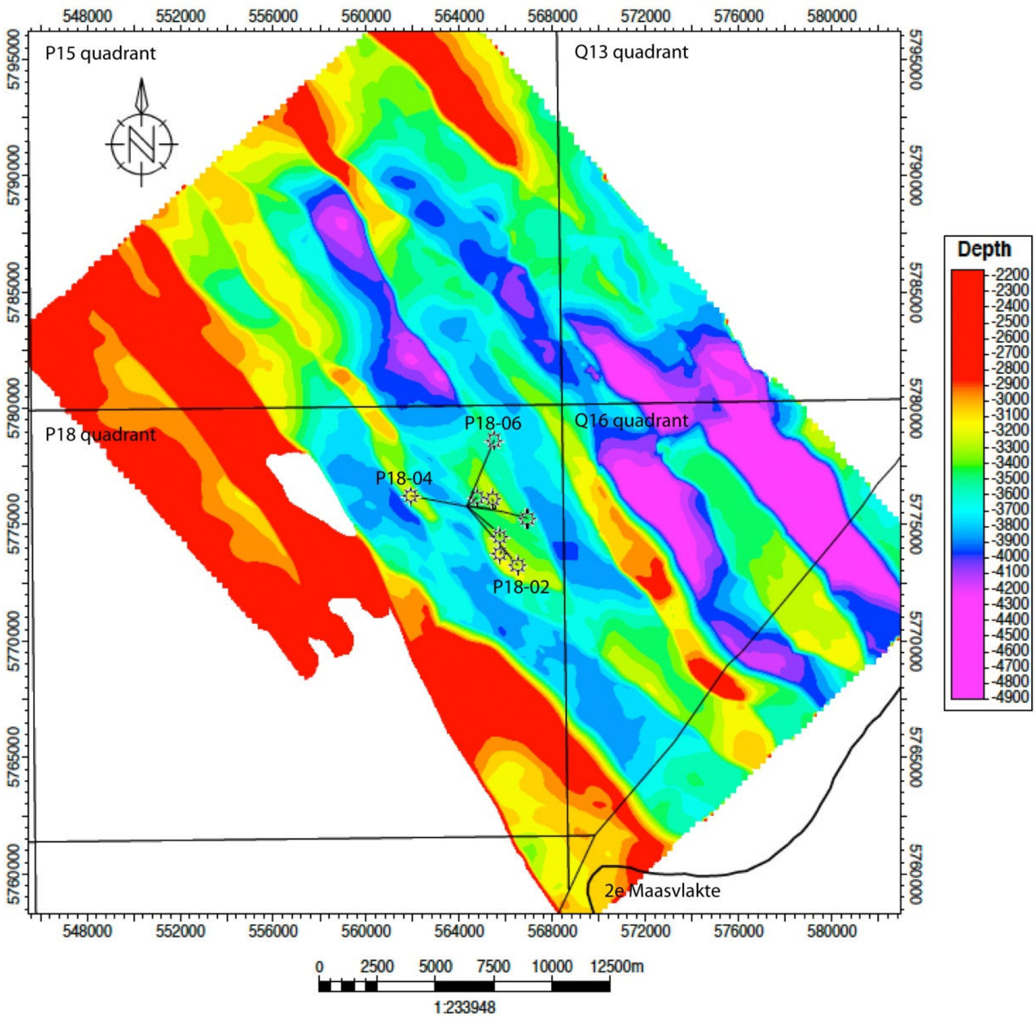

Figure 3.4: Contour map of the top Bunter (= top P18 reservoirs) in the offshore part of the West Netherlands Basin.

The rifting occurred in several discrete pulses of short duration in the time-span from Kimmeridgian to Barremian. Rifting gradually ceased during the Aptian-Albian (Van Wijhe, 1987), but subsidence of the WNB continued into the Late Cretaceous (van Balen et al., 2000).

Post-rift/Inversion

Compressional forces during the Late Cretaceous caused the inversion of the West Netherlands Basin (Van Wijhe 1987). On seismic, major fault zones display reverse movements, indicating that older basin-bounding faults were reactivated. Many of the oil-bearing anticlinal structures have been formed during this phase (De Jager et al., 1996; Racero Baena and Drake, 1996). The overall style of the inversion movements, with both a reverse vertical and a horizontal component, suggests they developed in response to transpression (dextral- strike-slip; Van Wijhe, 1987; Dronkers and Mrozek, 1991; Racero Baena and Drake, 1996).

3.4.2. Depositional setting

The Triassic sediments are of epicontinental character and were deposited in aeolian, fluvial, lacustrine, coastal and shallow-marine environments (Geluk, 2007). They are subdivided into two groups (Figure 3.5):

- The Lower Germanic Trias Group (Late Permian–Early Triassic), comprising mainly fine-grained clastic deposits with sandstone and oolite intercalations. In the P18 area, it consists predominantly of sandstones.
- The Upper Germanic Trias Group (Middle–Late Triassic) comprising an alternation of fine-grained clastics, carbonates and evaporites with subordinate sandstones.

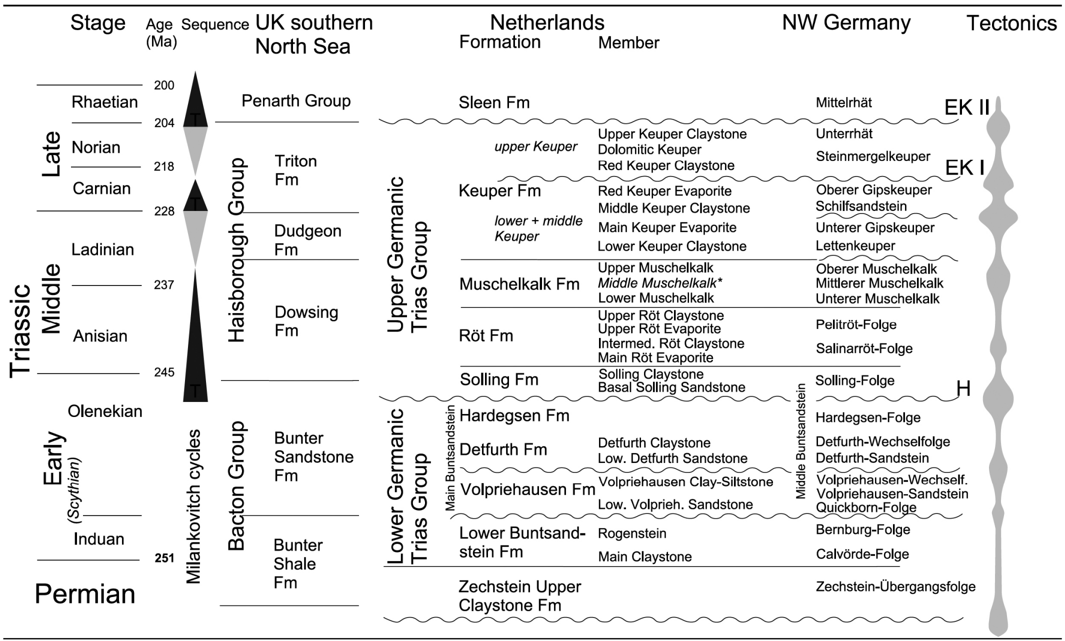

Figure 3.5: (Geluk, 2007; after Van Adrichem Boogaert and Kouwe 1994, Johnson et al. 1994, Geluk 1999 and Kozur, 1999; ages after ISC 2003; sequences after Gianolla and Jacquin 1998): Transgressive sequences in black, regressive sequences in grey. EK I: main Early Kimmerian Unconformity, base Norian; EK II: Early Kimmerian II Unconformity, base Rhaetian; H: Hardegsen Unconformity. * Middle Muschelkalk comprises the Muschelkalk Evaporite and Middle Muschelkalk Marl.

It is formed by the Hardegsen or Base Solling Unconformity, which forms a regionally well-correlatable event (Ziegler, 1990; Geluk & Röhling, 1997, 1999; Geluk, 2005). Directly above lie the claystones and evaporates of the Solling Claystone and Röt formations that form the caprock to the P18 reservoirs.

3.4.3. Source rock and charging

The gases in the P18 and other Triassic reservoirs in the West-Netherlands Basin have either a pure Westphalian (Carboniferous) or a mixed origin (De Jager et al., 1996). Based on the carbon-isotope ratios, carbon molecular gas ratios and nitrogen isotope ratios, Gerling et al. (1999) also concluded that Carboniferous and Upper Permian gas fields in the western part of the Southern North Sea Basin are of a mixed origin, with a low maturity terrestrial source and a more mature marine source. The terrestrial source is a thick succession of Westphalian sediments, which contains humic source rocks in coals and shales. The average coal content of the Westphalian A and B succession is about 5.5% (Dusar et al., 1998), and the TOC of the coals is at least 70% (Van Bergen, 1998). The second source could be a Namurian (Carboniferous) marine source rock.

Generation of the gas and migration into the P18 reservoirs was modelled by van Balen et al. (2000). They concluded that generation set in at about 240 Ma, accelerated at 160 Ma, and levelled out towards the present. In the P18 area, generation continues until now, whereas in the central and northern parts, the generation rate strongly declined at about 150 Ma. The charging occurred between 150 Ma and 80 Ma. This is in agreement with K/Ar dating of diagenetically formed illite, from which the age of gas emplacement for a well in the Broad Fourteens Basin was inferred to be 140 Ma (Lee et al., 1985). As the WNB has a similar tectonic history as the Broad Fourteens Basin (Van Wijhe et al., 1987), the timing of gas emplacement can also have been similar.

3.5. Reservoir geology

3.5.1. Structure and faults

The structures that contain the reservoirs are bound by a system of NW-SE oriented faults in a horst and graben configuration, with a sinistral strike-slip component (Figure 3.6). The top of the reservoir compartments lies at depths between 3175 m and 3455 m below sea level (Figure 3.7).

Block P18-02 is the main block, and is bounded by two normal faults, the F19 fault and the F20 fault. A closer look at the offsets of these reservoir-bounding faults (Figure 3.8) indicates that they are sealing due to juxtaposition of reservoir zones against impermeable shales of the Altena Group. Inside P18-02, compartment P18-02I, which is the largest compartment of the three, is separated from compartment P18-02II by fault F14, the offset of which is insufficient to be sealing by juxtaposition (Figure 3.8). Indeed, production data suggest that there is partial communication between the two compartments across this fault (pers. comm. N. Vera of TAQA). It is likely that the sealing capacity of this fault depends on a pressure threshold, and that this threshold is exceeded due to depletion of the compartment after production. Compartment P18-02III is separated from P18-02II and P18-02I by fault F18, which has enough offset to be sealing by juxtaposition, except for a small region at the southern end (Figure 3.8). However, no or very minor pressure communication was observed between the P18-02I/ P18-02II compartments and the P18-02III compartment (pers. comm. N. Vera of TAQA), which suggests that the F18 fault is sealing.

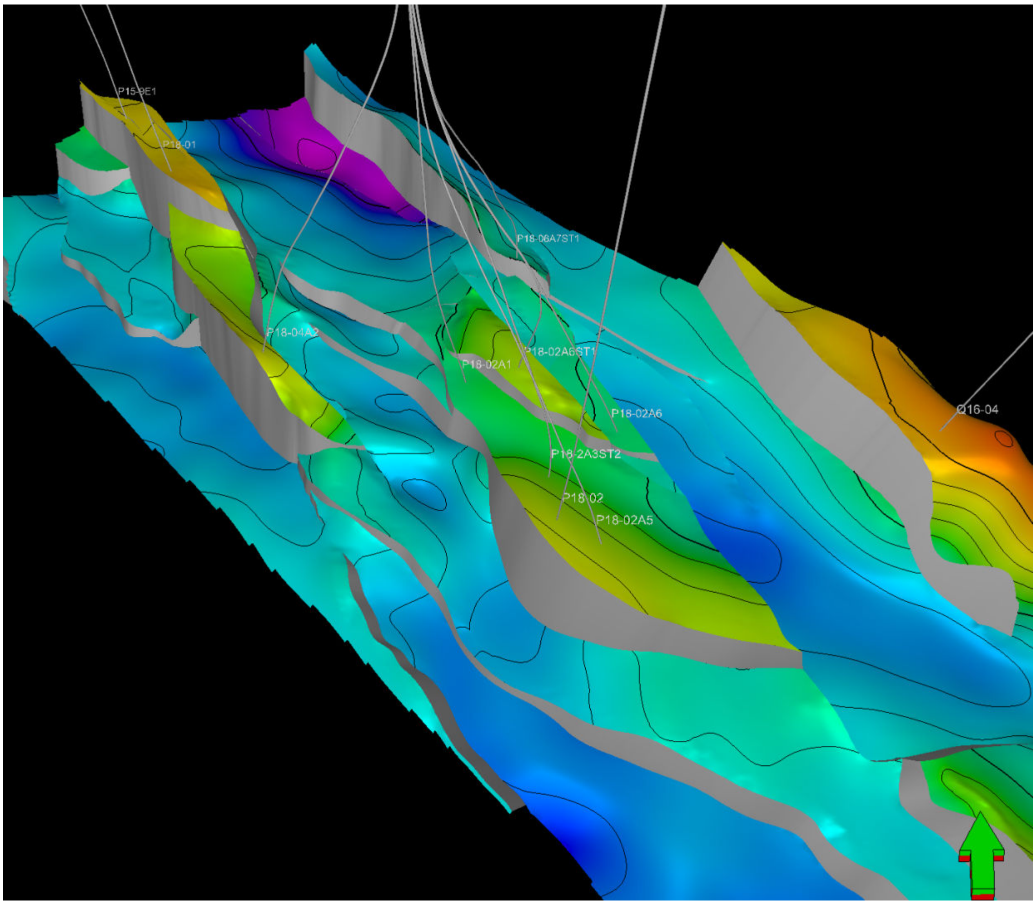

Figure 3.6: 3D view of the top of the P18 reservoirs. Faults are shown in grey.

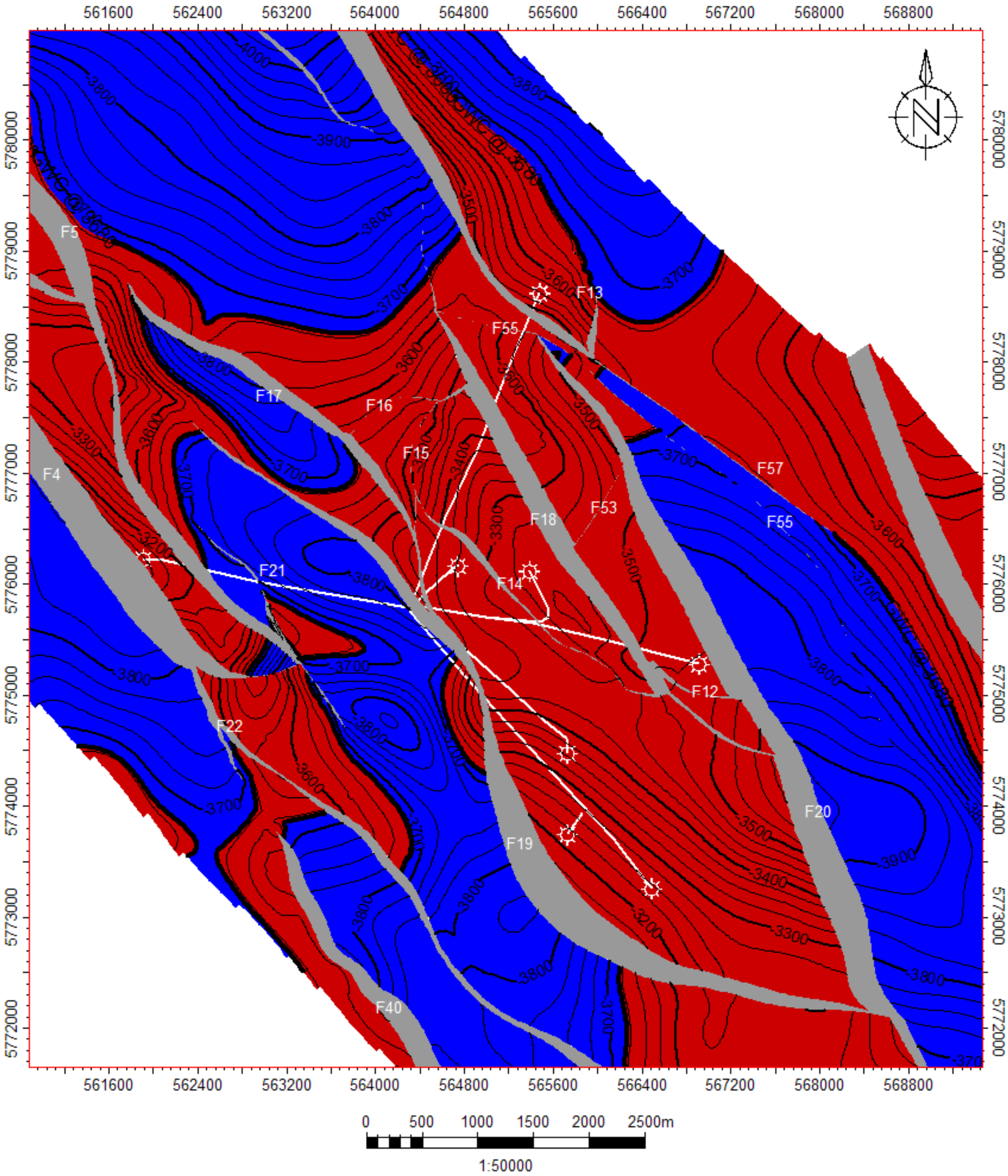

Figure 3.7: Contour map of the top of the reservoir, with faults bounding the compartments in grey. Fault identifiers and locations of the wells at the top of the reservoir are indicated in white. Colouring indicates pore fluid contents based on a GWC of 3680 m SSTVD; red: gas, blue: water

Block P18-04 is located to the northwest of the main block. It is bounded by faults F4 and F5 to the west and east respectively, and separated from the P15-E field by fault F3 (Figure 3.8). All three have sufficient offset to be sealing by juxtaposition, which is supported by production data (e.g. different pressures).

Block P18-06 is located to the northeast of the main block. It is bounded by faults F13 and F57, of which only F13 has enough offset to be sealing by juxtaposition.

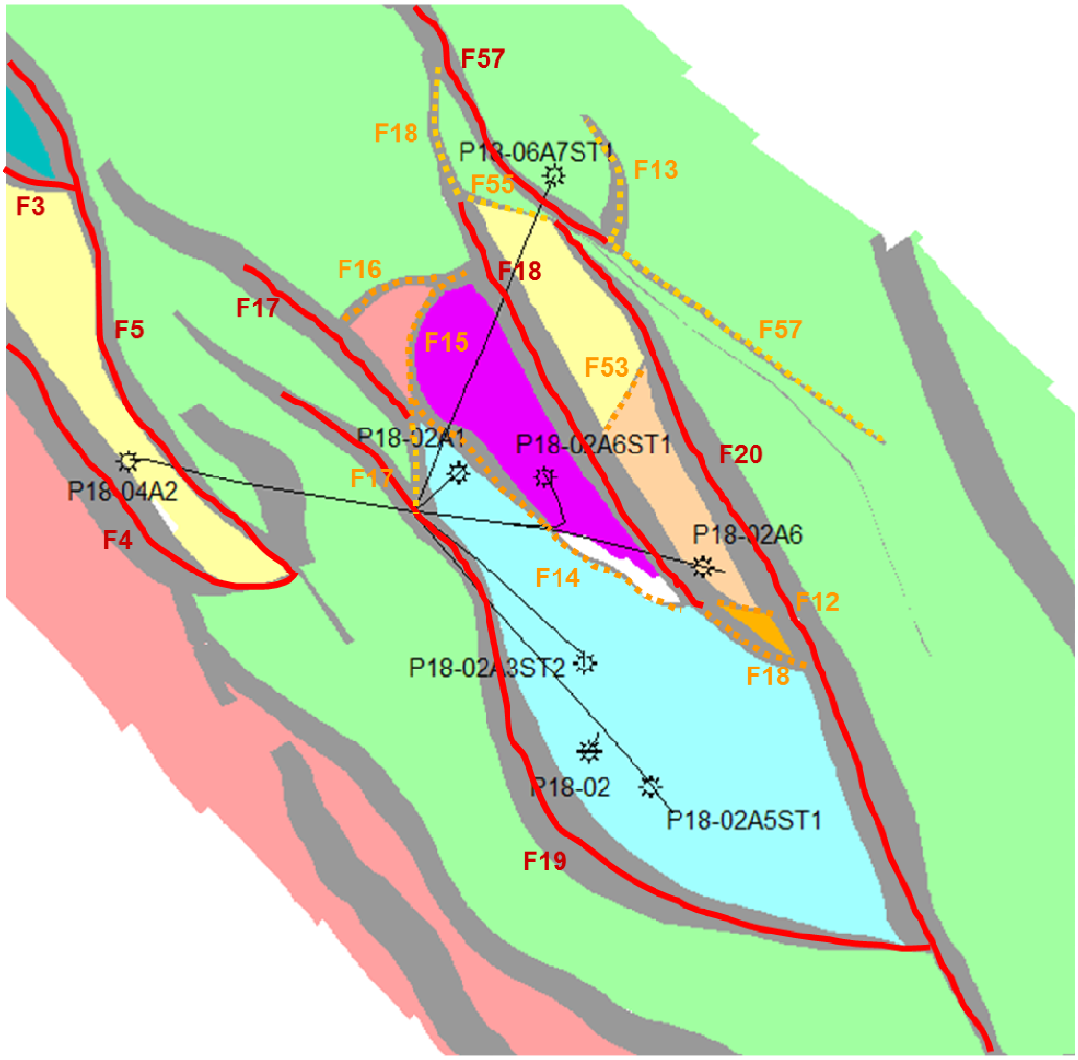

Figure 3.8: Map view of the P18 field, with the different reservoir compartments indicated in different colours. Faults that have enough offset to juxtapose reservoir against non-reservoir are indicated with bold red lines, and faults that do not have enough offset, i.e., where reservoir is juxtaposed against reservoir, are indicated with dotted orange lines.

3.5.2. Lithologies

The reservoir rocks of the P18 belong to the Main Buntsandstein Subgroup, a cyclic alternation of (sub-) arkosic sandstones and clayey siltstones. The Volpriehausen Formation is mainly of fluvial origin, but also contains substantial aeolian sediment. It consists of braided river deposits interbedded with dune deposits, and subordinate flood-plain and crevasse-splay deposits (Ames and Farfan, 1996). It is composed of a Lower Volpriehausen Sandstone Member and an Upper Volpriehausen Sandstone Member. The Volpriehausen Formation is a clean sandstone with a blocky appearance on Gamma-ray logs (Figure 3.9 & Figure 3.10) that contains high percentages of calcite and dolomite (Geluk et al., 1996).

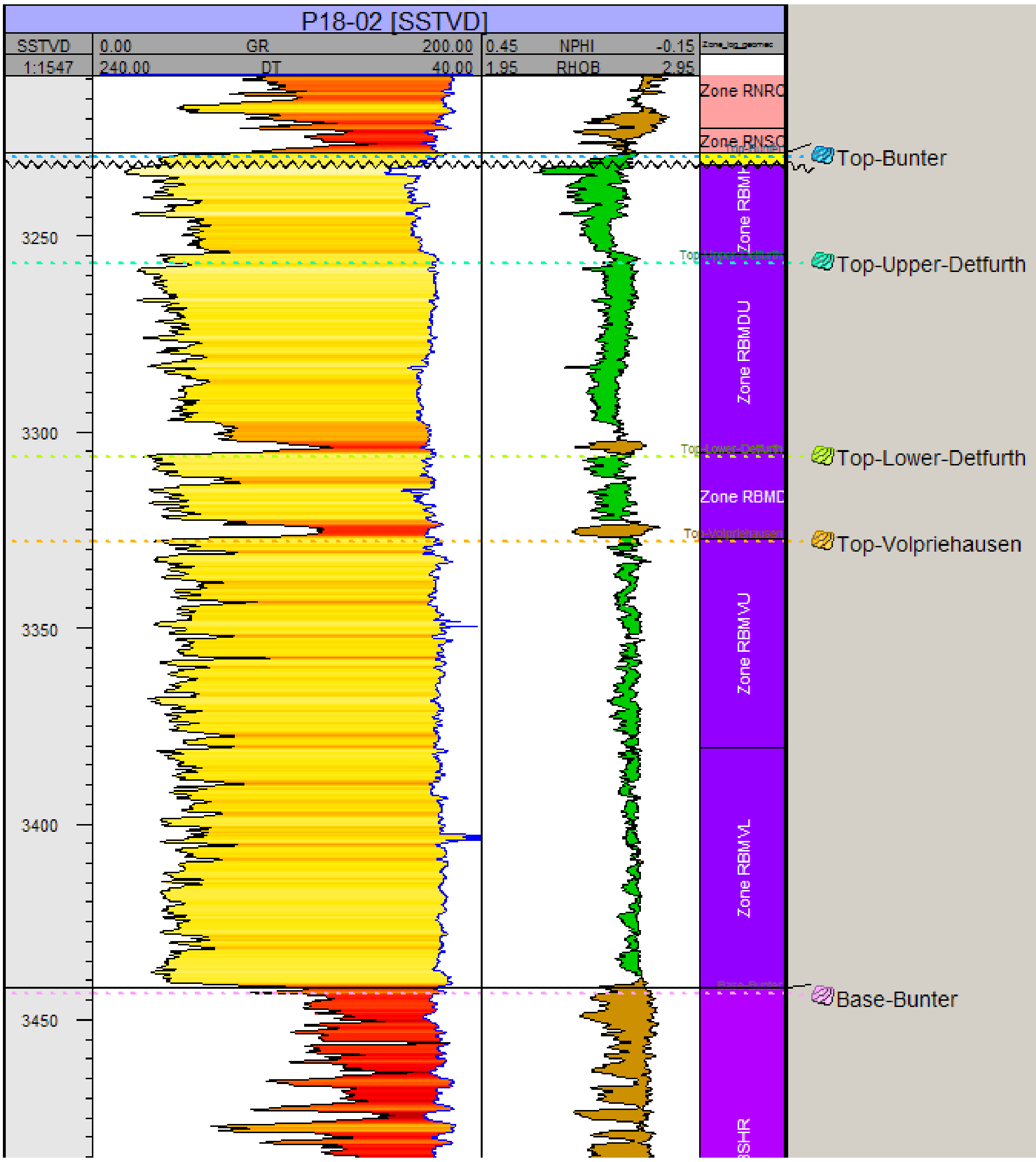

Figure 3.9: GR-log (red-yellow colouring), sonic log (blue), neutron porosity (NPHI) log, and bulk density (RHOB) log over the reservoir interval in the P18-02 exploration well.

On Gamma-ray logs, it is clearly distinguished from the Rogenstein Claystone Member below by a marked increase in Gamma-ray readings. The Rogenstein Claystone member forms the basal seal to the reservoirs (Figure 3.10). Only wells P18-02-A1, P18-02-A2, P18-02-A3ST2, and P18-02-A5 penetrate the entire Volpriehausen Formation. Its thickness in the wells ranges between 101 m and 115 m (Table A1 in Appendix A).

The Detfurth Formation is composed of a Lower and an Upper Detfurth Sandstone Member. It consists mainly of aeolian sediment (dunes), and some fluvial deposits (Ames and Farfan, 1996). The Lower Detfurth Sandstone Member forms one of the best reservoir intervals in the P18 fields. It is marked by low gamma-ray values (Figure 3.9 & Figure 3.10) due to its high quartz grain content and because it is quartz-cemented (Geluk et al, 1996). It is distinguished from the Volpriehausen Formation by a well-correlatable interval of high gamma-ray readings (Detfurth Unconformity) and two clearly recognizable coarsening upwards sequences (Figure 3.9 & Figure 3.10).

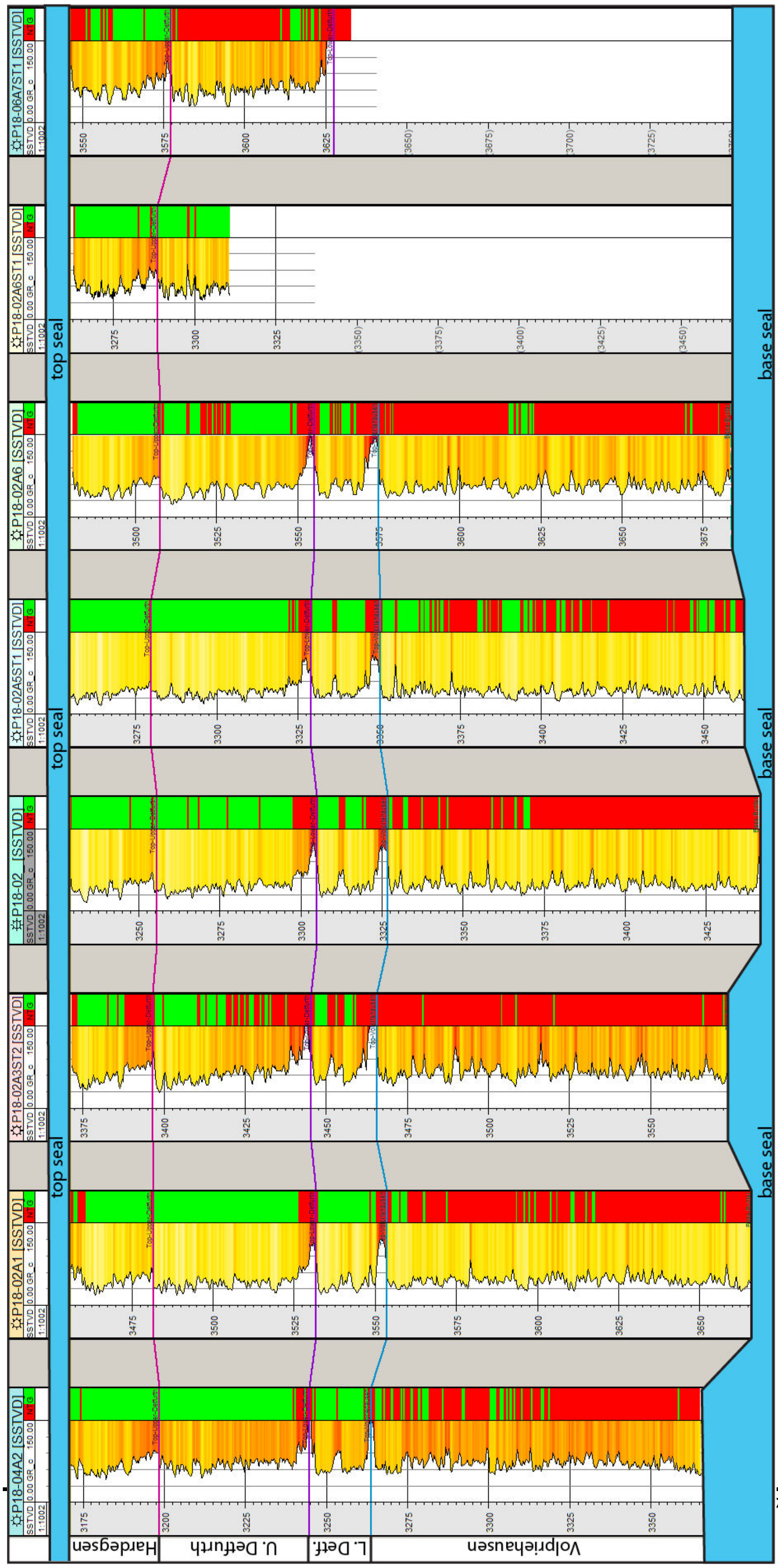

Figure 3.10: Log panel through the production wells of the P18 field. GR-logs on the left side, with colouring indicative of GR reading, yellow: low (sand), red: high (clay). Net Pay logs on the right side, red: no-pay zone, green: pay zone.

It is penetrated by all the wells except well P18-02-A6ST1. Well P18-02-A7ST1 only penetrates the top. Its thickness in the wells ranges between 19 m and 22 m (Table A2 in Appendix A).

The Upper Detfurth Sandstone Member is separated from the Lower Detfurth Sandstone Member by a second well-correlatable interval of high-Gamma-ray readings and a single coarsening-upward sequence (Figure 3.9 & Figure 3.10). It is penetrated by all the wells, although not completely by well P18-2A6ST1. Its thickness ranges between 47 m and 50 m (Table A3 in Appendix A).

The Hardegsen Formation is characterized by sandstones, and is recognized by a marked increase in the Gamma-ray values compared to the underlying Detfurth Formation. Furthermore, it displays a well-developed overall coarsening-upward pattern with low Gamma-ray values towards the top (Figure 3.9 & Figure 3.10). It consists mainly of aeolian deposits and is penetrated by all the wells. Its thickness in the wells ranges between 24 m and 33 m (Table A4 in Appendix). Above the Hardegsen Formation, gamma-ray values increase again, first mildly, and then strongly and abrupt (Figure 3.9). This mild increase is due to the transition from Hardegsen Formation to the Solling Sandstone Member, which here is included in the Hardegsen reservoir zone. The strong increase is due to the transition from the Solling Sandstone Member to the Solling Claystone Member that forms the basal part of the caprock to the P18 reservoirs (Figure 3.10).

3.5.3. Petrophysics

Wells

Data on the petrophysical properties of the reservoir intervals (N/G, PHI, S_w) in the wells were provided by TAQA. They are displayed in tables A5, A6, A7, and A8 in the Appendix A. The Free Water Level (FWL) was determined by TAQA either from pressure-depth gradients or from mapped spill points. However, there is much uncertainty on the actual position of the FWL in the three blocks. For instance, in the P18-02 block, the lowest-known-gas was found at 3506 m (base perforation) in well P18-02A6, but the structural spill point of the P18-02 block is mapped at 3635 m in the NW corner of the block (Figure 3.7). A discussion on the position of the FWL and significance for GIIP estimates and history matching can be found in the report of WP3.02 on the reservoir engineering aspects of this feasibility study.

Average values of porosity and connate water saturation per field are displayed in Table 3. Average porosity in the Hardegsen formation ranges between around 7-13% and in the Detfurth Sandstone Members slightly lower around 5-9%. Maximum porosities encountered in the clean sandy parts of both formations are around 21 %.

The average permeabilities are calculated by TAQA based on the average porosities using a porosity-permeability relation. Although its origin is unclear, it is likely that this relation is based on core measurements. However, an attempt to reproduce this relationship from such measurements failed. Clearly, the permeabilities are highest in the Hardegsen Formation, with a range between 2 and 207 mD. In the Detfurth Sandstone Members they range between 0.1 and 0.8 mD. The combined thickness of both formations is approx. 100 m. The Volpriehausen has a much lower porosity that ranges between 3 and 5%. Permeabilities are very low, i.e., less than 0.1mD. The thickness of the Volpriehausen is also approx. 100 m.

Average water saturations range between 0.24 and 0.47 in the Hardegsen Formation, between 0.43 and 0.57 in the Upper Detfurth Sandstone Member, between 0.32 and 0.42 in the Lower Detfurth Sandstone Member, and between 0.78 and 0.92 in the Volpriehausen Formation.

Table 3: Average (arithmetic) petrophysical properties of the reservoir intervals per block in the wells of the P18 field. "N/G" stands for "Net-To-Gross", as calculated by dividing the amount of sand (Vshale cut-off: < 0.35, PHI cut-off: > 0.02) in m by the total thickness of the formation, "PHI" indicates the average porosity (cut-off: > 0.02) of the bulk, "Sw" indicates the average water saturation (Vshale cut-off: < 0.35, PHI cut-off: > 0.02), and "k" indicates the average permeability as calculated using a porosity-permeability relation. "N.F.P." stands for not fully penetrated.

P18-02				
	Hardegsen	**Upper Detfurth**	**Lower Detfurth**	**Volpriehausen**
Thickness (m)	26.4	48.8	21	111
N/G	0.98	0.94	0.79	0.70
PHI	0.125	0.092	0.079	0.039
S_w	0.267	0.428	0.418	0.778
K (mD)	128.0	0.8	0.3	0.0
P18-04				
	Hardegsen	**Upper Detfurth**	**Lower Detfurth**	**Volpriehausen**
Thickness (m)	24	47	19	101
N/G	0.99	0.87	0.81	0.33
PHI	0.131	0.092	0.065	0.049
S_w	0.240	0.470	0.390	0.920
K (mD)	207.0	0.8	0.1	0.0
P18-06				
	Hardegsen	**Upper Detfurth**	**Lower Detfurth**	**Volpriehausen**
Thickness (m)	33	49	N.F.P.	N.F.P.
N/G	0.81	0.91	N.F.P.	N.F.P.
PHI	0.074	0.048	0.059	0.030
S_w	0.470	0.570	0.320	outside gasleg
K (mD)	1.8	0.0	0.1	0.0

Table 4: Average modelled petrophysical properties of the reservoir intervals per block in the P18 field.

P18-02				
	Hardegsen	**Upper Detfurth**	**Lower Detfurth**	**Volpriehausen**
Thickness (m)	26.6	49.1	21.5	116.2
PHI	0.107	0.077	0.066	0.033
S_w	0.401	0.650	0.624	0.936
P18-04				
	Hardegsen	**Upper Detfurth**	**Lower Detfurth**	**Volpriehausen**
Thickness (m)	29	49	19	111
PHI	0.111	0.076	0.064	0.0245
S_w	0.348	0.61	0.688	0.99
P18-06				
	Hardegsen	**Upper Detfurth**	**Lower Detfurth**	**Volpriehausen**
Thickness (m)	26.9	47.5	19.1	110.7
PHI	0.054	0.029	0.036	0.019
S_w	0.770	0.890	0.660	0.940

Model

An important step in the quality control of the reservoir model is to verify that the property model honours the original data on the petrophysical properties from the wells, as presented above. Property modelling, i.e., interpolation of measured values of porosity and permeability between the wells, was done by TAQA in RMS assuming that the distribution of the properties resembles a Gaussian distribution. Water saturation was modelled with a height-saturation function. Table 4 displays the average modelled values of thickness, porosity and water saturation for the three blocks in the P18 field. When comparing these values to the average values of thickness, porosity, and water saturation in the wells (Table 3) it can be concluded that the average thicknesses of the reservoir intervals in the model agree well with those in the wells, and that it somewhat underestimates the porosities. Far more striking however is that the model substantially overestimates the water saturation by values ranging between 0.07 and 0.34. Permeabilities in the supplied property model were of low confidence, and have not been included in this report.

3.6. Seals

3.6.1. Primary Seal

The primary seal to the P18 reservoirs is formed by siltstones, claystones, evaporites and dolostones of the Solling Claystone Member, the Röt Formation, the Muschelkalk Formation, and the Keuper Formation that discomformably overlie the reservoir. The Solling Claystone Member consists of red, green and locally grey claystones that where deposited in a lacustrine setting just after the tectonic movements of Hardegsen phase during a major transgression (Geluk et al., 1996). It is the first laterally extensive claystone above the reservoir rocks of the Main Buntsandstein. In well P18-02, it has a thickness of approx. 5 m (Figure 3.11). The Röt Formation consists of thin-bedded claystones, and is approx. 40 m thick. The Muschelkalk Formation consists of claystones, dolomites, and evaporates, and is approx. 70 m thick. All these rocks contain variable amounts of nodular anhydrite cementation (Spain and Conrad, 1997). The Keuper Formation consists of claystones intercalated with zones of anhydrite and gypsum, and is approx. 40 m thick. In total, the thickness of the primary seal in well P18-02 is approx. 155 m.

Faults are present in this primary seal. However, these faults appear to be sealing. Reservoir closure is obtained through impermeable zones above and below the reservoir interval (Figure 10), in combination with juxtaposition of permeable reservoir facies against impermeable non-reservoir facies of the Altena Group (secondary seal, see below). A closer look at the 3D seismic reveals that, although most of the reservoir-bounding faults do not continue further upward into the overburden than the shales of the Altena Group, some reverse faults that where formed during the inversion phase appear to originate around the fault tips of the older reservoir-bounding faults (Figure 3.14). However, inversion in the area of the P18 field was relatively weak. Therefore, it is unlikely that these inversion faults are reactivation faults that originate from movement along the older basin-bounding faults. Although impossible to rule out completely, it is not likely that the sealing properties of the basin-bounding faults have been compromised.

3.6.2. Secondary and higher seals

Directly above the primary seal lies the Altena Group, a thick succession of marine claystones, siltstones and marls of Early Jurassic age with excellent sealing quality. It also contains the Posidonia Shale Formation that is easily recognized on seismic due to its excellent reflectivity. The Altena Group has a thickness of approx. 500 m in the P18-02 well (Figure 3.14). The rest of the overburden is formed by several geological formations, some of which can also be assumed to have good sealing properties. The North Sea Supergroup is the shallowest succession in the overburden, and consists mostly of siliciclastic sediments. It has a thickness of approx. 1000m, and consists of the Lower, Middle and Upper North Sea Groups. The bases of the Upper and Lower North Sea Groups are marked by distinct unconformities. The Lower North Sea Subgroup comprises Paleocene and Eocene, predominantly marine deposits, the Middle North Sea Group includes mainly Oligocene, marine strata, and the Upper North Sea Group consists of marine to continental, Miocene and younger sediments. The North Sea Supergroup overlies the Chalk Group unconformably. On seismic, it appears as largely unfaulted, although sub-seismic scale faults might be present. Clayey sequences are abundant, especially in the lower part. These could very well act as secondary seals.

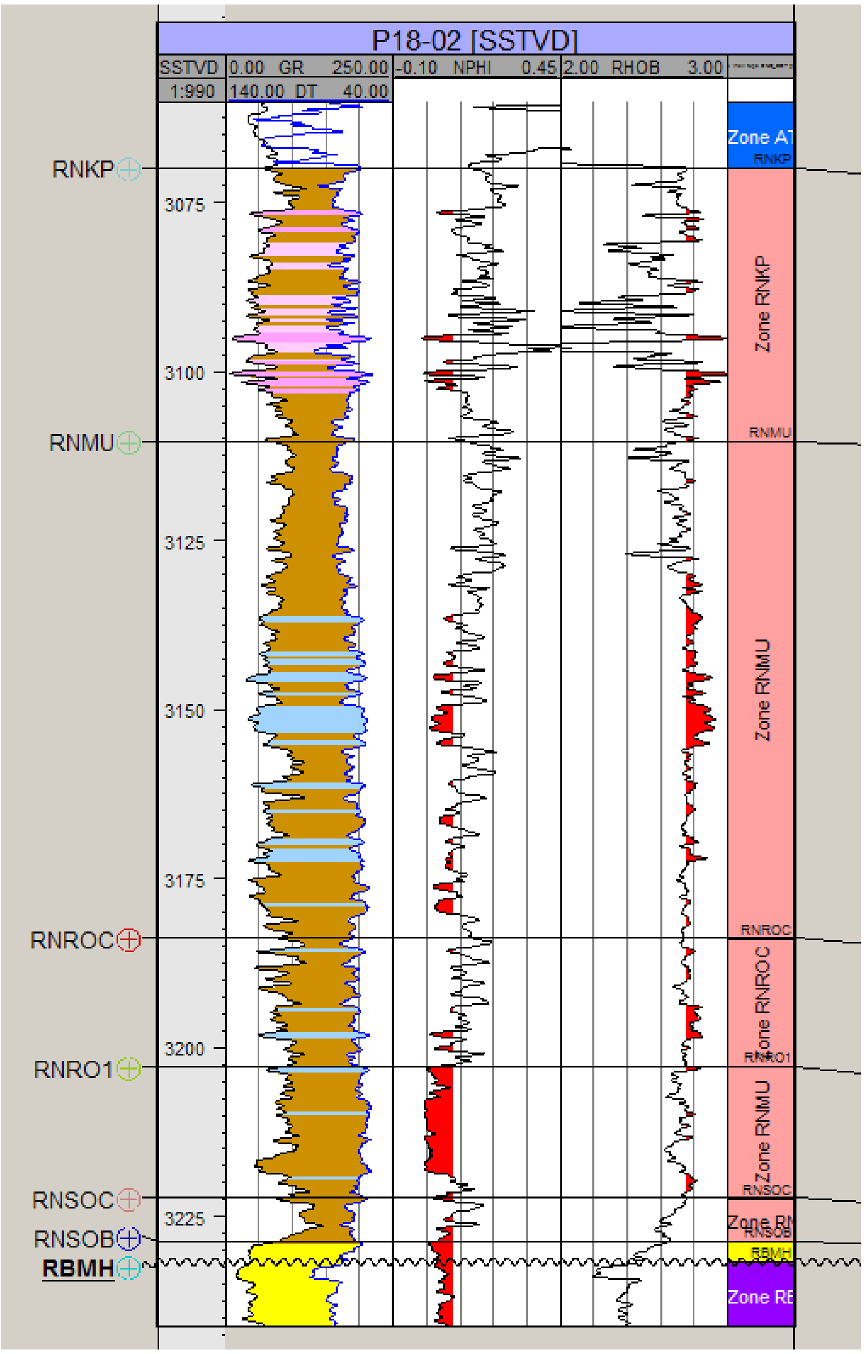

Figure 3.11: GR-log, sonic log, neutron porosity log and bulk density log of the primary seal in the P18-02 explo-ration well. RBMH: Hardegsen Formation = top reservoir (unconformity). Colouring indicates lithology, yellow: sand, brown: shale, blue: dolomite, light pink: anhydrite, dark pink: gypsum.

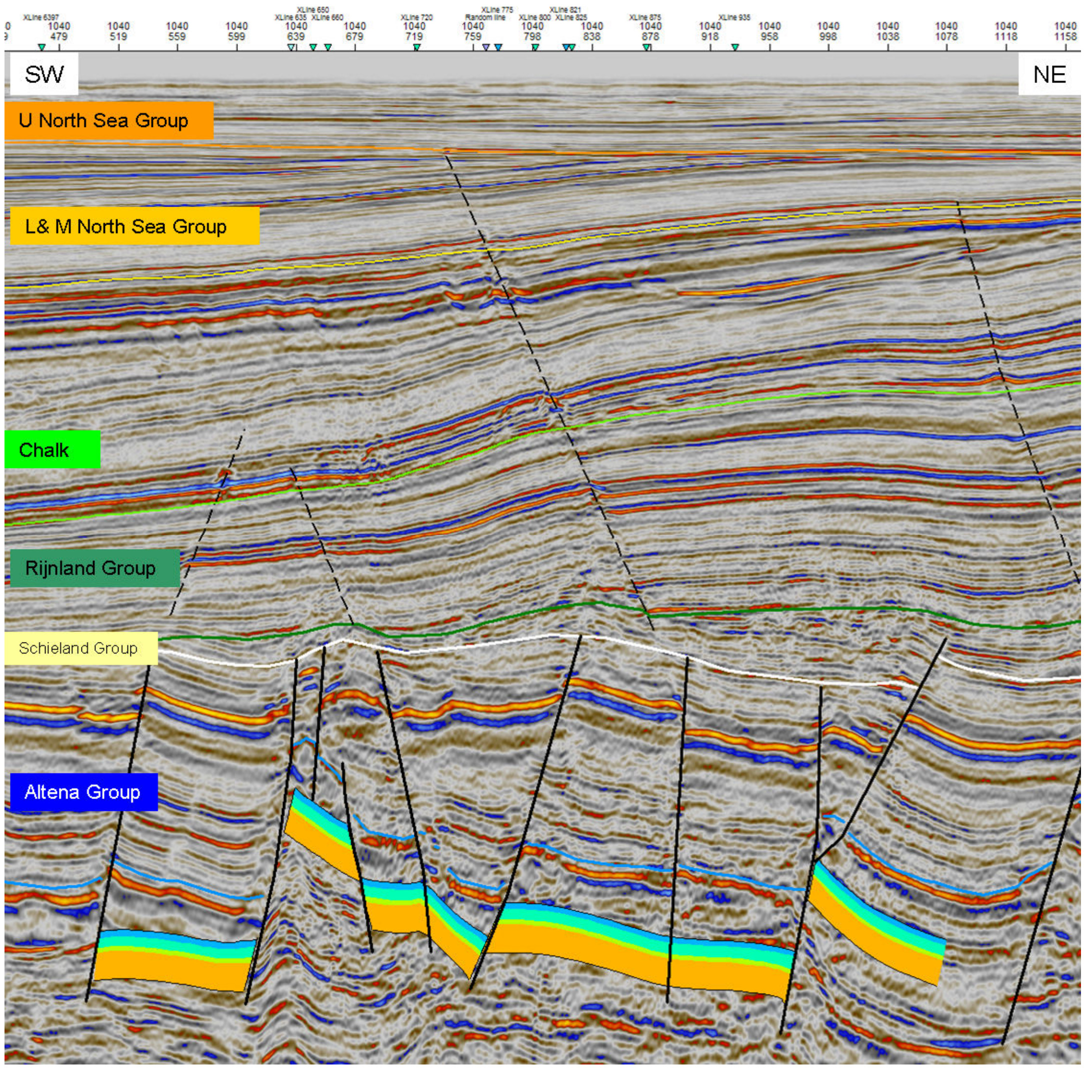

Figure 3.12: Seismic cross-section (inline 1040 in TAQA seismic cube) through the P18 field, displaying the reservoir interval (coloured layering), the main bounding faults to the reservoirs (bold lines), the main stratigraphic units in the overburden and the faults in the overburden (dashed). Position of cross-section is indicated in Figure 3.114.

The Upper Cretaceous Supergroup has a thickness of approx. 1400m and consists of the Ommelanden Formation, the Texel Formation and the Texel Greensand Member. During the Late Cretaceous, the influx of fine-grained clastics into the marine realm (Lower Cretaceous) diminished. A fairly uniform succession of marls and limestones of the Texel and Ommelanden Formations developed. These sediments have an earthy texture and are commonly known as 'chalk'. The sealing properties of these formations are questionable although few of the larger faults penetrate this interval. The Lower Cretaceous Supergroup has a thickness of approx. 1000m, and consists of the Holland Formation, the Vlieland Claystone Formation and the Vlieland Sandstone Formation. At locations in close proximity to the P18 field, some of the sandstone layers present in this interval are gas or oil bearing (e.g. Rijswijk Member, Rijn Member), which demonstrates the sealing quality of the numerous claystone intervals in this succession. The Lower Cretaceous appears largely unfaulted, which further increases the sealing potential of these rocks. However, it is expected that some sub-seismic scale faults are present throughout the Upper and Lower Cretaceous supergroups.

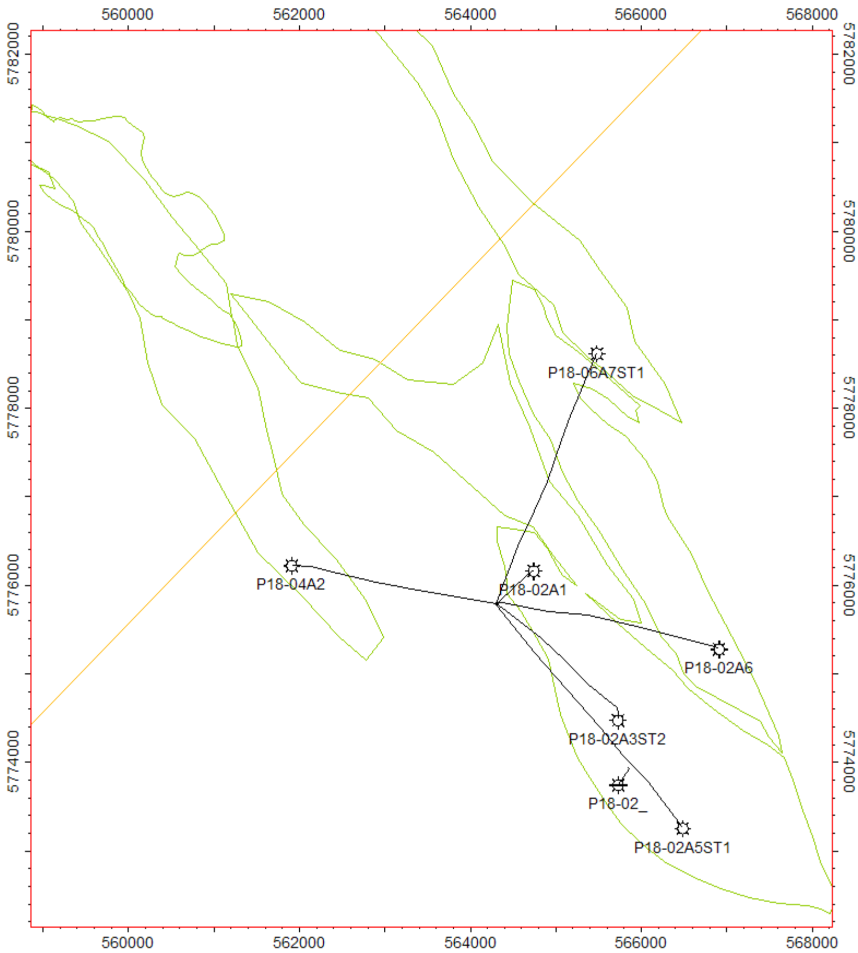

Figure 3.13: Map view of the P18 field, with position of the seismic cross-section of Figure 11 indicated in orange.

3.6.3. Shallow gas accumulations

On 3D seismic small bright spots and disturbances (diameter approx. 100m) along and near fault lines can be identified (Figure 3.15). It is likely that these bright spots and disturbances are related to shallow gas. Origin of the gas could be biogenic, but it could potentially also have originated deeper, in which case it must have migrated upward and possibly also laterally through transmissive faults and permeable layers. Considering the excellent sealing quality of the primary seal of the P18 reservoir, and the difference in age and dip of the faults in layers above and below the Altena Group, it is unlikely that these potential shallow gas accumulations are related to the P18 reservoirs from which gas is produced. More likely, it originates from either the Posidonia Shale Formation in the overlying Altena Group, which is responsible for charging many Upper Jurassic and lower Cretaceous reservoirs in the vicinity (De Jager et al., 1996), or from shallower layers by biogenic processes.

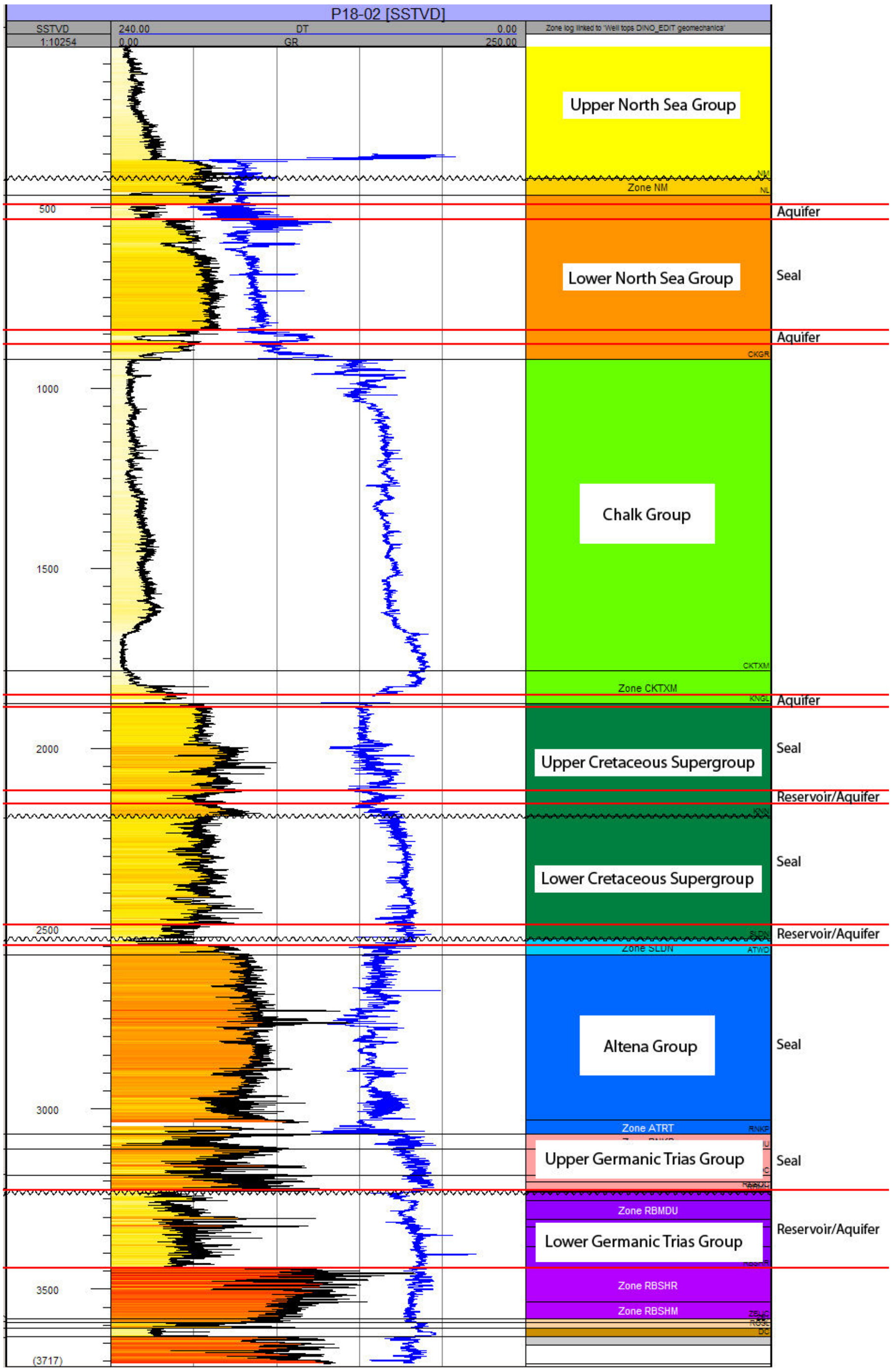

Figure 3.14: Stratigraphy and logs (GR in black with red-yellow colouring, sonic in blue) of the reservoir interval and overburden of the P18 field, with aquifers and seals indicated.

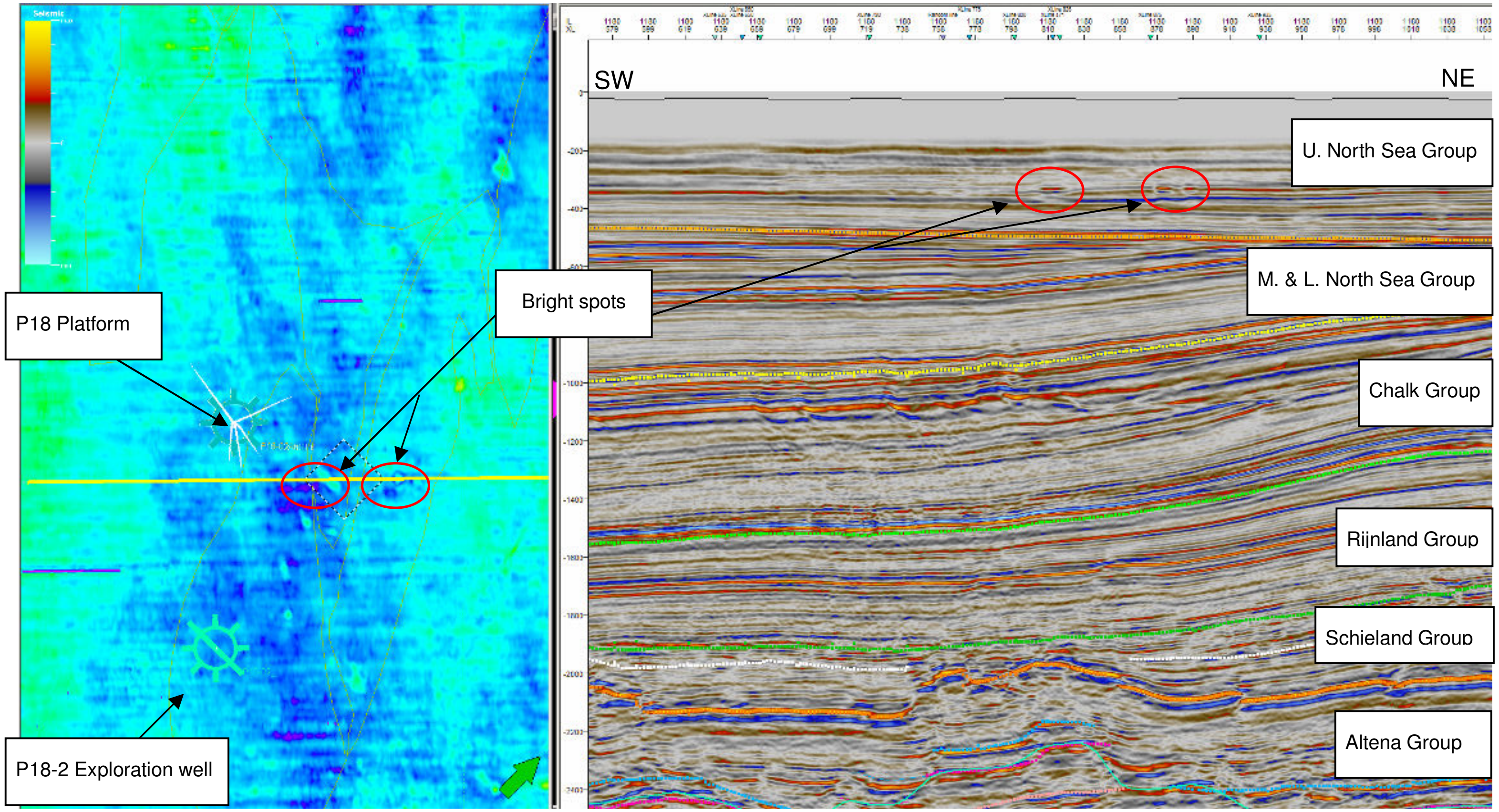

Figure 3.15: Left: map of the RMS amplitude between 250ms and 350ms TWT. Note the greenish blobs slightly east of the P18 structure. Right: Seismic section trough the P18 structure, note the elevated amplitudes between 250ms and 350ms TWT.

3.7. GIIP: estimates and sensitivity

Estimates of GIIP (Gas Initially In Place) are important, because they are an indication of the volume of CO_2 that can be stored. A GIIP estimate can be made based on different sources of information. Here, two independent sources have been used, a static GIIP estimate based on the static geological model, and a dynamic GIIP estimate, based on production data, i.e., plots of pressure/depth (P/z) vs. cumulative production (see also Chapter 4 reservoir engineering). The GIIP estimate from the production data is very accurate, i.e., it has a low uncertainty attached to it because it is directly based on production. It is a direct indication of the connected volume, i.e., the pore volume connected to the wells. Table 5 displays the GIIP estimates for the three blocks in the P18 field. Static GIIPs for both the original geological model of TAQA (RMS format) and the rebuilt one of CATO-2 (Petrel format) are given to indicate the close match between the two models. Evidently, the static model underestimates the GIIP.

Table 5: Static and dynamic GIIP estimates (in BCM) of the three blocks in the P18 field.

GIIP						
	GWC(m)	**Static (TAQA)**	**Static (CATO-2)**	**Dynamic**	**ΔGIIP**	**%**
P18-02	3680	12.40	12.45	13.40	0.95	7.1
P18-04	3377	2.58	2.58	3.20	0.62	19.3
P18-06	3680	0.35	0.36	0.62	0.26	41.9
Sum		15.33	15.39	17.22	1.83	10.6

A sensitivity analysis of the static GIIP estimates was done to assess the sensitivity of the estimates to uncertainty in structure, depth of GWC, porosity and water saturation. For block P18-02, the discrepancy between static and dynamic GIIP is only about 7%, which can easily be attributed to differences in porosity and/or average water saturation between the wells and the property model (see Tables 3, 4). However, for blocks P18-04 and P18-06 the discrepancy is much larger, and can be only partly explained by such differences.

For block P18-04, lowering the water saturation to 0.37, which is on the low side of the average as determined from well P18-04A2, and increasing the porosity to 0.13, which is on the high side of the average as determined from the wells, increases the static GIIP from 2.58 BCM to 2.78 BCM, which still leaves a gap of 0.5 BCM. However, when taking into account the structural uncertainty, this 0.5 BCM can be accounted for, as is shown in Figure 16. Spatial resolution in the reservoir model is 50m, i.e., a single grid cell has sides of 50 m. In the example of Figure 16, the left edge of the reservoir interval, which is formed by a fault (not explicitly shown), falls 50m (one cell) short of the actual position of the fault as identified from seismic. In fact, the position of the fault that bounds the reservoir interval in the model is slightly different from the actual position as identified on seismic. Consequently, a potential GIIP of 0.5 BCM is lost easily in the entire P18-04 block, calculated roughly by multiplying the difference of 50m by the length (3km) and thickness (150m) of the reservoir.

For block P18-06, structural uncertainty adds only 0.07 BCM to the static GIIP due to the low porosity. However, here the water saturation in the reservoir model far exceeds the values as determined from well P18-06A7ST1 (Table 3 & Table 4). Lowering the water saturation from 0.84 (average in the reservoir model) to values in the range of 0.6-0.7 is enough to match the static GIIP with the dynamic GIIP for this block. Furthermore it can be said that te p/Z curve as displayed in Figure 4.5 also suggest a low permeability around the producer and a higher permeability elsewhere. This was not reflected in the original geological model as supplied by TAQA.

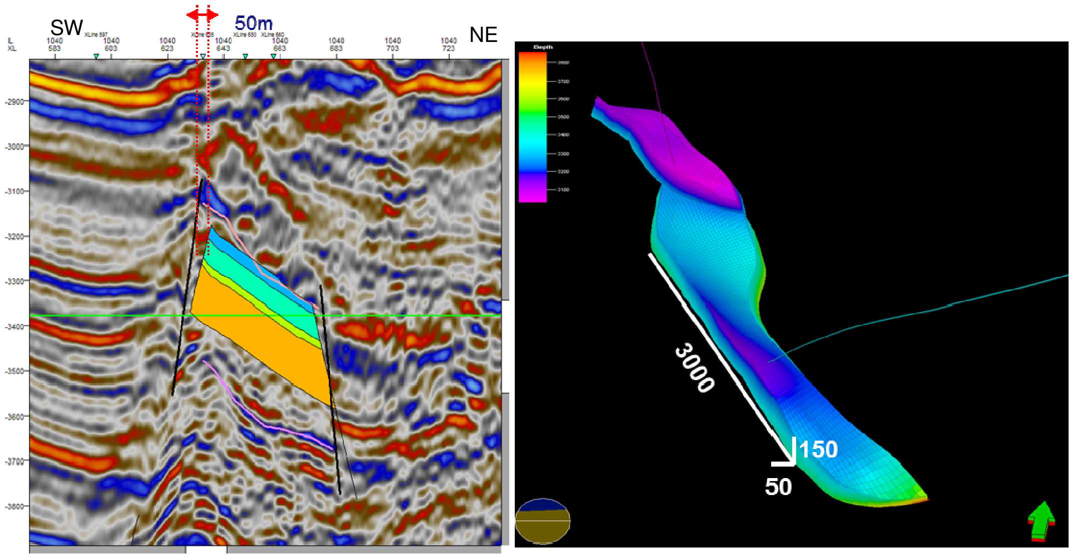

Figure 3.16: Example of structural uncertainty in the reservoir model. Left figure displays a seismic cross-section through block P18-04 (position indicated by red line in right figure), with the modelled reservoir interval in block P18-04 (coloured layering), which does not fully reach up to the faults (solid black lines) as interpreted from the seismic (mismatch approx. 50m). Green line indicates the GWC in this block. Left figure displays a 3D view of the reservoir interval of block P18-04.

3.8. Conclusions and recommendations

3.8.1. Conclusions

- A new static geological model was built in Petrel to overcome problems with the original model as built by TAQA in RMS. A comparison between the two models (depth and continuity of marker horizons, lateral position and dip of faults, statistics and spatial distribution of petrophysical properties) showed that the differences are negligible, i.e. the new model closely resembles the original model. Findings in this report are based on this new model.
- A velocity model supplied by TAQA proved to be unusable for the purpose of time-depth conversion of the seismic cube supplied by TAQA in two-way-travel time, which was needed to quality control the geological model. Therefore, a new velocity model was built, based on regional-scale velocity modelling work performed in-house at TNO, newly interpreted seismic, and well tops in combination with additional velocity log data from wells.
- Quality control of the new static geological model was achieved by comparing the lateral position and dip of faults and depth and continuity of marker horizons in the model to the depth-converted 3D seismic data. It was concluded that there are small differences, mainly in lateral position and dip of faults, which are not negligible. Differences in fault dip can be attributed to differences in time-depth conversion due to the use of different velocity models. However, differences in the lateral position of faults in the order of 50-100m (1-2 voxels in the reservoir-scale model) can only be traced back to the original seismic interpretation. This has implications for GIIP estimates (see below)

- The structures that contain the P18 reservoirs are bound by a system of NW-SE oriented faults in a so-called “horst and graben” configuration. They subdivide the P18 field into three blocks. Block P18-02 has three compartments, and blocks P18-04 and P18-06 each have one. The top of the compartments lies at depths between 3175 m and 3455 m below sea level. Blocks are bound by normal faults that are sealing because of juxtaposition of permeable reservoir intervals with impermeable intervals above the reservoir. At compartment level, production data suggests that faults are sealing, except for fault F14 between compartments P18-02I and P18-02II, which is not sealing in the current situation.
- The reservoir rocks in the P18 field belong to the Triassic-aged Main Buntsandstein Subgroup, a cyclic alternation of (sub-) arkosic sandstones and clayey siltstones of mixed fluvial/Aeolian origin. Four zones are distinguished in the reservoir; they correspond to the subdivision of the Main Buntsandstein Subgroup into the Volpriehausen Formation, the Upper and Lower Detfurth Formation and the Hardegsen Formation. Gross reservoir thickness in the production wells ranges between 200m and 214m. Average NTG of the individual zones ranges between 0.62 and 0.96, and increases from base to top over the reservoir interval.
- Average porosity in the Hardegsen Formation ranges between around 7-13% and in the Detfurth Formation slightly lower around 5-9%. Maximum porosities encountered in the clean sandy parts of both formations are around 21 %. Permeabilities are highest in the Hardegsen Formation, with a range between 2 and 207 mD. In the Detfurth Formation they range between 0.8 and 0.1 mD roughly. The combined thickness of both formations is approx. 100 m. The Volpriehausen Formation has a much lower porosity that ranges between 3 and 5%. Permeabilities are also low, and range between 0.01-0.05mD. The thickness of the Volpriehausen Formation is also approx. 100 m. Permeabilities were calculated by TAQA using a porosity-permeability relation, the origin of which could not be traced. Average water saturations range between 0.24 and 0.47 in the Hardegsen Formation, between 0.43 and 0.57 in the Upper Detfurth Sandstone Member, between 0.32 and 0.42 in the Lower Detfurth Sandstone Member, and between 0.78 and 0.92 in the Volpriehausen Formation.
- An important step in the quality control of the reservoir model is to verify that the property model honours the original data on the petrophysical properties from the wells. The average thicknesses of the reservoir intervals in the property model agree well with those in the wells, but the property model somewhat underestimates the porosities. Far more important however, especially for GIIP estimates, is that the model substantially overestimates the water saturation by values ranging between 0.07 and 0.34. Also, it is not clear how the original property model was populated by TAQA, which severely limits our abilities to reproduce and adapt the property model to improve the match with the well data and the production figures.
- The primary seal to the P18 reservoirs is formed by siltstones, claystones, evaporites and dolostones of the Solling Claystone Member, the Röt formation the Muschelkalk formation, and the Keuper formation that discomformably overlie the reservoir. Total thickness of this primary seal is approx. 150m.
- Faults are present in this primary seal. However, these faults appear to be sealing. Reservoir closure is obtained through impermeable zones above and below the reservoir interval, in combination with juxtaposition of permeable reservoir facies against impermeable non-reservoir facies of the Altena Group (secondary seal). Although most of the reservoir-bounding faults do not continue further upward into the overburden than the shales of the Altena Group, some reverse faults that where formed during the inversion phase appear to originate around the fault tips of the older reservoir-bounding faults. However, inversion in the area of the P18 field was relatively weak. Therefore, it is

unlikely that these inversion faults are reactivation faults that originate from movement along the older basin-bounding faults. Although impossible to rule out completely, it is not likely that the sealing properties of the basin-bounding faults have been compromised.
- Dynamic GIIP of the P18 field, estimated based on production data, i.e., plots of pressure/depth (P/z) vs. cumulative production, is 17.22BCM. GIIP estimates obtained from the static model of the reservoir are substantially lower, 15.39BCM. For block P18-02, the discrepancy between static and dynamic GIIP is only about 7%, which can easily be attributed to differences in porosity and average water saturation between the wells and the property model. For block P18-04 and P18-06, the discrepancy is likely attributed to a combination of under- and overestimated property values (porosity, water saturation) and structural uncertainty, i.e., reservoir-bounding faults that are slightly off in lateral position and dip compared to the 3D seismic.

3.8.2. Recommendations

- GIIP estimates as obtained from the static model suffer from structural uncertainty, i.e., reservoir-bounding faults that are slightly off in lateral position and dip compared to the 3D seismic. A reinterpretation of the faults in the reservoir model directly from the 3D seismic data will improve the quality of the reservoir model, and the GIIP estimates.
- GIIP estimates suffer from discrepancies in petrophysical properties such as e.g. porosity and water saturation between the reservoir model and the values from the production wells. An effort can be made to improve the match between the property model and the wells, especially for block P18-06 that is planned to be filled with CO_2 first, where the mismatch in GIIP is 40%.
- Facies-based property modelling will improve the quality of the model by adding heterogeneity to the reservoir based on geological concepts. Such heterogeneity, which is inevitably present in any reservoir, may have large effect on the injection in and subsequent migration of CO_2 through the reservoir.

3.9. Acknowledgements

This research has been carried out in the context of the CATO-2-programme. CATO-2 is the Dutch national research program on CO_2 Capture and Storage technology (CCS). The programme is financially supported by the Dutch government (Ministry of Economic Affairs) and its consortium partners. TU Delft acknowledges Schlumberger for the use of Petrel™, Schlumberger's reservoir modelling suite. We thank Andrew van de Weerd en Arie Speksnijder of PanTerra Geoconsultants for valuable comments that improved this report.

3.10. References

Ames, R., and Farfan, P.F., 1996. "The environment of deposition of the Triassic Main Buntsandstein Formation in the P and Q quadrants, offshore the Netherlands", in: Rondeel, H.E., Batjes, D.A.J. and Nieuwenhuijs,W.H. (eds): "Geology of Gas and Oil under the Netherlands", Kluwer Academic Publishers (Dordrecht), p. 167–178.

Beutler, G., 1995. "Stratigraphie des Keupers", Bundesanstalt fuїr Geowissenschaften und Rohstoffe (Hannover), Archive number 113087 (unpublished report): 147 pp.

De Jager, J.J., 2007. "Geological Development", in: Wong et al. (eds): "Geology of the Netherlands", Royal Netherlands Academy of Arts and Sciences (Amsterdam), p. 5-26

De Jager, J., Doyle, M.A., Grantham, P.J. and Mabillard, J.E., 1996. "Hydrocarbon habitat of the West Netherlands Basin", in: Rondeel, H.E., Batjes, D.A.J. and Nieuwenhuijs, W.H. (eds): "Geology of gas and oil under the Netherlands", Royal Geological and Mining Society of the Netherlands (KNGMG), Kluwer Academic

Publishers (Dordrecht), p. 191-209.

Dronkers, A.J. and Mrozek, F.J., 1991. "Inverted basins of the Netherlands", First Break 9, p. 409-425

Dusar, M., Bless, M.J.M., Burger, K., Demaret, M., Hardy, M., Langenaeker, V., Lie Sun Fan, Paproth, E., Piérart, E., Somers, Y., Streel, M. & Wouters, L., 1998. "De steenkool verkenningsboring Hechtel-Hoef", Geological Survey Belgium Professional Paper 286: 129 pp.

Geluk, M.C., 2007. "Triassic", in: Wong et al. (eds): "Geology of the Netherlands", Royal Netherlands Academy of Arts and Sciences (Amsterdam), p. 85-106

Geluk, M.C., 2005. "Stratigraphy and tectonics of Permo-Triassic basins in the Netherlands and surrounding areas", Ph.D. thesis, Utrecht Univerity, 171pp.

Geluk, M.C., 1999. "Palaeogeographic and structural development of the Triassic in the Netherlands – new insights". In: Bachmann, G.H. & I. Lerche (eds): The Epicontinental Triassic 1. Zentralblatt für Geologie und Paläontologie.

Geluk, M.C. and Röhling, H.-G., 1999. "High-resolution sequence stratigraphy of the Lower Triassic Buntsandstein: a new tool for basin analysis", in: Bachmann, G.H. and Lerche, I. (eds): "The Epicontinental Triassic 1". Zentralblatt für Geologie und Paläontologie 7-8: p. 545–570.

Geluk, M.C. and Röhling H.-G., 1997. "High-resolution sequence stratigraphy of the Lower Triassic 'Buntsandstein' in the Netherlands and northwestern Germany", Geologie en Mijnbouw 76, p. 227–246.

Geluk, M.C., Plomp, A., and van Doorn, Th.H.M., 1996. "Development of the Permo-Triassic succession in the basin fringe area, southern Netherlands", in: Rondeel, H.E., Batjes, D.A.J. & Nieuwenhuijs,W.H. (eds.): "Geology of gas and oil under the Netherlands", Royal Geological and Mining Society of the Netherlands (KNGMG) / Kluwer Academic Publishers (Dordrecht), p. 57-78.

Gerling, P., Geluk, M.C., Kockel, F., Lokhorst, A., Lott, H.K. and Nicholson, R.A., 1999. "NW European gas atlas – new implications for the Carboniferous gas plays in the western part of the Southern Permian Basin", in: Fleet, A.J. and Boldy, S.A.R. (eds.): "Petroleum geology of Northwest Europe – Proceedings of the Fifth Conference", Geological Society (London): 799-808.

Gianolla, P., and Jacquin, Th., 1998. "Triassic sequence stratigraphic framework of Western European Basins", Mesozoic and Cenozoic Sequence Stratigraphy of European Basins. SEPM Special Publication 60, p. 643–650.

Johnson, H., Warrington, G. and Stoker, S.J., 1994. "6. Permian and Triassic of the Southern North Sea", in: Knox, R.W.O'B., and Cordey, W.G. (eds): "Lithostratigraphic nomenclature of the UK North Sea", British Geological Survey (Nottingham).

Kozur, H., 1999. "The correlation of the Germanic Buntsandstein and Muschelkalk with the Tethyan scale", In: Bachmann, G.H., and Lerche, I. (eds): "The Epicontinental Triassic", Zentralblatt für Geologie und Paläontologie 7–8, p. 701–725.

Lee, M., Aranson, J.L. and Savin, S.M., 1985. "K/Ar dating of time of gas emplacement in Rotliegendes sandstone, Netherlands". American Association of Petroleum Geologists Bulletin 69: p. 1381-1385.

Racero-Baena, A., and Drake, S.J., 1996. "Structural style and reservoir development in the West Netherlands oil province". in: Rondeel, H.E., Batjes, D.A.J. & Nieuwenhuijs,W.H. (eds.): "Geology of gas and oil under the Netherlands", Royal Geological and Mining Society of the Netherlands (KNGMG), Kluwer Academic Publishers (Dordrecht), p. 211-227.

TAQA Energy B.V., 2008. "CO_2 offshore Storage Deep Under the Dutch North Sea", promotional material

Van Adrichem Boogaert, H.A., and Kouwe, W.F.P., 1994. "Stratigraphic nomenclature of the Netherlands; revision and update by RGD and NOGEPA, Section E Triassic", Mededelingen Rijks Geologische Dienst 50.

Van Balen, R.T., Van Bergen, F., De Leeuw, C., Pagnier, H., Simmelink, H., Van Wees, J.D. & Verweij, J.M., 2000. "Modelling of the hydrocarbon generation and migration in the West Netherlands Basin, the Netherlands", Netherlands Journal of Geosciences 79, p. 29–44.

Van Bergen, F., 1998. "Basin modelling and hydrocarbon generation in the WNB-an organic petrological and organic geochemical approach", Internal report Netherlands Institute of Applied Geoscience TNO – National Geological Survey (Utrecht) 98-148B: 120 pp.

Van Wijhe, D.H., 1987. “Structural evolution of inverted basins in the Dutch offshore”, Tectonophysics 137, p. 171-219.

Wolburg, J., 1967. “Zum Wesen der Altkimmerischen Hebung, mit einem Überblick über die Muschelkalk- und Keuper-Entwicklung in Nordwest-Deutschland”, Zeitschrift der deutschen Geologischen Gesellschaft 119, p 516–523.

Yealding, G., 2002. “Hydrocarbon Seal Quantification”, in: Koestler, A.G., and Hunsdale, R. (eds.): “NPF Special Publication 11”, Norwegian Petroleum Society (NPF), published by Elsevier Science B.V. (Amsterdam), p. 1-15.

Ziegler, P.A., 1990. “Geological atlas of western and central Europe, part 2”, Geological Society Publishing House (Bath), 239 pp.

4. Reservoir study

4.1. Introduction

In this chapter, reservoir engineering aspects of CO_2 storage in the P18-2, P18-4 and P18-6 reservoirs are discussed. This includes an initial assessment of the storage capacity and maximum injection rates. The dynamic reservoir study comprised both an analytical reservoir study and a reservoir simulation study.

4.2. Analytical reservoir study

4.2.1. Introduction

In order to get a basic understanding of the behaviour of the P18 field during CO_2 injection an analytical model is used. The most important aspects of this model are:

- The reservoir is modeled as a single tank that is gradually filled with CO_2.
- The geometry of the reservoir and the location of the wells are modeled implicitly using an average shape factor and drainage area for the wells.
- The analytical model uses the volume/material balance to calculate the average reservoir pressure given Gas Initially In Place (GIIP), initial reservoir pressure, reservoir pressure at end of production period ("abandonment pressure"), and cumulative CO_2 injected. Well inflow performance (injectivity) is based on the single phase semi steady state inflow model, using pseudo pressure. Given the average pressure from the aforementioned calculation and either BHP or required injection rate, the injection rate or BHP is calculated, respectively. CO_2 injected, average reservoir pressure, and well injectivity are calculated with a time step size of one year.

The model requires a number of basic input parameters with respect to the reservoir. This data includes reservoir depth, size, average thickness, temperature, initial and abandonment pressure, average permeability and required injection rate.
The injection scenario used in this analytical study is 1.1 Mton/year which equals 1.52 MNm^3/day[1].
Additionally a maximum FBHP constraint is applied, which is case specific and must be determined by the geomechanical engineer.
The most important output of the model will be the cumulative CO_2 injected and the injectivity each year. In section 4.2.2 these resulting injection capacity and rates are presented and discussed for the three compartments of P18.

The next step to improve the accuracy and resolution of the results a reservoir simulator should be used. This will be the subject of section 4.8.

4.2.2. P18 analytical study results

The input as used for the analytical study of P18 is presented Table 6. A summary of the model results is shown in Table 7. In P18-2 and P18-4 the target rate of 1.1 Mt/y is realised and the total injection period needed to fill up the reservoir to the initial pressure is 28 years and 7 years

[1] The density of CO_2 at normal conditions (temperature is 0℃ and pressure is 1 atmosphere) are used in this study, which equals to 1.9768 kg/m^3.

respectively. In contrast the target rate cannot be realised in P18-6. The low permeability gives rise to a high FBHP in order to realise the target rate, exceeding the maximum allowed FBHP.

Table 6: Input parameters for P18

Parameter	Units	P18-2	P18-4	P18-6
Number of wells for injection		1	1	1
First year of injection	Year	2015	2015	2015
Gas initially in place (GIIP)	GNm3	13.35	3.2	0.6
Average depth of reservoir	Meter	3500	3220	3561
Reservoir temperature	°C	126	117	117
Initial pressure	Bar	375	340	377
Abandonment pressure	Bar	20	20	45
Average thickness	Meter	220 m	94.0	70
Average permeability	mDarcy	64	103	0.9
Well Dietz shape factor		0.232	0.232	0.232
Reservoir drainage area	m^2	2371791	1456000	366600

Table 7: Result analytical study P18

	Units	P18-2	P18-4	P18-6
Cumulative CO_2 injection	Mton	31.83	8.78	1.48
Injection period	Year	2015-2043	2015-2022	2015-2021
Target rate realised?		Yes	Yes	No

4.3. Dynamic reservoir study

4.3.1. Overview of P18 field

The P18 field can be divided in 3 independent reservoir compartments, respectively P18-2, P18-4 and P18-6. Static properties of the P18 field as described in Petrel were used as input for the compositional flow simulation in MoReS. The results of these dynamic simulations in MoReS will be discussed in this section. The initial geological model (Roxar) received from TAQA Energy B.V. was converted into a petrel model, the number of gridblocks of which was reduced in order to make it feasible for a reservoir simulation. The actual reservoir appears to have no active aquifer, as the p/Z curve is a straight line. In addition the permeability below the gas-water contact (GWC) is small compared to above the GWC.

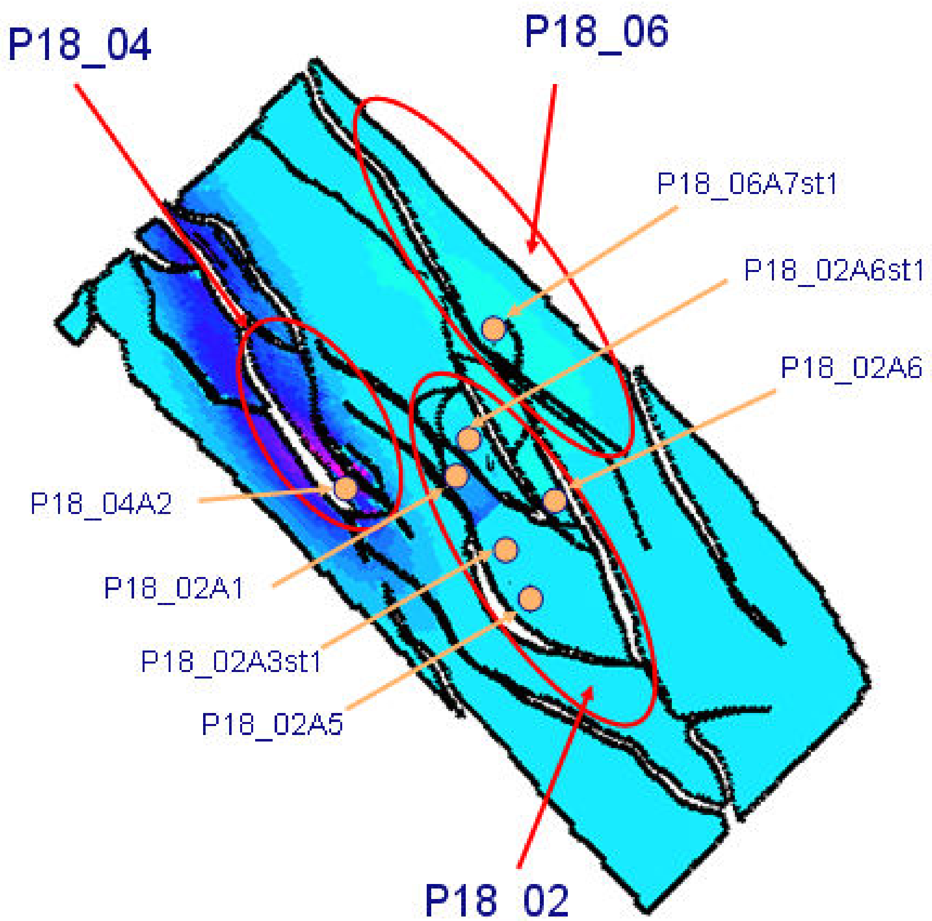

Figure 4.1: Overview of P18 field

Table 8: below gives a summary of the properties of the P18 field found after the history match.

	Units	P18	P18_2	P18_4	P18_6
Average gridblock dimensions	Meter	i-direction=65 , j-direction=100, k-direction=30			
Simulator grid dimensions		i-direction=77 , j-direction=175, k-direction=4			
Initial fraction of components		C1(0.94), C3p(0.07),C2(0.024),CO_2(0.013), N_2 (0.015),			
Average permeability	mDarcy	94	64	499	30
Average (volume weighted) porosity		0.068	0.06	0.11	0.08
GWC (gas water contact)	Meter	Depends on compartment	-3680	-3377	-3680
GIIP (gas initially in place)	GNm3	18.7	14.4	3.19	1.1GNm3
Initial pressure	bar	Depends on compartment	375 bar	340 bar	377 bar
Production start datum		1st January 1994	1st January 1994	6th March 1997	15th July 2003

4.3.2. Production data

The gas rates provided by TAQA Energy B.V. were daily rates for each well. These rates were averaged to monthly rates to reduce the simulation time. The gas rates for well P18_02A6 and P18_2A6ST1 are uncertain, because it was unclear how much gas was produced for each individual well, as only the total combined gas rates of both wells was measured. In the simulations performed the gas rates were divided over the two wells by the ratio of the well KH. For the wells P18_2A1 and P18_2A3ST2 the production data before 1997 was considered unreliable. However, the cumulative gas production until this time was known, therefore a constant gas rate between 1994 and 1997 is used during the history match of P18-2.
The shut-in pressure measurements of well P18_6A7ST2 are subject to uncertainty; because the well is perforated in a low permeability environment reliable shut-in pressures need long-shut in periods. The shut-in periods vary from 4 to 51 days. Furthermore the initial pressure is not measured directly but derived from the P18-2 field.

4.3.3. Simulation constraints

The MoReS (version 2010.1) reservoir simulator is used to history match the P18 model. The history match simulations were constrained by monthly production data of each individual well and a minimum BHP of 1 bar. It is important to note that non-darcy flow is not modelled in this study.

4.4. History match of P18-2

The process of history matching starts with an implementation of the gas production history of each well in the model (as provided by TAQA Energy B.V.).

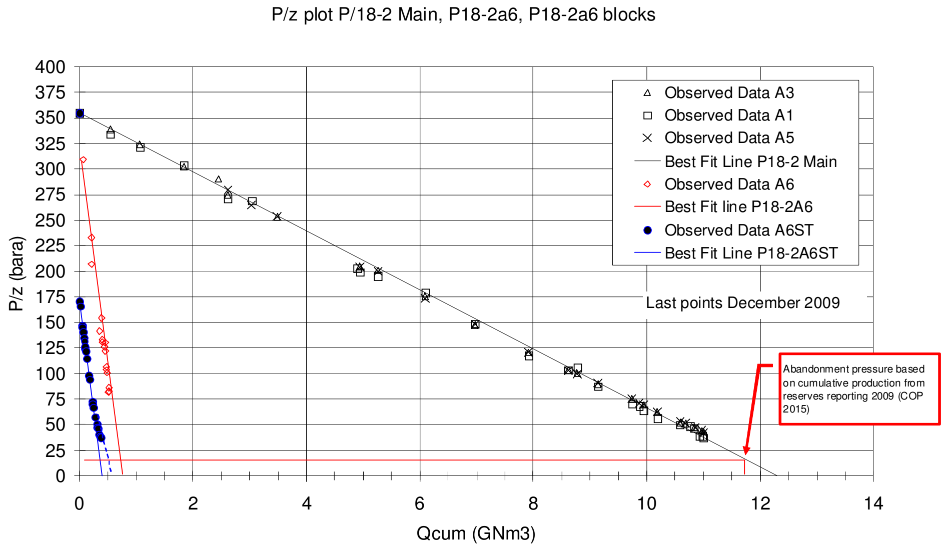

Figure 4.2: Production history for the wells A1, A3ST2, A5, A6 and A6ST1

The gas-initially-in-place and initial pressure are known from the p/Z plot derived from field measurements (Figure 4.2). From this linear p/Z curve it is assumed there is no active aquifer**.**

Once a material balance match is achieved, the subsequent step is to match the bottom hole pressures (BHP). Using the provided BHPs over the period of 1994-2010 a match could be achieved by making adjustments to fault transmissibility, well productivity indexes and absolute permeability.

P18-2 consists of three blocks, where block I and II are connected (Figure 4.3). This can be determined from the pressure data from the wells in each individual block. The data show no indication of a connection between block III and the other two blocks.

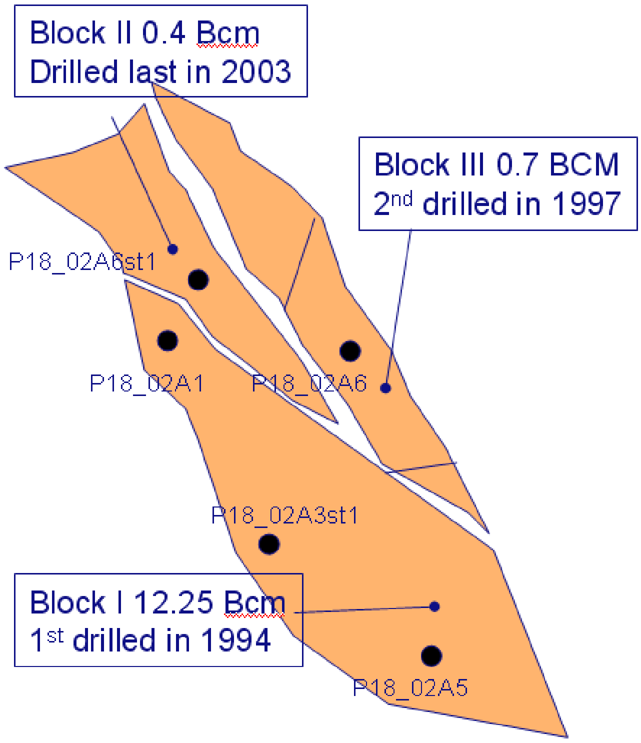

Figure 4.3: Overview block I, II and III in P18-2

In Table 9 an overview is given of the stock tank gas volumes (in GNm3) determined by the p/Z curves and determined by the dynamic model. The sensitivity with respect to the gas water contact (GWC) and porosity are shown as well. In order to get the correct mass balance a porosity multiplier very close to one should be applied.

Table 9: Volumes of block I, II and III of P18-2 in GNm^3

	Volume in Block I and II	Volume Block III	Total Volume Block I, II and III	GWC (m)	porosity multiplier
p/Z	12.65	0.7	13.35		
base case	13.6	0.81	14.4	3680	1
Case 1	13.4	0.78	14.2	3660	1
Case 2	12.9	0.70	13.6	3620	1
Case 3	11.4	0.67	12.0	3680	0.9
Case 4	12.4	0.73	13.1	3680	0.95

In this study the base case is used for further simulation. After the first simulations it became clear additional changes to the permeability and well KH are needed to reproduce the measured shut-in pressures of the wells. In order to get a reasonable history match the fault transmissibility was changed between block I and block II (equal to 0.2). In 2003 the well P18_02A6ST1 in block II came on stream and the reservoir pressure in this well was equal to 158 bar, which is significant lower than the initial reservoir pressure measured (375 bar) in block I. This observation indicates a connection between both block I and II.

The permeability around well P18_02A1 was lower in the original geological model than the average permeability of block I. To increase the flow performance around this well the low permeability region is multiplied by a factor of 5. For the other wells (P18_02A3ST1 and P18_02A5) in block I another permeability multiplier was needed to get a reasonable history match, the whole block I was multiplied by a factor of 2. The pressure behaviour of the model corresponds with the measured shut in pressures of the wells in block I (see figure).

In Block II the geological model was not able to produce the measured gas rates, a permeability multiplier of 10 and a well KH multiplier of 5 were applied. Although, the model and measurements are not in perfect agreement; the characteristic behaviour is captured with this model. This block is significantly higher (less deep) then block I and III, it is possible that the absolute permeability is estimated very conservatively, as a result of diagenesis.

In block III no additional changes to the flow performance of the original geological model were made. The measured pressure behaviour is captured well by the dynamic model. The average permeability and porosity of each block of the static model and the history matched model of compartment P18-2 are given in

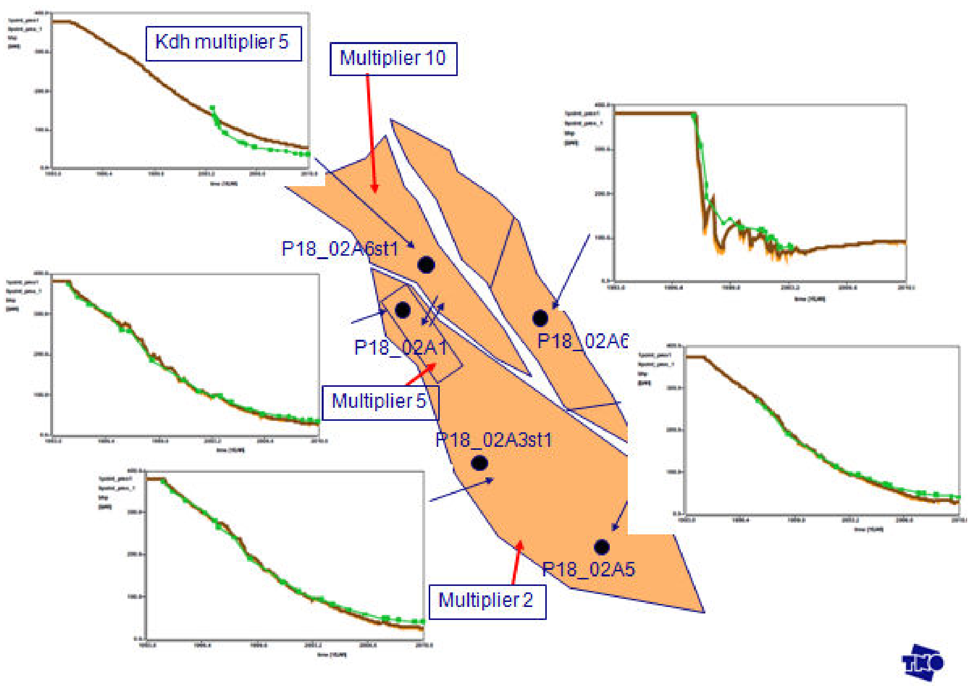

Figure 4.4: Overview P18_2 of the pressure behaviour of each individual well after applying permeability and well KH multipliers. The green line with markers represents the measured shut-in pressure, the dark lines are the simulated nine-point reservoir pressures.

Table 10: Properties of P18-2 of static model and History Matched (HM) model.

	Initial average porosity	averaged porosity in HM model	Initial average permeability (mDarcy)	Average permeability in HM model (mDarcy)
P18_02 block I	0.065	0.065	17.0	43.5
P18_02 block II	0.061	0.061	11.7	117
P18_02 block III	0.057	0.057	7.0	7.0

4.5. History match of P18-4

The P18-4 compartment is a reservoir, which consists of one block and is bounded by faults (Figure 4.1). Well P18-04A2 is drilled in the southern part of this compartment.
The first step is to get a material balance match; from the p/Z curve the GIIPP was estimated to be 3.2 GNm3 (Figure 4.5). However the dynamic model had only 2.0 GNm3 initial in place. This discrepancy can be explained by the interpretation of the fault along the long side of P18-4 compartment. Shifting the south-eastern boundary by the order of 50 meters will give us exact the volume needed to match the material balance. Instead of remodelling the structure of the geological model a porosity multiplier of 1.3 was used to get the correct volume in the dynamic model.

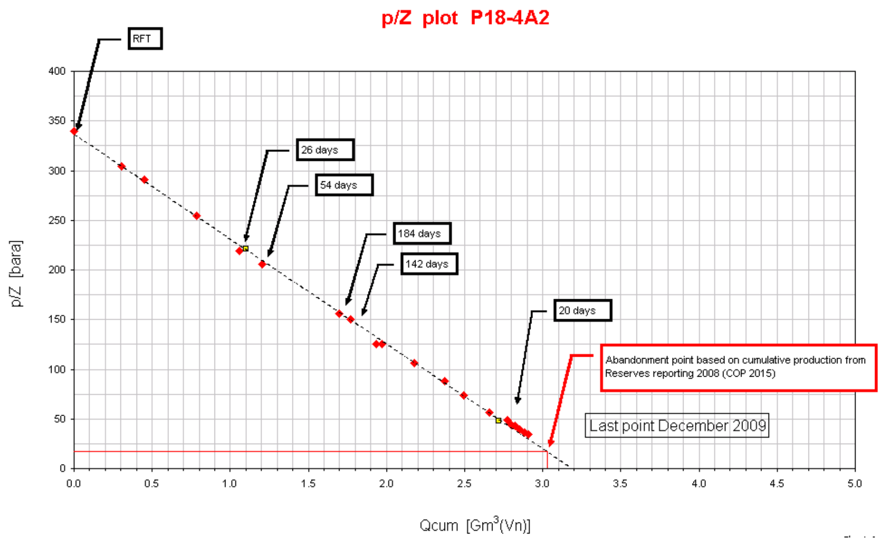

Figure 4.5: p/Z curve of P18-4, the number of days in the black boxes are the shut-in periods

Table 11: Volumes of compartment P18-4 in GNm^3

	Volume P18_4	GWC (m)	porosity multiplier
p/Z	3.2		
base case	2.0	3377	1
Case 1	3.2	3377	1.3
Case 2	2.3	3400	1
Case 3	2.7	3450	1

After simulating Case 1, the reservoir pressure behaviour of P18_4 corresponds very well with the measured shut in pressures of well P18_4A2 as can be seen in Figure 4.6. Additional changes to flow parameters (e.g. permeability) are not needed to model the characteristics of the P18-4 field. The average permeability and porosity of the static and history matched model of compartment P18-4 are given in Table 12.

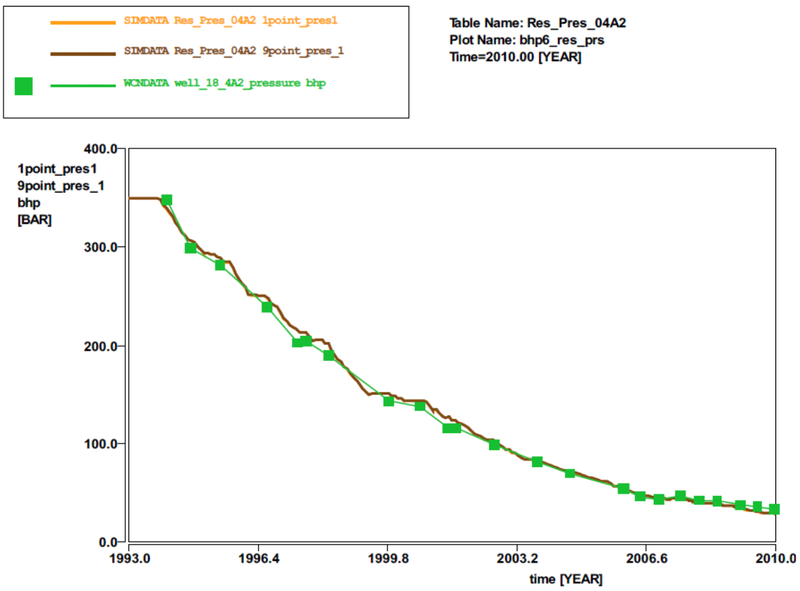

Figure 4.6: Reservoir pressure of the dynamic P18 model (brown line), measured shut in pressures (green markers) of well P18_4A2.

Table 12: Properties of P18-4 of static model and History Matched (HM) model

	Initial average porosity	averaged porosity in HM model	Initial average permeability (mDarcy)	Average permeability in HM model (mDarcy)
P18_04	0.086	0.111	499.	499

4.6. History match of P18-6

P18-6 is a significant lower permeable compartment (Table 8). Well P18_06A7ST1 is the only well in this compartment and located near the southern boundary, surrounded by faults on the east and southern side. The volumes according to the p/Z curve and the dynamic model are not corresponding with each other. In order to get correct volumes in the dynamic model the GWC or the water saturation (S_w) or the porosity or a combination of these could be changed. The GWC is initially at 3680m, however the volumes are not sensitive to the GWC, because the porosity is very low in these lower layers By changing the porosity with a multiplier 1.4 the volume in the dynamic model corresponds with the volumes from p/Z analysis. However as mentioned before, the p/Z curve is subject of uncertainty because of short shut-in periods (Figure 4.7). An underestimation of the initial volume in place is therefore plausible. In our simulation a porosity multiplier of 1.6 is used, because with smaller volumes an early water breakthrough is observed in the simulations. The absolute permeability was multiplied by 9 and a well KH multiplier of 60 was used to simulate the measured production rates. The physical reason behind the multipliers as described above are discussed in Section 3.7.

In Figure 4.8 the measured and simulated pressures are compared and a reasonable history match is found here. The average permeability and porosity of the static model and the history matched model of compartment P18-6 are given in Table 14.

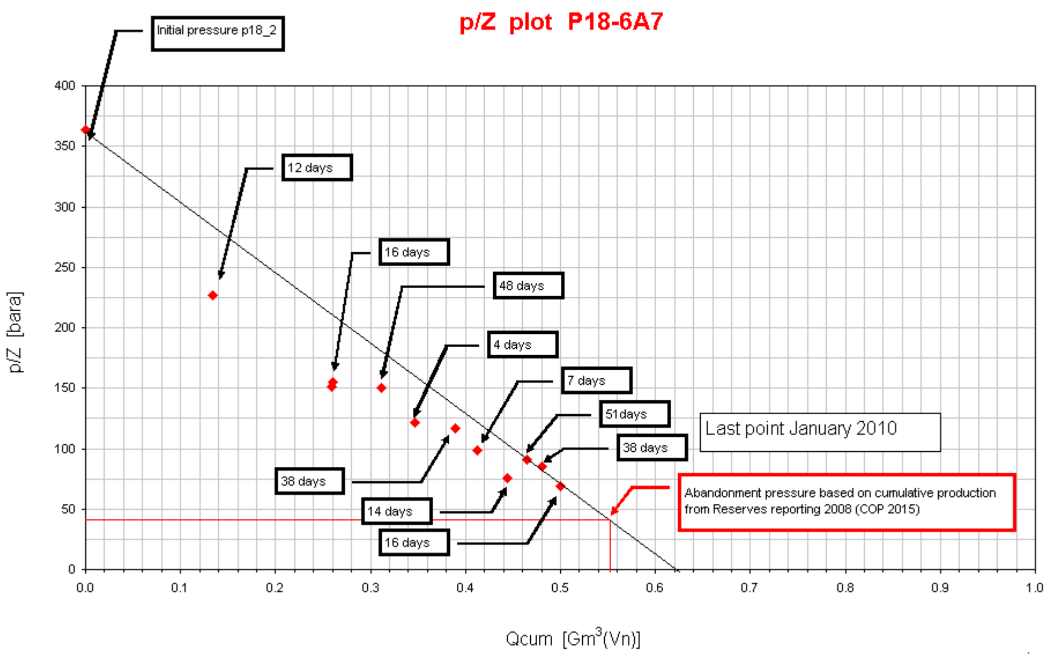

Figure 4.7: p/Z curve of P18-6, the number of days in the black boxes are the shut-in periods

Table 13: Volumes of compartment P18-6 in GNm^3

	Volume P18-6	GWC(m)	Porosity multiplier
p/Z	0.62		
base case	0.33	3680	1
Case 1	0.67	3680	1.4
Case 2	1.1	3680	1.6
Case 3	0.36	3700	1
Case 4	0.42	3750	1

Table 14: Properties of P18-4 of static model and History Matched (HM) model

	Initial average porosity	averaged porosity in HM model	Initial average permeability (mDarcy)	Average permeability in HM model (mDarcy)
P18_06	0.047	0.075	3.3646	29.67

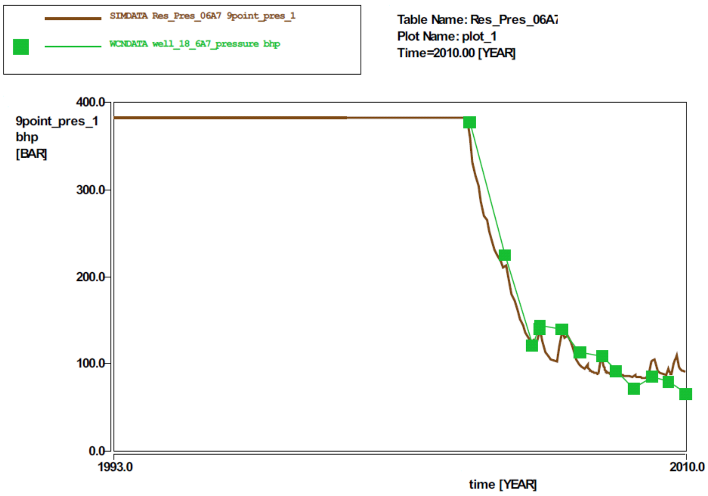

Figure 4.8: Reservoir pressure of the dynamic P18 model (brown line) , measured shut in pressures (green markers) of well P18_6A7ST1.

4.7. Discussion and conclusion of the history match

The static model of P18 from TAQA Energy B.V. has large uncertainties (as discussed in the geolocial study of P18). The volumes from the p/Z analysis do not correspond with the static model, especially for compartment P18-4 and P18-6. In compartment P18-2 it is not known from which block, which volume is produced, however these are relatively small volumes.

- In P18-2 is permeability the most adapted parameter, in block II a multiplier of 10 is used and a KH multiplier of 5 on the well itself, which means a multiplier on the flow performance of 50. This is an extreme value; therefore the predictive power of the model in this region has a high uncertainty.

- In P18-4 no adjustment has to be made to the flow performance, the volume balance is incorrect. TNO found an explanation of this mismatch. The structural re-interpretation of this compartment gives the correct volumes of this compartment
- In P18-6 porosity and permeability had to be adapted to get a reasonable history match. The p/Z curve is not a straight line and the initial pressure is not measured directly. Therefore the estimated GIPP are very uncertain. In the dynamic model a higher volume was needed to reproduce the measurements. Furthermore the permeability in the static field of this compartment was multiplied with a factor 9 and the well KH with factor 60. The flow performance of the well is increase by a very extreme factor (520). Using this gives us a reasonable history match, however the uncertainty of this compartment is very high and any prediction taken from this model should be interpreted with care.

4.8. Injection study of P18

4.8.1. Introduction

The injection study of P18 is performed with the adjustments mentioned earlier in the history matching part in this report (section 4.14, 4.15.and 4.16). The yearly average injection target rate is 34.93 kg/s (equals 1.1 Mton/year) for each individual well, with a maximum of 47 kg/s. The annual injection profile proposed by EON is shown in Figure 4.9. The results with this specific injection rate are similar to the results with a constant injection rate of 1.1Mton/year. In this section the results of a constant injection rate are presented.
In P18 four wells are assigned as injection well, P18_02A1, P18_02A6 (because block III is isolated from block I and II), P18_04A2 and P18_6A7ST1

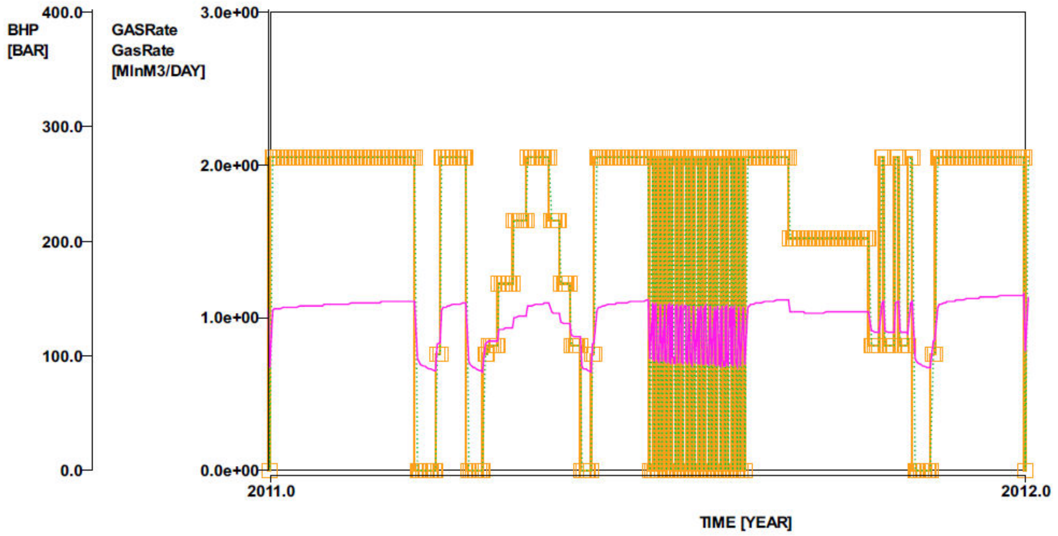

Figure 4.9: Annual injection CO_2 profile proposed by EON with average 1.1 Mton/year. Green dashed line is target rate, the orange line is the simulated injection rate. Pink line is the BHP of the well A1

4.8.2. Results and discussion

The forecast injection rate and pressure behaviour of compartment P18-2, P18-4 and P18-6 are shown in Figure 4.10, Figure 4.11 and Figure 4.12 respectively. The forecast shown here is performed with a slow start up phase until 2014 and after that a constant injection rate of 1.1

Mton/year. Furthermore the injection well is constrained by a maximum BHP pressure equal to the initial reservoir pressure of each particular compartment. The reason for this choice is to prevent the final reservoir pressure (after the CO_2 injection) to become higher than the initial reservoir pressure. If the final reservoir pressure is higher than the initial reservoir pressure this could cause fractures, which can possibly result to a leakage path.

A summary of the capacity of each compartment is given in Table 15: Results compositional reservoir simulation study

.

As shown earlier in the analytical study the target injection rate in P18_02A1 and P18_05A2 is realized and the cumulative CO_2 injection is comparable with previous results from the analytical study.
Well P18_02A6 in block III can inject the target rate only for a few months. The BHP needed for the target rate is constrained by the maximum allowed BHP (375 bar). It is important to realize that block III is still at a relative high reservoir pressure (90 bar), because it possible to inject more CO_2 in block III if the reservoir pressure is reduced to a lower abandonment pressure. The discrepancy between the analytical study and the simulation study on the cumulative injection can be the reason of this difference.
In P18-6 the low permeability in the area give rise to a low injection rate. In our simulations the injection rate is immediately constraint by the maximum flowing BHP.
The drawdowns (BHP – 9 point pressure) for each injection well are shown in Figure 4.13. For injector P18_02A6 has a maximum value of 330 bar. This low permeable block (7mDarcy) and a target rate of 47 kg/s give rise to this high drawdown. In contrast to P19_4A2 a high permeable (499mDarcy) the target rate can be reached by only a maximum drawdown of 5 bar. Furthermore as mentioned before the drawdown of P18_02A1 and P18A7ST1 is maximum of 50 bar and 8-bar, respectively.
Several processes may increase or decrease the injectivity of the CO_2 with respect to the current simulations. Salt precipitation may decrease, while fracturing may increase the predicted injectivity. Another aspect, which has shown up in field tests is that the change from production to an injection well leads an increased injection. This is possibly due to the small parts which are blown out of the near-well area.

Table 15: Results compositional reservoir simulation study

			P18-2			**P18-4**	**P18-6**
		Units	P18_02A1	P18_02A6	Total	P18_04A2	P18_6A7ST1
Cumulative CO_2 injection	Dynamic simulation study	GNm^3 Mton	14.7 29.1	0.7 1.3	15.4 30.4	4.1 8.1	0.3 0.6
	Analytical study	Mton	31.8			8.8	1.5
Target rate realized?			Yes	No		Yes	No

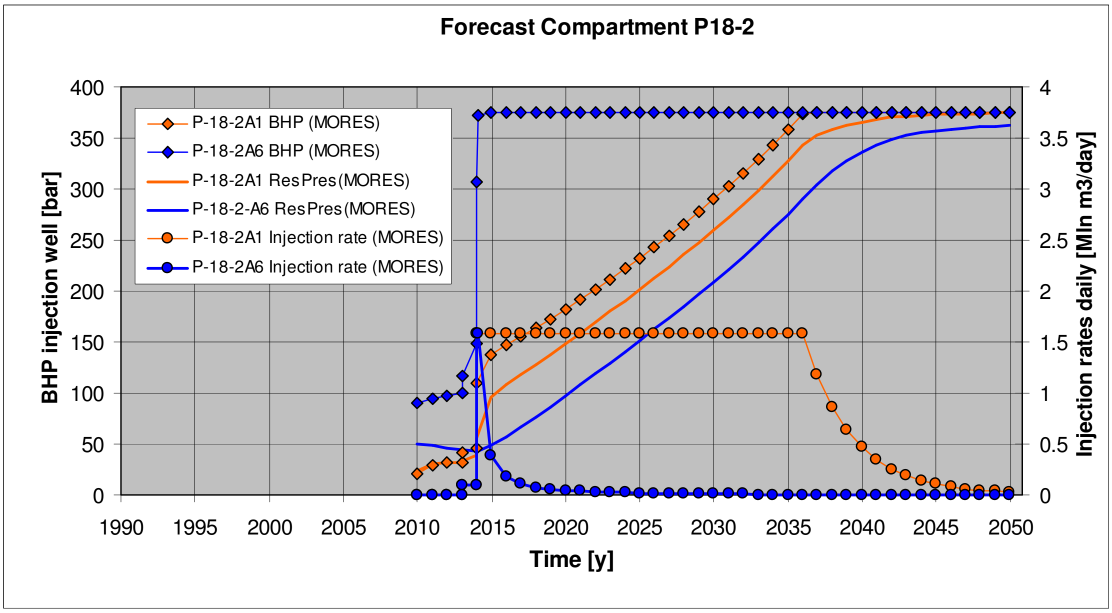

Figure 4.10: Injection behaviour of compartment P18-2, with average injection rate of 1.1 Mton/year

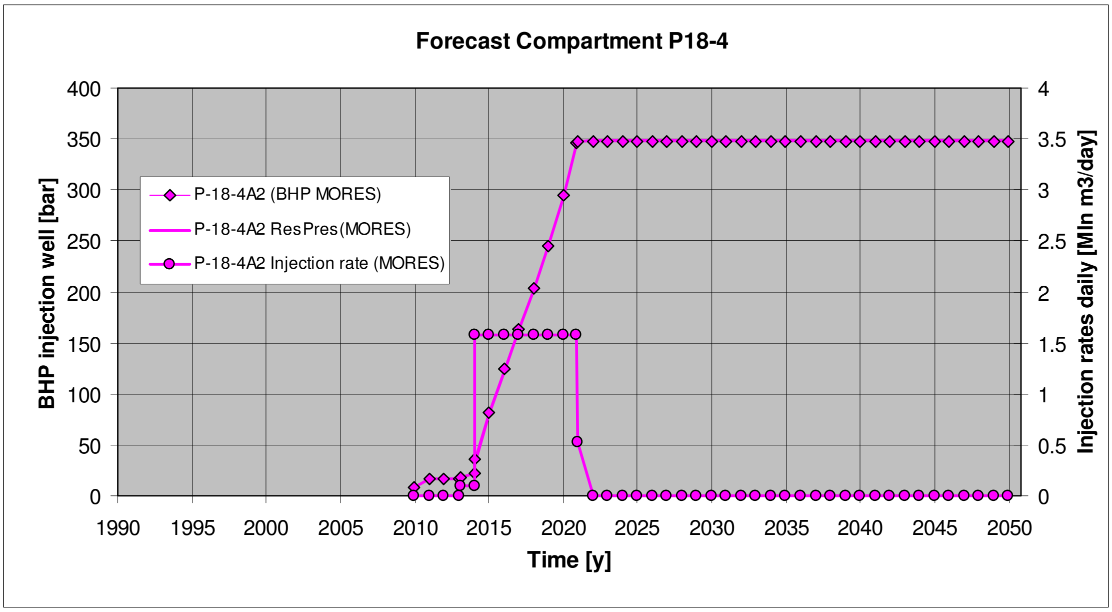

Figure 4.11: Injection behaviour of compartment P18-4, with average injection rate of 1.1 Mton/year

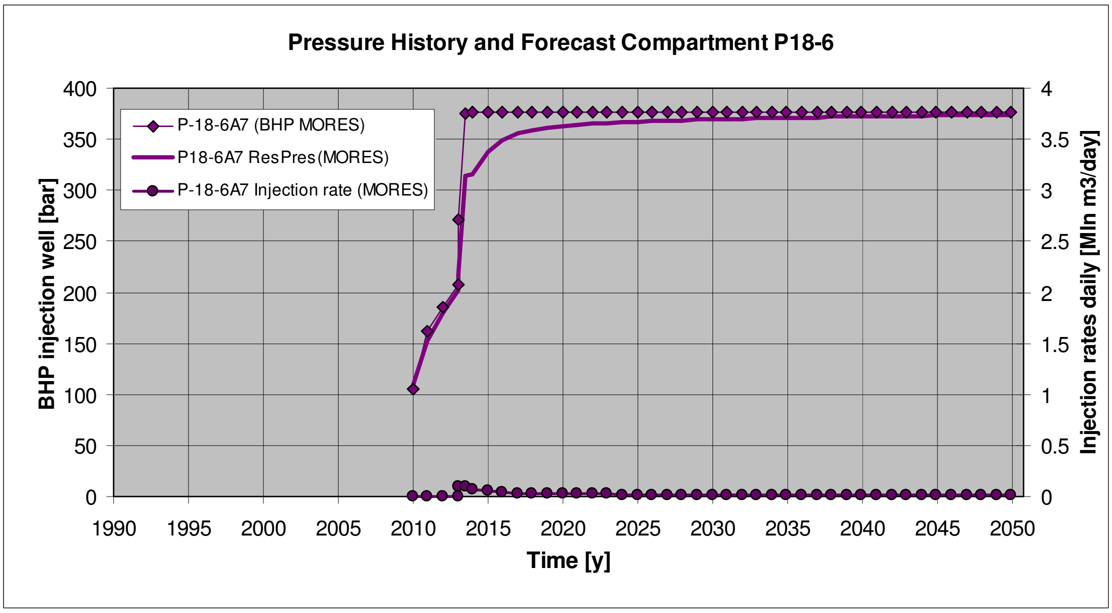

Figure 4.12: Injection behaviour of compartment P18-6, with average injection rate of 1.1 Mton/year

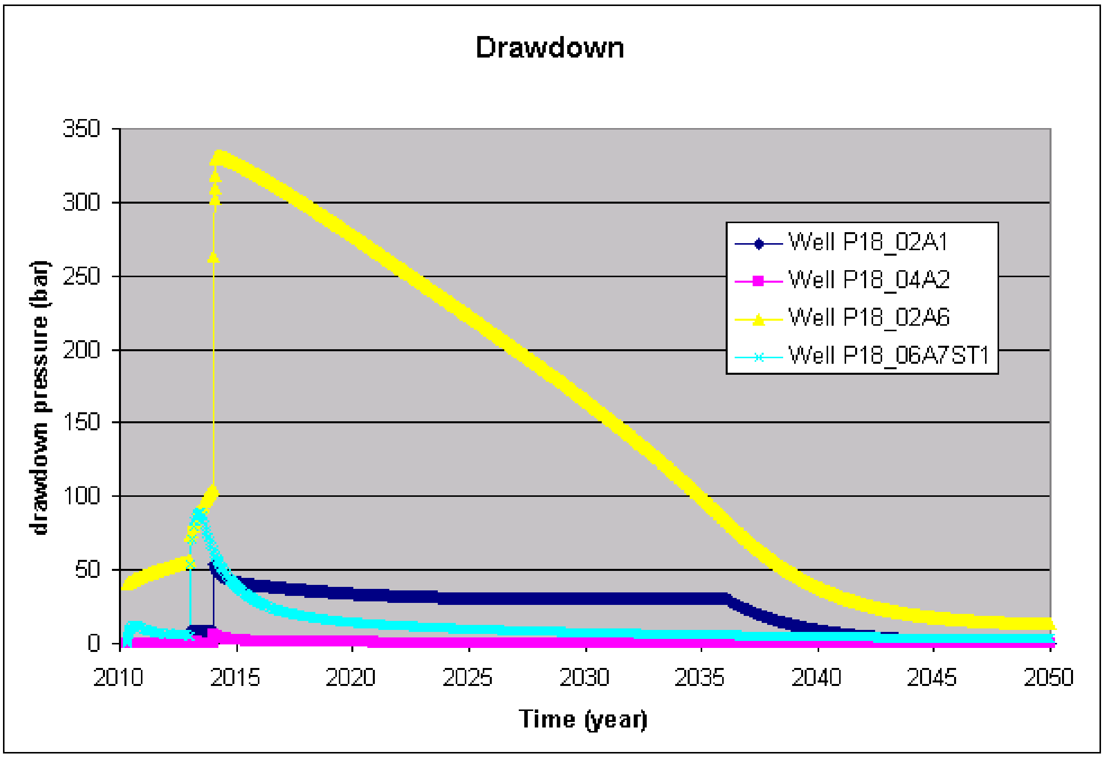

Figure 4.13: Drawdown of each individual well in P18

4.8.3. Conclusion

The conclusions of the injection study of P18 are:

- Simulations show that in P18-2 block I and II the target rate of 1.1 Mton/year is possible and a total of 30.4 Mton CO_2 can be injected.
- In well P18-2A1 the target is possible; however in P18_2A6 the target rate is not feasible.
- Simulations show that in P18-4 the target rate of 1.1 Mton/year is possible and a total of 8.1 Mton CO_2 can be injected.
- Simulations show P18-6 the target rate is not feasible and a range of 0.5 to 1.6 Mton can be injected in this compartment..

All these conclusions need to be interpreted very carefully, because of the uncertainties in the static and history matched model of P18 as discussed in section 4.17.

4.9. Thermal aspects of reservoir modelling of P18

4.9.1. Introduction

TAQA Energy B.V. plans to inject CO_2 into the various mature P18 compartments. These compartments are deep (over 3 km depth) and quite permeable. This in connection with the off-shore nature of the injected and the associated cooler temperatures of the injected CO_2 means that it is essential to include thermal aspect and processes, such as the Joule-Thompson cooling, impact on induced fracturing etc. in the feasibility study.

Most current reservoir models do not allow to model thermal effects together with a description of the PVT, according to the EOS. In a similar former project, TNO has been successful in modelling the thermal impact of injection into the Barendrecht reservoir. As this was a NAM field, we applied the Shell reservoir model MoReS. TNO at that moment was not allowed to use the Shell model for other producers. It was therefore decided to translate the MoReS input files into those for Eclipse300 (+ thermal). After trying hard with several approaches, and after several talks with Schlumberger it was concluded that the current version of Eclipse cannot properly model the thermal effects of CO_2 injections into a depleted (composition) gas reservoir.

4.9.2. P18 thermal reservoir study

The next approach was to ask Shell to make the MoReS simulator available for TNO reservoir engineers to work on reservoirs within CATO2. Shell agreed to this and allowed the use of MoReS for the P18 and P15 fields operated by TAQA Energy B.V., and the K12-B blocks operated by GDF Suez E7P Nederland B.V. It was therefore possible use the still innovative pseudo-thermal approach as used for the Barendrecht for the P18 fields. During the modelling for P18, we tested the modelling of the C_p of the liquid phase which was found to be reasonable. Furthermore we changed the way MoReS manages the time steps of the simulation as a function of the temperature changes over all grid blocks in the previous time step.

In other to include small-scale processes in the simulation, a radial sector model was used with very small (1.5 cm) grids directly adjacent to the injection well and much larger grids, further away from the well. The total radius of the flow domain was 2 km. The permeability of the reservoir rock, the initial pressure and temperature were 100 mDarcy, 20 bar and 399 K, respectively.

Together with TAQA, a workflow was set up which included integration of the modelling efforts of the TAQA contractor Genesis and TNO Within the framework, Genesis was responsible for modelling the transport from the on-shore CO_2 source, and the transport/behaviour of CO_2 within the injection well. For various scenario's Genesis modelled the injection rate, bottom hole pressures and temperatures, which subsequently were applied as input data for the reservoir simulation as conducted by TNO.

Genesis provided the data on a number of injection scenarios. Two of these were subsequently modelled by TNO (Bottom Hole Temperatures of 285 K and 259 K, respectively) and an injection rate of 47 kg/s or 1.5 MTon/year.

Figure 4.14 shows the predicted temperatures (BHT = 285 K) around the injection well after 1 day and 1 year of injection, respectively.

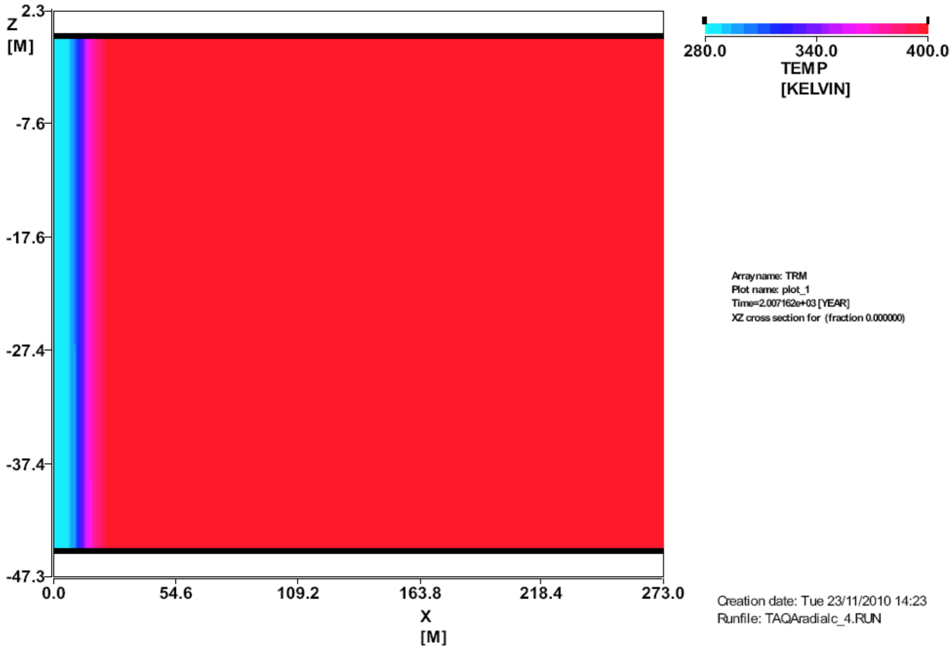

Figure 4.14: Temperature profiles after 1 day of injection.

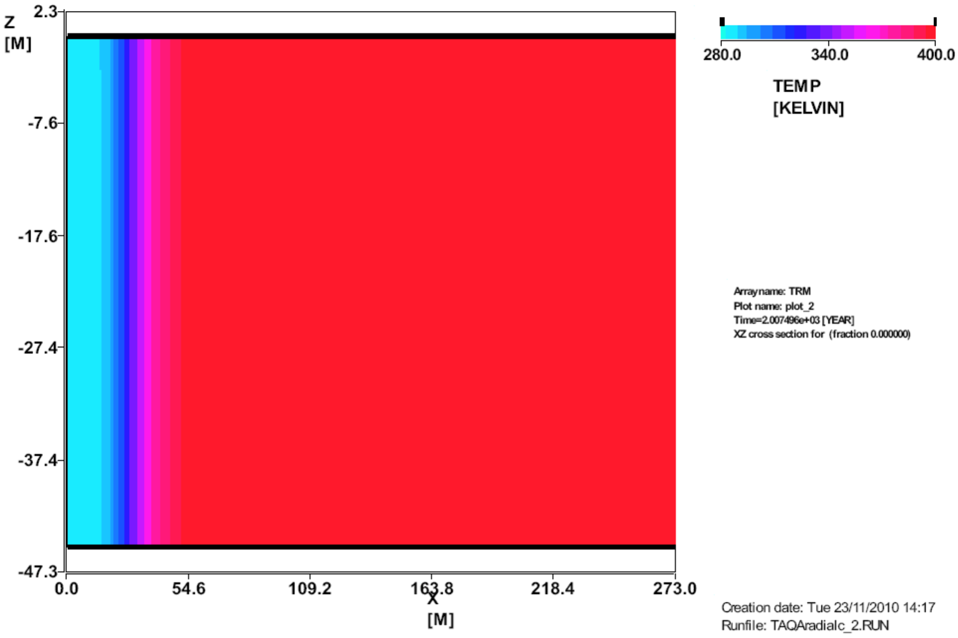

Figure 4.15: Temperature profiles after 1 year of injection.

The temperature propagation in the reservoir depends on the heat capacity of the matrix; the heat capacity used in this study is 2560 kJoule/m^3/K.
Figure 4.14 shows that temperatures, close to the injection well, drop several degrees within 1 day. Subsequently, the temperature drops rapidly from the initial temperature of the reservoir to that of the injected fluid in the area around the well. The initial cooling is focused on the grid block, directly adjacent to the injection well. Only after this grid has reached the temperature of the injected fluid, the cooling continues in the next grids. After 1 year of injection (Figure 4.15) a very small area near well area has reached a new temperature plateau (at that of the injected fluid). This area will increase with a continued injection under the same conditions. For smaller injection rates the advance of the temperature front will be slower, while for higher rates the speed of advancement will increase. Both figures show a large temperature gradient at the boundary between the new plateau and the rest of the reservoir.

The 12.3 ^{o}C of the new temperature plateau is at the high range at which hydrate formation may occur (after the bottom hole has reached 80 bar) Predicting the exact impact of temperature changes and the strong temperature gradient within the reservoir is complex. Not only the fluid properties (for example hydrate formation), but also timescales and degree of drying of the near well area should be considered. Other complicating processes are the thermally induced fracturing and its impact of these fractures on the fluid flow.

The impact of fluctuations of the injection rates and that of a complete shut-in on the temperature profile within the reservoir were also modelled. During the various scenario's, no temperatures below those of the injected fluid were observed. This means that the Joule Thompson effect is neglectable just after the start of the injection as well as right after a shut-in.

As mentioned before the pseudo thermal approach is still under investigation. For certain (more or less random) injection rates, the model was not stable leading to sudden and random stops (due to non-conversion problems) in the middle of a simulation. Investigation this problem, it was found that this was connected with a phase (flash) change within the well bore (for example from vapour to liquid at a certain temperature and pressure. The associated instant changes in density and viscosity of the CO_2 lead to the instability and non-conversion during that time-step. This was solved by slightly changing the injection rates.

The cold injection scenario (159 K) lead to near well temperatures, which rapidly reach 273 K, which resulted in the reservoir simulator to stop (273 K is internal threshold of MoReS). Predicting the impact of freezing conditions within the reservoir is complex. The aforementioned thermal effects are likely to be more pronounced at the lower temperatures. The cold injection may also result in freezing of the connate water in the reservoir.

To the best of our knowledge, it is unknown whether freezing conditions lead to risks or technical problems during the injection. It was therefore concluded that for at the moment some heating of the CO_2 is required before injection in other to stay out of the freezing - and even the hydrate conditions in the near well area. Only after further investigation or a pilot test has shown that colder injection is feasible, it may be possible to reduce the temperature of the injected CO_2.

conditions of the formation water and mineral assemblage before stage 3, which are used in the model.

Stage 3: conditions of P18 reservoir and cap rock after CO_2
The effects of CO_2 injection on the reservoir rock and cap rock (seal) are computed in the 'CO_2 scenario'. The results of stage 2 are used with an increase of the CO_2 partial pressure. The following three terms are then modeled:

- No mineral reactions (drop in pH), representing the short-term effects;
- Selection of mineral reactions (carbonates and sulfides), representing the mid-term effects (in the order of years to decades);
- Full suite of mineral reactions, representing the long-term effects (in the order of thousands of years).

Stage 4: reference scenario; equilibrium assemblage without CO_2 *injection*
Most often, the mineral assemblage of a reservoir or cap rock and the corresponding computed formation water chemistry represent a meta-stable configuration. This is because the reservoir and cap rock are not yet in thermodynamic equilibrium, due to very slow mineral reactions. Besides, several minerals have not been into contact with formation water due to their presence as inclusions or due to the presence of clay coatings around detrital minerals (Peters, 2009). For this reason, a reference equilibrium assemblage has been modeled in which the final mineral assemblage is computed without CO_2 injection. The resulting mineral assemblage can than be compared to the initial mineralogy and the mineralogy after CO_2 injection. Subsequently, the effect of CO_2 injection on the final reservoir assemblage of the reference equilibrium mineralogy is computed and compared to the initial CO_2 injection assemblage.
Furthermore, the sensitivity of final mineral assemblage to formation water chemistry is shortly investigated (section 5.2.5). This is important since the methodology of the formation water computation holds some uncertainty and subjectivity.
Possible geochemical effects of O_2 impurity in the CO_2 stream are investigated in section 5.2.6

All figures of reservoir and cap rock mineral assemblage are given in Appendix B in such a way that they can be easily compared.

5.1.3. Modelling approach

During the modeling, the following constraints were imposed for finding a delicate balance in the mineral-water-gas system:

- A fixed amount of water is available, which is not refreshed (batch reaction in a closed system);
- For each simulation it is checked that the error in the electrical balance between the anions and the cations in the connate water is below 0.05%;
- In the *PHREEQC* model all partial pressures of the gases in the pores are specified and it is assumed that these partial pressures are maintained (i.e. instantaneous supply);
- Ideal gases and ideal gas mixtures are assumed in *PHREEQC*, which is a simplification as CO_2 behaves as a supercritical fluid at the temperature and final pressure conditions at injection depth. Nonetheless, the solubility of CO_2 is corrected for supercritical behaviour by adjusting its partial pressure, using the fugacity coefficient and the Poynting correction. As a result, a lower partial pressure is used as input in order to (artificially) achieve the solubility corresponding to the supercritical behaviour;
- N_2 and CH_4 are present as an inert gas and do not chemically react.

5. Geochemical study

Summary

The effects of CO_2 injection on reservoir and cap rock in the P18 reservoir is predicted by geochemical modeling, using *PHREEQC*. The modeling results show that short-term mineralogical and porosity changes, induced by dissolved CO_2 and corresponding pH decrease, are negligible. On the long-term (thousands of years) mineral reactions will result in a porosity *de*crease of 0.3 percentage point (pp) for the reservoir and a porosity *in*crease of 0.2 pp for the cap rock. The presence of O_2 as an impurity in the CO_2 stream does not seem to have significant consequences regarding the short-, mid- and long-term geochemical effects of CO_2 storage.

5.1. Geochemical modelling

5.1.1. Introduction

TAQA is investigating the possibilities for CO_2 injection in the P18 depleted gas field for geological storage. CO_2 dissolution and subsequent aqueous dissociation will lower the pH of the connate (formation) water, which will influence the chemical equilibrium between gas, connate water and rock mineralogy. Interactions between these three phases will occur, leading to a new equilibrium. This could result in a change in porosity and permeability of the reservoir and cap rock, and affect their storage integrity. Data was collected on the chemical composition of the reservoir and cap rock, on gas currently present and on connate water, together with current and future reservoir conditions like pressure and temperature. This data was used in the geochemical modeling code *PHREEQC* in order to investigate the geochemical effects of CO_2 injection on subsurface characteristics.

PHREEQC computes the chemical equilibria of aqueous solutions interacting with mineral assemblages and gases by means of batch-reaction calculations (Parkhurst and Appelo, 1999). The development of the effects in time is considered on a qualitative base; quantification would require further study.

5.1.2. Stages and scenarios

The modeling approach consists of four stages. During the first stage the available data is organized and evaluated. During the following stage the pre-operational (i.e. before CO_2 injection) conditions are established. In the third stage the geochemical consequences of CO_2 injection are computed. Finally a reference scenario without CO_2 injection is also computed.

Stage 1: data inventory and evaluation

1. Define the mineral composition, porosity and water saturation of the reservoir (Main Buntsandstein) and cap rock;
2. Define the measured composition of the formation water;
3. Define the current gas composition in the formation;
4. Define the pressure and temperature conditions at the injection depth.

Stage 2: pre-operational conditions (before CO_2 *injection)*

During the second stage the initial composition of the solution (the speciation of the dissolved ions) and the corresponding rock mineralogy are computed. *PHREEQC* adjusts the pH of the formation water accordingly. Formation water and mineral assemblage are compared to the measured compositions and adjustments are made, if necessary. The results define the

With respect to the latter constraint we initially observed the following (overall) reaction during our preliminary *PHREEQC* simulations:

$$CH_4\ (g) + SO_4^{2-} + H^+ \rightarrow HCO_3^- + H_2O + H_2S\ (g)$$

In the case of a relatively high CH_4 partial pressure and sufficient SO_4^{2-} the equilibrium of this reaction will shift to the right. The preliminary simulations predicted that this would lead to dissolution of anhydrite ($CaSO_4$). It is not considered likely that these reactions will be predominant during the next few thousand years due to two reasons. Firstly the given reaction with CH_4 and SO_4^{2-} requires a very high activation energy and is very slow. Secondly it is frequently observed that anhydrite has been in equilibrium with CH_4 (for example in the P18 field) for thousands of years. Therefore it is unlikely that anhydrite will dissolve. Rather than eliminating the reactions given above from the *PHREEQC* database, the problem was solved by replacing CH_4 by the inert Ar gas in the model.

5.1.4. Reservoir and cap rock conditions

The sample analyses of the P18 reservoir (Hardegsen, Upper Dethfurth and Lower Dethfurth formations) show that the average porosity is 8.8% with a water saturation of 0.42 (Cantwell, 1992). The volume percentages of rock, gas and water in the reservoir are therefore 91.2%, 5.1% and 3.7% respectively. In the model 1.0 dm^3 of formation water is used, which corresponds to 1.4 dm^3 of gas and 24.6 dm^3 of minerals.
The porosity of the cap rock is 1% and it is assumed that the water saturation is 100%.

<u>Pressure and temperature</u>
The initial pressure in the P18 reservoir is 20 bar. The average temperature is 106℃ and total final pressure is defined as 356 bar (20 bar below the initial gas pressure before gas production). The initial and final pressure conditions are shown in Table 16. Pressure and temperature conditions of the cap rock after CO_2 injection are assumed to be equal to the conditions in the reservoir rock.

Table 16: Initial and final condition of the reservoir gas.

Component	Initial conditions			Final conditions		
	Composition (mol%)	Px (atm)	Log Px (-)	Composition (mol%)	Px (atm)	Log Px (-)
C1	98.26	19.91	1.30	5.52	19.91	1.30
CO_2	1.24	0.25	-0.60	94.45	331.33	2.09
N_2	0.5	0.10	-1.00	0.03	0.10	-1.00
Total	100	20.26			351.34	

<u>Rock composition</u>
The reservoir rock composition is defined from several rock samples of the Hardegsen, Upper Dethfurth and Lower Dethfurth formations (Cantwell, 1992). Average values are taken (Table 17). The rock sample from the Volpriehausen formation was excluded as it is expected that CO_2 will not be injected in this formation, based on porosity measurements. The sealing formation of the P18 Bundsandstein formation consists largely of quartz, with lesser amounts of e.g. dolomite, illite, anhydrite and siderite (Table 18).

Gas composition

The composition of the gas phase currently present in the reservoir is known. In the model all alkanes are represented by C1 (CH_4) (Table 16).

Table 17: Composition of reservoir rock of the P18 field based on sample analyses and experimental mineral densities and mol masses. The volume (dm3) and number of moles are in correspondence to a total rock volume of 24.6 dm3.

Mineral	Composition (wt%)	Volume (dm^3)	Amount (Mole)
Quartz	78.1	19.38	856.15
Anorthite	2.3	0.54	5.45
K-feldspar	5.7	1.47	13.59
Dolomite	5.8	1.33	20.66
Anhydrite	0.1	0.02	0.40
Albite	0.1	0.02	0.17
Kaolinite	0.7	0.17	1.63
Clinochlore-14A	1.3	0.32	1.58
Illite	2.8	0.66	4.83
Smectite-Na	3.1	0.66	5.06

Table 18: Composition of cap rock of the P18 field based on sample analyses and experimental mineral densities and mol masses. The volume (dm3) and number of moles are in correspondence to a total rock volume of 99 dm3.

Mineral	Composition (wt%)	Volume (dm^3)	Amount (Mole)
Quartz	60.7	62.1	2734.62
Anorthite	2.9	2.8	28.12
K-feldspar	3.7	3.9	35.47
Dolomite	11.8	11.2	173.69
Anhydrite	7.0	6.4	138.57
Pyrite	0.5	0.3	12.19
Siderite	2.4	1.6	55.54
Clinochlore-14A	0.7	0.7	3.55
Illite	10.1	9.9	71.43
Smectite-Na	0.2	0.1	1.0

5.1.5. Pre-operational conditions

The balance between rock mineralogy and water chemistry is delicate. Measured compositions of both are subject to local variability and measurement errors. Because the measured salt concentration of the connate water in the P18 field is unexpectedly very low, the formation water of P06-A2, which is located near P18, is used for comparison with the computed chemistry of the formation water in the reservoir. This is done by equilibration of pure water with surplus amounts of minerals present in the reservoir and a NaCl concentration of 130 g/kg water. Subsequently, it is compared to the formation water of P06-A2. It is computed that several minerals show extensive dissolution and precipitation of secondary minerals. To avoid this, the amount of the dissolving minerals is lowered until no significant conversion occurs. Several new minerals are

still computed to precipitate in low amounts (glauconite, muscovite and pyrite). Due to the lowering of dissolution of illite, smectite, K-feldspar and anorthite, the amounts of precipitating minerals are so low that they could have been overlooked during mineral analysis. Therefore they are included in the assessment. Mesolite and saponite are computed to dissolve, but these do not naturally occur in regular sandstones. Furthermore, dolomite is computed to transform completely into dolomite-ord and, K-feldspar into microcline. These precipitates and conversions are excluded from the simulation since they do not represent current conditions. Dolomite and K-feldspar thus represent meta-stable phases.
The pH of the computed formation water has a value of 5.8. The computed water chemistry and the measured chemistry of P06-A2 are shown in Figure 5.1. The computed concentration of chloride, magnesium and sodium are close to the measured values of P06-A2. For iron, calcium and potassium, the computed and measured values are significantly different. The high iron concentration in the measured sample(s) might be an artefact caused by corrosion of well material. Other differences might be caused by contamination from, for example, drilling muds. Furthermore, water samples can locally be very different due to local mineralogy differences, and this water sample is from another location. In section 5.2.5 the results of a sensitivity analysis on formation water chemistry are given.
The rock composition corresponding to the computed formation water is shown in Appendix B Figure 12.1.

For the computation of cap rock formation water, the same methodology is used as for the reservoir. Small amounts of albite, diaspore, glauconite and muscovite were predicted to precipitate. These have been included in the modeling since these minerals occur frequently in natural sandstones. The mineral assemblage of the cap rock is shown in Appendix B, Figure 12.4. The pH of the computed formation water has a value of 6.1.

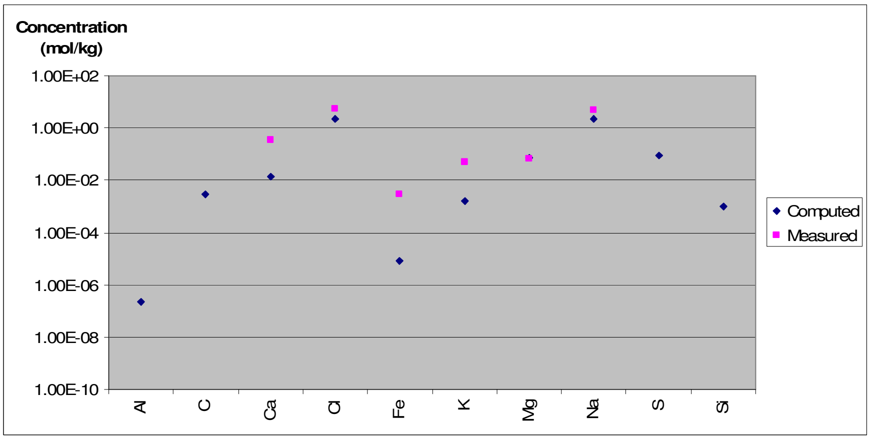

Figure 5.1 Computed and measured formation water composition (initial).

5.2. Geochemical effects of CO_2 injection

5.2.1. Introduction

In this section the effects of CO_2 injection on reservoir and cap rock are described. Three terms were defined describing the qualitative modeling of the processes. The results for the reservoir and cap rock are described in section 5.2.2 and 5.2.3 respectively. Results for the mineral assemblage of reservoir and cap rock, as well as initial rock mineralogy are shown in this section, as well as in Appendix B for easy comparison.

5.2.2. Reservoir rock

Short term effects on connate water

In this scenario the effect of increased CO_2 partial pressure (356 bar) is computed, while excluding mineral dissolution and precipitation.
As expected, the pH of the connate water drops due to the increasing dissolution and dissociation of CO_2. The following reactions take place:

$$CO_2\,(g) + H_2O \rightleftharpoons HCO_3^- + H^+$$
$$HCO_3^- \rightleftharpoons CO_3^{2-} + H^+$$

A relatively high CO_2 partial pressure will shift the first and second reaction more to the right and decreases the pH. The pH in the reservoir is computed to decrease to a value of 3.5, which is expected to be the condition directly after injection. The rates of mineral reactions are assumed to be much slower than the dissolution rate of the CO_2 in the water. Mineral reactions will buffer the pH (see following sections) and a pH of 3.5 is therefore considered to be the minimum. The carbon concentration in the formation water increases as a result of CO_2 dissolution.

Carbonate and sulfide mineral reactions (mid term)

On the mid-term the effect of increased CO_2 partial pressure is computed, while also allowing dissolution and/or precipitation of carbonates and sulfides. In the reservoir, a small amount of dolomite and pyrite dissolve (0.03 and 0.17% of the amounts initially present, respectively) due to the dissolution of CO_2. Some anhydrite and an insignificant amount of dawsonite precipitates. These dissolution and precipitation reactions slightly buffer the pH, to a value of 4.2 but the porosity is not affected. Also, the composition of the formation water does not change significantly, except for an increase in carbon concentration caused by the CO_2 dissolution in the brine.

Full suite of mineral reactions (long term)

The effect of increased CO_2 partial pressure on the total rock mineralogy describes the conditions of thermodynamic equilibrium. This will take thousands of years to establish since most mineral reactions are very slow. Furthermore, minerals can be (temporarily) inaccessible to formation water due to their presence as mineral inclusions or to clay coatings surrounding them (Peters, 2009).
The results on the final formation water, compared to the initial formation water, and the final reservoir mineral assemblage are shown in Figure 5.2 and in Appendix B, Figure 12.2 respectively. The following main reactions occurred:

<u>Dissolution</u>

$CaAl_2(SiO_4)_2 + 8\ H^+ \rightarrow Ca^{2+} + 2\ Al^{3+} + 2\ SiO_2 + 4\ H_2O$ (Anorthite)

$Mg_5Al_2Si_3O_{10}(OH)_8 + 16\ H^+ \rightarrow 2\ Al^{3+} + 3\ SiO_2 + 5\ Mg^{2+} + 12\ H_2O$ (Clinochlore-14A)

$K_{0.6}Mg_{0.25}Al_{1.8}Al_{0.5}Si_{3.5}O_{10}(OH)_2 + 8\ H^+ \rightarrow$
$0.25\ Mg^{2+} + 0.6\ K^+ + 2.3\ Al^{3+} + 3.5\ SiO_2 + 5\ H_2O$ (Illite)

$KAlSi_3O_8 + 4\ H^+ \rightarrow Al^{3+} + K^+ + 2\ H_2O + 3\ SiO_2$ (K-feldspar)

$Al_2Si_2O_5(OH)_4 + 6\ H^+ \rightarrow 2\ Al^{3+} + 2\ SiO_2 + 5\ H_2O$ (Kaolinite)

$Ca_{0.02}Na_{0.15}K_{0.2}Fe^{2+}{}_{0.29}Fe^{3+}{}_{0.16}Mg_{0.9}Al_{1.25}Si_{3.75}H_2O_{12} + 7\ H^+$
$\rightarrow 0.02\ Ca^{2+} + 0.15\ Na^+ + 0.16\ Fe^{3+} + 0.2\ K^+ + 0.29\ Fe^{2+} + 0.9\ Mg^{2+}$
$+ 1.25\ Al^{3+} + 3.75\ SiO_2 + 4.5\ H_2O$ (Smectite)

<u>Precipitation</u>

$1.5\ K^+ + 2.5\ Fe^{3+} + 0.5\ Fe^{2+} + 0.5\ Mg^{2+} + Al^{3+} + 7.5\ SiO_2 + 9\ H_2O$
$\rightarrow K1.5Mg_{0.5}Fe_3AlSi_{7.5}O_{20}(OH)_4 + 14\ H^+$ (Glauconite)

$HCO_3^- + Mg^{2+} \rightarrow MgCO_3 + H^+$ (Magnesite)

$K^+ + 3\ Al^{3+} + 3\ SiO_2 + 6\ H_2O \rightarrow KAl_3Si_3O_{10}(OH)_2 + 10\ H^+$ (Muscovite)

$Fe^{2+} + HCO_3^- \rightarrow FeCO_3 + H^+$ (Siderite)

Due to these reactions, *the porosity decreases with 0.3 percentage point (pp) to 8.5%, based on the specific density of the different minerals*. Possible porosity effects due to geomechanical processes are not taken into account. Dissolution of minerals might cause mechanical compaction of the reservoir, thereby causing additional porosity decrease.

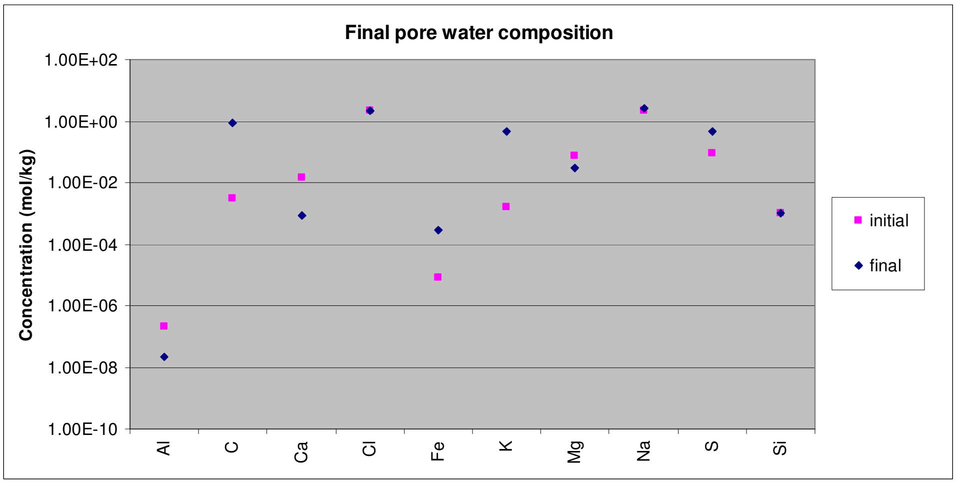

Figure 5.2 Initial and final computed formation water composition.

5.2.3. Cap rock seal

Effects on connate water (short term)

If CO_2 would dissolve and diffuse into the formation water of the cap rock, the pH could decrease to a value of 3.2. Unlike in the reservoir, the pH drop will not occur throughout the formation within the injectivity period, because a *boundary* between reservoir and cap-rock is affected. We then might expect CO_2 diffusion could start at the reservoir - cap rock boundary, and CO_2 could possibly slowly migrate up, into the cap rock.

Carbonate and sulfide mineral reactions (mid-term)

On the mid-term, small amounts of anhydrite and siderite (less than 0.01% of the initial amounts present) will dissolve, thereby buffering the pH to a value of 4.3. Precipitation of other carbonates and sulfides does not occur and the effect of dissolution on porosity is negligible. The iron concentration in the brine increases significantly to a value of $2.55 \cdot 10^{-3}$ mol/liter due to the dissolution of siderite, but the amount of anhydrite dissolution is too small to have any effect on the calcium concentration.

Full suite of mineral reactions (long term)

On the long-term, mineralogical changes are predicted to occur. Illite, K-feldspar, anorthite, clinochlore, and siderite are (almost) completely dissolved, while muscovite, glauconite and diaspore have precipitated in significant amounts (Appendix B, Figure 12.5). *These mineralogical changes correspond to a porosity increase of 0.2 pp (equal to an increase of 20%).* The final formation water chemistry is shown Figure 5.3.

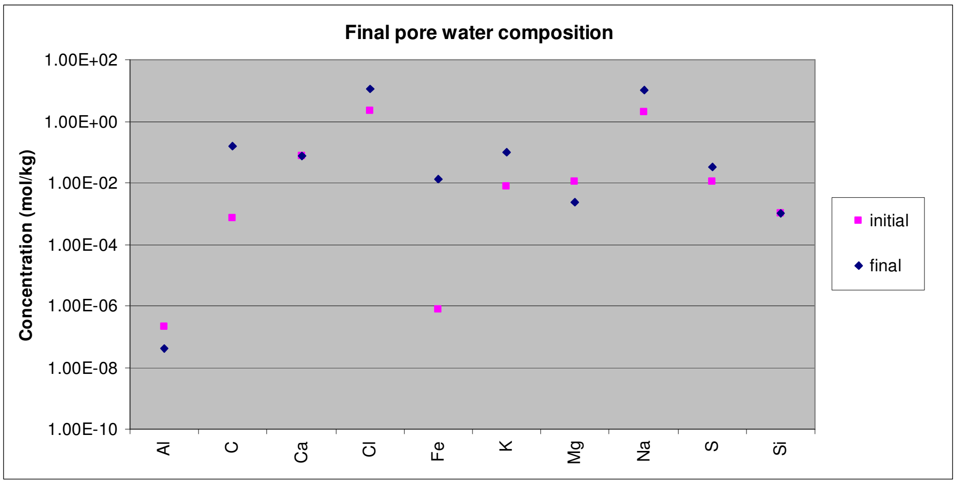

Figure 5.3: Initial and final formation water composition of the cap rock.

5.2.4. Reference scenario; equilibrium assemblage

The computation of the long-term mineralogical changes in the reference scenario show that significant changes would occur in the reservoir and cap rock, even without CO_2 injection, due to their current meta-stable conditions (Appendix B, Figure 12.3 and Figure 12.6 respectively).
The porosity of the reservoir increases by 0.1 pp, compared to a decrease of 0.3 pp in the CO_2 scenario. In the equilibrium stage of the cap rock, the porosity is predicted to increase by 0.3 pp, while it increases by 0.2 pp in the CO_2 injection scenario.
CO_2 injection into a reservoir with the computed reference assemblage results in exactly the same mineralogical changes, and thus porosity change, for the reservoir and cap rock as CO_2 injection into a reservoir (with a cap rock) with the meta-stable assemblage (Appendix B, Figure 12.2 and Figure 12.5 respectively). This shows that the meta-stability of the reservoir and cap rock do not affect the mineralogical changes caused by CO_2 injection.

5.2.5. Formation water sensitivity

As explained in section 5.1.5, several minerals are computed to completely dissolve when computing the chemistry of the formation water, thereby supplying the ions required for precipitation of new, secondary minerals. In order to obtain a mineral assemblage close to the measured one, a limited amount of the dissolving minerals was supplied in the calculation of the formation water. For sensitivity analysis, these amounts were multiplied by a factor of ten, allowing the precipitation of larger amounts of secondary minerals. In another run, the precipitation of secondary minerals was excluded. The results show that for both cases there is negligible effect on the mid- and long-term mineral assemblage and the porosity change of the reservoir and cap rock, even if the initial pH is significantly different. Hence, the formation water sensitivity of the P18 reservoir and cap rock is small.

5.2.6. O_2 impurity

The captured CO_2 can contain some O_2, which is maximally 160 ppm. To study the possible effect of O_2 on the reservoir, 0.05 bar of O_2 is used as input in the model (log P_x is -1.30), corresponding to 160 ppm.

The model results show that only a fraction of the O_2 is predicted to dissolve on the short-term , having no additional effect on the pH of the formation water compared to the baseline scenario. Mid-term effects are small. Slightly more pyrite and anhydrite will dissolve and precipitate, respectively, compared to the baseline. The iron, in the reduced state, remains in the formation water. All oxygen is used to oxidize sulfur from pyrite for anhydrite precipitation. The effects of these reactions on porosity are negligible.
Increasing the O_2 partial pressure by 10 (corresponding to 1600 ppm O_2 in the CO_2 gas stream), in order to investigate a worse case scenario, would lead to complete pyrite dissolution and slightly more anhydrite precipitation , since more oxygen is in the system to oxidize sulfur from pyrite. The iron from pyrite is oxidized and precipitated as hematite. The porosity change is still negligible.
Long-term effects do not differ from the baseline scenario.

5.3. Conclusions

When CO_2 is injected into a reservoir system with cap rock, the pH of the formation water will initially decrease to a value of 3.5 and 3.2 for the reservoir and cap rock respectively, due to the formation of carbonic acid. Dissolution of small amounts of carbonate and sulfides, which is predicted to occur on the mid-term (in the order of years to decades), will buffer the pH to a value of 4.2 and 4.3 respectively. The effects on mineralogy and porosity are negligible.
It is predicted that the mineralogical assemblage will have been changed significantly once thermodynamic equilibrium is established, which may take thousands of years. *The corresponding porosity change is a decrease of 0.3 pp (to 8.5%) for the reservoir rock and an increase of 0.2 pp (to 1.2%) for the cap rock*.

Since the initially computed formation water and mineral assemblage of both reservoir and cap rock are not in equilibrium reference calculations were performed to investigate the equilibrium assemblage without CO_2 injection. The results show that the assemblage changes significantly. However, if CO_2 injection would occur in the reference assemblage, the mineralogy and porosity change would be equal to CO_2 injection into a reservoir with cap rock in a meta-stable phase. Furthermore, the final mineral assemblage is relatively insensitive to the methodology of formation water computation.

The presence of O_2 as an impurity in the CO_2 stream is predicted not to have a significant effect on the short-term. On the mid-term the model shows a slight increase in pyrite dissolution and anhydrite precipitation. Effects on porosity are negligible. Long-term effects are similar to the baseline and therefore also to the reference.

5.4. References

Cantwell W., 1992. Final Report of Mineralogical Analysis for Amoco Netherlands Petroleum Company, Well number P/18-2 and P/18-3, The Netherlands.

Peters C.A., 2009. Accessibilities of reactive minerals in consolidated sedimentary rock: An imaging study of three sandstones. Chemical Geology 265; p198-208

6. Top seal and fault integrity study

6.1. Introduction

6.1.1. Background

This chapter presents the results of the top seal and fault integrity assessment conducted in the framework of the technical feasibility study of geological CO_2 storage in the depleted P18 Field. The study was undertaken within the framework of CATO-2 project, WP3.3. Caprock and fault integrity.

6.1.2. Scope and objective

CO_2 injection into depleted hydrocarbon reservoirs will change the state of stress in a reservoir-seal system due to various phenomena: poro-mechanical effects caused by changes in the pore fluid pressure; buoyancy effects caused by changes in the pore fluid density; thermal effects caused by changes in the pore fluid temperature; and chemical effects caused by changes in the pore fluid chemistry.

As a result of induced stress changes top seals can be mechanically damaged, pre-existing sealing faults and fractures can be re-activated, or new fracture systems can be created, allowing fluid migration out of the storage complex. Besides the effects on the containment, CO_2 injection could also induce ground movement, which can be either aseismic - in the form of ground surface uplift, or (micro-)seismic - caused by a sudden slip on pre-existing discontinuities or faults.

The objective of this study is to evaluate the impact of induced stress changes, resulting from past gas extraction and future CO_2 injection in P18 Field, on top seals and faults.
The impact on the containment will be evaluated by assessing:

- The mechanical integrity and the potential for induced hydro-fracturing of top seals.
- The mechanical integrity and the potential for re-activation of faults, as fault slip can make previously sealing faults conductive and induce seismic events at the injection site.

The impact on the environment will be evaluated by assessing the induced ground/seabed movement, i.e. subsidence and uplift.

Mechanical and transport rock properties may change over time due to mineral reactions between the injected CO_2 and the rock (reservoir, caprock and fault gouge). Experimental testing program is currently under way at the HPHT lab of Utrecht University to quantify the long-term effects due to CO_2-rock interaction for P18. The results of these tests were not available at the time when this study was completed and therefore not considered in this report.

6.1.3. Approach

The input data for this study were supplied by TAQA Energy B.V.

The following data and models developed within the framework of the CATO-2 project were used in this study:

- Regional geological Petrel model of P18 constructed by TU Delft and reservoir scale Petrel model constructed by TNO.
- Reservoir MoReS model and analytical model developed by TNO.
- Rock mechanics properties of the top seal determined by the experimental testing program at Utrecht University.
- The following tasks and activities were defined and carried out in this study:
- Geomechanical field characterization - by using well logs analysis, experimental rock mechanics tests and in situ stress data analysis.
- Development of geomechanical models - by using a finite element (FE) approach.
- Assessment of top seal mechanical integrity - by using analytical and numerical geomechanical models.
- Assessment of fault seal integrity - by using a fault seal analysis tool based on the Shale-Gouge Ratio, analytical and numerical geomechanical models.
- Assessment of induced ground, i.e. seabed deformation - by using a semi-analytical model for prediction of subsidence/uplift.

6.2. Geomechanical field characterization

6.2.1. Field description

P18 Field is located in the P block of the Dutch offshore. The reservoir structure of P18 comprises 3 compartments bounded by a system of NW-SE oriented faults in a horst and graben pattern.

The main compartment P18-2 comprises 3 segments (Figure 6.1). The largest segment P18-2 is drained by 3 wells: P18-2A1, P18-2A3 and P18-2A5. Wells P18-2A6 and P18-2A6st drain other two segments. The segment drained by well P18-2A6 is not in communication with other two segments of this compartment. Well P18-2A1 will be used as the CO_2 injector. The initial pressure in P18-2 is 375 bar and GWC is at 3680 m. Reservoir temperature is 126℃. P18-2 is in production since October 1993.

Compartment P18-4 is drained by one well P18-4A2 which will be used as CO_2 injector. Compartment P18-4 is not in communication with other two compartments. The initial pressure in P18-4 is 340 bar and GWC is at 3377 m. P18-4 is in production since March 1994.

Compartment P18-6 is drained by one well P18-A67 which will be used as CO_2 injector. Compartment P18-6 is not in communication with compartment P18-4 (different GWC) and appears (according to Chapter 4) not to be in communication with compartment P18-2 (equal GWC). The initial pressure in P18-6 is 375 bar and GWC is at 3680 m. P18-6 is in production since March 2004.

The reservoir rocks consist of sandstones intercalated with thin layers of shale. The reservoir belongs to the Main Buntsandstein Group and comprises the following parts:

- 25 m thick Hardegsen (RBMH), good producer;
- 50 m thick Upper Detfurth (RBMDU), fair producer;
- 25m thick Lower Detfurth (RBMDL), fair producer;
- 120m thick Volpriehausen (RBMVU+RBMVL), poor producer.

Hardegsen and Upper Detfurth are the main gas producers.

The primary top seal overlying the Bunter reservoir is a 50 m thick layer of the lower part of Upper Germanic Trias (RN). This layer comprises (from top to base):

- Röt Claystone Member (Mb) (RNROC),
- Main Röt Evaporite Mb (RNRO1),
- Solling Claystone Mb (RNSOC).

The primary top seal, as defined above, is covered by a 100 m thick upper part of Upper Germanic Trias (Muschelkalk, RNMU and Keuper, RNKP) and a 3-400 m thick Altena Group (AT) which can also be regarded as a part of the primary seal.

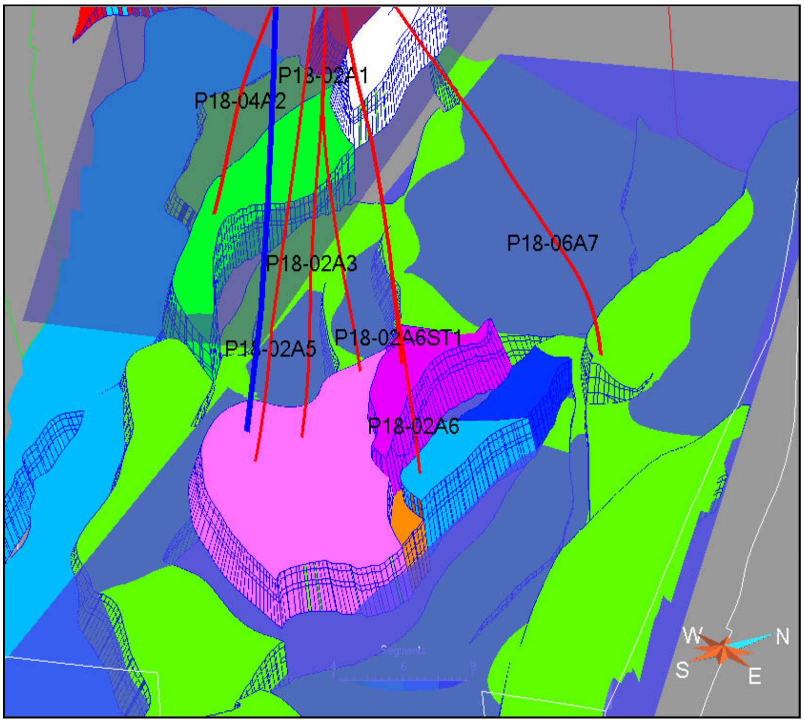

Figure 6.1: Reservoir structure showing compartment P18-2, which consist of 3 segments (in the middle), compartment P18-6 (penetrated by well P18-06A7) and compartment P18-4 (penetrated by well P18-04A2).

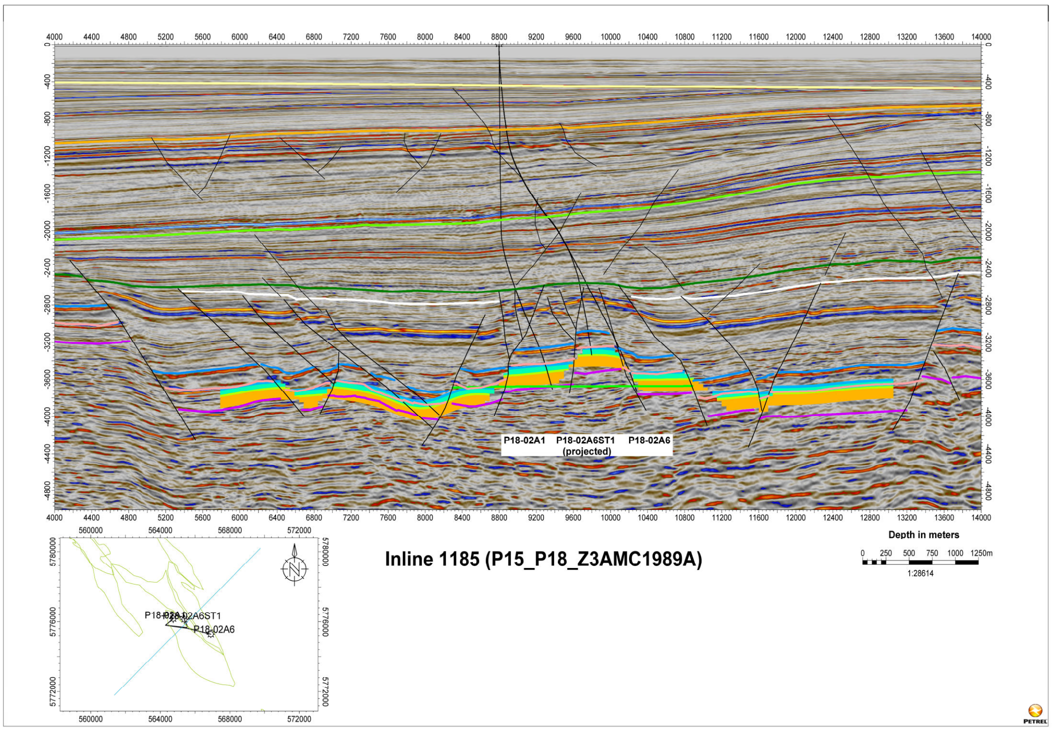

Figure 6.2: Interpreted seismic section along Inline 1185 through the P18 Field. The Bunter reservoir is shown in solid colours.

6.2.2. Lithological differentiation of the top seal

Detailed lithological determination of the top seal was performed in order to differentiate various lithologies present in the formations overlying the Bunter P18 reservoir. Bulk top seal lithologies were determined using gamma-ray, density, sonic and neutron-porosity logs. The most complete well-log suites were available from wells P18-2, P18-A-03-S2 and P18-A-06, which we used in analysis. The following lithologies could be resolved: shale, dolomite, anhydrite and gypsum.

The primary top seal overlying the Bunter reservoir is represented by the lower part of Upper Germanic Trias (RN), namely Röt Claystone Mb, Main Röt Evaporite Mb and Solling Claystone Mb. The lithologies present in these layers, according to well logs interpretation, comprise thin beds of shales with anhydritic cementation (Figure 6.3). The average thickness amounts to about 50 m, with a range of 41-68 m. This zone is continuous above compartment P18-2 with variable anhydritic content in shales (Figure 6.4). We assume that the seal above P18-2 is representative for the whole P18 Field.

The core from Röt and Solling (i.e. the primary top seal as defined above) was taken from well P15-14 in the neighbouring block P15 in an earlier study and analysed using standard geologic and petrophysical techniques including mercury-injection capillary-pressure tests (Spain and Conrad, 1997). The results showed that the true top seal for the P15 hydrocarbon accumulations is provided by thinly interbedded and interlaminated shale and very fine-grained sandstone to siltstone. These lithofacies contain type A seals which are capable of supporting gas-column heights in excess of 300 m. The P15-top seal quality may also be representative for the neighbouring P18 block as hydrocarbon accumulations in the Buntsandstein are present in both blocks.

The lower part of Upper Germanic Trias (i.e the top seal as defined above) is covered by a 100 m thick upper part of Upper Germanic Trias (Muschelkalk, RNMU and Keuper, RNKP) and a 3-400 m thick Altena Group (AT) which can also be regarded as a part of primary top seal.

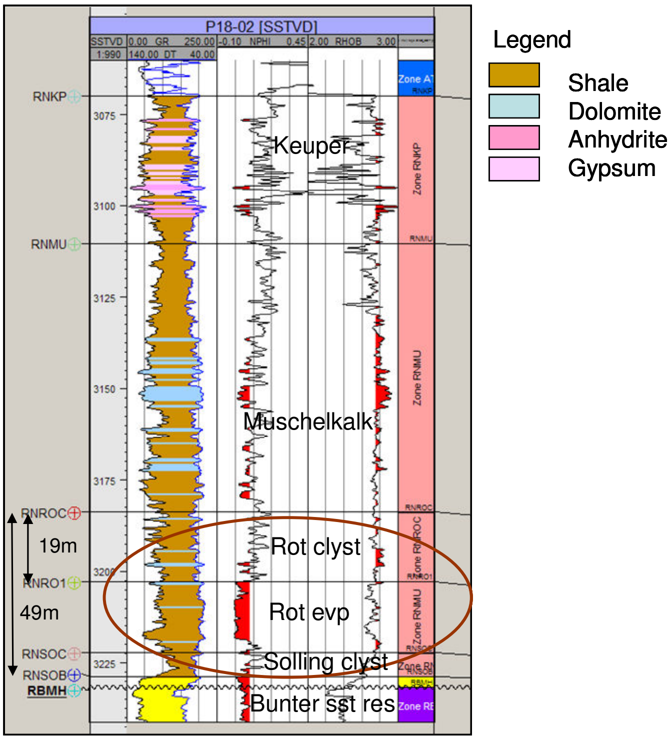

Figure 6.3: Lithological differentiation of the top seal based on well logs from well P18-02. The primary top seal is represented by Solling claystone, Röt evaporites and Röt claystone. Muschelkalk and Keuper could also be regarded as a part of primary top seal.

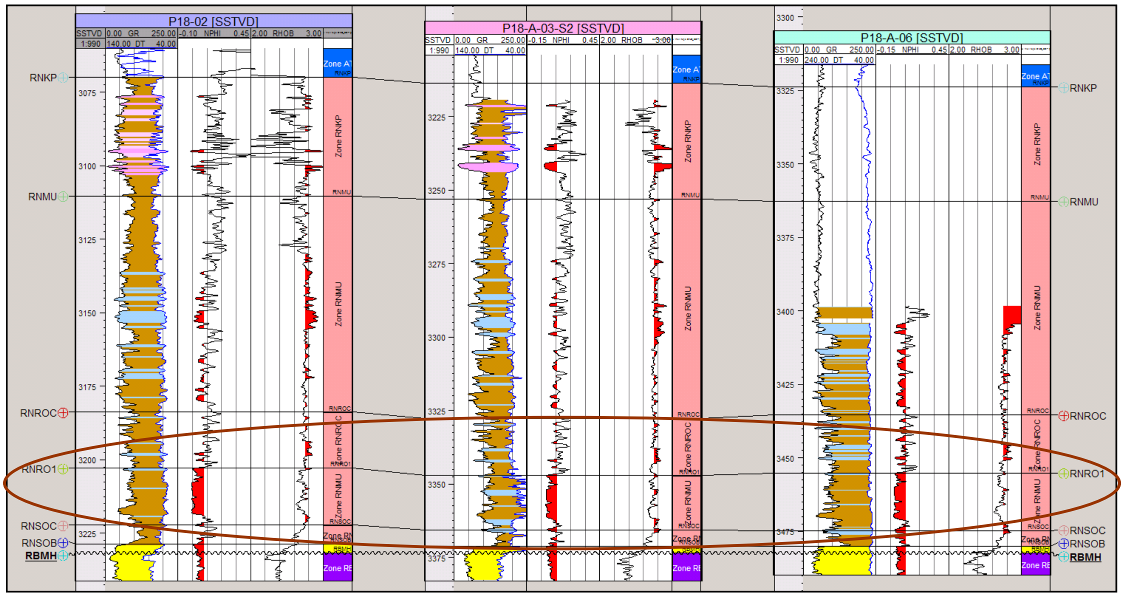

Figure 6.4: Well correlation section showing lithologies of the top seal in compartment P18-2. The primary top seal is represented by Solling claystone, Röt evaporates and Röt claystone. Muschelkalk and Keuper could also be regarded as a part of primary top seal.

6.2.3. Geomechanical characterization of the top seal and overburden formations

Experimentally derived rock properties

Experimental testing program within the CATO-2 project is currently under way at the HPT lab of Utrecht University to quantify the long-term effects due to CO_2-rock interaction for P18 (Utrecht University report, 2010). As a part of the testing program, permeabilities of the reservoir rock were measured on samples taken from P18 field. However, caprock core was not available from P18 field. Therefore permeabilities and mechanical properties were measured on samples taken from the Röt/Solling caprocks in the Q16 gas field, which is presumed to be analogous to the P18 field.

First results show that reservoir rocks are generally 2-3 orders of magnitude more permeable than caprocks. For most samples measured permeability of the reservoir rock is on the order of 10^{-15} m^2 to 10^{-16} m^2 and permeability of the caprock on the order of 10^{-18} m^2.

A summary of the caprock strength properties for the Röt/Solling caprocks from the Q16 gas field is shown in Table 19. Based on the measured properties, the caprock is a hard and competent rock. Generally we find that the mechanical properties fall within a reasonable range for similar materials. At this stage, due to a lack of suitable samples, no analysis has been conducted on the mechanical properties of the reservoir rocks of the P18 gas field.

Well log-derived rock properties

Besides the experimental test data on the caprock strength mentioned above, no other experimental data on the strength and elasticity of other formations were available. Therefore, geomechanical properties of the overburden and the underburden required for geomechanical analyses were derived indirectly from the available well logs. The most complete well-log suites were available from wells P18-2, P18-A-02, P18-A-03-S2 and P18-A-06.

For determination of dynamic elastic properties both compressional- (V_p) and shear (V_s) wave velocities are required. Shear velocities were measured in wells P18-A-02 and P18-A-06. They had to be estimated for other two wells using lithology-dependent empirical relationships from the literature (for clastic sediments from Castagna et al., 1985; for anhydrite from Rafavick et al, 1984, and for dolomite from Greenberg and Castagna, 1992).

Dynamic Young's modulus (*Edyn)* was then derived from well logs and converted to the static Young's modulus (*Estat),* which is required in geomechanical analyses, according to the formulas given below:

$$E_{dyn} = \rho V_s^2 .(3V_p^2 - 4V_s^2)/(V_p^2 - V_s^2) \qquad (6.1)$$

$$E_{stat} = 0.74 \cdot E_{dyn} - 0.82 \quad \text{(from Eissa and Kazi, 1988)} \qquad (6.2)$$

Well-log derived elastic rock properties clearly indicate stiffness contrast (i.e. difference in Young's elasticity modulus) between different lithostratigraphic and geomechanical units. The obtained absolute values of Young's moduli, however, possibly overestimate the expected values and therefore were downscaled by the ratio *Elab / Ewell-logs* for the caprock (as direct measurements of mechanical rock properties were only available for the caprock). This approach gives a value of E=20 GPa for the Bunter sandstone reservoir, which is a realistic value based on analogy with other Bunter reservoirs in the Netherland such as the Barendrecht-Ziedewij gas field (Winningsplan Barendrecht-Ziedewij, 2003).

Summary of the differentiated geomechanical units and their geomechanical properties is given in Table 20. The successive lithostratigraphic units with relatively small thickness, similar in lithology and mechanical properties were joined into one unit.

Table 19: Caprock strength summary. The properties were determined by triaxial tests performed in HPT lab of Utrecht University.
E=Young's elasticity, UCS=unconfined compressive strength, μ=friction coefficient (corresponds to a friction angle φ=28°), C=cohesion.

Caprock strength summary, Samples from Q-16 field

Sample #	Lithology	σ_1 (MPA)	$(\sigma_1\text{-}\sigma_3)_{max}$ (MPa)	E (GPa)	UCS (MPa)	μ	C (MPa)
#57	Röt	5	91.94	21.15	93.315	0.536	27.92
#59	Röt	20	147.74	31.64			
#55	Röt	35	149.87	23.69			
#60	Röt/Solling	50	180.83	29.11			

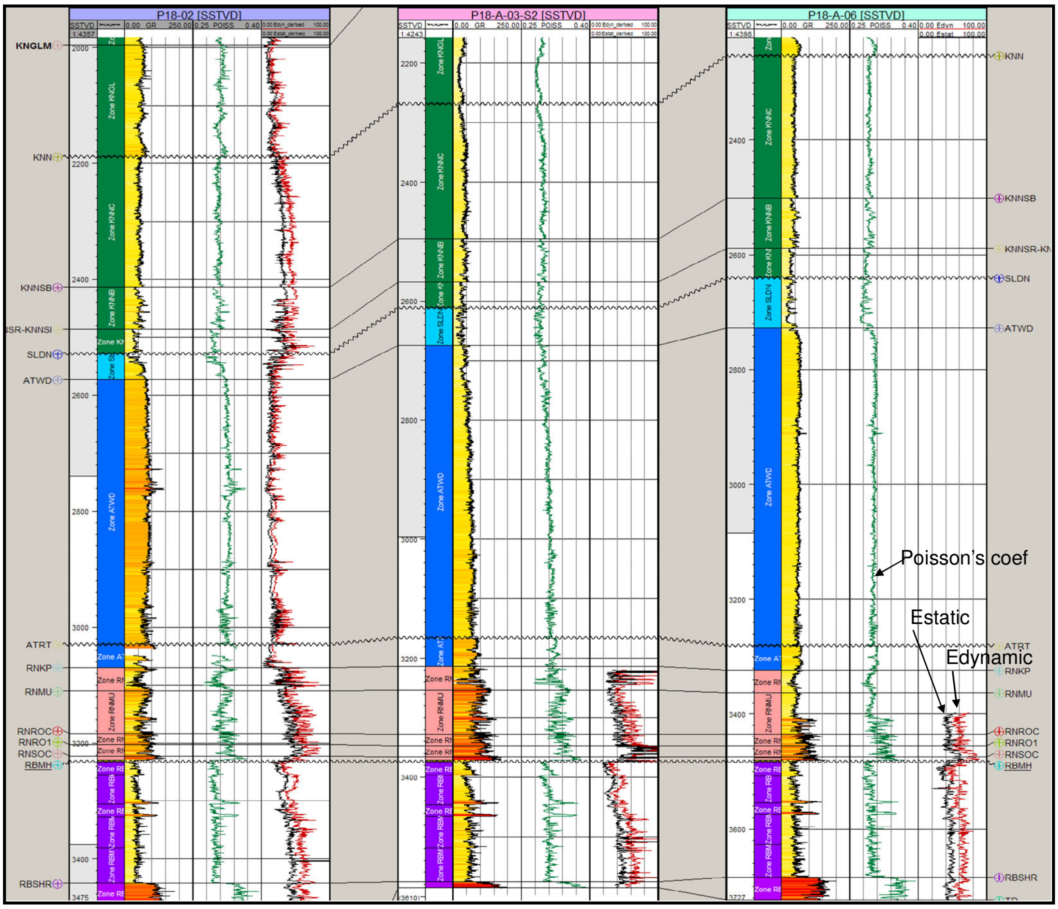

Figure 6.5: Well correlation section showing gamma-ray log and calculated Poisson's coefficient (range from 0.25-0.4) and Young's elasticity modulus (range from 0-100 GPa).

Table 20: Geomechanical properties for the differentiated geomechanical units in the P18 gas field.

Unit No	Stratigraphic unit	Thickness* [m]	Depth top* mTVDss	Density** [kg/m3]	Young's modulus*** E [GPa]	Poisson's coeff.*** v [-]
1	Upper North Sea Group, NU	417	33.5	1960	0.5	0.3
2	Middle and Lower North Sea Group, NM+NL	503	451	2600	5	0.3
3	Chalk Group, CKGR	956	920	2300	20	0.17
4	Rijnland Group, KN	652	1876	2650	17	0.30
5	Schieland Goup, SL	44	2528	2100	13	0.30
6	Altena Group, (AT)	497	2573	2600	15	0.30
7	Upper Germanic Trias (RN) (Keuper Fm, Muschelkalk Fm, Röt Claystone Mb, Röt Evaporite Mb, Solling Claystone Mb) **Primary top seal**	162	3070	2600	26****	0.30
8	Lower Germanic Trias (RB) = Hardegsen Fm (RBMH) + Upper Detfurth Sandstone Mb (RBMDU) **Reservoir, upper part, good producer**	74	3232	2600	20	0.2
9	Lower Germanic Trias (RB) = Lower Detfurth Sandstone Mb (RBMDL) + Volpriehausen Sandstone Mb (RBMV) **Reservoir, lower part, poor producer**	137	3305	2600	25	0.2
10	Rogenstein Mb, RBSHR + Main Clayst Mb, RBSHM (Lower part of Lower Germanic Trias)	140	3442	2600	29	0.30
11	Zechstein Group, ZE (Permian)	27	3582	2100	20	0.35
12	Slochteren Fm, ROSL + Carboniferous, undefined (DC)	>23	3608	2650	30	0.25

*Thickness and depth based on exploration well P18-02 as this well penetrates all the units down to the Carboniferous base.

**Rock density assumed based on common values for different lithologies.

***Elastic rock properties derived indirectly from well logs from P-18-A-02 and P18-2.

****Young's modulus of the caprock measured in laboratory test on samples from Röt/Solling caprock performed by Utrecht University.

6.2.4. In situ stress

The orientations and magnitudes of the principal in situ stresses are the key input parameters required for geomechanical analyses. In the West Netherlands Basin the minimum in situ stress is horizontal and the stress regime is extensional or normal-faulting (i.e. the largest principal stress is vertical).

The regional minimum in situ stress (Shmin) orientation in the West Netherlands Basin is in northeast-southwest direction (World Stress Map, Reinecker et al., 2005). Field data from P18 show that *Shmin* orientation in well P18-2A6 is 55E - 235NW, which is in agreement with regional stress orientation (Figure 6.6). Determination of stress orientation in well P18-2A6 was based on borehole breakouts analysis (*Schlumberger report, 1977*).

The magnitude of *Shmin* is determined from leakoff test data from wells in P18 (). The estimate is based on a polynomial fit to all but one leakoff test data as a function of depth (D):

$$Sh\min = 2.2 * 10^{-6} D^2 + 1.08 * 10^{-2} D \qquad (6.3)$$

This relationship fits data better than for example the relationship for the North Sea region provided by Breckels and van Eekelen (1982).

The largest principal vertical stress (*Sv=Smax*) is calculated assuming a lithostatic gradient of 2.25 bar/10m. The hydrostatic stress is determined from water density of 1.078 kg/l measured on a sample taken from a neighbouring field. Based on the given stress and pressure gradients, the initial total stresses in the P18 reservoir at a reference depth of 3400 mTVD amount to *Sv*=765 bar (76.5 MPa) and *Shmin*=622 bar (62.2 MPa). The initial fracturing gradient is *FG*=1.8 bar/10m.

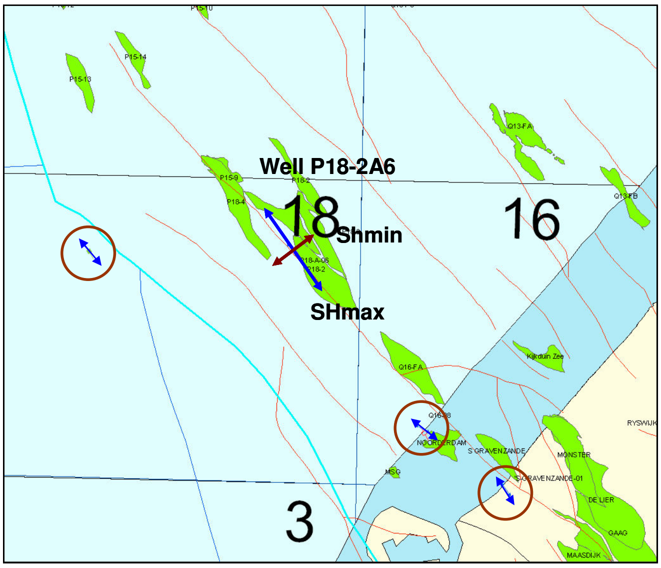

Figure 6.6: Map showing horizontal stress orientations in P18, determined from borehole breakouts in well P18-2A6, and in some neighbouring fields (data from World Stress Map).

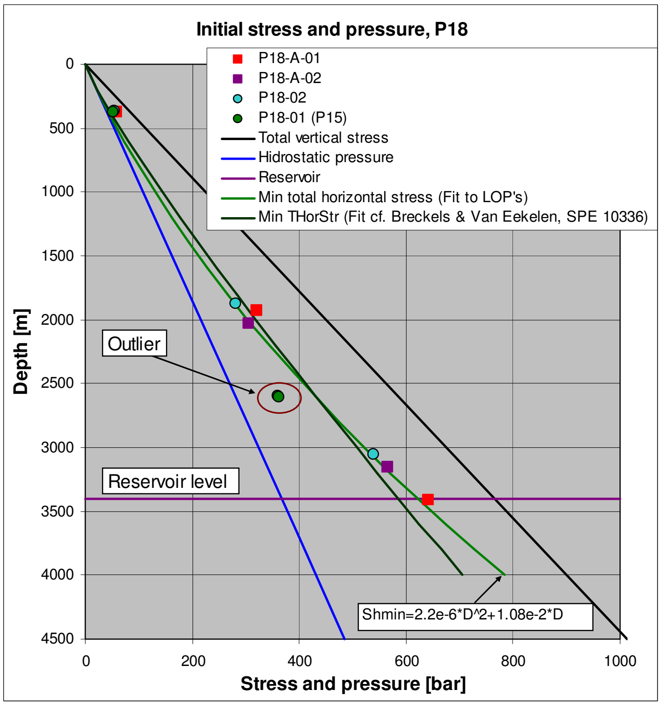

Figure 6.7: Leakoff test data from wells in P18 used to determine magnitude of the minimum total horizontal stress (Shmin) as a function of depth (h). Total vertical stress is calculated from an assumed lithostatic gradient of 2.25 bar/10m. Hydrostatic pressure is calculated from water density of 1.078 kg/l measured on a sample taken from the neighbouring Q16-8 field.

6.3. Geomechanical numerical model

6.3.1. Schematisation and mesh

A two-dimensional (2D) finite element (FE) model of the P18 gas field was developed using a general-purpose FE program DIANA (TNO, 2010). The numerical model represents a plane strain model based on an interpreted seismic cross-section along Inline 1185 running in a SW-NE direction (Figure 6.2).

The location and orientation of the cross-section was chosen in such a way to be able to evaluate the maximum poro-mechanical effects of CO_2 injection on the mechanical seal integrity and fault stability:

- The modelling plane is perpendicular to the maximum horizontal stress, which implies that both the maximum principal (vertical) stress and the minimum horizontal stress lie in the modelling plane.
- The plane is perpendicular to the main geological structure and boundary faults oriented in a NW-SE direction. The (largest) true dip is visible on the modelling plane.
- The plane intersects all three segments of compartment P18-2 which enables studying the overall impact of possibly different pressure increase in each of the three segments.
- The chosen cross-section through compartment P18-2 is also representative for other two compartments P18-4 and P18-6, which are structurally less complex since each of these two compartments forms a single structure compartment.

General drawdown of a 2D modelling approach is that a strike-slip stress regime and strike-slip movement on faults can not be modelled. Current study aims at investigating the potential for normal and reverse faulting, for which a 2D modelling approach is appropriate.

The developed finite element model of P18 preserves the structural complexity of the interpreted seismic cross-section (Figure 6.8 & Figure 6.9). Model dimensions are 10 by 6 km. The model consists of a total of 8,700 elements and 17,700 nodes. Quadratic triangular plane strain elements (the CT12E element type in DIANA notation) were used to model the geomechanical units. 5 boundary faults and 4 faults in the overburden were modelled by using the 1m-thick interface elements which are suitable for modelling the fault slip behaviour (the CL12I element type).

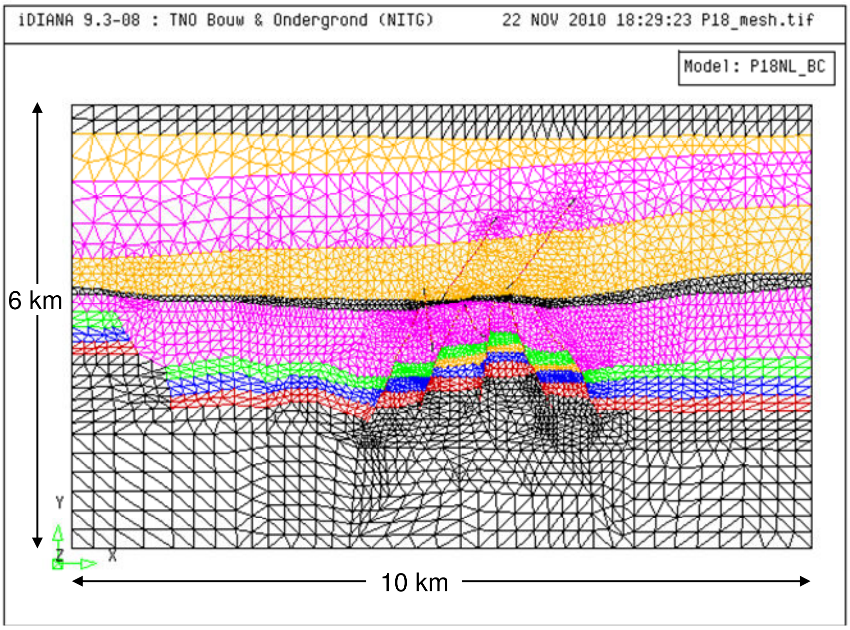

Figure 6.8: Mesh for a two-dimensional plane strain finite element DIANA model of the P18 field.

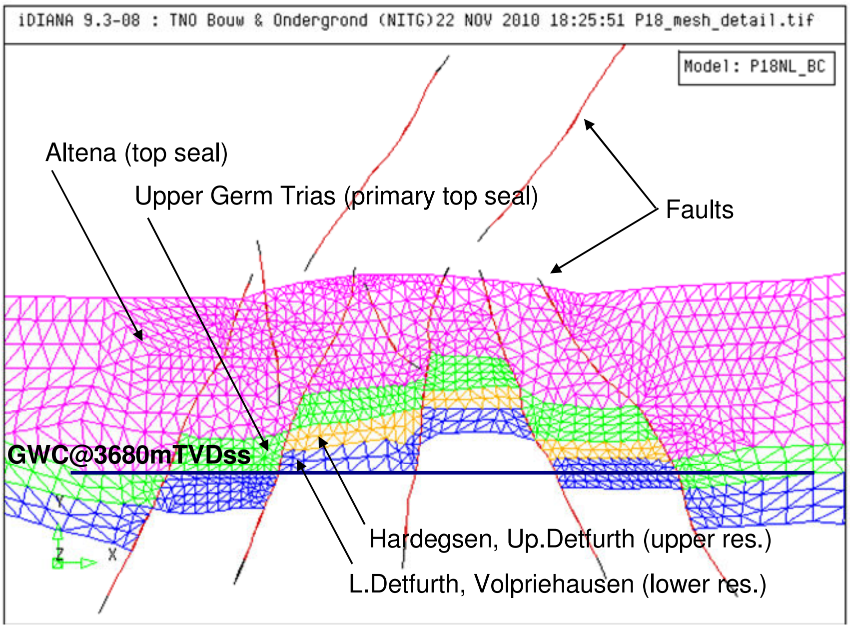

Figure 6.9: Enlarged central part of the mesh showing the main faults, reservoir and top seal.

6.3.2. Boundary and initial conditions

Structural boundary conditions were defined by imposing displacement constraints along the model boundaries. Vertical displacements were not allowed along the bottom boundary, while the top boundary was free to move in any direction. The lateral boundaries were constrained in horizontal direction.

The initial vertical stress was introduced in the numerical model by combining the following loads (Figure 6.10):

- The weight of the formations, which is calculated by applying the gravity load on the model.
- The initial pressure of 375 bar in the reservoir above the GWC.
- The hydrostatic pressure in other model units except the reservoir.
- The initial reservoir pressure on the fault segments that laterally bound reservoir blocks.
- Hydrostatic pressure on all other fault segments which do not bound reservoir blocks.

The initial horizontal stress was introduced in the numerical model by defining and applying the ratio of horizontal-to-vertical effective stress Ko'= σ3'/σ1' = Sh'/Sv'.
A value of Ko=0.81 was used for the total stresses, which is equivalent to a value of Ko'=0.63 for the effective stresses. This value was derived from a minimum horizontal stress gradient of 1.82 bar/10m based on the leakoff test data (Section 6.2.4).

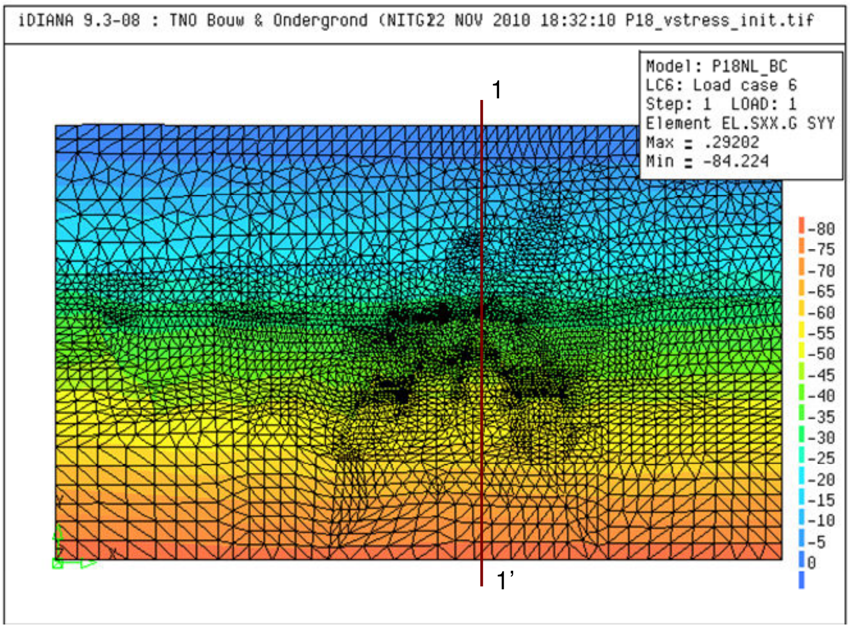

Figure 6.10: Initial vertical effective stress in the finite element model of the P18 field. Compressive stresses are negative.

6.3.3. Pressure loads

Pressure histories and pressure forecasts are required for geomechanical analyses. Measured pressure data from all wells in P18 were supplied by TAQA. TNO developed analytical models of CO_2 injection and calculated pressure forecasts for each of the three compartments (Figure 6.11, Figure 6.12 and Figure 6.13). TNO also performed a full-scale reservoir simulation modelling using MoReS. Simulation scenarios assumed that the reservoir compartments will be re-pressurized close to the initial pressure.

Pressures from analytical estimates were use in analytical geomechanical analyses. Pressures from MoReS simulation were used in numerical finite element geomechanical analyses. Besides the BHP in injectors from MoReS simulations (shown in Figure 6.11, Figure 6.12 and Figure 6.13), the average reservoir pressure were also required for FE modelling. This pressure represents the input loads for DIANA FE simulations. The evolution of the average reservoir pressure in each segment of the P18-2 compartment determined from MoReS output is presented inFigure 6.14, Figure 6.15 and Figure 6.16. Note that the pressure evolution in the reservoir is different in the upper part of the reservoir (Hardegsen and Upper Detfurth, which are good producers) from that in the lower part of the reservoir (Lower Detfurth and Volpriehausen, which are poor producers). An overview map showing the location of different compartments and segments in the P18 field is presented in Figure 6.17.

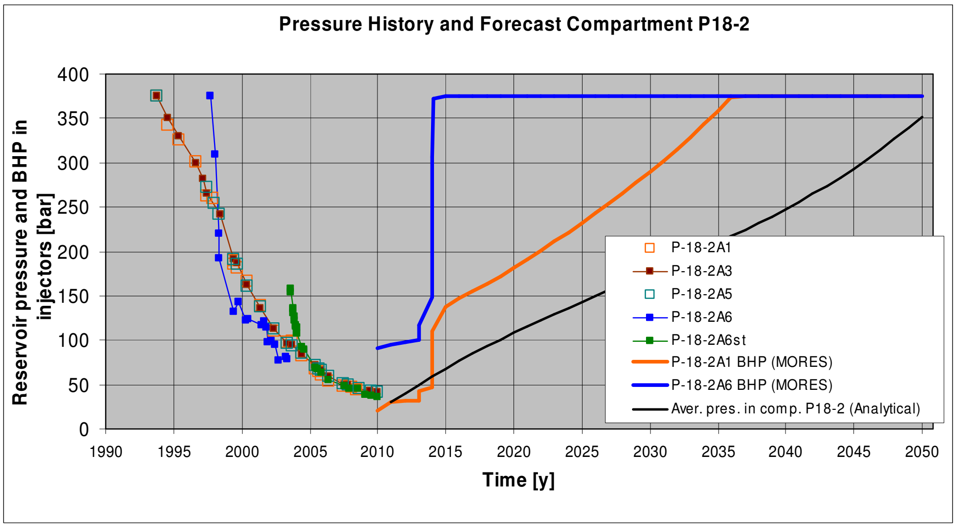

Figure 6.11: Measured pressure data in compartment P18-2 and pressure forecasts based on an analytical model and MoReS simulations performed by TNO.

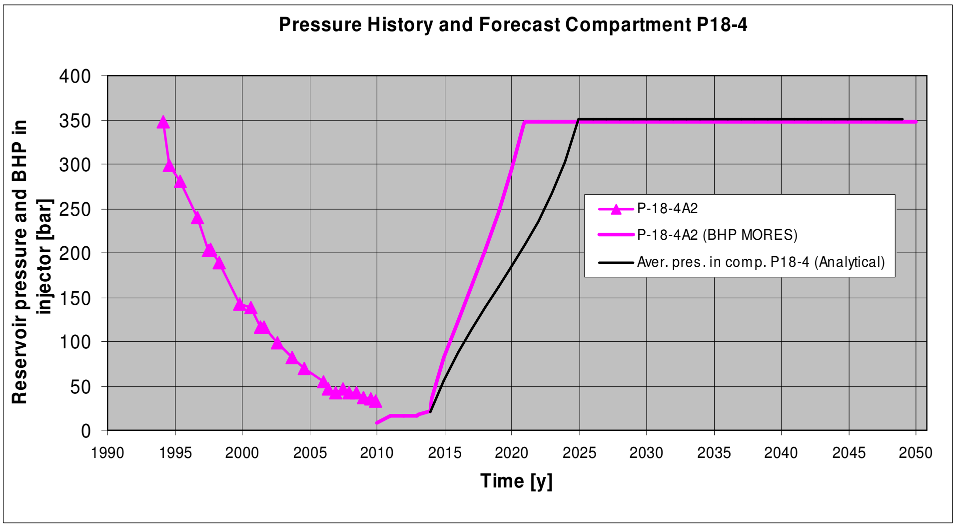

Figure 6.12: Measured pressure data in compartment P18-4 and pressure forecasts based on an analytical model and MoReS simulations performed by TNO.

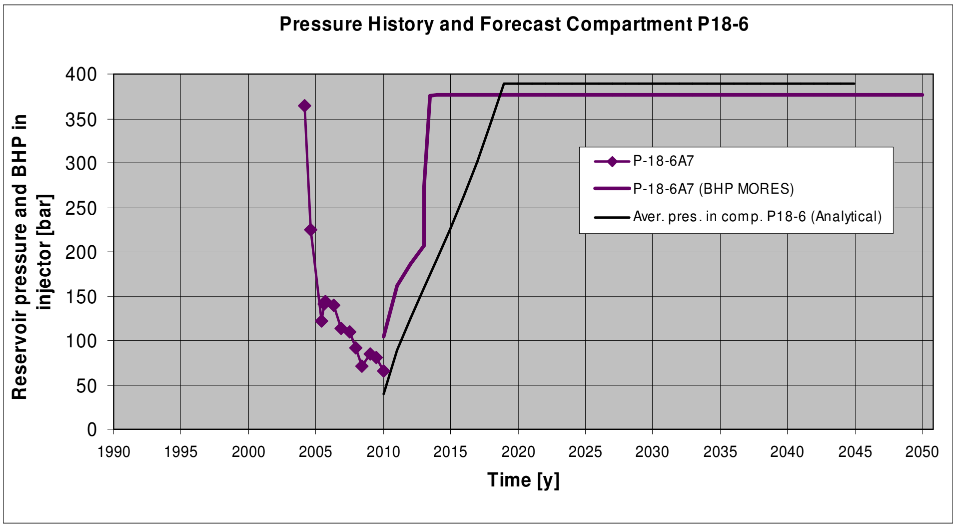

Figure 6.13: Measured pressure data in compartment P18-6 and pressure forecasts based on analytical models of CO_2 injection developed by TNO.

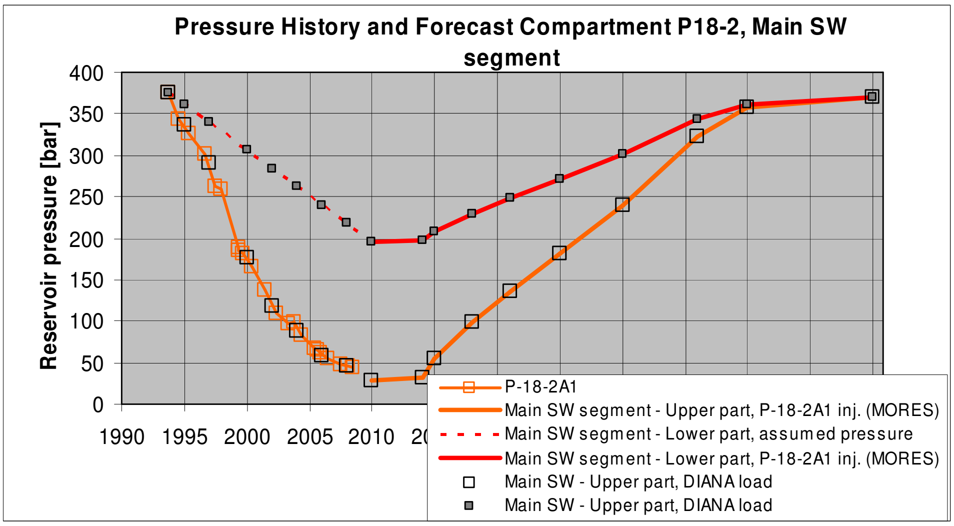

Figure 6.14: Input pressure loads for DIANA FE analysis derived from MoReS simulations. The Main SW segment of compartment P18-2 with the injector P-18-2A1.

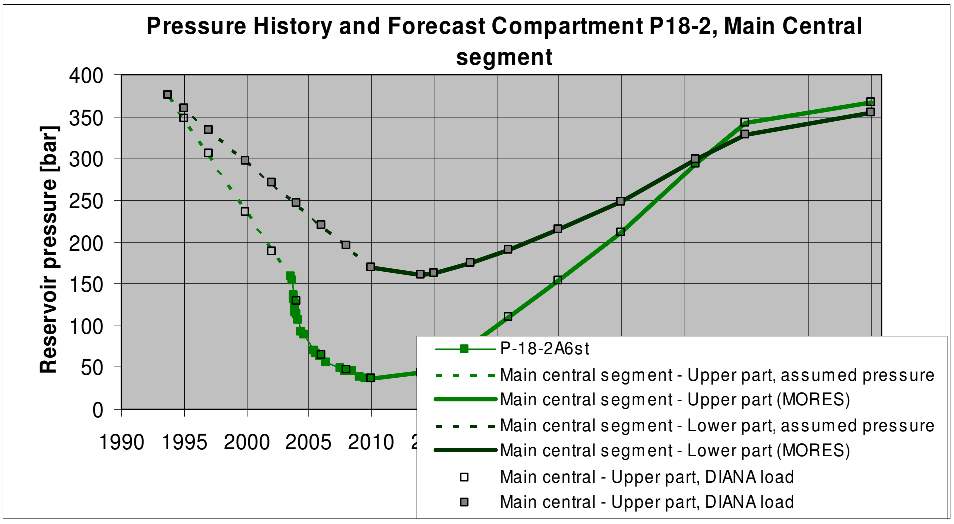

Figure 6.15: Input pressure loads for DIANA FE analysis derived from MoReS simulations. The Main central segment of compartment P18-2 (II) connected to the Main SW segment with the injector P-18-2A1.

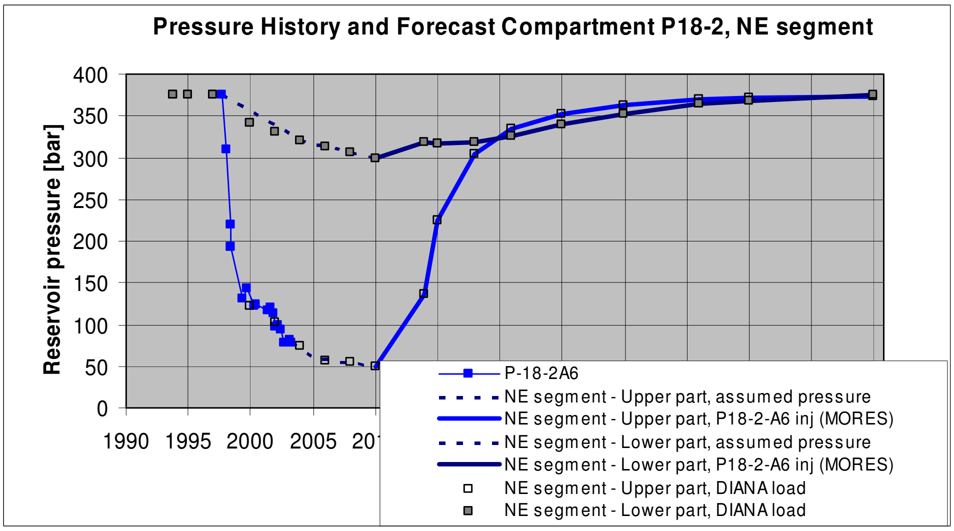

Figure 6.16: Input pressure loads for DIANA FE analysis derived from MoReS simulations. The NE segment of compartment P18-2III, not connected with the other two segments, with the injector P-18-26.

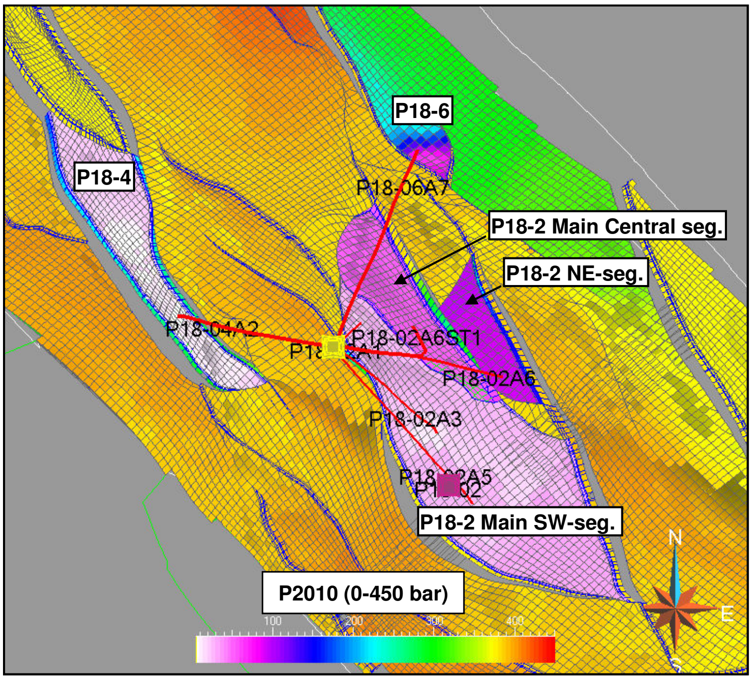

Figure 6.17: Top view of the P18 field showing the location of different compartments and segments. It should be noted that the main central segment and NE seg. are also referred to as sub-compartments P18-2II and P18-2III, respectively.

6.3.4. Calculation scenarios

The Base case scenario and four sensitivities were defined and calculated. The material properties for the differentiated geomechanical units and the initial state of stress were the same in all the runs (described in Sections 6.2.3 and 6.2.4). The sensitivities considered the impact of different pressure evolution in various segments of compartment P18-2.

- BC: Base case (BC).
  The pressure evolution is the same in all three segments of compartment P18-2. The pressure evolution is equal to that of the upper part of the Main SW- segment (Figure 6.14).
- S1: Segments re-pressurization sensitivity (S1-NEseg).
  The pressure evolution is the same in the two connected segments of compartment P18-2 (the Main SW-segment and the Main central segment, P18-2II), but different from that in the third, NE-segment. The pressure evolutions are equal to that of the upper part of the Main SW-segment (Figure 6.14) and the upper part of the NE-segment (P!8-2III), respectively (Figure 6.15).
- S2: Aquifer depletion sensitivity (S2-NEseg-AQdepl).
  As S1, with addition of pressure change in the aquifer supporting the NE segment.
- S3: Reservoir sub-division sensitivity, with aquifer depletion (S3-NEseg-AQdepl-2LAYres).
  As S2, with addition of differential pressure evolution in the upper and lower part of the reservoir segments.
- S4: Reservoir sub-division sensitivity, without aquifer depletion (S4-NEseg-2LAYres).
  As S3, but without pressure change in the aquifer supporting the NE-segment.

6.4. Top seal integrity assessment

6.4.1. Potential for induced fracturing of top seal due to CO_2 injection

Analytical model

The risks associated with hydraulic fracturing of the reservoir rock are related to the possibility of forming fractures in the top seal allowing vertical CO_2 migration, possible spill paths for lateral CO_2 migration and direct charging of faults by injected CO_2. Conditions for safe CO_2 injections without fracturing of the reservoir rock are met when the bottom hole pressure (BHP) in the injection well is lower that the minimum in situ stress (Shmin) in the reservoir. Both parameters are dynamic and evolve during depletion and injection period. Evolution of the Shmin was estimated using available data, current practices and methods, while evolution of reservoir and injection pressures (BHP) was based on analytical CO_2 reservoir engineering forecasts. Comparison of the Shmin and the BHP predictions for the Base Case (Figure 6.18) and several variations around it (Figure 6.19) show that the BHP will not exceed the Shmin, which implies that CO_2 injection will not induce fracturing of the reservoir rock in the three compartments under consideration. This conclusion applies to the compartments re-pressurized up to the initial reservoir pressure.

Besides the poro-mechanical effects considered above, it is necessary to consider the impact of thermal effects caused by a difference in temperature between the injected CO_2 and the host reservoir rock. The main consequence of thermal effects is additional decrease of the Shmin in the near-well area promoting easier fracturing of the reservoir rock. Stress reduction due to cooling was estimated analytically using the following expression (Zoback, 2007):

$$\Delta\sigma_T = \alpha\, E\, \Delta T / (1-\nu) \qquad (6.4)$$

$\Delta\sigma_T$ is the thermal stress change, α is the linear coefficient of thermal expansion, E is the Young's modulus of elasticity of the reservoir rock, ν is the Poisson's coefficient and ΔT is the temperature difference between the injected fluid and the reservoir rock.

For a value of α=1E-5 $°C^{-1}$, ΔT=10°C and typical values of the elastic parameters for the Bunter sandstone given in Table 20, the thermal stresses in the near-well area can reach 2.25 MPa. This is the maximum value which is representative for the worst case conditions. In the reality the thermal effects will be lower and can be predicted more accurately with pseudo-thermal MoReS simulator.

Combined poro-mechanical and thermal effects of CO_2 injection suggest that induced fracturing can occur in the latest stage of CO_2 injection, when the pressure in reservoir compartment is approaching the initial pressure. At this stage the BHP can exceed the Shmin if the difference in temperature between the CO_2 and the reservoir rock is more than 50°C (Figure 6.20). In case of fracturing of the reservoir rock, there is a risk of fracture growth into the caprock and mechanical damage of the top seal. Although limited fracture growth into the seal may not be harmful, induced fractures still provide access routes for CO_2 and brine penetration into the seal. The potential for fracture growth into the top seal is dependent on several geological, geomechanical, reservoir and well engineering parameters and has to be studied separately in case of intentional hydro-fracturing of the reservoir.

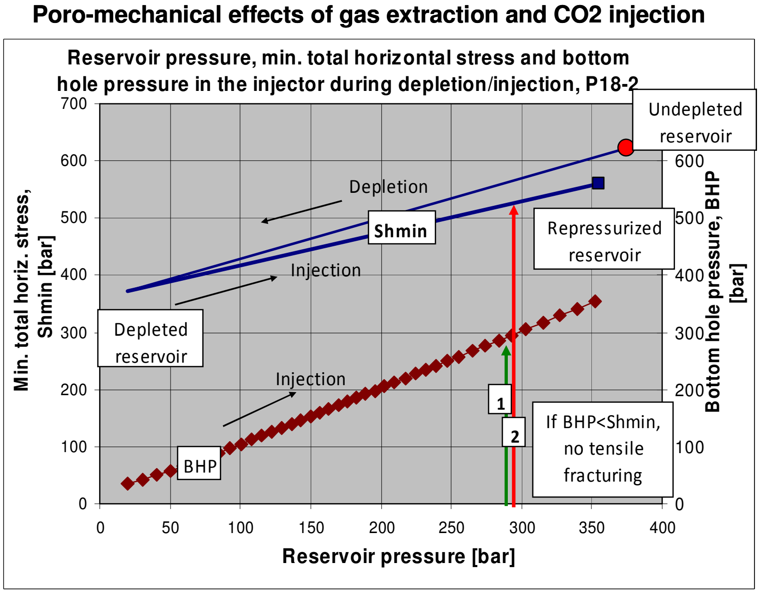

Figure 6.18: Analytical estimates of the maximum admissible injection pressures in compartment P18-2 that will not cause fracturing of the reservoir rock and top seal (excluding thermal effects). The conditions for safe injection are met when the bottom hole pressure (BHP) in the injection well is lower than the minimum in situ stress (Shmin) in the reservoir.

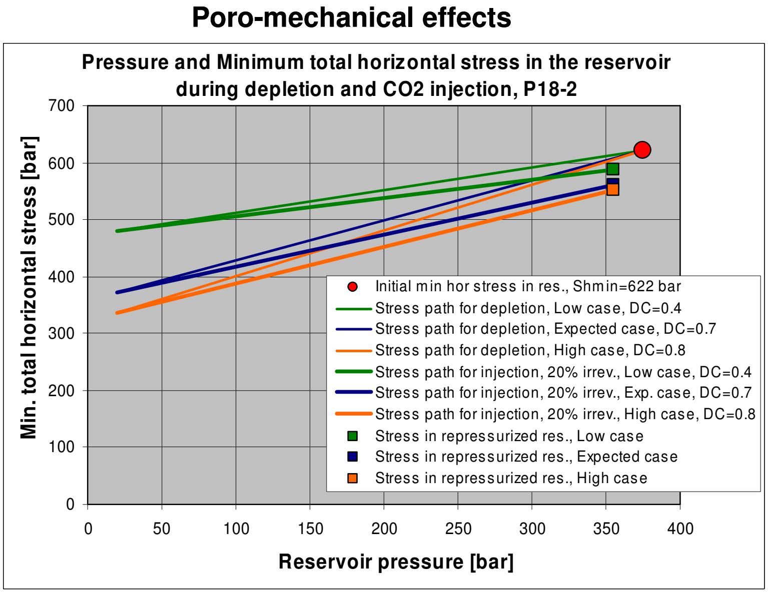

Figure 6.19: Analytical estimates of the possible reservoir stress paths in compartment P18-2 for depletion and injection. DC=depletion constant defined as DC=$\gamma h=\Delta Shmin/\Delta p$.

Poro-mechanical and thermal effects

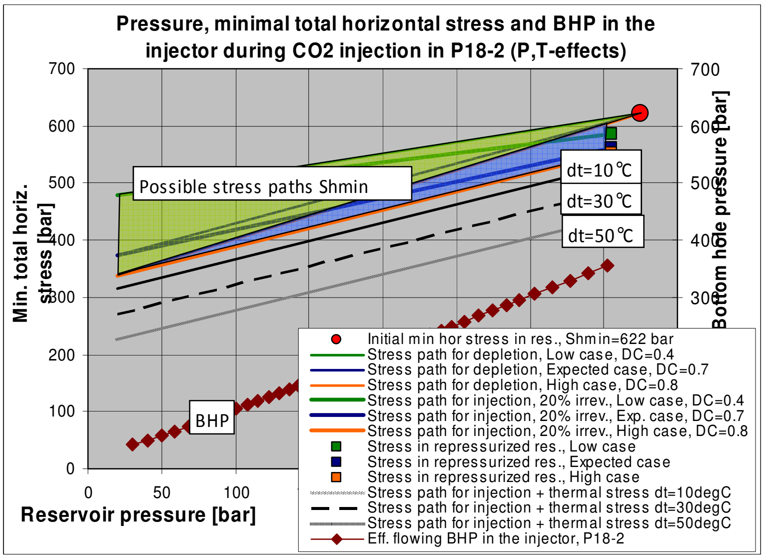

Figure 6.20: Analytical estimates of the maximum admissible injection pressures in compartment P18-2 that will not cause fracturing of the reservoir rock and top seal (combined poro-mechanical and thermal effects). The conditions for safe injection are met when the bottom hole pressure (BHP) in the injection well is lower than the minimum in situ stress (Shmin) in the reservoir decreased by the thermal stresses. DC=depletion constant; dt=temperature difference between injected CO_2 and reservoir rock.

Numerical model

Numerical analysis was performed to assess the mechanical impact of reservoir depletion and re-pressurization on the reservoir rock and the top seal. The numerical model makes possible investigating the stress perturbations within the reservoir and in its surroundings taking into account the poro-mechanical effects. Note that the model cross-section intersects compartment P18-2 as explained in Chapter 6.3.

In the reservoir, the largest stress change occurs at the end of depletion period (2010), when the reservoir is depleted from the initial 37.5 MPa (375 bar) down to 3 MPa (30 bar). Depletion causes an increase in the (compressive) vertical effective stresses in the depleted reservoir which is approximately equal to the rate of depletion (Figure 6.21 and Figure 6.22). At the same time, the horizontal effective stresses also increase. This increase is, however, much smaller and amounts to about 1/4 the increase in the vertical effective stress. From the elasticity theory it follows that dSh'= dSv'*v/(1-v) , where dSh', dSv' are the change in the horizontal and vertical effective stresses, respectively, and v is the Poisson's coefficient.

Changes of the vertical, horizontal and shear stress in the reservoir and its surrounding due to depletion are shown in Figure 6.23, Figure 6.24 and Figure 6.25. As discussed above, both the vertical and horizontal effective stresses in the reservoir increase .The rate of stress change is much lower in the surrounding rock than in the reservoir, usually by one order of magnitude.
The pattern of vertical stress change shows typical arching effects with stress relaxation above the reservoir (i.e. vertical stress becomes less compressive) and stress concentration at the abutments (stress becomes more compressive,Figure 6.23).
The pattern of horizontal stress change shows the opposite effects with regard to the vertical stress change. Above the reservoir, horizontal stresses become more compressive, while in the abutments horizontal stresses become less compressive (Figure 6.24).

The pattern of shear stress change shows the largest changes in the reservoir at the areas where reservoir segments partially overlap (Figure 6.25). In the surrounding rock, the largest change in the shear stress can be observed in the vicinity of the edges of the depleting reservoir (Figure 6.24).

During injection period, the stress development in the reservoir and its surrounding is the opposite of the stress development during depletion. The stress change, which is maximal when the reservoir is fully depleted, gradually reduces as the reservoir is re-pressurized back to the initial pressure. In a hypothetical case of a pure elastic response, production-related stress change would practically vanish at the end of injection period.

Initial stress before depletion

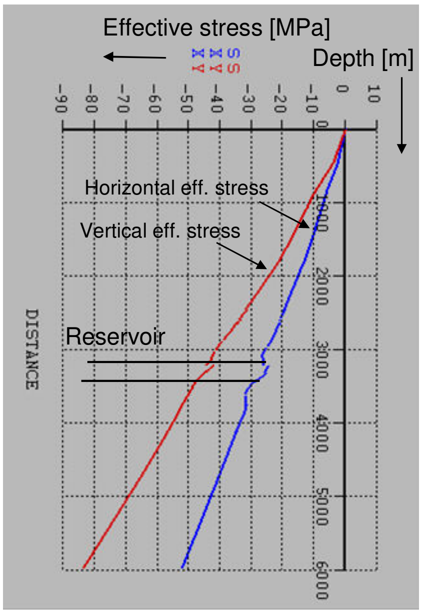

Figure 6.21: Vertical and horizontal effective stress versus depth before depletion.

Stress in depleted reservoir

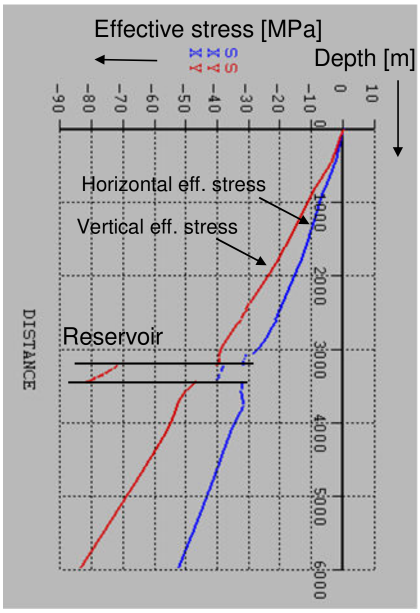

Figure 6.22: Vertical and horizontal effective stress versus depth after depletion.

Change in the vertical effective stress for depleted reservoir

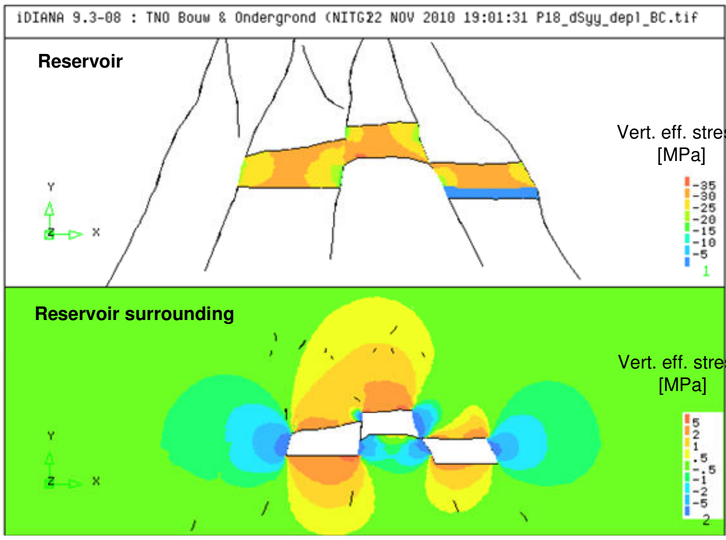

Figure 6.23: Change in the vertical effective stress in the depleted P18 field for the Base Case (compartment P18-2). Compressive stresses are negative.

Change in the horizontal effective stress for depleted reservoir

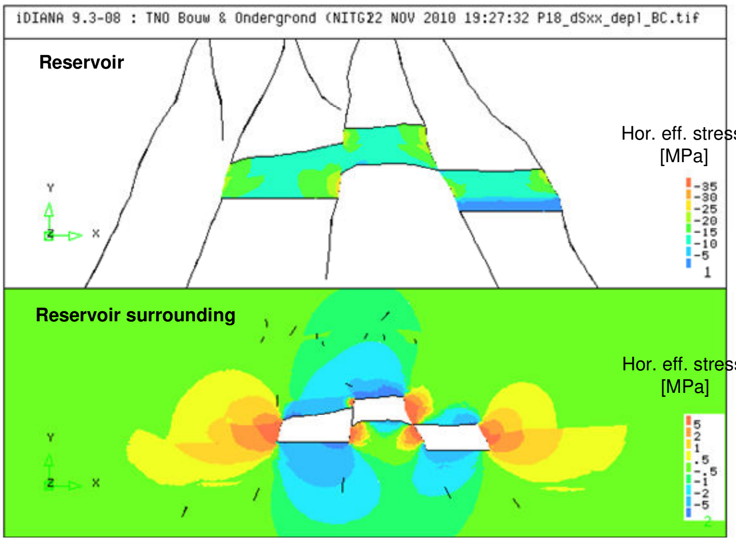

Figure 6.24: Change in the horizontal effective stress in the depleted P18 field for the Base Case (compartment P18-2). Compressive stresses are negative.

Change in the shear stress for depleted reservoir

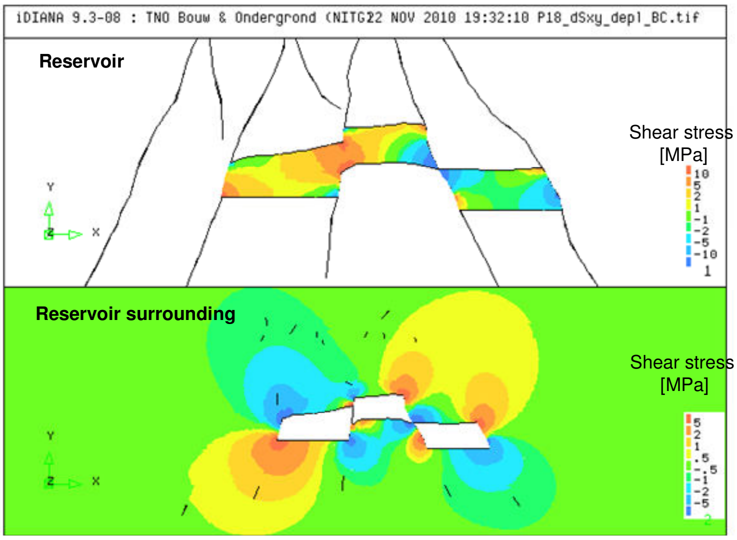

Figure 6.25: Change in the shear stress in the depleted P18 field for the Base Case (compartment P18-2).

Additional analysis was performed to identify locations in the model which are mostly affected by the induced stress changes. We defined a parameter called the mobilised shear strength (MSS) which can be calculated by dividing the shear stress (τ) by the normal effective stress (σ), i.e. MSS= τ / σ. By plotting this parameter for the whole model, we can identify locations with the largest MSS values where the rock material is close to, or at failure. For the case of depleted reservoir, the largest values of MSS are nearby the edges of the reservoir segments (Figure 6.26). For a number of monitoring points located in the critical areas we plotted the stress path diagrams (Figure 6.27 to Figure 6.29). The stress path diagrams show the stress evolution during reservoir depletion and future CO_2 injection at the selected monitoring points located in the reservoir and the top seal.

The stress paths for the reservoir rock show a significant increase of both normal effective stress (~ 20 MPa) and shear stress (~10 MPa) during depletion period (Figure 6.27). In order to assess the mechanical effect of depletion on the reservoir rock, we can compare the relative position of the stress paths with the Mohr-Coulomb shear strength criterion thought to be representative for the reservoir rock (cohesion c=2 MPa and friction angle Fi=25°). From the comparison it is apparent that the stress paths do not show critical behaviour, i.e. the paths are not converging towards the failure envelope.
During injection, the stress paths development is in the opposite direction, towards the initial state of stress before gas production. In the ideal case of pure elastic behaviour of the reservoir rock and the surrounding rock, re-pressurization of a depleted reservoir back to the initial pressure would undo the production-related stress perturbations.
Hence, the stress change and the related mechanical impact on the reservoir rock are the largest at the time when the reservoir is fully depleted.

The stress paths for the top seal show predominantly shear stress change during depletion, while changes in the normal effective stress are minor (Figure 6.28 and Figure 6.29). The direction of shear stress change is, however, different in the top seal (element 226) and the side-seal (elements 325 and 928). The stress development is non-critical, i.e. away from the failure envelope, in the top seal and critical, i.e. towards the failure envelope, in the side seal.
In order to assess the mechanical effect of depletion on the seal, we compare the relative position of the stress paths with the Mohr-Coulomb shear strength criterion based on the experimental data obtained in HPT lab of Utrecht University (c=27 MPa and Fi=28°; Figure 6.28 and Figure 6.29). Apparently, the induced stresses can mobilise at most 50% of the shear strength of the seal material, which suggests elastic deformation only. The second failure envelope with c=7 MPa and Fi=28° is hypothetical and shows the strength of the top seal necessary to initiate shear failure.
During injection, the stress paths development is in the opposite direction, towards the initial state of stress before gas production.

In conclusion, the largest stress changes and the associated mechanical effects affecting the top- and side seal are expected near the edges of the reservoir segments, where stress concentrations occur. Plastic deformation of the reservoir rock and the seal may occur locally at these locations, having in mind the natural variability of (shear) strength which can exist in these rocks.

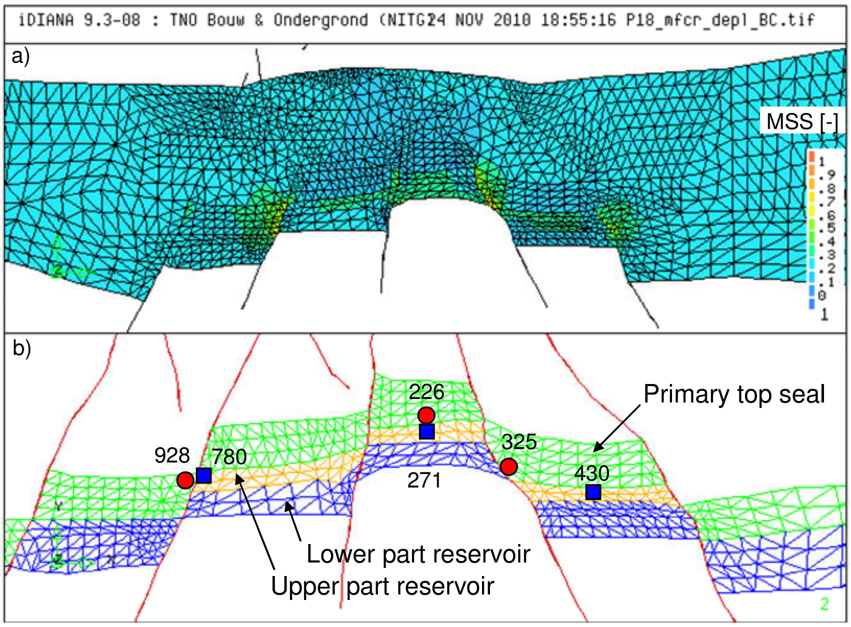

Figure 6.26: Mobilised shear strength (MSS) of the rock for the case of depleted reservoir (MSS=Shear stress / Normal effective stress). b) Location of the selected monitoring points (i.e. the finite elements) used to present the results of FE analysis in Figure 6.28 to Figure 6.29.

Feasibility study P18

Stress paths for the reservoir rock for depletion, Base case

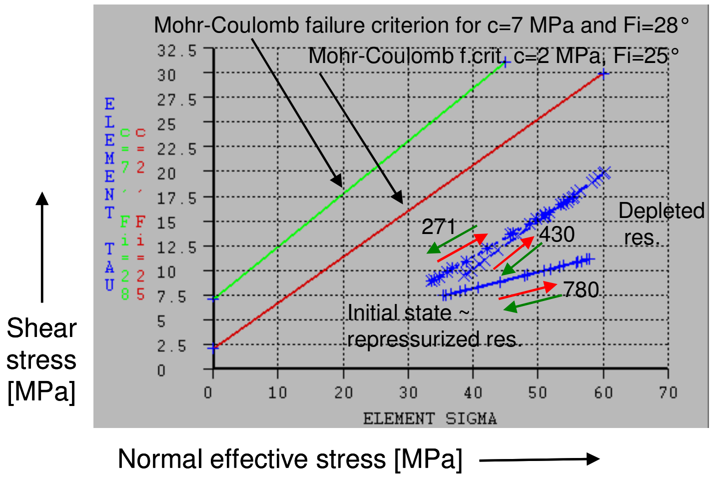

Figure 6.27: Stress paths for the monitoring points in the reservoir for depletion (Base case). The direction of stress development is shown by red arrows. The Mohr-Coulomb failure envelope with c=2 MPa and Fi=25° for the reservoir rock is based on the assumed shear strength parameters. During injection, the stress paths development is in the opposite direction, towards the initial state before gas production (shown by green arrows).

Stress paths for the top seal for depletion, Base case

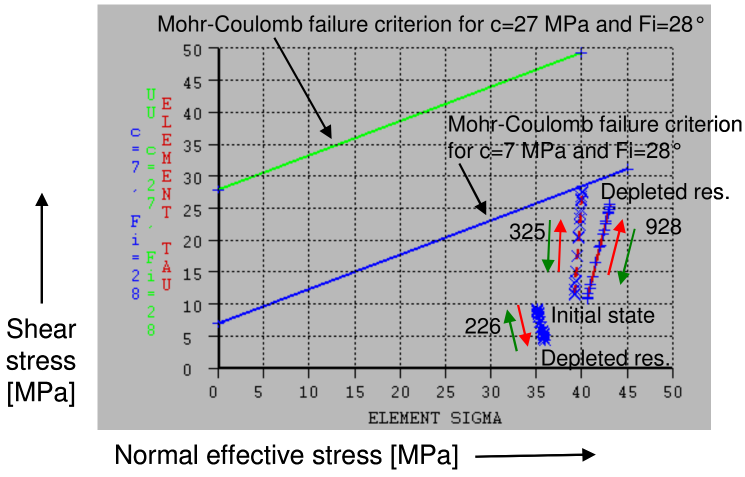

Figure 6.28: Stress paths for the monitoring points in the top seal for depletion (Base Case). The direction of stress development is shown by red arrows. Location of the selected elements is presented in Figure 6.26. The Mohr-Coulomb failure envelope with c=7 MPa and Fi=28° is based on the experimental data obtained in HPT lab of Utrecht University. The Mohr-Coulomb failure envelope with c=7 MPa and Fi=28° is hypothetical and shows the strength of the top seal necessary to initiate shear failure. During injection, the stress paths development is in the opposite direction, towards the initial state before gas production (shown by green arrows).

Stress paths for the top seal for depletion, Sensitivity S4: Reservoir subdivision into lower and upper parts with different pressure evolutions

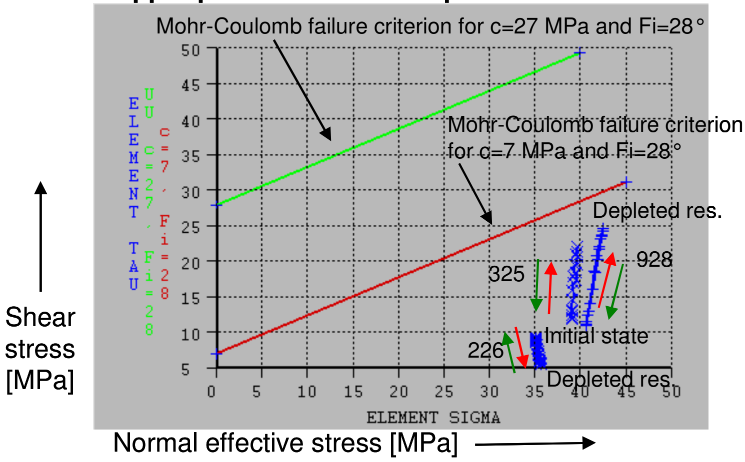

Figure 6.29: Stress paths for the monitoring points in the top seal for depletion (Sensitivity S4). The direction of stress development is shown by red arrows. The Mohr-Coulomb failure envelope with c=7 MPa and Fi=28° is based on the experimental data obtained in HPT lab of Utrecht University. The Mohr-Coulomb failure envelope with c=7 MPa and Fi=28° is hypothetical and shows the strength of the top seal necessary to initiate shear failure. Note that the stress path at the monitoring point 325 does not reach the hypothetical failure envelope as in the Base case due to different pressure evolution in the upper and lower part of the reservoir (Figure 6.28).

6.5. Fault seal integrity assessment

6.5.1. Fault seal analysis

The sealing capacity of the faults that intersect and bound the Bunter reservoir was determined as a function of Shale Gouge Ratio (SGR), i.e. using the clay smear approach (e.g. Yielding, 2002). In the SGR method, hydraulic properties of faults are determined by the amount of shale contained in the fault rock. The SGR depends on the lithology of the host rock and on the throw of a particular point on the fault plane. Continuous smears and significant sealing capacity are present when SGR>0.2. Besides the SGR method, juxtaposition maps were made to investigate juxtaposition of different lithologies across the faults and identify potential leak points (Allan, 1989). The SGR analysis and juxtaposition maps were calculated on the reservoir-scale Petrel model of P18.

The boundary faults of all three compartments are found to be sealing (Figure 6.30). Field production data indicate that P18-2, P18-4 and P18-6 represent separate pressure compartments. The boundary faults of the three main compartments of P18 have such large throws that they juxtapose the reservoir Bunter sequence against the sealing Upper Germanic Trias (RN) and occasionally against a lower part of Altena (AT). None of the faults offsets the top of the Altena Group, so that the shales of Altena will always seal off formations below.

The internal faults which split compartment P18-2 into three segments are mostly conductive (Figure 6.31). These faults have much smaller throws then boundary faults. Generally, reservoir sand is juxtaposed against sand across the internal faults and the SGR is low. Most of the internal faults are therefore permeable. The only exceptions are fault F12 and F18, which have a larger SGR and therefore either one, or both of them, are sealing. This was supported by field data which showed the absence of pressure communication between the segment drained by well P18-02A6 and the other two segments of compartment P18-2, which are in mutual pressure communication.

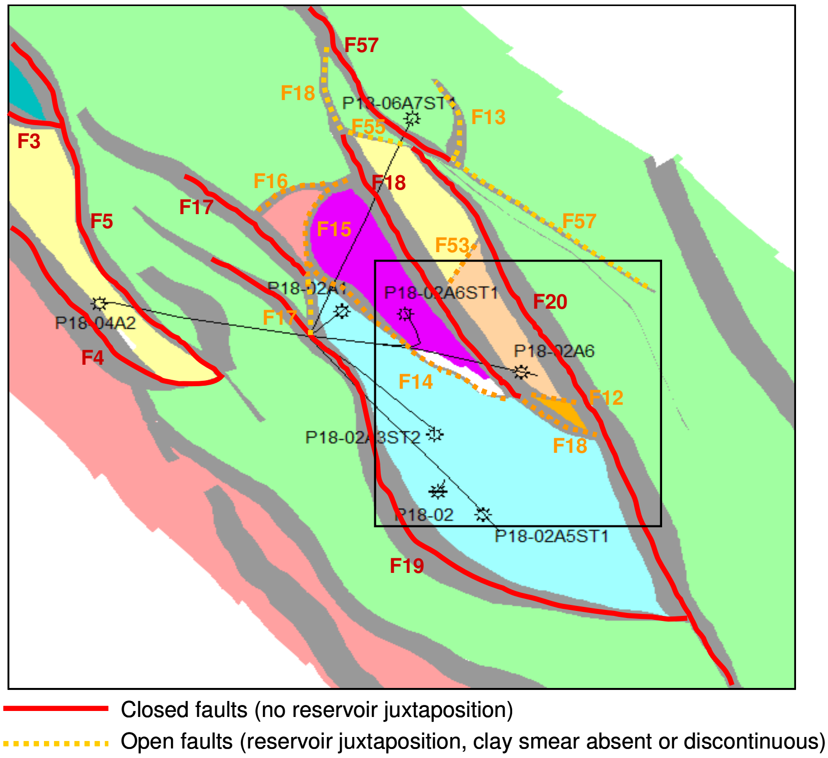

Figure 6.30: Top view of P18 showing sealing capacity of faults determined as a function of Shale Gouge Ratio (SGR).

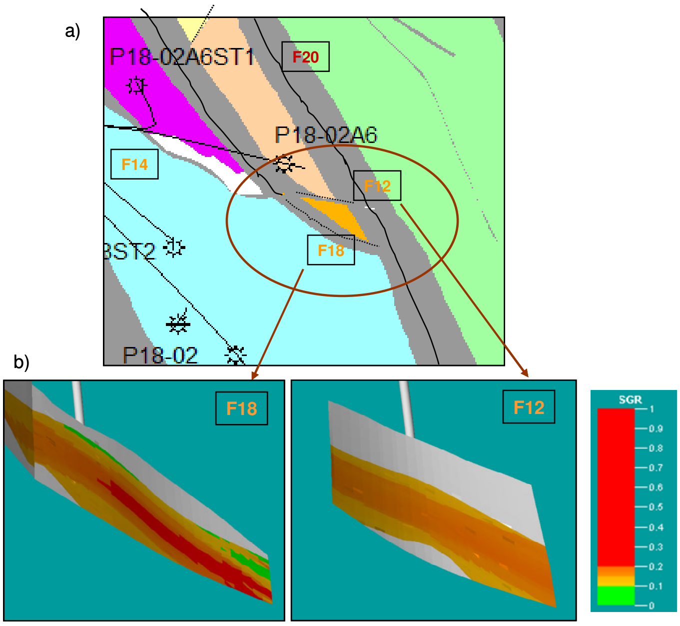

Figure 6.31: a) Top view of a part of compartment P18-2 and b) the Shale Gouge Ratio (SGR) for sealing capacity assessment of faults F12 and F18. According to the SGR, either one or both faults can be sealing (continuous smears and significant sealing capacity are present when SGR>0.2). Field data showed no pressure communication between well P18-02A6 and other wells in compartment P18-2.

6.5.2. Fault stability analysis

Analytical model

Gas extraction and CO_2 injection may cause fault re-activation, i.e. sudden slip movement along faults, which can change their sealing characteristics in such a way that previously sealing faults become conductive to fluid flow. In addition, micro-seismic events (earth tremors) and seismic events of low intensity can occur at the injection site.

The potential for fault re-activation due to gas extraction and CO_2 injection in P18 was estimated by using the Mohr-Coulomb stress circles. A Mohr-Coulomb circle represents the state of stress at the reference depth of 3400mTVDss in undepleted, depleted and re-pressurized compartment P18-2 (Figure 6.32). Note that the effective stresses are used in fault stability analyses. The failure criterion for faults is plotted in the same graph, based on the common shear strength properties of faults (cohesionless faults with a friction coefficient of 0.6).

The initial state of stress in undepleted reservoir, represented by the black circle, is below the Mohr-Coulomb failure line which implies that the fault is stable (Figure 6.32).
During production period, the effective stresses in the reservoir increase and the Mohr-Coulomb stress circles grow in size but do not reach the failure criterion for faults (Figure 6.32). This implies that the faults were stable throughout the production period.
The past history of induced seismicity associated with gas production from fields in the West Netherlands showed no seismic activity in this region.

During the injection period, the state of stress is basically reversed with respect to the depletion period. The state of stress in the undepleted reservoir and the repressurized reservoir differ only slightly, depending on the assumptions about the degree of reversibility of the reservoir stress paths (Figure 6.33 and Figure 6.34).

Finally, we present the effects of a hypothetical case of direct CO_2 injection into a fault or fracture zone (Figure 6.35). In this case representative for the worst case conditions, the effective normal stress on fault would decrease as much as the pressure increases, while the shear stress on fault would not change. This means that the reservoir stress path is now horizontal, leading to faster fault reactivation under lower injection pressures than in the previous cases. Once the critical conditions for fault re-activation have been reached, further injection would lead to ongoing fault instability characterized by stress build-up and release and induced seismicity.

State of stress after depletion

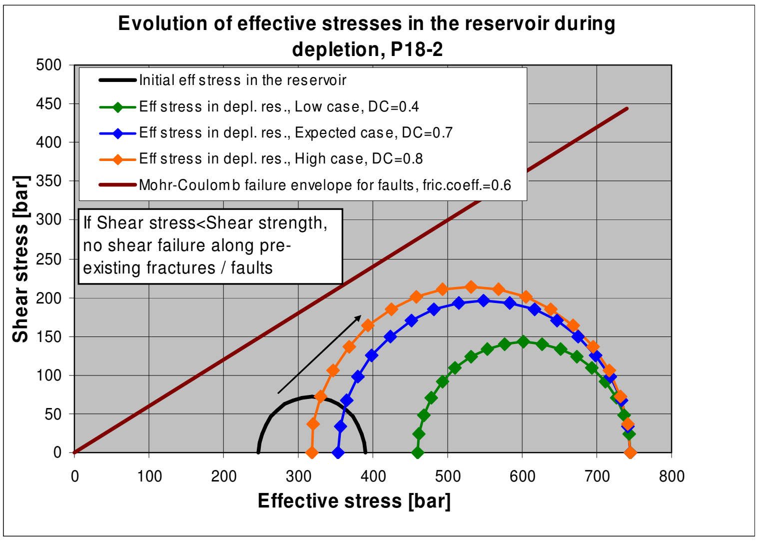

Figure 6.32: Evolution of the effective stresses in the reservoir compartment P18-2 during depletion.

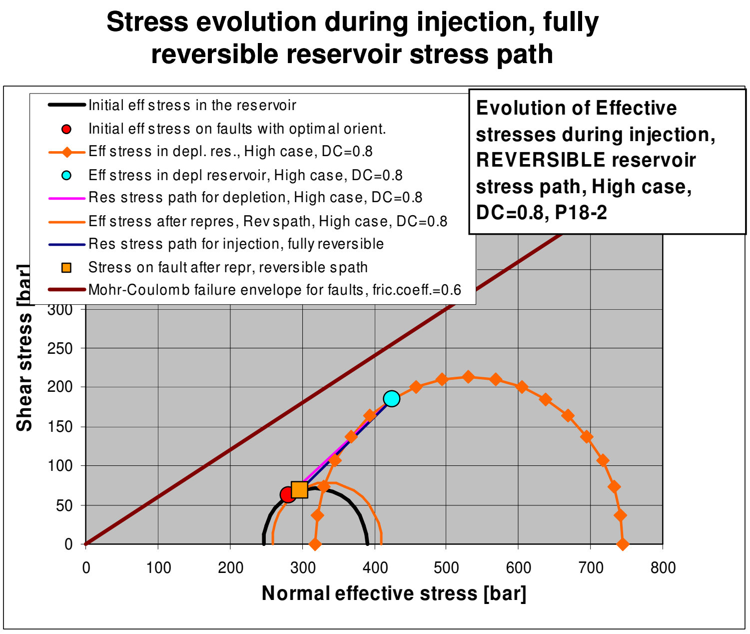

Figure 6.33: Evolution of the effective stresses in the reservoir compartment P18-2 during depletion and subsequent CO_2 injection. The case of fully reversible reservoir stress path.

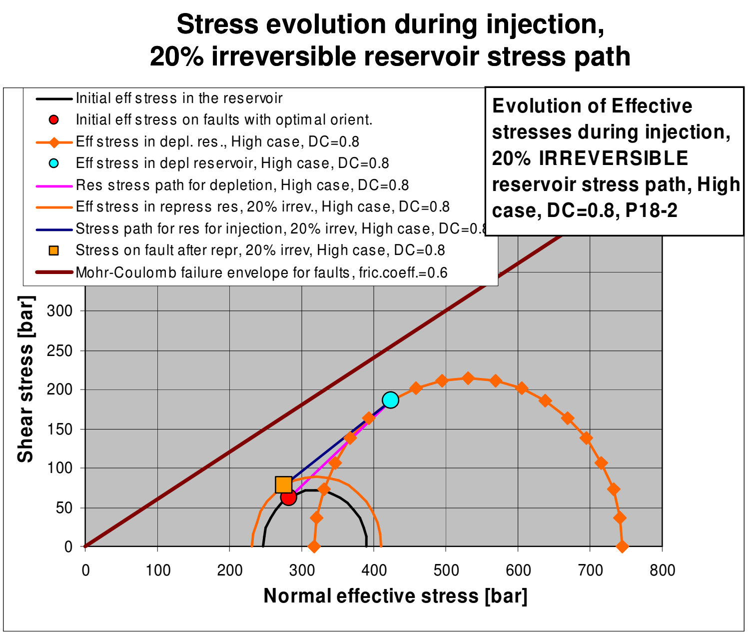

Figure 6.34: Evolution of the effective stresses in the reservoir compartment P18-2 during depletion and subsequent CO_2 injection. The case of 20% irreversible reservoir stress path.

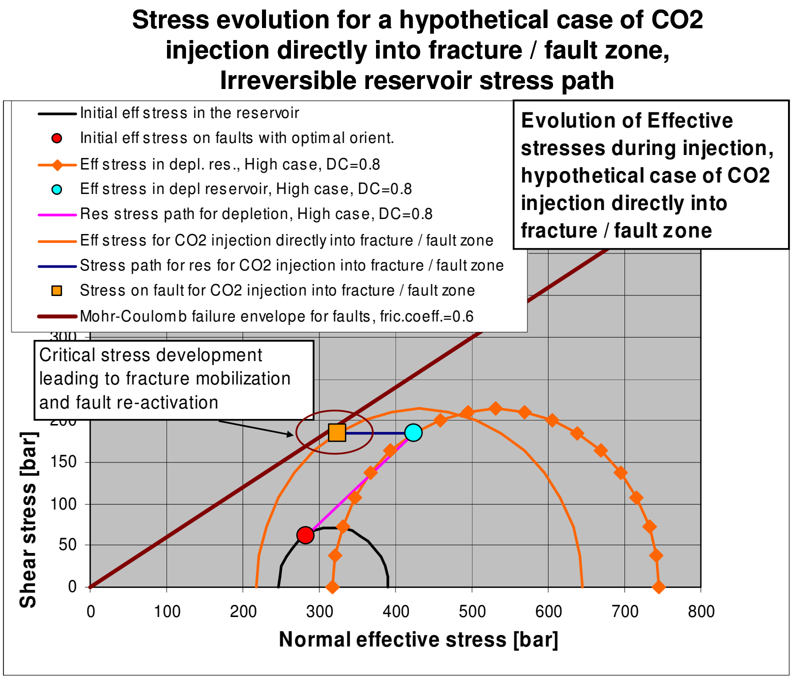

Figure 6.35: Hypothetical case of the effective stress evolution in the reservoir compartment P18-2 during depletion and subsequent CO_2 injection directly into fracture or fault zone. The case of fully irreversible reservoir stress path.

Numerical method

Numerical analysis was performed to assess the mechanical impact of production- and injection-related stress changes on the stability of faults. We defined a parameter called the mobilised friction coefficient (MFC) which can be calculated by dividing the shear traction (ts) by the normal traction (tn'), i.e. *MFC= ts / tn'*. The normal traction is a stress component perpendicular to the fault and the shear traction is a component parallel with the fault. By plotting the MFC we can identify the fault segments with the largest MFC values which are close to, or at failure, indicating fault slip and re-activation. We assumed that the faults are cohesionless, with a friction coefficient of μ=0.6. When the MFC value is approaching the critical value of 0.6, the fault is at risk of failure.

For the case of undepleted reservoir, the values of MFC > 0.5 occur only at two locations in the model, one of which is at the fault tip (Figure 6.36a). For the case of depleted reservoir, the values of MFC > 0.5 occur at several locations nearby the edges of the depleting reservoir segments (Figure 6.36b). However, the average values of MFC calculated for each finite element representing faults do not reach a critical value of 0.6 during depletion period and subsequent repressurization. The MFC values plotted along faults are lower than the critical value of 0.6, which indicates that the faults are stable (Figure 6.37).

We selected a number of monitoring points on the fault segments located in the critical areas to analyze further the induced stress changes (Figure 6.38). The stress path diagrams show that none of the stress paths reaches the assumed Mohr-Coulomb failure envelope for faults, which indicates that the faults are stable (Figure 6.39). Most of the stress paths, however, are converging towards the failure envelope, which means that the stress development is critical.

During injection, the stress paths development on the faults is in the opposite direction, towards the initial state of stress before gas production. The effective stresses decrease and, assuming a fully elastic response of the subsurface, return back to the initial state of stress before hydrocarbon production. In such an idealistic case, the stress paths on the fault for depletion and injection fully overlap.

In conclusion, the calculated scenarios show that the potential for reactivation of fault segments bounding the depleting/expanding reservoir compartments is low. The largest stress changes and the associated mechanical effects on faults occur near the edges of the reservoir compartments, where stress concentrations occur. Fault slip may occur locally at these locations, having in mind the natural variability of shear strength in fault rocks and local perturbations of the in situ stress nearby faults.

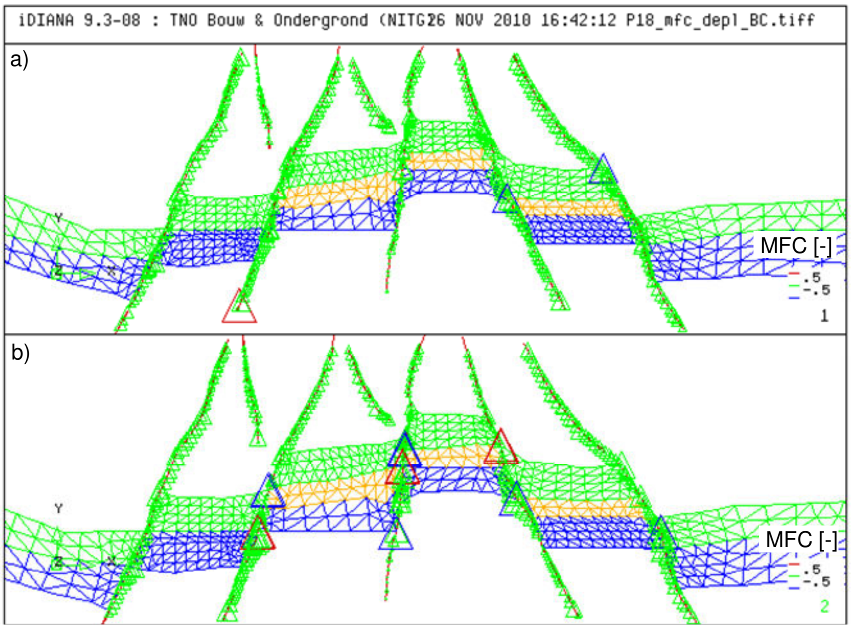

Figure 6.36: a) Mobilised friction coefficient (MFC) on the faults a) for the case of undepleted reservoir, before start of production, and b) for the case of depleted reservoir (Base case).

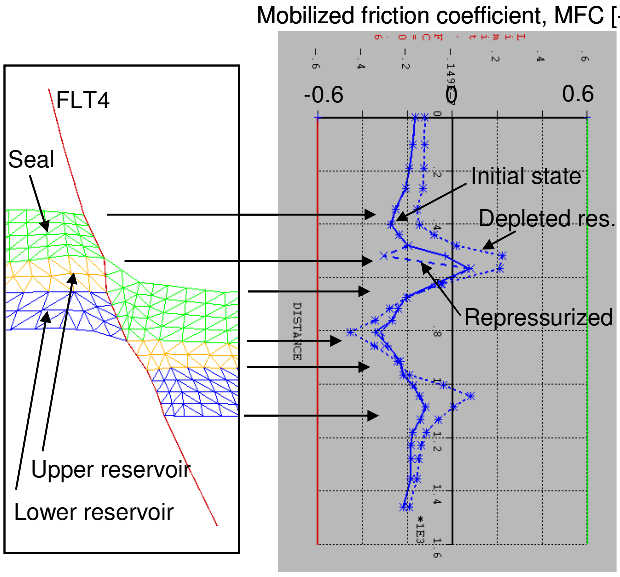

Figure 6.37: Mobilized friction coefficient (MFC) along the fault FLT4 for the initial state of undepleted reservoir, depleted reservoir and repressurized reservoir. Location of FLT4 is presented in Figure 6.38.

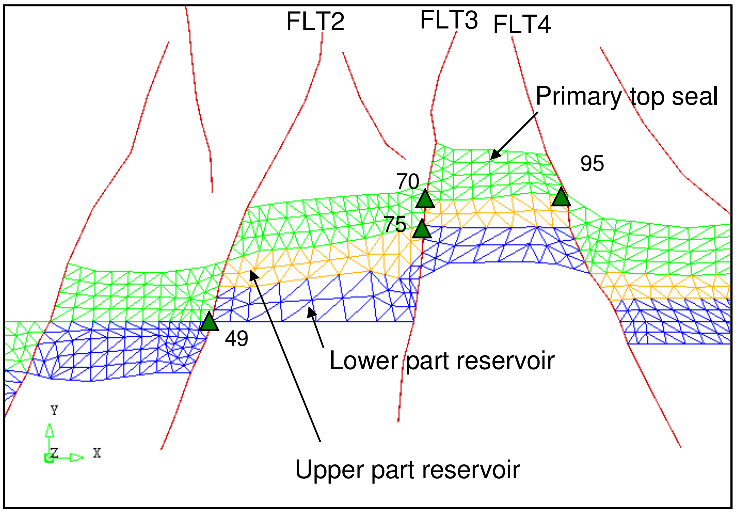

Figure 6.38: Location of the selected monitoring points (i.e. the finite elements) on the faults used to present the results of FE analysis in Figure 6.39.

Stress paths for the faults for depletion and injection, Base case

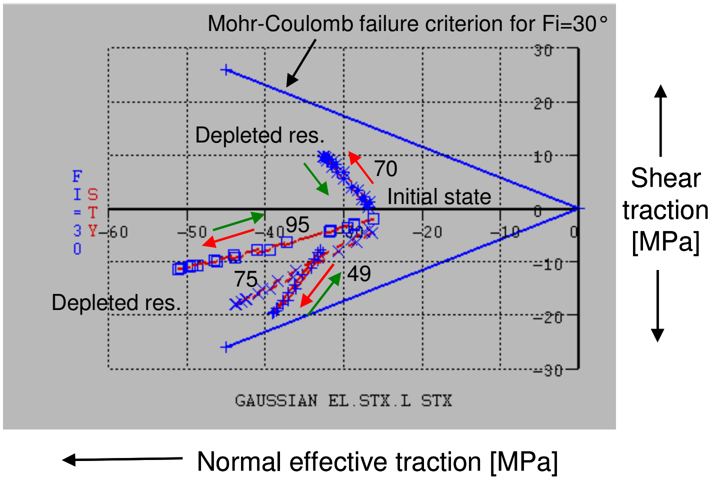

Figure 6.39: Stress paths for the monitoring points on the faults for depletion (Base case). The direction of stress development is shown by red arrows. The Mohr-Coulomb failure envelope with Fi=30° (μ~0.6) is based on the assumed shear strength parameters for faults. During injection, the stress paths development is in the opposite direction, towards the initial state before gas production (shown by green arrows).

6.6. Induced seabed deformation

Production- and injection-related seabed deformation was estimated by using a semi-analytic modelling tool called *AEsubs* developed by TNO (Fokker and Orlic, 2006).
AEsubs requires as input the pressure from reservoir simulator, the compaction coefficient (*Cm*) of the reservoir rock and the elastic properties of the overburden and underburden formations. The formations are represented as horizontal layers with elastic, or visco-elastic, properties changing per layer. The forward model for subsidence/uplift prediction uses combinations of analytical solutions to the elastic equations, which approximate boundary conditions. First, a solution is found for a single point source of compaction or expansion. In the following step this solution is integrated over each grid block of the reservoir model to calculate the subsidence/uplift of the ground surface.

In the case of P18 field, the pressures from MoReS simulations were used as input to *AEsubs* (Figure 6.40). The elastic properties of the overburden and underburden formations were derived from Table 20 (Figure 6.41).
Data on the compressibility of the reservoir Bunter sandstone in the P18-field were not available. Therefore we used a value from another field with the Bunter reservoir, which is presumed to be analogous to the P18 field.
For the Base case, a value of Cm=0.5e-5 1/bar from the Barendrecht-Ziedewij field was used (Winninggsplan Barendrecht-Ziedewij, 2003).
Because the greatest uncertainty in the input parameters for subsidence/uplift calculations usually lies in the compressibility of the compacting/expanding reservoir, we have defined an additional scenario called High case with the compressibility of Cm=0.75e-5 1/bar, which is 50% larger than in the Base case.

Input data on reservoir compaction were supplied in the form of compaction/expansion grids with the calculated product of:

$$Cm\ V\ dp \qquad (6.5)$$

where:
Cm is the coefficient of uniaxial compaction,
V is the compacting/expanding volume, i.e. the volume of each grid block in the reservoir model, and
dP is the pressure change in each grid block with respect to the initial pressure.

The results indicate that the maximum production-related subsidence amounts to 5 to 7.5 cm (Table 21). Such a minor subsidence of seabed is usually considered to be of little practical importance.
During injection period, the production-related subsidence will be reduced due to the injection-related seabed deformation, i.e. uplift. In the case of an elastic reservoir, the subsidence could vanish at the end of injection period when the reservoir is re-pressurized back to the initial pressure. However, it is more likely that injection-related seabed deformation will largely, but not fully, reduce the effects of production-related seabed deformation leaving a few cm of residual subsidence.

Table 21: Maximum subsidence due to gas production and subsequent CO_2 injection in P18.

Time	Maximum subsidence [cm]	
	Base Case, Compaction coefficient Cm=0.5e-5 1/bar	High Case, Compaction coefficient Cm=0.75e-5 1/bar
End production / start CO_2 injection (2010)	5	7.5
Compartment P18-6 : BHP injector P-18-6A7 = Pinit reservoir (2014)	5.1	7.6
Compartment P18-4 : BHP injector P18-4A2 = Pinit reservoir (2021)	3.7	5.5
Compartment P18-2 : BHP injector P18-2A1 = Pinit reservoir (2036)	1.5	2.2
End of injection in all the compartments (2050)	0.6	1

End of gas production (2010) | End of CO2 injection in P18-4 (2021)

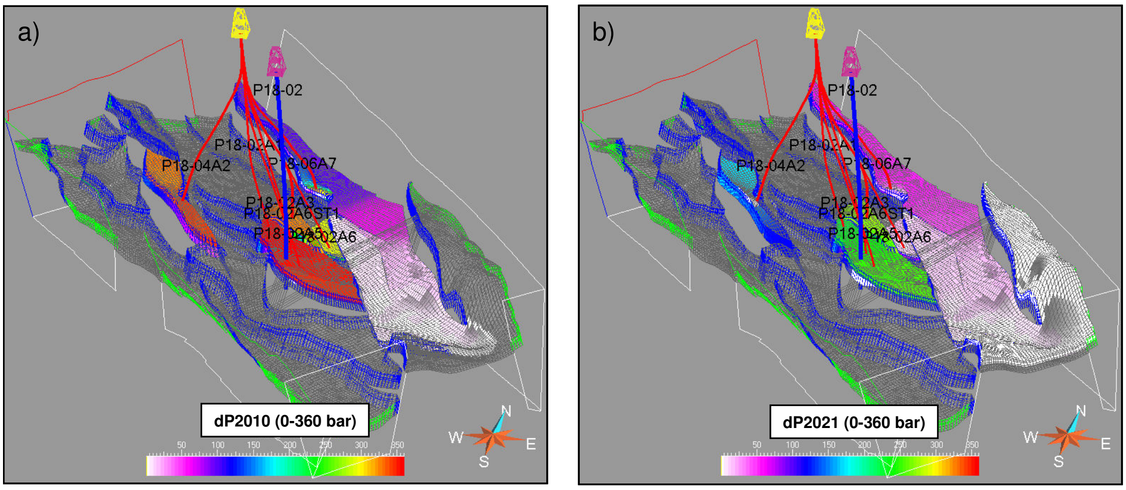

Figure 6.40: Pressure change with respect to the initial pressure in the P18 field a) at the end of gas production period (year 2010) and b) at the end of CO_2 injection in compartment P18-4 (2021). MoReS simulation results.

Base Case, Subsidence 2010,
End of gas production, Cm=0.5e-5 1/bar,
Max subs = 5 cm

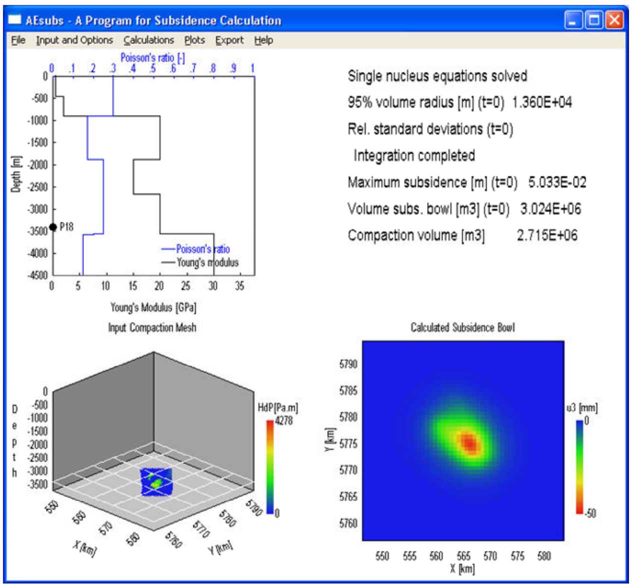

Figure 6.41: Seabed subsidence at the end of reservoir depletion (2010). The input for subsidence calculations are the pressures from MoReS simulations, the compaction coefficient for the reservoir rock Cm=0.5x10E-5 1/bar and the elastic properties of different formations in the subsurface. Maximum subsidence amounts to 5 cm.

6.7. Conclusions

Top seal integrity and fault stability do not represent critical factors for injection and storage of CO_2 in the depleted P18 field.
The primary top seal overlying the Bunter reservoir is represented by a 50 m thick layer of the lower part of Upper Germanic Trias. The seal comprises (from top to base): Röt Claystone Member, Main Röt Evaporite Mb and Solling Claystone Mb. The primary top seal is covered by a 100 m thick upper part of Upper Germanic Trias (Muschelkalk and Keuper) and a 300-400 m thick Altena Group which also represent sealing formations.

No direct measurements of the sealing characteristics of the primary top seal were available. The measurements on core from Röt and Solling taken from well P15-14 in the neighbouring block P15 can be used as analogue for the P18 field. The true top seal in P15 is provided by thinly interbedded and interlaminated shale and very fine-grained sandstone to siltstone. These lithofacies contain type A seals which are capable of supporting gas-column heights in excess of 300 m.

The anhydrite content in the primary seal is variable. As anhydrite can react with CO_2 in the presence of water, it is necessary to quantify the effects of possible geochemical reactions on the mechanical and transport properties of bulk/intact anhydrite and fault gouge anhydrite material.

The primary top seal (Röt and Solling) is comprised of a hard, brittle and competent rock. The rock strength properties of the top seal were determined by triaxial tests on core in HPT lab of Utrecht University. The value of rock properties are as follows: Young's modulus E=20 to 30 GPa, unconfined compressive strength UCS= 93 MPa, cohesion c=27 MPa and friction angle φ=28°.

The largest stress changes and the associated poro-mechanical effects on the top- and side seals occur when the reservoir is fully depleted. The largest stress changes occur near the edges of the reservoir compartments (and segments) where stress concentrations occur. Due to high strength of the top seal, the poro-mechanical effects on the bulk/intact top seal are expected to be weak. However, plastic deformation of the top seal (and the reservoir rock) may occur locally at the edges of depleting/expanding compartments, having in mind the natural variability of (shear) strength which can exist in these rocks.

Combined poro-mechanical effects, due to pore pressure increase, and the thermal effects, due to injection of cold CO_2 into the hot reservoir, may cause hydro-fracturing of the reservoir rock and possibly, the top- and side seals. The risk of induced hydro-fracturing increases in the later stage of CO_2 injection when the reservoir is almost re-pressurized to the initial pressure.

Risks associated with induced fracturing of the reservoir rock are related to the possibility of forming:

- Fractures in the top seal allowing CO_2 migration out of the containment.
- Possible spill paths for lateral escape of CO_2 from the containment.
- Pathways for direct hydraulic communication between the injection well and faults, leading to direct charging of faults by the injected CO_2 and, consequently, to fault instability and slip, which may affect sealing capacity of faults.

The boundary faults of all three compartments are found to be sealing. These faults have large throws and juxtapose the reservoir Bunter sequence against the sealing Upper Germanic Trias and occasionally a lower part of Altena.
The internal faults which split compartment P18-2 into three segments are mostly conductive.

These faults have much smaller throws then boundary faults. Generally, reservoir sand is juxtaposed against sand across the internal faults and the shale gouge ratio (SGR) is low.

The largest stress changes and the associated poro-mechanical effects on faults occur near the edges of the depleting/expanding reservoir compartments. The potential for fault reactivation generally increases during reservoir depletion, but likely does not lead to fault slip and reactivation. However, fault slip may occur locally at the edges of reservoir compartments, having in mind the natural variability of shear strength properties in fault rocks and local stress perturbations nearby faults.
During injection, the potential for fault reactivation generally decreases providing that the CO_2 is not injected directly into the fault zone and the thermal effects of injection are negligible.

The P18 field was not seismically active during production period, based on the KNMI database of recorded induced seismic events associated with hydrocarbon production in the Netherlands. No production-related induced seismicity has been recorded so far in other hydrocarbon fields in the Western part of the Netherlands. The detection limit of the KNMI seismic network was M2.5 until 1995 and M1-1.5 on Richter scale afterwards.

Current seismic analysis practices do not allow predictions of the magnitude of possible future seismic events related to fluid injection into reservoirs. Quantitative Probabilistic Seismic Hazard Analysis (PSHA) of induced earthquakes associated with CO_2 injection is not yet possible because of lack of data.

The effects of production and subsequent CO_2 injection on seabed deformation are minor. The maximum production-related subsidence amounts to 5 to 7.5 cm, which is considered to be of little practical importance. During injection period, the production-related subsidence will be reduced.

Geomechanical-related risks of fracturing and fault re-activation can be (partially) reduced by:

- Injecting CO_2 with bottom hole pressures (BHP) which are below fracturing condition.
- Avoid overpressurizing the reservoir above the initial pressure.
- Keeping a safe distance between the injection wells and faults to avoid direct charging of faults by injected CO_2 through natural or induced fractures.
- Managing thermal effects of injection

References

Papers

Allan, U.S., 1989. Model for hydrocarbon migration and entrapment within faulted structures. AAPG Bull. 73, 803-811.

Breckels, I.M., van Eekelen, H.A.M., 1982. Relationship between horizontal stress and depth in sedimentary basins. *Journal of Petroleum Technology*, 34(9): 2191-2199. SPE paper 10336.

Castagna, J.P., Batzie, M.L., Eastwood, R.L., 1985. Relationships between compressional-wave and shear-wave velocities in clastic sillicate rocks. Geophysics, Vol. 50, No 4, 571-581.

DIANA Version 9.3, 2009. Program and User's Documentation. TNO Diana B.V.

Eissa, E.A. and Kazi, A., 1988. Relation between static and dynamic Young's Modulus of rocks. *Int. J. Rock Mech. Min. Sci.*, Vol. 25, No. 6, 479-482.

Greenberg, M.L., Castagna, J.P., 1992. Shear-wave velocity estimation in porous rocks: Theoretical formulation, preliminary verification and applications. *Geophysical Prospecting.* 40, 195-209.

Rafavich, F., Kendall, C.H.St.C., Todd, T.P., 1984. The relationship between acoustic properties and the petrographic character of carbonate rocks. *Geophysics* 49, 1622-1636.

Spain, D., Conrad, C., 1997. Quantitative analysis of top-seal capacity: offshore Nethrlands, southern North Sea. Geologie en Mijnbouw, Kluwer, 76: 217-226.

Reinecker, J., Heidbach, O., Tingay, M., Sperner, B., Müller, B., 2005. *The release 2005 of the World Stress Map* (available online at www.world-stress-map.org).

Yielding, G., 2002. Shale gouge ratio – calibration by geohistory. In: A.G.Koestler, A.G., Hunsdale, R. (Eds), *Hydrocarbon Seal Quantification*. NPF Spec. Publ. 11, Elsevier, Amsterdam, 1-15.

Zoback, M. D., 2007, Reservoir Geomechanics, Cambridge University Press, 464p.

Reports

Winningsplan P18a, P18c, P15c, 2003.

Winninggsplan Barendrecht-Ziedewij, 2003.

Schlumberger, 1997. Report on processing and interpretation of ultrasonic borehole imager (UBI) data.

Utrecht University, 2010. Report on mechanical properties and permeability of Röt and Solling claystones from the Q16 gas field and permeability of P18 reservoir rocks. CATO-2 progress report 1.10.2010.

7. Well integrity study

7.1. Executive summary (restricted)

CO_2 storage is being considered in TAQA's P18 gas field. In the context of the CATO-2 project the suitability of the existing wells in the field is being investigated for injection and long-term storage of CO_2. The well integrity assessment covers the operational phase of the injection project (decades) and the long-term post-abandonment phase. The study aims at the evaluation of the relevant well system barriers to identify potential showstoppers and recommendations on remedial actions and abandonment strategies. This report presents progress until September 2010, but does not describe the final conclusions of the well integrity assessment of the P18 field.
The P18 field comprises 3 reservoir blocks, penetrated by a total of 7 wells, some of which have been sidetracked. One of these sidetracks also penetrates the caprock and the reservoir.
One of the wells, P18-2, is plugged with several cement plugs. The current layout of plugs in P18-2 is inadequate for long-term containment of CO_2, as it provides likely migration pathways from the reservoir to shallower levels, bypassing the caprock. In order to improve the quality of this well, it is required to re-enter the well, which is technical feasible according to TAQA. Subsequently, the existing cement plugs should be drilled out and an abandonment plug of sufficient length should be positioned across the primary and/or secondary caprock. Since cement-to-casing bonding is poor, it is recommended to place pancake-type abandonment plugs.
Special attention is drawn to the sidetracked P18-2A6 well. From the limited available data it is uncertain how exactly the parent hole was suspended. It seems that the current layout is unsatisfactory for CO_2 storage. Moreover, since the parent well forms the only penetration to the P18-2 III block, it might be beneficial to not only properly abandon the parent well, but actually use it for CO_2 injection in that block in order to mitigate large pressure differences between the reservoir blocks. This would require adequate abandonment of the P18-2A6st sidetrack and fishing of the whipstock. Subsequently, the P18-2A6 parent well needs to be recompleted to enable CO_2 injection.
All other wells are readily accessible and can be remediated. Most of these show questionable cement sheath quality at caprock level from CBL data or lack data to verify this. Inadequate primary cement poses a risk to long-term integrity, but could also affect the operational phase. However, these wells can be accessed and, in order to prepare them for CO_2 storage, it is recommended to re-evaluate and, if required, remediate the cement sheath quality at least over caprock level.
When considering wells that will be used for CO_2 injection it is recommended to check the packer operating envelope against CO_2 injection scenarios. Potential elastomers and wellhead configuration should also be verified and adapted where required. Moreover, it is suggested to adjust completion materials (tubing, tubing hanger and packer) to corrosive circumstances, in case corrosion mitigation measures are not already in place.
Abandonment - either (re)abandonment of wells that will not play a part in injection or monitoring, or abandonment of injection and monitoring wells after injection ceases - can be designed specifically for CO_2 storage. At present, there are two general options to permanently seal a wellbore for CO_2 containment. If the quality of the primary cement sheath is ensured over critical intervals, traditional abandonment plugs can be positioned and tested at caprock level. Alternatively, and especially in the case of questionable cement sheaths, pancake plugs can be used at caprock level. This would involve milling out of the casing, annular cement and part of the formation, followed by placement of cement in the cavity. This procedure would effectively reduce the number of material interfaces, which could form potential migration pathways. However, this operation may pose difficulty particularly in horizontal or strongly deviated wells. Both of these

options should be accompanied by additional plugs higher up the well, according to common practice and as prescribed by governing abandonment regulations.

7.2. Introduction

CO_2 storage is being considered in TAQA's P18 gas field. In the context of the CATO-2 project the feasibility of injecting and storing CO_2 in the field is investigated with respect to the existing wells. The well integrity assessment aims to determine whether the existing wells are fit for CO_2 injection and long-term containment as currently planned, covering the operational phase of the injection project (decades) and the long-term post-abandonment phase. The study comprises the identification of potential showstoppers and recommendations on remedial actions and abandonment strategies.
Potential migration from the reservoir along wells is generally considered as the major hazard associated with CO_2 storage (e.g. Gasda et al., 2004; Pruess, 2005, Carey et al., 2007). With respect to the evaluation of long-term integrity of the geological storage system, the quality of wells penetrating the storage reservoir therefore must be taken into account.
The well system forms a potential conduit for CO_2 migration because wellbore cement may be susceptible to chemical degradation under influence of aqueous CO_2 or to mechanical damage due to operational activities. Wet or dissolved CO_2 forms a corrosive fluid that could induce chemical degradation of the oil well cement (e.g. Bruckdorfer, 1986; Scherer et al., 2005; Barlet-Gouédard et al., 2006), potentially enhancing porosity and permeability. It could also stimulate corrosion of steel, which may lead to pathways through the casing steel (Cailly et al., 2005). Furthermore, operational activities (e.g. drilling, pressure and temperature cycles) or natural stresses can result in mechanical degradation of the cement sheath through the development of tensile cracks or shear strain, enabling highly permeable pathways to develop (Shen and Pye, 1989; Ravi et al, 2002). Finally, poor cement placement jobs or cement shrinkage could cause the loss of bonding between different materials (debonding) and lead to annular pathways along the interfaces between cement and casing or host rock (Barclay et al., 2002).

7.2.1. History of the P18 field

The P18 field consists of several reservoir blocks. The reservoirs are situated in the Main Buntsandstein Subgroup and are primarily capped by the Solling and Röt Claystone Members (RNSOC and RNROC, respectively). In turn, these are overlain by a secondary caprock, the Muschelkalk and Keuper formations (RNMU and RNKP, respectively). The P18 reservoirs are penetrated by eight wellbores. They are listed in Table 22

Table 22: Overview of reservoirs, compartments and wells in the P18 field

	Reservoir	*Block*	*Well*	*NLOG-name*	*Drilled*	*Comments*	*Status*
1	**P18-2**	P18-02-I	P18-2	P18-02	1989		Suspended
2		P18-02-I	P18-2A1	P18-A-01	1990	Previously P18-03	Producing
3		P18-02-I	P18-2A3	P18-A-03	1993	Sidetracks -S1,-S2	Producing
4		P18-02-I	P18-2A5	P18-A-05	1997		Producing
5		P18-02-III	P18-2A6	P18-A-06	1997		Shut-in
6		P18-02-II	P18-2A6st	P18-A-06ST	1997	Sidetrack from P18-2A6	Producing
7	**P18-4**		P18-4A2	P18-A-02	1991		Producing
8	**P18-6**		P18-6A7	P18-A-07	2003	Sidetrack -S1	Producing

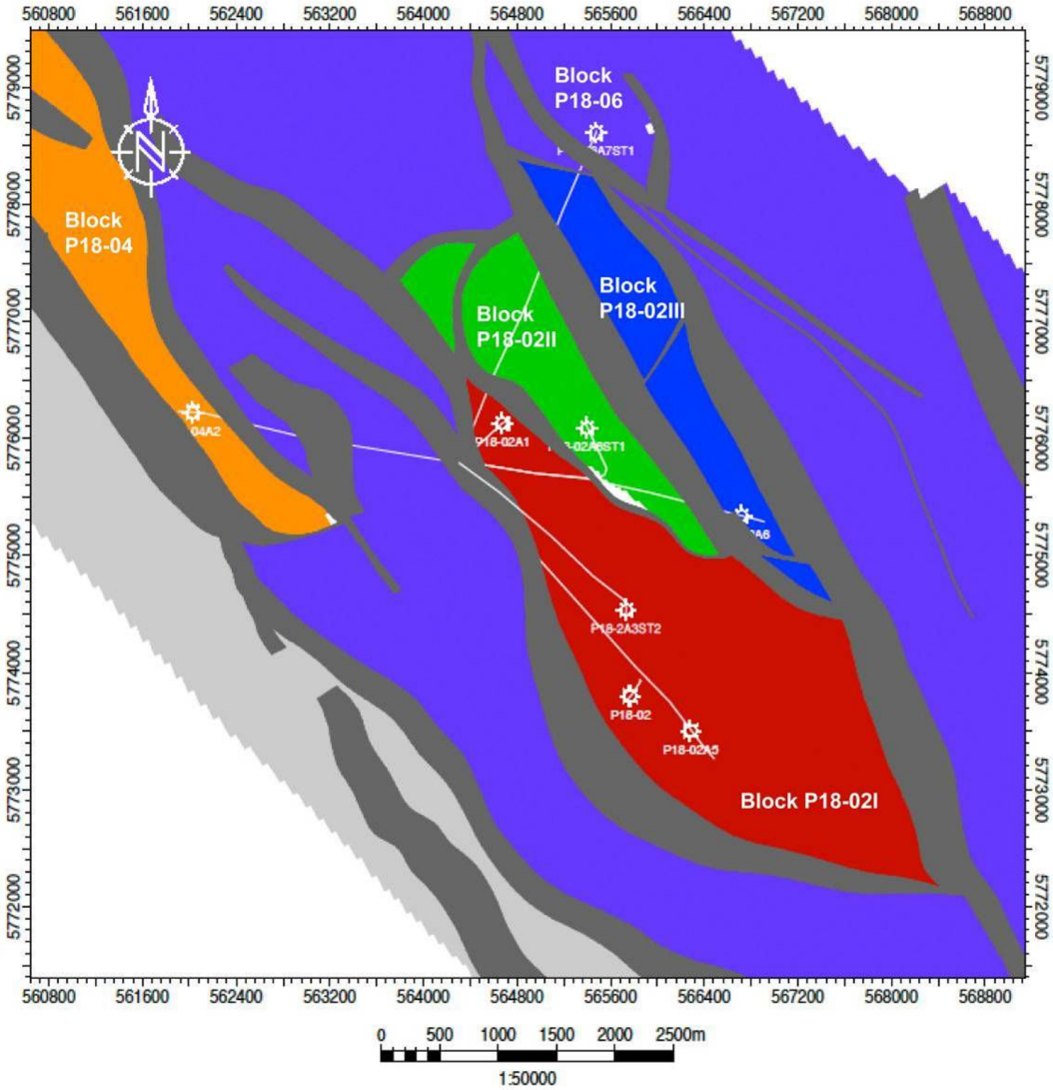

Figure 7.1: Layout of the P18 field, with position of wells at the top of the reservoir interval (top Bunter).

7.2.2. Data availability

Table 23 shows the well data that TAQA provided for the study. This data forms the basis of the evaluation presented in this report.

Table 23: Data available for the P-18 wells

Wells/boreholes	P18-2A1	P18-2A3	P18-2A5	P18-2A6	P18-6A7	P18-4A2	P18-2
Well status	Producing	Producing	Producing	Producing[1]	Producing	Producing	Abandoned
Spud date	11-1993	14-5-1993	18-11-1993	17-11-1996	7-2003	4-6-1991	11-3-1989
Abandonment date							28-5-1989
Final Well Report	N/A	x	x	x	N/A	x	x
Well/completion diagrams	x	x	x	x	x	x	x
Casing and cementing reports		x		x		x	x
Drilling reports	x	x	x	x		x	x
Well tests	N/A	x	x	x			N/A
Cementing and corrosion logs (mentioned in EOWR)	CBL (7" L)	CBL-VDL (5" L)	USIT-CBL (5"L), CBL-CET (7" L)[2]	USIT-CBL (7" L)[3]	N/A	N/A	CBL (7", 9 5/8")
Openhole logs over reservoir section only	x		x	x	x	x	x
Stratigraphy along the well	x	x	x	x	N/A	x	x
Annulus pressure reports	N/A	N/A	N/A	N/A	N/A	N/A	
Production data	Dec 1993 – March 2010	Dec 1993 – March 2010	Dec 1993 – March 2010	June 1997 – April 2003	Dec 1993 – March 2010	Dec 1993 – March 2010	

[1] Present production from sidetrack P18-2A6st

[2] Cement bond log mentioned in EOWR, but data not physically available

[3] Cement bond log available for pilot hole (P18-2A6) only

7.2.3. Methodology

As part of the CATO-2 project, the objective of the current study is to evaluate whether the wells in the P18 field are fit for CO_2 injection and long-term containment of the injected CO_2 as currently envisaged. To this purpose the integrity of the wells in the operational and post-operational period is assessed under the assumptions listed in

Table 24 and using the methodology discussed in Table 25. Note that all well depths in this report are stated in measured depth along hole (MDAH), unless specifically listed otherwise.

Table 24: Assumptions of feasibility study

Only existing producing wells will be converted for injection	As a starting point to this study, no information was available on which well(s) will be converted to injection well(s). It is assumed that TAQA will not re-use the abandoned well for injection.
Initial reservoir pressure	The maximum reservoir pressure during the injection project will not exceed the original reservoir pressure (ca. 350bar)
Cold injection	The temperature of the injected CO_2 will be much lower than the ambient temperature in the well (the undisturbed geothermal gradient), i.e. injected CO_2 will not be pre-heated before injection. Therefore, injection will introduce additional thermal-induced stresses to the well tubulars.
Only existing wells	Only existing wells will be evaluated in this study. The evaluation of specifications for (potential) integrity of any future wells that may be drilled in the field is not within the scope of this work..
Dry CO_2 injection	It is assumed that dry CO_2 will be injected.

Table 25: Methodology used in assessing the feasibility of injection using P18 wells

Identify well barriers	Identification of well barriers that keep the well fluids inside the wellbore and prevent uncontrolled discharge to the overburden—above the caprock—and to the atmosphere. These typically include the cement section outside the production casing adjacent to the caprock and the production casing itself.
Assess the evidence for failure	Assessment of potential evidence suggesting failure of the identified barriers, based on information on well history.
Direct evidence	Direct measurements of the quality of the barrier: - Measurements that show that the barrier was not installed properly (e.g. cement bond logs, pressure tests) - Measurements that show that the barrier may have been breached during the productive life of the well (annular pressure information).
Indirect evidence	Indirect evidence that the barrier might be compromised will be used when direct evidence is unavailable (e.g. drilling information on kicks, cement losses).
Define robustness criteria	Robustness criteria will be defined to state which barriers (e.g. wetted areas of pipes) need to be 'upgraded' to be fit-for-CO_2 storage by defining (where applicable).
Data gaps	Data gaps will be identified when insufficient information is available to guide our analysis of the barrier.

7.3. Definition of well integrity barriers

This chapter presents the principal well integrity barriers that are investigated in the scope of the present study. The barriers are illustrated for a generic P18 well, which was constructed based on the information provided by TAQA. The evaluation of well barriers includes the definition of failure and robustness criteria applied to the identified barriers in the field. Robustness criteria can be distinguished into two types: mandatory criteria and recommended, “nice-to-have” criteria.

1. Primary cement across primary caprock
2. Production liner
3. Production casing
4. Wellhead
5. Production tubing (with completion elements like SC-SSSV)
6. Primary cement outside production casing
7. Production liner hanger
8. Production packer

A. A-annulus
B. B-annulus

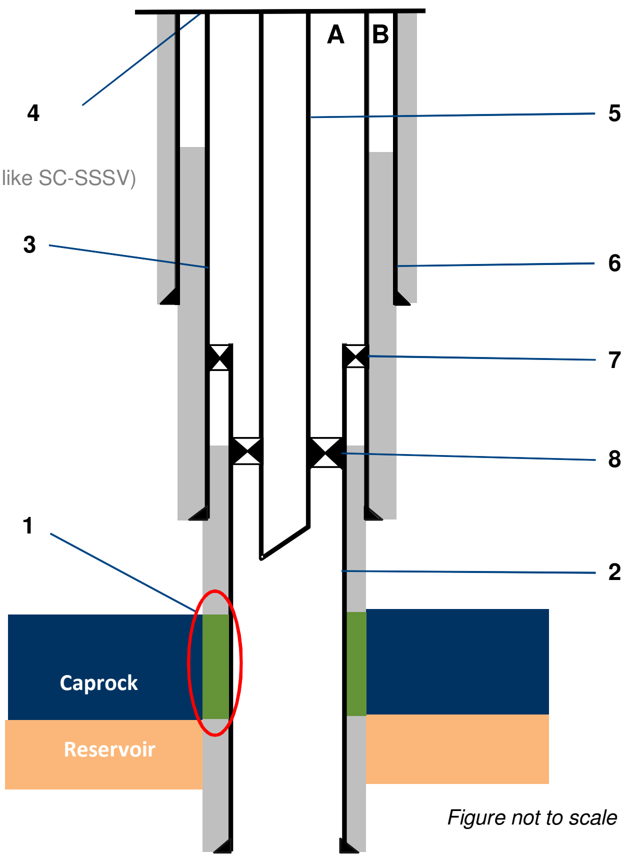

Figure 7.2: Generic P18 well showing the well barriers.

7.4. Primary cement across the caprock

The most obvious evidence that the cement across the primary caprock failed during production life is the confirmed presence of reservoir gas in the B-annulus, after the production liner and wellhead are tested OK The robustness of the primary cement across the caprock is assessed using the criteria summarised in Table 26.

Table 26: Robustness criteria used in assessing quality of primary cement across caprock

		Mandatory	Recommended ("nice-to-have")
Direct evidence	Good (preferably recent) quality cement bond log showing good cement quality across the caprock	×	
Indirect evidence	No prediction of serious defects such as microannuli and cracks created in the cement due to injection of cold CO_2.	×	
	No large caving/hole washouts in the openhole across caprock		×
	No significant fluid/cement loss during placement		×
	Chemical resistance of the cement to CO_2 attack		×
	No 'high-pressure' well operation that could have compromised the cement across caprock		×
	Good centralisation i.e. if the pipe was well-centralised, then *all factors being equal,* a better quality cement operations is expected		×

Note 1: The cement bond log does not measure the absolute hydraulic isolation of the cement; it only provides an indication of the quality of the bond from which hydraulic isolation can be inferred. The industry rule of thumb is that good bonding is defined by a CBL reading of about 1-2 mV and a minimum of 3 m of well-bonded cement for a 7" casing/liner. This minimum length does not reflect the potential chemical interaction of acidic fluids with wellbore cement.
Note 2: Hydraulic isolation is best evaluated using the combination of cement bond log and azimuthal cement log. However, azimuthal logs (e.g. USI, Isolation Scanner) are not available for the P18 wells.

7.5. Production liner

A pressure test during setting of the liner could tell whether or not the liner itself failed. Failure below the liner hanger is not necessarily a showstopper if the other barriers above the leak still hold. In addition, failure due to any plastic salts in the overburden during the production life of the well was evaluated.
The recommended robustness criterion for the liner for CO_2 injection and storage involves the wetted area of the liner to be made of corrosion-resistant alloy. However, this criterion can be relaxed if the amount of free water in the injected CO_2 stream is expected to be very low.

7.6. Production casing

Like the production liner, the production casing is usually tested when it is set. It is investigated whether the casing passed this test. In addition, the impact (if applicable) of plastic salt layers is investigated that may impinge upon the intermediate casing. Direct evidence for failure of the production casing during producing life could include annular pressure communication between the A and B annuli, noise logging and pressure testing of the production casing.

7.7. Wellhead

The wellhead provides the main barrier between the well and the atmosphere, and typically is tested during installation and periodically during operation. In this study, the results of these tests are investigated, evaluating whether the wellhead passed the tests. In addition, the materials used to construct the metallic and non-metallic components of the wellhead are investigated to assess if they are fit for CO_2 injection.

7.8. Production tubing

The evidence for failure of the production tubing is almost always direct evidence. This includes (but is not necessarily limited to):

- failure of the tubing to hold pressure during initial installation;
- pressure communication between the A-annulus and the tubing;
- reservoir gas-cap on top the A-annulus; and
- depletion of fluid in the A-annulus

The production tubing provides the main wetted surface during CO_2 injection. Due to the corrosive nature of CO_2 (in the presence of free water), the main robustness criteria for the tubing are:

- the wetted areas (the i.d.) be made of CO_2-resistant material;
- tubing i.d. be sufficient to prevent erosion and high pressure losses due to friction during injection; and
- the tubing be designed to withstand the thermal stresses (due to contraction) that injecting cold fluid will impose on the pipe.

7.9. Primary cement outside production casing

The evidence of failure of this cement sheath is similar to that of the primary cement sheath across the caprock, as described in section 0. Particular care should be taken to evaluate the quality of the cement at the shoe, as the quality of the cement there is the primary barrier to an outer annulus becoming a leak path.

7.10. Production liner hanger

The production liner hanger is an additional barrier between the reservoir and the production casing. Evidence of failure of the liner hanger could include the presence of reservoir fluids in the A-annulus and/or failure of hanger test during installation.

7.11. Production packer

The production packer isolates the corrosive reservoir fluids from the production casing, and 'forces' the fluids to enter the tubing. In addition, the packer may bear some of the tubing loads (depending on how the completion is set). Like the production tubing, evidence for failure of the packer is almost always directly observed. It includes:

- Failure of pressure test during initial installation;
- Loss of annulus fluid levels;
- Presence of reservoir fluids inside the production casing during production life; and
- Pressure communication between the production tubing and the production casing.

There is insufficient information available to distinguish tubing failure from packer failure; therefore, for the remainder of this report, the tubing and production packer will be grouped as one barrier: tubing and completion barrier.

7.12. Well integrity assessment

This section involves the application of the defined failure modes and robustness criteria to the wells of the P18 field in order to evaluate their suitability for CO_2 injection and long-term containment.

7.12.1. P18-2A1

This well was spudded in 1993 and has produced gas ever since. Available drilling and completion information suggests that no problems occurred during the drilling or completion phase of the well. Refer to the schematic of the well in Figure 7.3.

Cement barrier across the primary caprock

The 222 m thick Middle Bunter Sandstone (RBM) reservoir is topped by the primary caprock (25m thick), the Solling (RNSOC) and the Röt Claystone (RNROC) members. A cement bond log was run across the 7" liner, covering the reservoir, the primary caprock and the lower part (21 m) of the secondary caprock, with top of cement (TOC) found at 3,477 m. The CBL-VDL log shows poor casing-cement bond in the liner lap above the perforations, including the primary caprock section, and mainly good bonding below the perforations.

Cement barrier across the secondary caprock

The Muschelkalk (RNMU) and Keuper (RNKP) formations (141 m thick) are believed to act as the secondary caprock. As mentioned above, a cement bond log was run across the lower part of the secondary caprock, showing poor bonding. Across the 9⅝" casing string, which traverses most of the secondary caprock, no cement bond logs were run.

However, there is indirect evidence suggesting that the casing bond may be adequate. This evidence includes the fact that no problems were encountered during drilling or cementing, such as loss of cement or mud. Furthermore, the well is vertical and the production casing was centralised with at least six centralisers, suggesting good centralisation. There is no information about the condition of the hole, e.g. washouts, or sort of centralisers used.

Production liner and casing

Both the 7” and 9⅝” liner/casing strings were pressure tested OK to 5,000 psi for 20 min. The 7” liner consists of 29 lb/ft N-80 casing and the 9⅝” casing is 53.5 lb/ft HC-95 material. According to reports, neither of the two strings is made of Cr13 steel. There is no data on annulus pressures; therefore, there is no information on possible communication between the completion and casing.

Production tubing and completion

The completion is 4½”/5” L80 Cr13 tubing. Since it is made of Cr13 steel, it is fit for CO_2 injection. However, a retrievable packer is used. This packer could become unseated during CO_2 injection depending on the packer operating envelope[2].
There is no information available on the wellhead and type of elastomers (if any). Therefore, the suitability of the wetted areas of the wellhead or any elastomers for CO_2 conditions cannot be evaluated.

[2] The packer operating envelope shows the tensile, compressional and burst loads that the packer is designed to handle. In essence, it shows the conditions under which the packer can operate. Operating the packer outside this envelope would result in failure of the packer – and loss of well integrity.

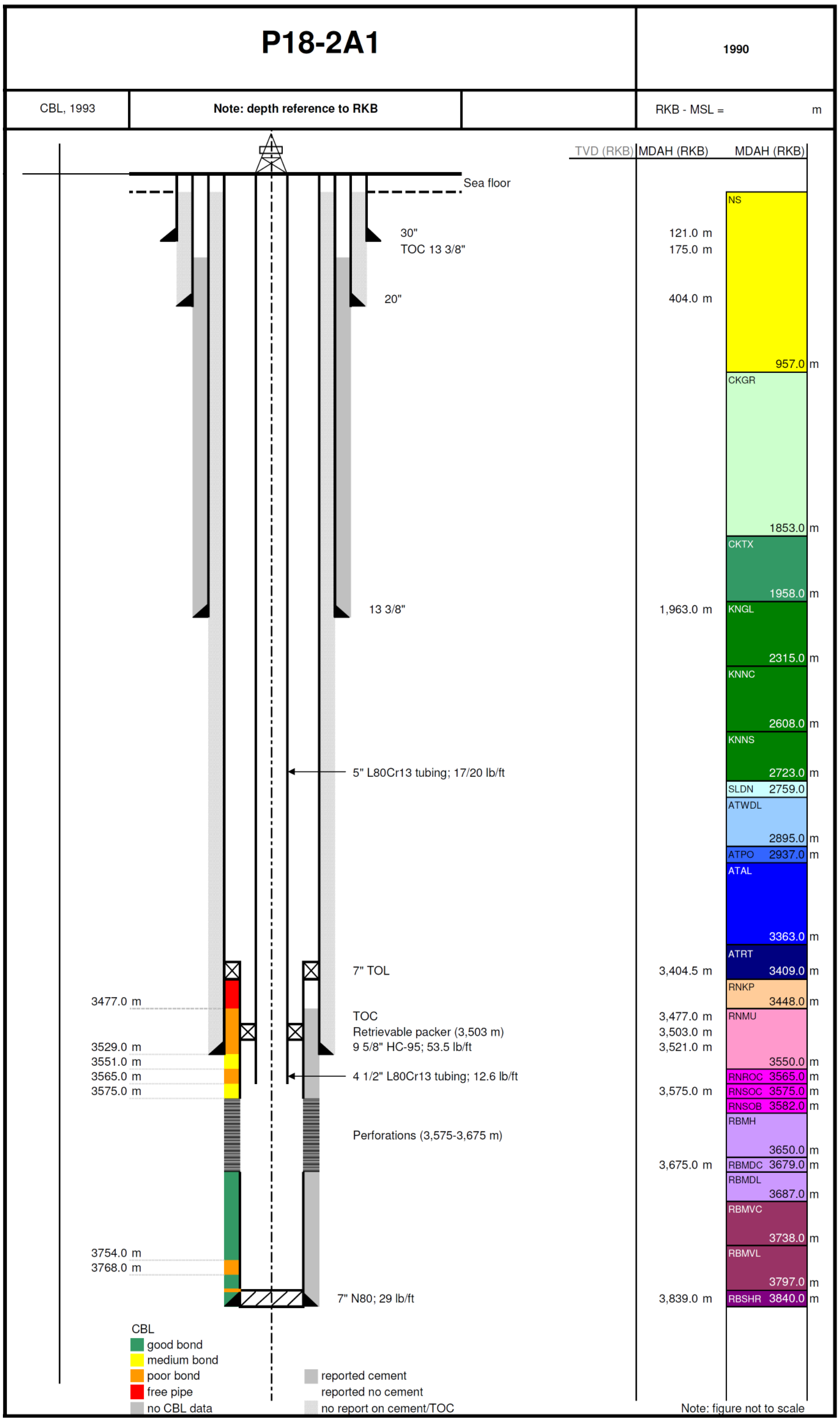

Figure 7.3: P18-2A1 well schematics with CBL interpretation (left hand side) and stratigraphy (right hand side).

Conclusion

Information from available cement bond logs suggest poor casing-cement bond across the upper part of 7” liner. This implies inadequate hydraulic isolation over the primary caprock and parts of the secondary caprock. No information is available for the 9⅝” casing cementation. However, successful casing tests, presence of casing centralisers and the absence of cementing and drilling problems provide favourable boundary conditions for a successful cementing job. It is suggested that the cement sheath be re-evaluated before considering it for CO_2 injection by checking annulus pressures or running cement bond logs over the intervals in question. Although the casing strings themselves are not made of Cr13 steel, the completion is and therefore would be fit for CO_2 injection. Furthermore, the packer operating envelope should be checked against CO_2 injection scenarios by performing a tubing stress analysis and if needed workover to be performed. Furthermore, elastomers and wellhead information should also be checked.

7.12.2. P18-2A5

Well P18-2A5 was spudded in November 1996. The well was sidetracked once because of wellbore instability problems across the Aalburg (ATAL) shales (4,058m). A cement plug was set from 3,830m to inside the 9⅝” casing and the 8½” sidetrack drilled below the 9⅝” casing shoe. After successfully sidetracking the well, a 7⅝” casing was run without success. The hole was cleaned and a 7” liner run and cemented in place. While drilling the 6” openhole section, mud losses occurred until the mud weight was lowered to 9.1ppg. The well schematic is shown in Figure 5 below.

Cement barrier across the primary and secondary caprock

The 327m thick Middle Bunter Sandstone (RBM) reservoir is topped by its primary caprock (69m thick), consisting of the Solling Claystone (RNSOC), the Main Röt Evaporite (RNRO1) and Röt Claystone (RNROC) members. The overlying Muschelkalk (RNMU) and Keuper (RNKP) formations (174m thick) are believed to act as the secondary caprock (see Figure 7.4). Conditions for cementing were good. Although mud losses occurred during drilling, no problems were mentioned during the cementing job. The casing string was centralized well by placing 1 centralizer on each joint and 3 m of cement were drilled above the liner top. A cement bond log is available across the 5” liner; it covers the reservoir and the caprocks. The log confirms overall good bonding across the caprocks, represented by low CBL amplitude and good formation arrivals from the variable density log (VDL). Incidentally, short poor-quality zones can be distinguished. The reported calculated top of cement is at 4,398 m (approximately top of the 5” liner).
The end of well report suggests that a cement bond log was also acquired across the 7” liner suggesting good casing-cement bond and top of cement (TOC) 50 m below the 9⅝” casing shoe. However, the log was not available for analysis. No problems occurred during drilling and cementing operations and the casing was centralized using solid spiral centralizers, providing good cementing conditions and supporting the reported result of the cement bond evaluation.

Production and intermediate liner

The 7” liner was pressure tested OK to 4,000psi for 15min. The 5” liner is 18 lb/ft N-80 and the 7” liner 29 lb/ft N-80 casing. According to reports, neither of the two strings is made of Cr13 steel.

Production tubing and completion

The well has been in production since Nov 1996. The tubing is 4½"/ 5½" L80Cr13 tubing, which is fit for CO_2 service. Due to the use of a retrievable packer, it is suggested that its operating envelope be checked against CO_2 injection scenarios by performing a tubing stress analysis and if needed workover to be performed. Elastomers and wellhead information was not available but should also be checked.

Other criteria

The pilot hole does not truncate the caprock or the reservoir and therefore should not act as an additional leakage pathway for CO_2. No information is available about annulus pressures or the cement quality across intermediate aquifer zones.

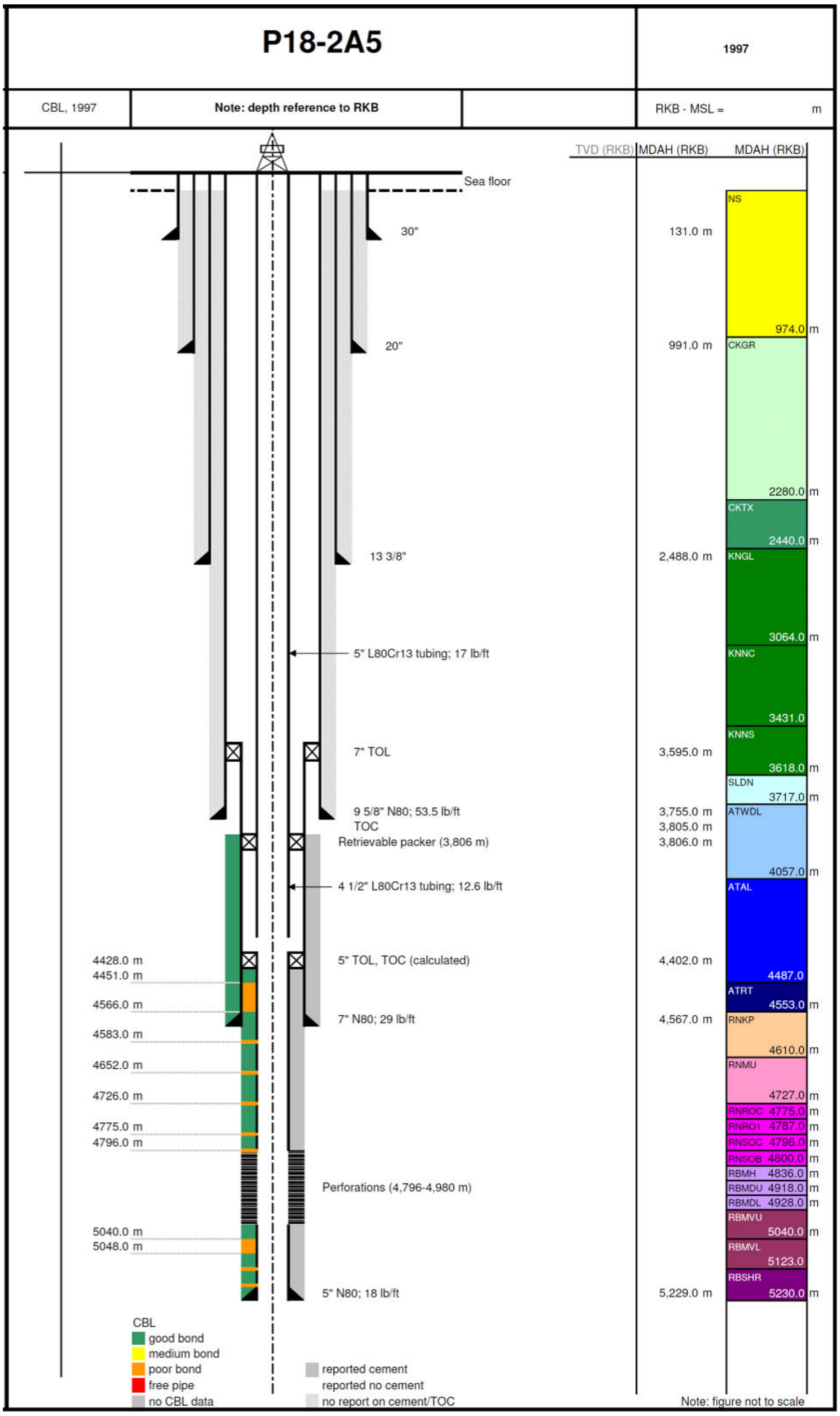

Figure 7.4: P18-2A5 well schematics with CBL interpretation (left hand side) and stratigraphy (right hand side).

Conclusion

The available information shows that good casing-cement bond exists across the majority of reservoir and caprock formations. Although the casing strings themselves are not made of Cr13 steel, the completion is, and therefore would be fit for CO_2 injection. It is recommended that the packer operating envelope is checked against CO_2 injection scenarios by performing a tubing stress analysis and, if required, workover to be performed. Furthermore, elastomers and wellhead information should be checked.

7.12.3. P18-2A6

Well P18-2A6 was spudded in November 1996. Mud losses occurred during drilling of the pilot hole. The bottomhole assembly got stuck at the bottom of the 12¼" openhole section in the Triassic Muschelkalk and needed to be fished. After the 9⅝" liner was set and cemented (TOC = 3,000m), a 13⅜" casing wear log indicated 25% wear on the casing, so a 9⅝" tie back casing string was run and cemented (TOC = 1,613m). See Figure 6.
While drilling the 8½" openhole section no problems occurred. The 7" liner was cemented successfully. Both the 9⅝" casing and the 7" liner were pressure tested OK to 5,000 psi and the well displaced to filtered completion brine.
The well penetrated the P18-2 III reservoir block. The well was sidetracked in 2003 (P18-2A6st, see section 7.12.4) to reach the P18-2 II reservoir block.

Cement barrier across the primary and secondary caprocks

The 256 m thick Middle Bunter Sandstone (RBM) reservoir is topped by its primary caprock (33 m thick), the Röt Claystone member (RNROC). The above Muschelkalk (RNMU) and Keuper (RNKP) formations (188 m thick) are believed to act as the secondary caprock (Figure 7.5).
A cement bond log is available across the 7" liner of the P18-2A6 well from 4,755 to 4,255m, which covers reservoir and both caprocks. The log suggests good casing-cement bond across several intervals in the reservoir section. However, cement bond is moderate to poor across the caprock with CBL amplitudes ranging between 10 and 30mV.
No cement bond logs are available across the 9⅝" casing string of the pilot hole. End of well reports indicate that mud losses occurred during drilling and while running the 9⅝" casing string in hole. This suggests non-ideal cement placement conditions.

Production casing and liner

Both the 9⅝" casing and the 7" liner of the pilot hole were pressure tested ok to 5000 psi. The 7" liner consists of 29 lb/ft N-80 and the 9⅝" casing of 53.5 lb/ft N-80 casing. According to reports neither of the two strings are made of Cr13 steel.

Production tubing and completion

The P18-2A6 pilot well was in production from June 1997 to April 2003. No information is available on the measures that were taken regarding the pilot hole when sidetracking the well. The pilot well report indicated that a retrievable packer was used in the well. If still applicable, it is suggested that the packer operating envelope be checked against CO_2 injection scenarios by performing a tubing stress analysis and - if needed - workover to be performed. Elastomers and wellhead information was not available, but should also be checked.

Other criteria

The P18-2A6 pilot hole traverses both the caprock and the reservoir and the available cement-bond log does suggest poor casing-cement bond across the caprock and parts of the reservoir. Due to the missing end of well report for the sidetrack (P18-2A6st), it is not clear how the pilot hole was abandoned. Therefore, there is uncertainty on whether a leak path exists along the original hole. No information is available about annulus pressures or the cement quality across intermediate aquifer zones.

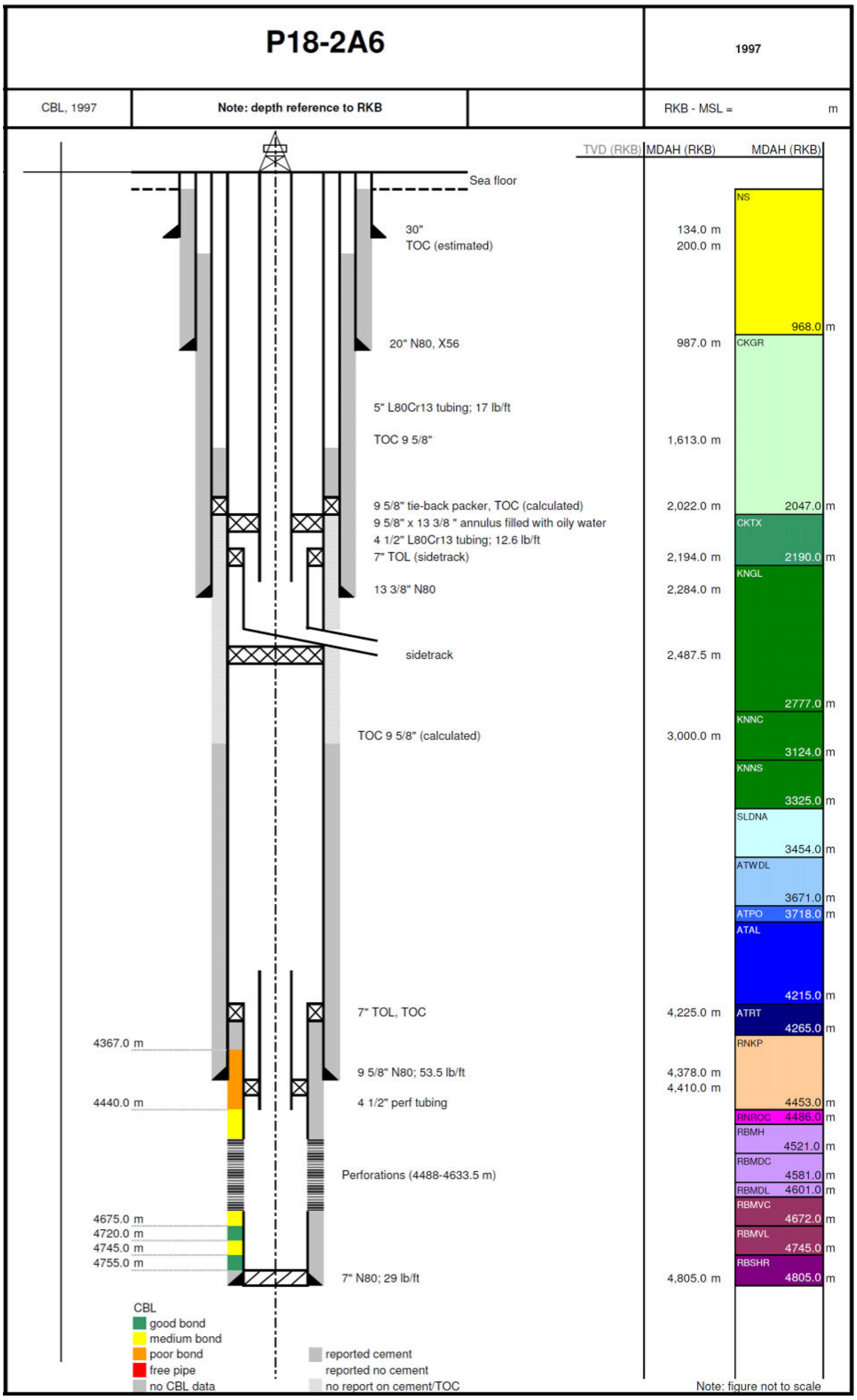

Figure 7.5: P18-2A6 well schematics with CBL interpretation (left hand side) and stratigraphy (right hand side).

Conclusion

Due to the missing information about the sidetracked well and the plugging of the pilot hole, no definite conclusion can be dawn on the suitability of the well for CO_2 storage. The cement bond log across the 7" liner of the pilot hole suggests poor casing-cement bond across the caprock with only a few good intervals across the reservoirs. As this poses a potential threat to long-term CO_2 containment, the abandonment of the pilot hole is crucial for well integrity. However, it is unclear how the pilot hole was abandoned and if the current layout is suitable for CO_2 storage. This issue needs to be clarified before CO_2 injection begins. Without the appropriate data available and proving the contrary, there is a probability that a leakage pathway exists at least along the 7" liner. It is suggested to check the packer operating envelope against CO_2 injection scenarios by performing a tubing stress analysis and if needed workover to be performed. Furthermore, elastomers and wellhead information should also be checked.

7.12.4. P18-2A6st

The P18-2A6 well was sidetracked in 2003 (P18-2A6st). The sidetrack's geometry consists of a 7" liner and a 4½" liner and is presented in Figure 7.6. Unfortunately, the reports on the sidetracked borehole were not available to this study.

Cement barrier across the primary and secondary caprocks

Information about the cementing and casing-cement bond across the 7" and 4½" liner was not obtained.

Production and intermediate liner

No information on pressure tests of the 7" and 4½" liner of the sidetracked borehole is available. The sidetrack's 7" liner consists of L80 Cr13 steel.

Production tubing and completion

The sidetracked well produced since June 2003. The sidetrack's tubing is 4½"/ 5½" L80Cr13 tubing, which is fit for CO_2 service. A retrievable packer is used; therefore, it is suggested that the packer operating envelope be checked against CO_2 injection scenarios by performing a tubing stress analysis and - if needed - workover to be performed. Elastomers and wellhead information on the mother well was not available, but should also be checked.

Other criteria

No information is available about annulus pressures or the cement quality across intermediate aquifer zones.

Conclusion

Due to the missing information about the sidetracked well, no conclusions can be drawn on the suitability of the P18-2A6 well or its sidetrack for CO_2 storage. Specifically, no information is available on the location and bonding quality of the cement in the sidetrack.
In addition, information about the sidetracked wellbore is crucial to decide on its suitability for conversion into a CO_2 injector or for long-term containment of CO_2. Although the casing strings across the reservoir and caprocks, are not made of Cr13 steel, the completion is and therefore would be fit for CO_2 injection.
It is suggested to check the packer operating envelope against CO_2 injection scenarios by performing a tubing stress analysis and if needed workover to be performed. Furthermore, elastomers and wellhead information should also be checked (as described in section 7.12.3).

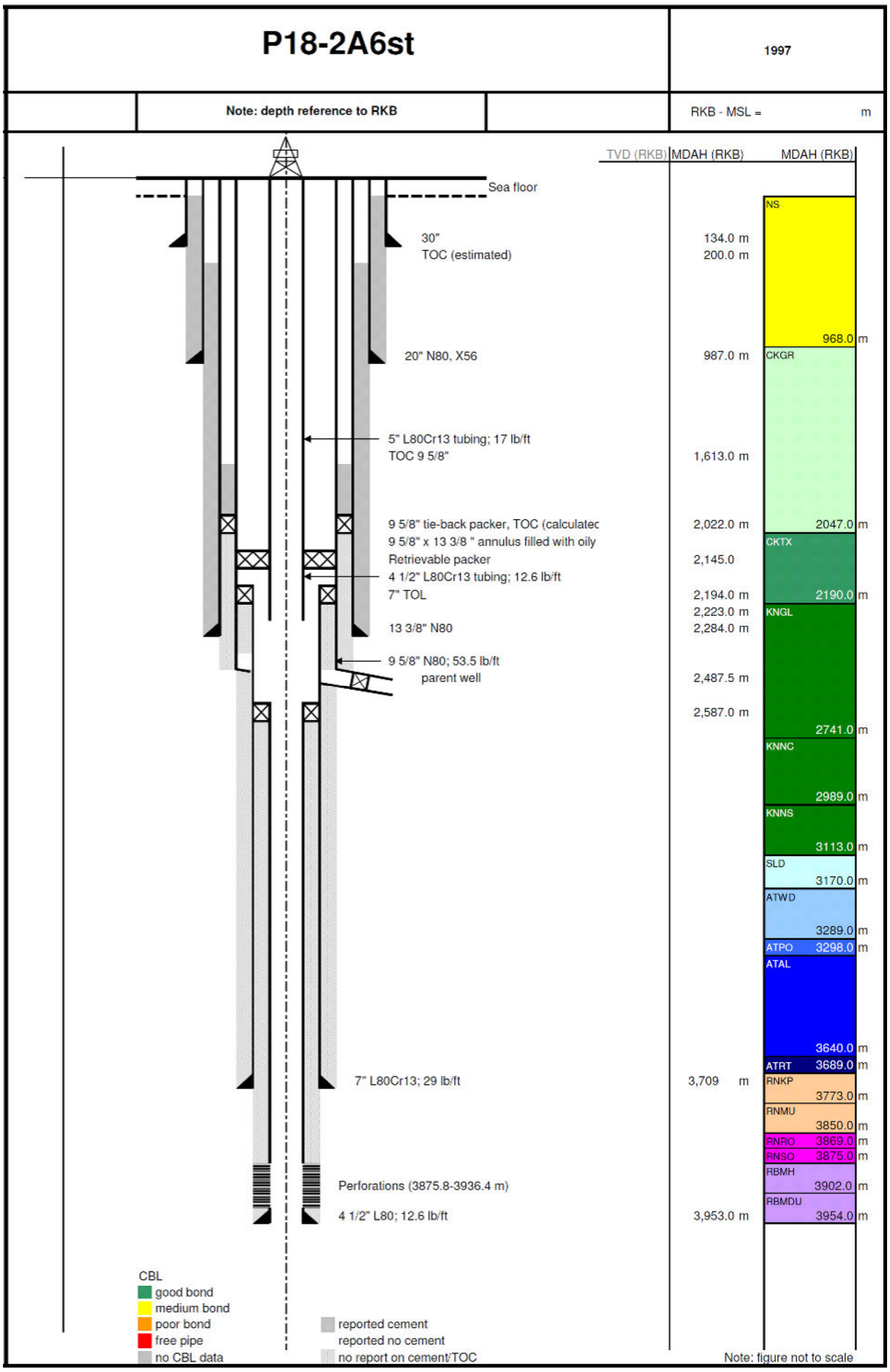

Figure 7.6: P18-2A6st well schematics, CBL interpretation (left hand side) and stratigraphy (right hand side).

7.12.5. Well P18-4A2

Well P18-4A2 was spudded in April 1991 and was temporarily suspended with three cement plugs. Subsequently, it was completed and brought on stream in June 2003. The end of well report suggests that no problems occurred during the drilling and cementing operations, except in the 9⅝" casing string, where mud losses were experienced. Refer to the schematic of the well in Figure 7.7.

Cement barrier across the primary and secondary caprocks

The 225 m thick Middle Bunter Sandstone (RBM) reservoir is topped by its primary caprock (24 m thick), the Solling (RNSOC) and Röt Claystone (RNROC) members, and the secondary caprock, the Muschelkalk (RNMU) and Keuper (RNKP) formations (120 m thick).
No cement bond logs are available for the 7" liner and the 9⅝" casing strings. The 7" liner was set across the reservoir, the primary and the secondary caprock. The end of well report indicates that no mud losses occurred during the drilling of the openhole section and no other problems occurred during the cement job itself. In combination with the in-gauge borehole and evenly spaced casing centralisers, this provides adequate conditions for proper cement placement across the formations of interest. The calculated top of cement is at the top of the 7" liner, at 3,924 m.
The 9⅝" casing string covers most of the secondary caprock. According to the end of well report 709bbls of mud were lost while setting the casing; moreover only four casing centralizers were used. Top of cement is estimated to be at around 2,000m. This suggests, *all other factors being equal*, the quality of the cement bond across the 9⅝" casing string to be worse than that across the 7" liner. However, as stated earlier, there is no data available to verify either of the cement bonds.

Production casing and liner

No information about pressure testing the 9⅝" casing and the 7" liner was available. The 7" liner consists is 32 lb/ft P-110 and the 9⅝" casing of 53.5 lb/ft N-80 casing. Neither string is made of Cr13 steel. Mud across 9⅝" casing interval showed CO_2/$CaCO_3$ contaminations and low to medium corrosion. Corrosion control is reported.

Production tubing and completion

The well has been in production since December 1993. The tubing is 4½"/ 5½" L80Cr13 tubing, which is fit for CO_2 service. Since the production packer is a retrievable one, it is suggested that the packer operating envelope be checked (by tubing stress analysis) that it is indeed fit for 'cold' CO_2 service. If needed, thereafter, a workover could be performed.
There was no information on packer/wellhead elastomers; it is recommended that this information be checked before start injection to confirm applicability for CO_2 service.

Other criteria

There is no information about annulus pressures or the cement quality across intermediate aquifer zones.

Conclusion

Reports indicate overall good cement placement conditions across the 7" liner, suggesting that good hydraulic isolation over the reservoir and the primary caprock and parts of the secondary caprock might exist.

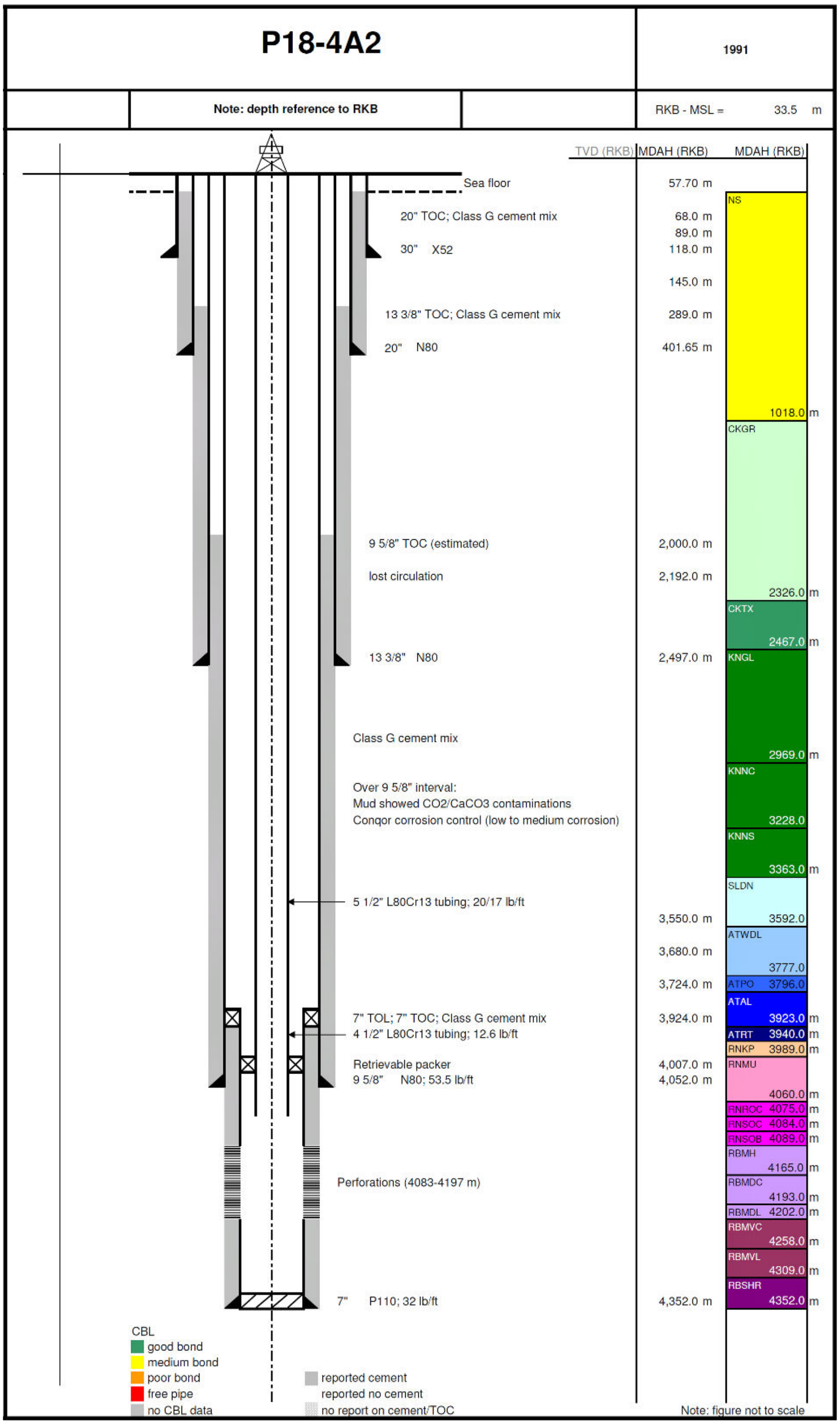

Figure 7.7: P18-4A2 well schematics with CBL interpretation (left hand side) and stratigraphy (right hand side).

Mud losses, which occurred while running, circulating and cementing the 9⅝” casing, and the limited number of centralisers, suggest that cement placement might not have been optimal. However, these observations are only an indirect inference of cement quality made in the absence of direct measured information; therefore, they need to be verified with the actual data. The casing strings are not made of Cr13 steel. The reported corrosion in the 9⅝” casing should be verified before converting the well to CO_2 service. However, the completion is made of Cr13 steel and therefore would be fit for CO_2 injection. It is suggested that the packer operating envelope is checked against CO_2 injection scenarios by performing a tubing stress analysis and if needed workover to be performed. Furthermore, elastomers and wellhead information should also be checked.

7.12.6. Well P18-6A7

Well P18-6A7 was spudded February 2003. The pilot well was sidetracked in the Ommelanden Formation (CKGR). The end of well report indicates that the first cementing stage on the 13⅜” casing did not enter the annulus due to plug problems and that only the second cementing stage was successful. The 3½” liner is not cemented. Refer to the schematic shown in Figure 7.8.

Cement barrier across the primary and secondary caprocks

The 95 m thick Middle Bunter Sandstone (RBM) reservoir is topped by its primary caprock (27 m thick), the Solling (RNSOC) and Röt Claystone (RNROC) members; the overlying Muschelkalk (RNMU) and Keuper (RNKP) formations (161 m thick) are believed to act as the secondary caprock (see Figure 9).
The 3½” liner covers the reservoir and the primary caprock, whereas the lower section of the 5½” liner is set across the secondary caprock. Casing-cement bond information is not available for the 5” liner and therefore, no statement on its cement quality can be made. The 3½” liner, positioned across the primary caprock, is reported to be uncemented.

Production liner and casing

No information about pressure testing the 3½” and 5½” liners was available. The 3½” liner consists is 9.5 lb/ft L-80Cr13 and the 5½” liner 18 lb/ft L-80Cr13 material.

Production tubing and completion

The well has been in production since July 2003. The tubing is 4½” L80Cr13 tubing, which is fit for CO_2 injection. Unlike the other production packer in the other wells, the production packer in well P18-6A7 is not retrievable. However, still it is recommended to confirm that the packer’s operating envelope is appropriate for the anticipated CO_2 injection service.
Elastomers and wellhead information was not available and should be checked also.

Other criteria

There is no information on annulus pressures or the cement quality across intermediate aquifer zones. The well is not located in the immediate vicinity of other boreholes, which truncate the caprock and could provide additional leakage pathways for CO_2.

Conclusion

There was limited data available for the P18-6A7 well. Due to missing cementing reports and cement bond logs across the 5½” liner, the casing-cement bond quality across the secondary caprock is highly uncertain. It is recommended to check this before start of injection. The 3½” liner, positioned across the primary caprock, is uncemented.
In addition, both liners and the completion are made out of Cr13 steel and are therefore fit for CO_2 injection. It is recommended that the packer operating envelope is checked against CO_2 injection scenarios by performing a tubing stress analysis and, if required, workover to be performed. Furthermore, elastomers and wellhead information should also be checked.

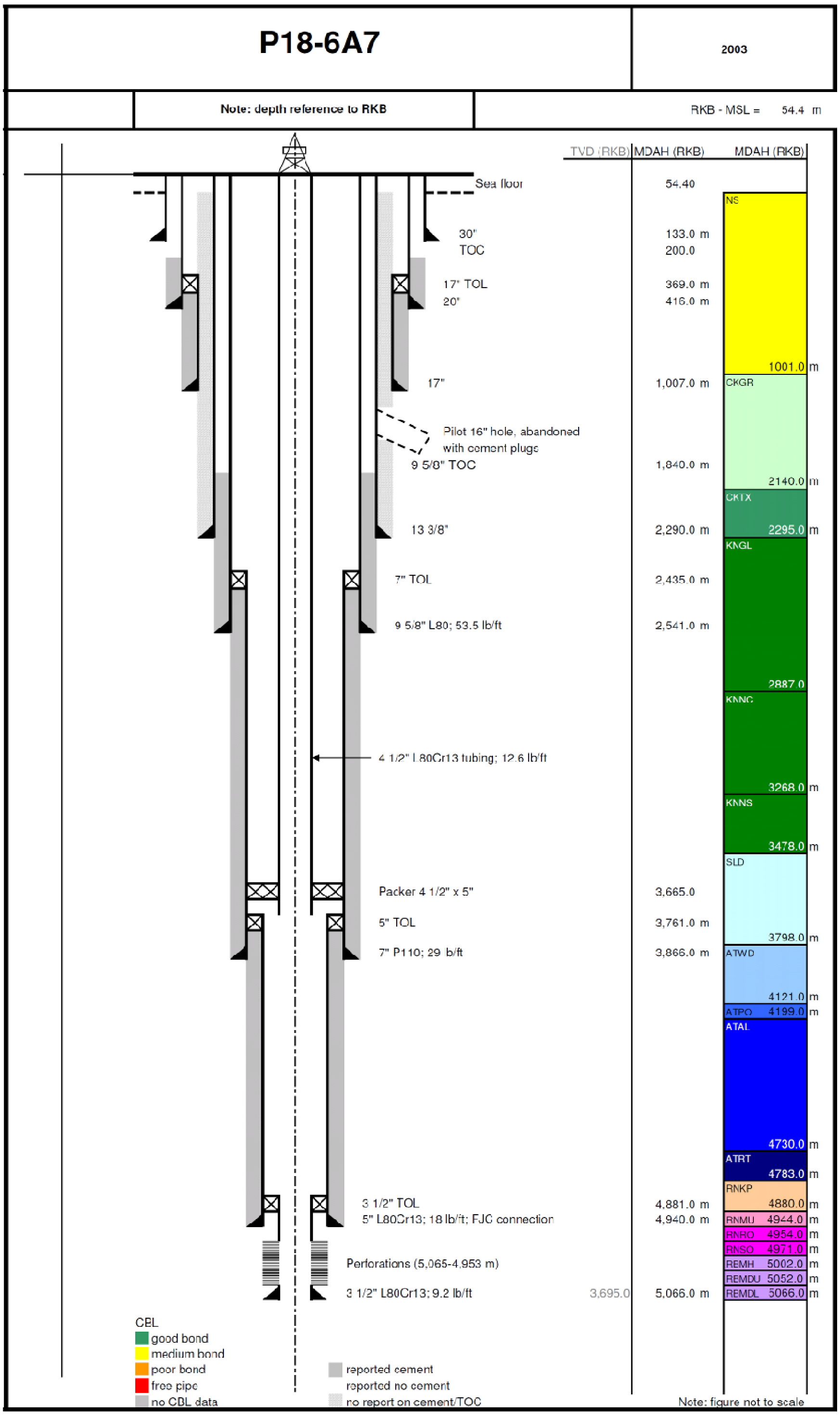

Figure 7.8: P18-6A7 well schematics with CBL interpretation (left hand side) and stratigraphy (right hand side).

7.12.7. Well P18-2

This well was spudded in March 1989 and suspended with four cement plugs after a DST test was performed in the Bunter Sandstone Formation. The end of well report does not mention any particular problems during drilling or cementing operations of the 7" liner. The current well configuration is shown in Figure 7.9.

Cement barrier across the primary and secondary caprocks

The 213 m thick Middle Bunter Sandstone (RBM) reservoir is topped by its primary caprock (33 m thick), the Solling (RNSOC) and Röt Claystone (RNROC) members; the overlying Muschelkalk (RNMU) and Keuper (RNKP) formations (131m thick) are believed to act as the secondary caprock. Refer to Figure 10.

The 7" liner covers the reservoir and both the primary and secondary caprocks. It was centralized with 47 centralisers within an in-gauge borehole. After running the cement bond log under pressure (1,000 psi), overall poor bonding was recorded with moderate to well bonded sections from 3,664-3,597m and 3,276-3,247 m, with top of cement at around 3,005m MD, inside the 9⅝" casing. See Figure 10.

The 9⅝" casing string was centralized with 32 centralisers. A cement bond log was acquired from 2,960 to 100 m, showing overall poor bonding. The top of cement was found at 1,932m and at 1,525 m, separated by a free pipe section on top of a multi-stage packer at 1,893 m.

Abandonment plugs

The deepest of the four cement plugs is located across the upper part of the reservoir section (Figure 10), directly above the perforations, but below the caprocks. The cement that was placed on a (presumably) mechanical plug extends only 1.5 m. The remaining cement plugs are located above the caprock intervals. The next plug is positioned at 3,006-2,896 m across the Aalburg Formation (ATAL) at the 7" liner hanger, with a length of 110 m – of which 60 m is situated above the liner hanger. At 1,915-1,846 m a cement plug is placed at the 13⅜" casing shoe and 9⅝" multi stage PKR, across the Texel Chalk Formation (CKTX). The uppermost plug extends from 154-85 m, covering the base of the 30" conductor pipe. Each of the cement plugs were pressure tested OK to 2,000 psi.

Production liner and casing

The 7" liner and 9⅝" casing string were pressure tested OK to 4,000 psi and 5,000 psi respectively. The 7" liner consists of 29 lb/ft N-80 and the 9⅝" casing of 47 lb/ft N-80 casing. Neither of them are made of Cr13 material.

Conclusion

Cement bond across the reservoir and caprocks generally shows poor results. The abandonment plugs are situated such that the first plug is positioned across the reservoir, whereas the remaining three are located considerably higher than the primary and secondary caprock. This combination does not provide adequate conditions for CO_2 storage. Aqueous CO_2 could affect the lowermost (1.5m thick) seal or associated poor bonded cement or penetrate the carbon steel casing above the plug, and as a result could easily bypass the primary and secondary caprock. Although the abandonment plugs were pressure tested OK, it is reasonable to expect that, in the long term, CO_2 could bypass the lowermost abandonment plug and migrate through the wellbore to levels above the primary and secondary caprock. Furthermore, the possibility of subsequent upward migration of the CO_2 cannot be excluded, given the poor quality of the cement bond adjacent to the 7" liner and the 9⅝" casing.

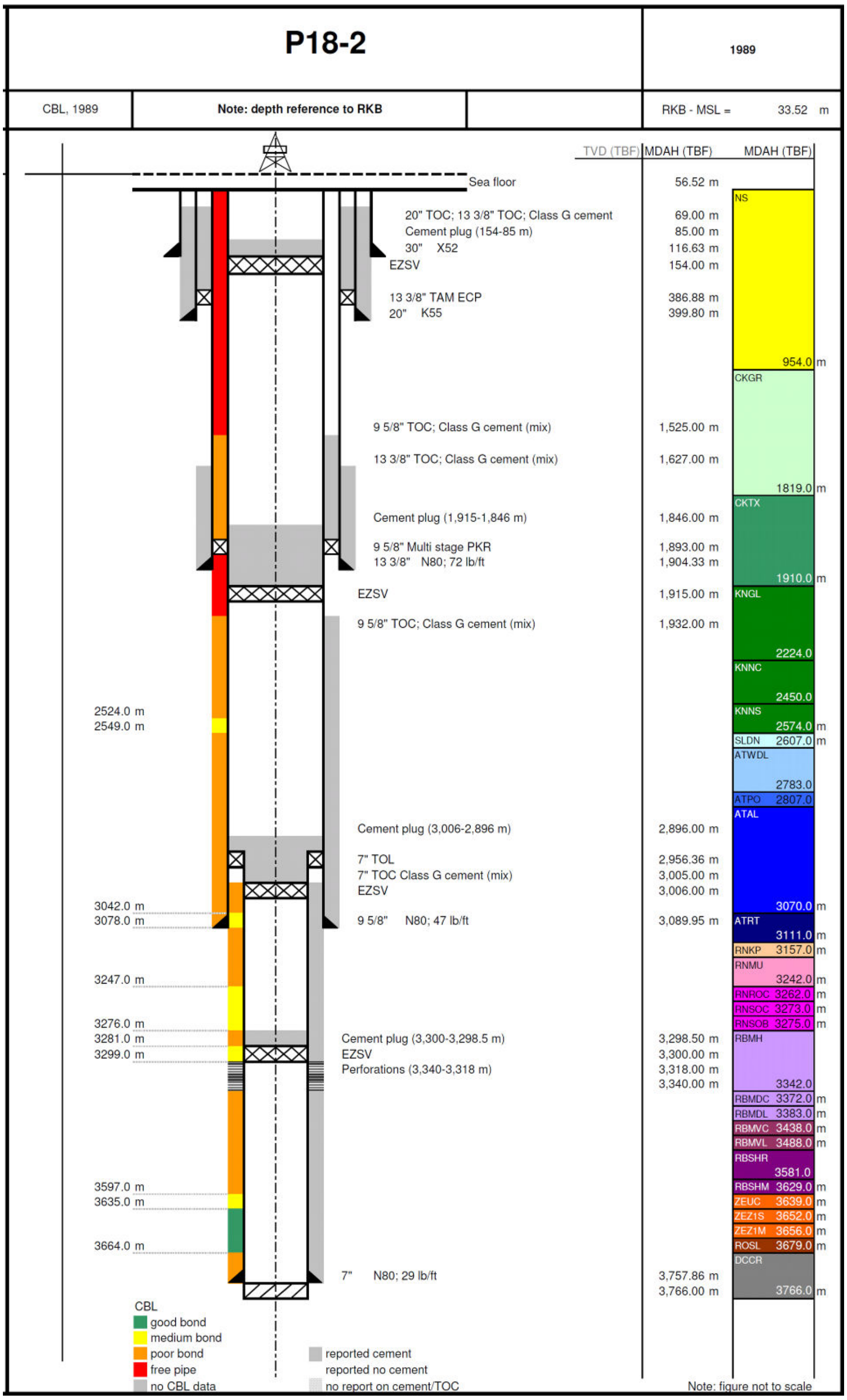

Figure 7.9: P18-2 well schematics with CBL interpretation (left hand side) and stratigraphy (right hand side).

7.13. Summary of integrity assessment of the P18 wells

In this section, the assessment of the integrity of the seven studied wells is summarized. As discussed in section 7.12, the integrity of the well barriers is evaluated using available direct and indirect evidence. Refer to Table 27 for a summary of the assessment.

Table 27: Summary of P18 well integrity evaluation

Well		*P18-2A1*	*P18-2A3*	*P18-2A5*	*P18-2A6*	*P18-2A6st*	*P18-4A2*	*P18-6A7*	*P18-2*
Barriers	*Cement sheath across primary caprock*	✗	✗	✓	✗	?	✓	✗	✗
	Cement sheath across secondary caprock	✗	✗	✓	✗	?	✗	?	✗
	Production casing and liner								
	Tested OK?	Y	Y	Y	Y	?	?	?	Y
	Cr13?	N	N	N	N	Y	N	Y	N
	Production tubing and completion	✓	✓	✓	?	✓	✓	✓	N/A
	Production packer	?	?	?	?	?	?	?	N/A
	Wellhead	?	?	?	?	?	?	?	?
	Abandonment plugs	N/A	N/A	N/A	N/A	N/A	N/A	N/A	✗
Comments (see below)		2, 3, 4	2, 3, 4	2, 3, 4	2, 3, 4	1, 2, 3, 4	2, 3, 4	1, 2, 3, 4	

✓ Direct evidence suggesting that barrier is of good quality or robust for CO_2 service

✓ Indirect evidence suggesting that barrier might be of good quality of robust for CO_2 service

✗ Direct evidence suggesting that barrier is not of good quality or robust for CO_2 service

✗ Indirect evidence suggesting that barrier might not be of good quality or robust for CO_2 service

? No data to suggest quality of barrier or robustness

1 No end-of-well report available

2 No information on annulus pressure during production life

3 Applicability of (retrievable) packer for cold CO_2 injection needs to be confirmed by tubing stress analysis

4 Applicability of wellhead and any potential elastomers to CO_2 service unknown

7.14. Long-term well integrity

7.14.1. Material degradation

Well material degradation can occur by several mechanisms on different timescales. While mechanical deformation of the wellbore may generally be associated with the operational life of the well or field, chemical degradation of well materials will take place on longer timescales. Under certain conditions aqueous CO_2 can chemically interact with well materials. Especially taking into account time spans of thousands of years, these processes may play a crucial role in the integrity of wells and therefore of storage reservoirs.
A review of laboratory experimental studies indicates that diffusion-based chemical degradation rates of cement are relatively low. Extrapolation of the general results shows a maximum of up to a few meters of cement that may be affected in 10,000 years. Even under very high temperatures, extrapolated degradation rates would result in a maximum of 12.4 m of cement plug degradation after 10,000 years of exposure to CO_2, assuming that diffusion processes define the degradation mechanism. In order to translate the experimental results to field situations, several limiting factors apply. Whereas cement samples in the laboratory in certain cases were immersed in a bath of supercritical CO_2, well material in reality will be partially surrounded by reservoir rock, limiting the available reaction surface, the supply of CO_2 and the transportation of reaction products. Furthermore, in specific field cases, especially in depleted gas fields, the availability of water necessary for degradation may be far more limited compared to the experiments. Moreover, injected CO_2 will push back the brine present in the storage formation. As dissolution will take place slowly, many wells may not come across the CO_2-water contact at or near critical levels, such as the cap rock. The presence of only connate water would significantly limit the chemical reactivity of CO_2, although CO_2 is expected to favourably dissolve water. Finally, higher salinity of formation water will likely decrease the solubility of CO_2 and reaction products, thus reducing cement degradation rates. Especially relative high concentrations of calcium and magnesium in the brine may limit the degradation of wellbore cement. Steel corrosion is much faster than cement degradation with rates up to mm's per year. However, also corrosion rates will be seriously reduced by the limited availability of water. A more detailed discussion is presented in IEA GHG (2009).
As a result of the above, the mechanical integrity and quality of placement of primary cement and cement plugs probably is of more significance than the chemical degradation of properly placed abandonment plugs. The presence or development of fractures or annular pathways in the cement or along material interfaces will strongly affect the bulk permeability of the cement sheath. These phenomena, which may be associated with either operational activities or degradation, will play an important role in leakage mechanisms and may significantly reduce the sealing capacity of the cement. Moreover, degradation in lateral direction, affecting the primary cement sheath and casing steel, is likely to compromise integrity in decades. As previously abandoned wells generally cannot easily be remediated, these wells form an element of especial attention in any prospective CO_2 storage project.

7.14.2. Integrity of the P18 wells

In the scope of the present study P18-2 is the only previously abandoned well. The lowermost abandonment plug is very thin and actually positioned below the primary caprock. In case the CO_2 in the reservoir will dissolve present (connate) water, the aqueous CO_2 is likely to interact with the cement sheath and carbon steel casing above this plug. In a timeframe of years to decades, the lateral barrier may be compromised, providing a pathway into the interior casing leading to higher levels, bypassing both the primary and secondary caprock. Given the poor quality of the annular cement sheath along the entire well, leakage pathways through the annulus cannot be excluded.

As described in sections 7.12 and 7.13, most of the P18 wells show questionable cement sheath quality at caprock level from CBL data (i.e. P18-2A1, P18-2A3, P18-2A6, P18-6A7) or lacked data to positively assess these (i.e. P18-2A6st, P18-4A2, P18-6A7). Even if CBL showed good bonding, the evaluated data was acquired prior to production, while bonding could have deteriorated as a result of induced temperature or pressure loading cycles during the production stage. Moreover, CBLs are unable to see thin channels along the material interface and, therefore, even good signal response does not necessarily imply full isolation. In order to prepare the accessible wells for CO_2 storage, cement sheaths should be verified with adequate techniques and if required remediated.

7.15. Conclusions and recommendations

From the perspective of well integrity, the feasibility of CO_2 storage in nearly depleted gas fields, is primarily determined by the accessibility of the wells penetrating the prospective storage reservoir. In the P18 reservoir blocks, only the P18-2 well was previously abandoned.
The lack of a cement abandonment plug at caprock level and the poor quality of the annular cement, cause the P18-2 well in its current state to be unsuitable for CO_2 storage application. In order to improve the quality of this well, it is required to re-enter the well, which is technical feasible according to TAQA. The existing cement plugs should then be drilled out and an abandonment plug of sufficient length should be positioned across the primary and/or secondary caprock. Since cement-to-casing bonding is poor, it is recommended to place pancake-type abandonment plugs (as described in section 7.15.2).
Special attention is drawn to the sidetracked P18-2A6 well. From the limited available data it is uncertain how exactly the parent hole was suspended. It seems that the current layout is unsatisfactory for CO_2 storage. Moreover, since the parent well forms the only penetration to the P18-2 III block, it might be beneficial to not only properly abandon the parent well, but actually use it for CO_2 injection in that block in order to mitigate large pressure differences between the reservoir blocks. This would require adequate abandonment of the P18-2A6st sidetrack and fishing of the whipstock. Subsequently, the P18-2A6 parent well needs to be recompleted to enable CO_2 injection.

7.15.1. Remediation and mitigation

When considering wells for CO_2 injection it is recommended to check the packer operating envelope against CO_2 injection scenarios by performing a tubing stress analysis and, if required, workover to be performed. Furthermore, potential elastomers and wellhead configuration should also be verified and adapted where required. Moreover, it is suggested to adjust completion materials (tubing, tubing hanger and packer) to corrosive circumstances, where applicable.
Most of the wells show questionable cement sheath quality at caprock level or lacked data to verify this. Inadequate primary cement imposes a risk to long-term integrity, but could also affect the operational phase. With respect to CO_2 injection and especially long-term containment, it is recommended to re-evaluate the cement sheath quality at least over caprock level by checking annular pressures or running cement bond logs over the intervals in question. Even when subsequent logging showed good bonding, temperature and pressure loading during production could have adversely affected the cement quality. If verification gives cause for remediation, e.g. cement or polymer squeezing should be considered.

7.15.2. Abandonment

For P18 all wells are still accessible. P18-2 requires re-abandonment, while all other wells will need abandonment in the future. For these wells abandonment can be designed specifically for CO_2 storage. After the most optimal injection well would be selected, the objectives for the other wells also need to be defined. Although forming a potential conduit to the surface, wells also form an invaluable source of information from the reservoirs. Serious thought should be directed at using specific wells for monitoring purposes, equipped with measurement devices.
At present, there are two general options to permanently seal a wellbore for CO_2 containment. If the quality of the primary cement sheath is ensured over critical intervals, traditional abandonment plugs can be positioned and tested at caprock level. Alternatively, and especially in the case of questionable cement sheaths, pancake plugs can be used at caprock level. This would involve milling out of the casing, annular cement and part of the formation, followed by placement of cement in the cavity. This procedure would effectively reduce the number of material interfaces, which could form potential migration pathways. However, this operation may pose difficulty, particularly in horizontal or strongly deviated wells. Both of these options should be accompanied by additional plugs higher up the well, according to common practice and as prescribed by governing abandonment regulations.

7.16. References

Barclay, I., Pellenbarg, J., Tettero, F.,Pfeiffer, J., Slater, H., Staal, T., Stiles, D., Tilling, G., Whitney, C., 2002. The beginning of the end: A review of abandonment and decommissioning practices. Oilfield Review, winter 2001/2002, Schlumberger, UK.

Barlet-Gouédard, V., Rimmelé, G., Goffé, B., Porcherie, O., 2006. Mitigation strategies for the risk of CO_2 migration through wellbores, IADC/SPE Drilling Conference, Miami, USA, February 2006 SPE paper 98924.

Bruckdorfer, R.A., 1986. Carbon dioxide corrosion in oilfield cements. SPE Rocky Mountain Regional Meeting, May 19-21 1986, Billings, Montana, SPE-15176.

Cailly, B., Le Thiez, P., Egermann, P., Audibert, A., Vidal-Gilbert, S., Longaygue, X., 2005. Geological Storage of CO_2: A State-of-the-Art of Injection Processes and Technologies, Oil & Gas Science and Technology – Rev. IFP, Vol. 60, No. 3, pp. 517-525

Carey, J.W., Wigand, M., Chipera, S., Gabriel, G. W., Pawar, R., Lichtner, P.C., Wehner, S.C., Raines, M.A., Guthrie Jr., G. D., 2007. Analysis and performance of oil well cement with 30 years of CO_2 exposure from the SACROC unit, West Texas, USA, Internat. J. of Greenhouse Gas Contr., 75–85.

Gasda, S.E., S. Bachu, and M.A. Celia, 2004. The Potential for CO_2 Leakage from Storage Sites in Geological Media: Analysis of Well Distribution in Mature Sedimentary Basins. Environ. Geol., 46 (6-7), 707-720

IEA Greenhouse Gas R&D Programme (IEA GHG), 2009. Long Term Integrity of CO_2 Storage – Well Abandonment, 2009/08, July 2009.

Pruess, K., 2005. Numerical Simulations Show Potential for Strong Non-isothermal Effects During Fluid Leakage from a Geologic Disposal Reservoir for CO_2, In: Dynamics of Fluids and Transport in Fractured Rock ,B. Faybishenko, P.A. Witherspoon and J. Gale (eds.), Geophysical Monograph 162, 81–89

Ravi, K., Bosma, M., Gastebled, O., 2002. Safe and Economic Gas Wells through Cement Design for Life of the Well. SPE Gas Technology Symposium, 30 April - 2 May 2002, Calgary. SPE-75700.

Shen, J.C. and Pye, D.S., 1989. Effects of CO_2 attack on cement in high-temperature applications. SPE/IADC Drilling Conference, February 28 – March 3 1989, New Orleans, Louisiana, SPE/IADC-18618.

Scherer, G.W., Celia, M.A., Prévost, J.-H., Bachu, S., Bruant, R., Duguid, A., Fuller, R., Gasda, S.E., Radonjic, M., Vichit-Vadakan, W., 2005. Leakage of CO_2 through abandoned wells: role of corrosion of cement. In: D.C. Thomas & S.M. Benson (eds.): Carbon Dioxide Capture for Storage in Deep Geologic Formations, Vol. 2, pp. 827-848.

8. Migration path study

8.1. Introduction

In order to assess the risk of migration of CO_2 through the overburden, an analysis is conducted to identify possible secondary containment and migration paths.

A static overburden model was assembled, based on both 2D and 3D seismic surveys and well information. On the basis of the overburden model and the selected migration scenarios, an evaluation of possible migration pathways was developed.

8.2. Available data and workflow

A geological model was constructed with Petrel modelling software (Schlumberger). The model comprises an area with a 14 km minimum radius surrounding the P18 gas field.
In vertical direction the model spans the total overburden of the reservoir.

The workflow for building the model is described in *CATO-2-WP3.1-Geological report P18 (December 2010).* In brief: Seismic interpretation of the overburden was performed, and subsequently the model was built on the basis of a fault model with a grid cell size of 250m x 250m. The model was converted from time to depth, and tied to the wells.

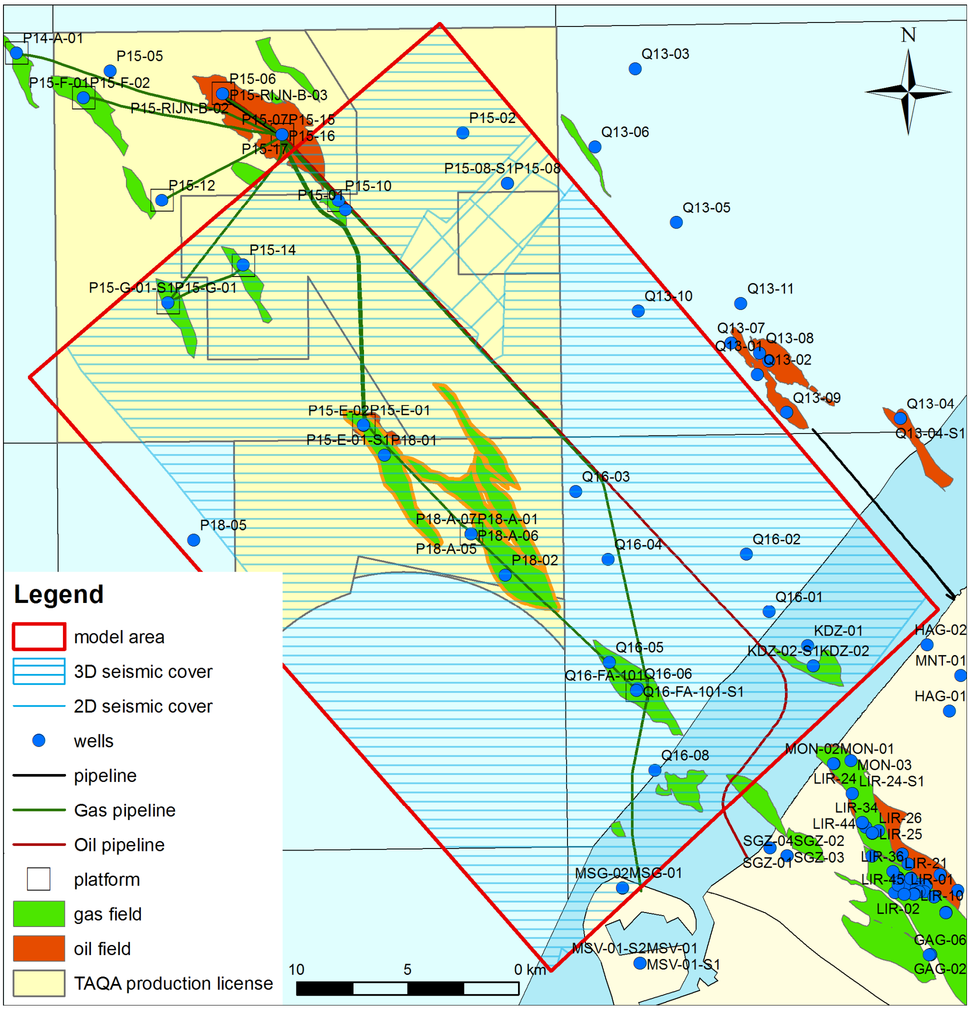

Figure 8.1: Location map of P18 model area. Target P18 gas fields are indicated with an orange boundary.

8.3. Geological model of the P18 Bunter reservoir and overburden

8.3.1. Field description

The P18 gas field is located in the P18 block in the Dutch North Sea, approximately 20 km North West of the coastline. The gas field was discovered in 1989 by the P18-02 exploration well, which found the Triassic Buntsandstein gas bearing. Production started in 1993. The 3 separate accumulations of the P18 gas field are being produced by a total of 6 production wells. The current operator of the field is TAQA Offshore B.V.

Reservoir

The Main Buntsandstein consists of several successive formations (Table 28). The producing interval is limited to the Hardegsen and Detfurth formation. The combined thickness is approximately 100 m, with an average porosity of around 10%. Average permeabilities range from 2-200 mD. The depth of the reservoir ranges approx. between 3200 m and 3600 m.

Table 28: General data on Main Buntsandstein Subgroup sandstones at the P18 location.

Formation	Porosity	Thickness
Hardegsen Fm.	10 % – 12 %	100 m (combined thickness)
Detfurth Fm.	9 % - 11 %	
Volpriehausen Fm.	5 %	100 m

Seal
The primary seal of the P18 reservoirs consists of siltstones, claystones, evaporites and dolostones of the Solling Claystone Member, the Röt formation, the Muschelkalk formation, and the Keuper formation. These formations span a total thickness of approximately 155 m.

8.3.2. Overburden

Directly above the primary seal, as identified in section 8.3.1, a thick succession of marine claystones, siltstones and marls is present. These sediments have excellent sealing quality and belong the Altena Group (Jurassic age). In the P18-02 well (Figure 8.2), the Altena Group has a thickness of approx. 500 m.
The Altena Group is successively overlain by:

- The Schieland Group, which consists of shales and (stacked) channel sands of the Nieuwekerk Fm. (Delft sandstone equivalent). The lateral continuity of the individual sandbodies (thickness 2-5m) is probably very limited.
- Lower Cretaceous Rijnland Group, which consist of marine sandstones, shales and marls. At the base of the Rijnland Group, the Rijn / Rijswijk sandstone is present. This sandstone is widely distributed in the P18 area. It is also known for its oil (P15) and gas (onshore) accumulations within the West Netherlands Basin. The sandstones are interpreted as transgressive sheet sands, with good lateral continuity. In the upper part of the Rijnland succession, the Holland Greensand is present. It consists of argillaceous sands and silts. The distribution is limited to the southern margin of the West Netherlands Basin. Although the Holland Greensand has good lateral continuity, permeability is in general low.
- Upper Cretaceous Chalk Group, which consist at the base of the formation of sands and marls and a thick layer (900 m) of limestones (Chalk). The distribution of the basal Texel Greensand is limited to the southern basin margin.
- The North Sea Group, which consists of siliciclastic sediments. Two major aquifers cam be distinguish; the Dongen sand, a basal transgressive sandstone, and the marine Brussels sand.

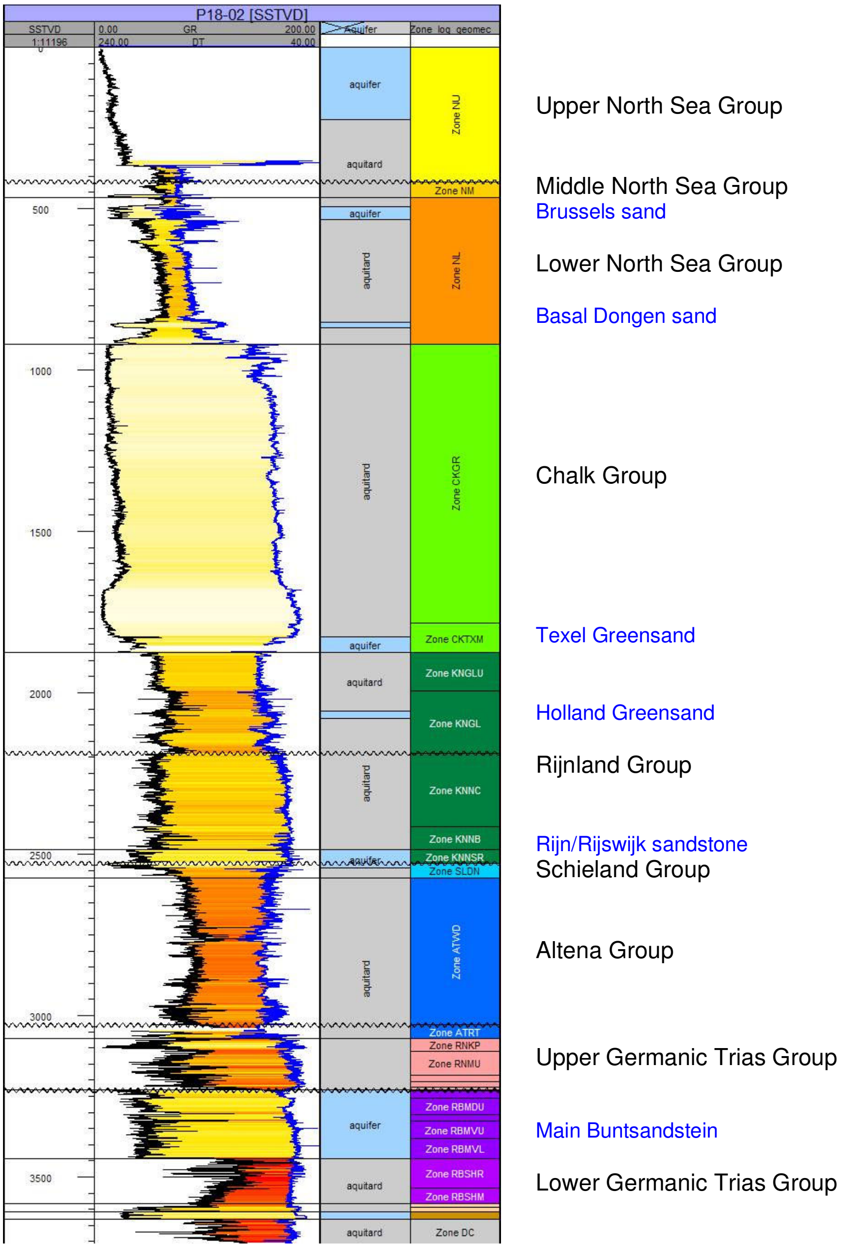

Figure 8.2: Composite well log (GR, DT) of P18-02 with main stratigraphic units and aquifer intervals

8.3.3. Faults

Faults present at reservoir level (Buntsandstein) in general continue till the Schieland group (white line) or base Rijnland Group (dark green line in Figure 8.3). Late Cretaceous inversion caused faulting of the sediments above the Base Cretaceous Unconformity (base Rijnland) These faults (dashed lines Figure 8.3) have limited displacement, but continue to the Upper North Sea Group.

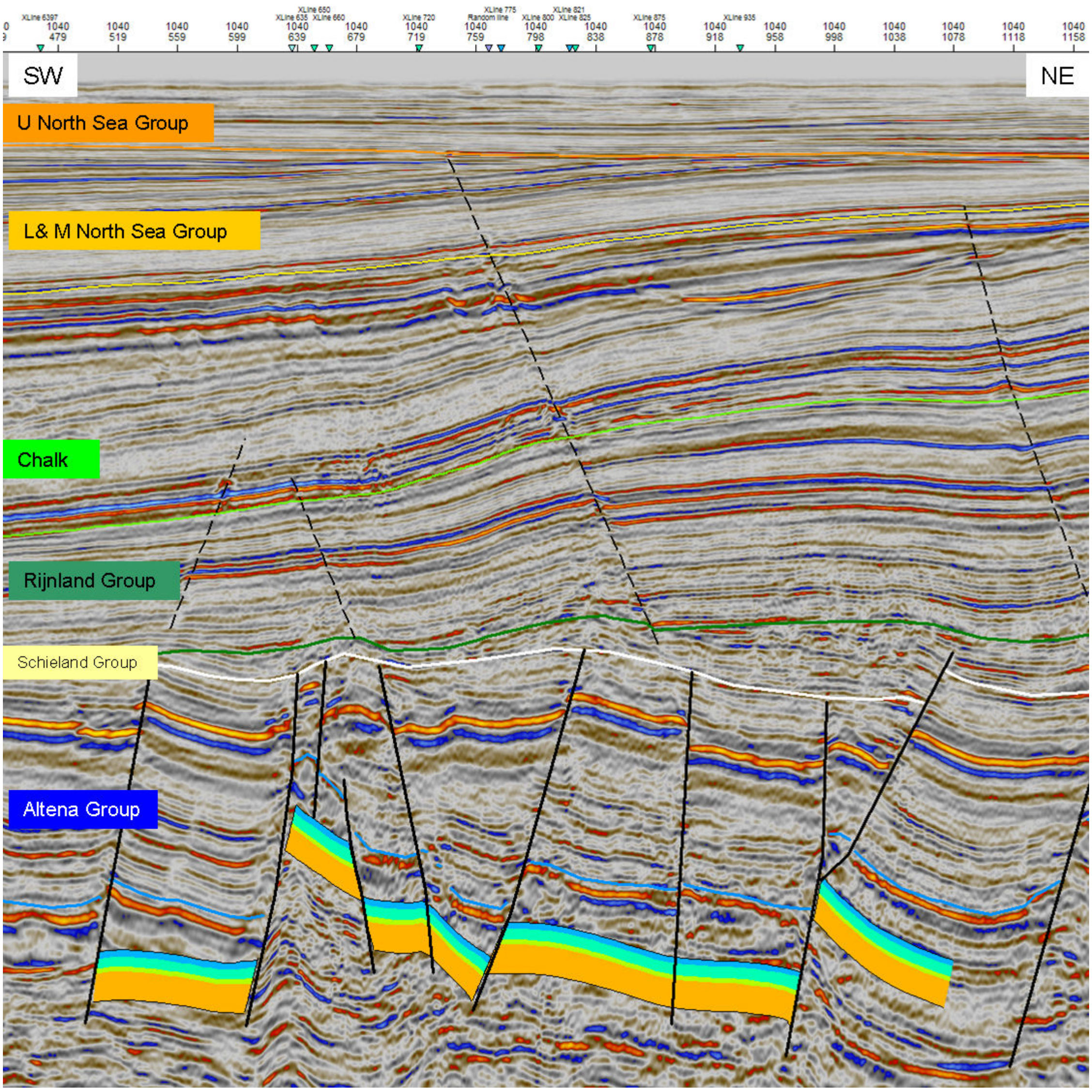

Figure 8.3: Seismic cross-section (inline 1040 of P15P18 seismic cube) through the P18 field, displaying the reservoir interval (coloured layering), the main bounding faults to the reservoirs (bold lines), the main stratigraphic units in the overburden and the faults in the overburden (dashed)

8.4. Migration scenarios

For the qualitative analysis three migration scenarios will be considered:

1. Aquifer spill reservoir:
    a. Buntsandstein
2. Induced fracture caprock:
    a. Migration into Rijn/Rijswijk sandstone
3. Wellbore shortcut:
    a. Migration into Rijn/Rijswijk sandstone
    b. Migration into Holland Greensand
    c. Migration into Texel Greensand
    d. Migration into Dongen & Brussel sandstone

8.4.1. Methods

Possible CO_2 migrations pathways were analyzed using the rapid trapping assessment tool PetroCharge Express of IES. With this tool a rapid analysis of the migration pathways based on the layer geometry is performed. The layer geometry was provided by the exported horizons from Petrel (regional scale model). The program uses the input top layer as bounding elements assuming these layers to be impermeable. Although in reality the layers are not completely impermeable the goal is to create a concept model from which migration routes within the layer can be deducted.
It should be noted that PetroCharge only looks at the geometry and does not describe various other aspects of flow. It was therefore decided to “inject” unreasonable large amounts of CO_2 within the considered leakage scenarios and to look at the trapping mechanisms in a worst case, when all other processes fail.

8.4.2. Results

Migration scenario: Buntsandstein

In case of “overfilling” the gas reservoir with CO_2 it might be possible that the CO_2 will pass by the original closure defined by the initial gas water contact. (GWC).

- Overfilling the P18-2 main compartment could lead to migration towards the Q16-4 structure (Figure 8.4, arrow 1) and the P16-FA field (Figure 8.4, arrow 4)
- Overfilling the P18-6 compartment could lead to migration towards the P15-10 field (Figure 8.4, arrow 2).
- Overfilling the P18-4 compartment in combination with migration along faults could lead to migration towards the P15-E and P15-14 field (Figure 8.4, arrow 3).

It must be mentioned that the structure drilled by the (dry) exploration wells Q16-04 and Q16-03, only minor amounts of gas were encountered. If the containment were to fail by a mechanism describes above, the most probable failure would that be of a sideseal in combination with reservoir juxtaposition with Jurassic sandstones from for instance the Nieuwekerk Formation.

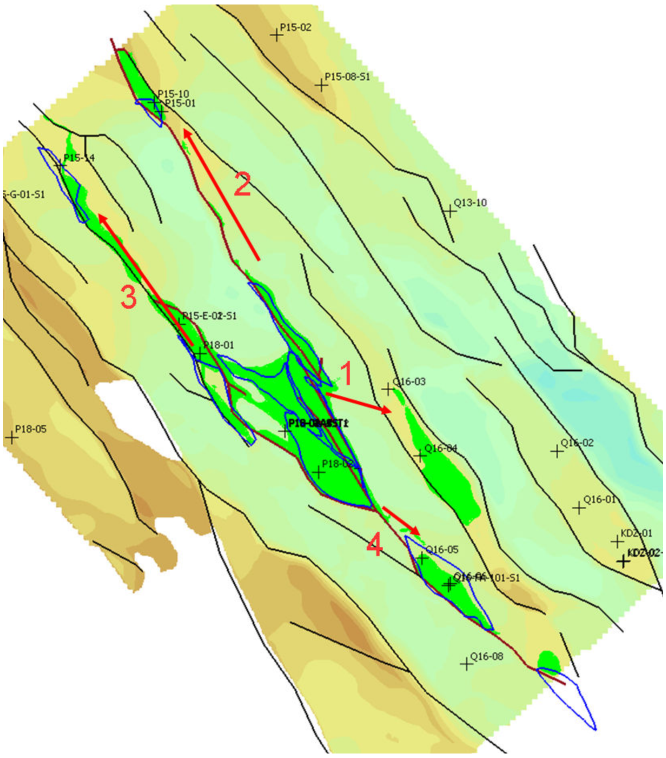

Figure 8.4 Structure map of Top Buntsandstein. Black lines indicate faults. Also shown are boundaries of gas accumulations and location of wells.

Migration scenario: Rijn/Rijswijk sandstone

In case of fault reactivation or shortcut via a wellbore, CO_2 can hypothetically migrate into the Rijn/Rijswijk sandstone aquifer.

- Spill originating from wells P18-A-01, P18-A-06 , P18-A-06-S1, P18-A-07 will migrate towards Q16-03 & Q16-04 structure (Figure 8.5, arrow 1).
- Spill originating from wells P18-02, P18-A-03, P18-A-05 will migrate towards Q16-FA structure (Figure 8.5, arrow 2).
- Spill originating from P18-A-02 well will migrate towards P15-9 (E) structure (Figure 8.5, arrow 3).

Migration scenario: Holland Greensand

In case of a shortcut via a wellbore, CO_2 can hypothetically also migrate into the Holland Greensand aquifer

- Spill originating from wells P18-A-01, P18-A-03, P18-A-06 , P18-A-06-S1, P18-A-07 will migrate towards Q16-03, Q16-04 structure (Figure 8.6, arrow 1)
- Spill originating from wells P18-02, P18-A-05will migrate towards Q16-FA structure (Figure 8.6, arrow 2)
- Spill originating from P18-A-02 well will migrate towards P15-9 (E) structure (Figure 8.6, arrow 3)

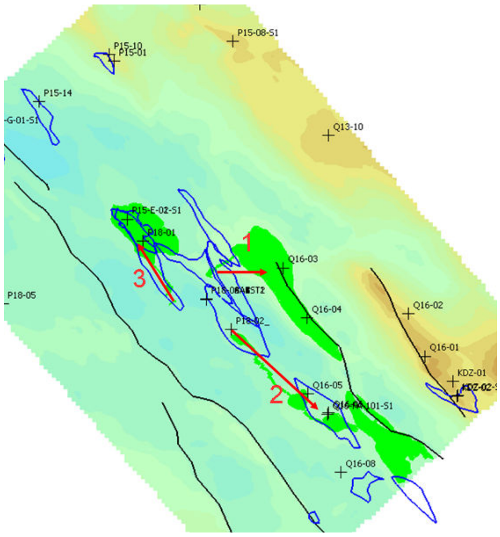

Figure 8.5: Structure map of the Base Rijnland Group. Black lines indicate faults. Also shown are boundaries of gas accumulations and location of wells.

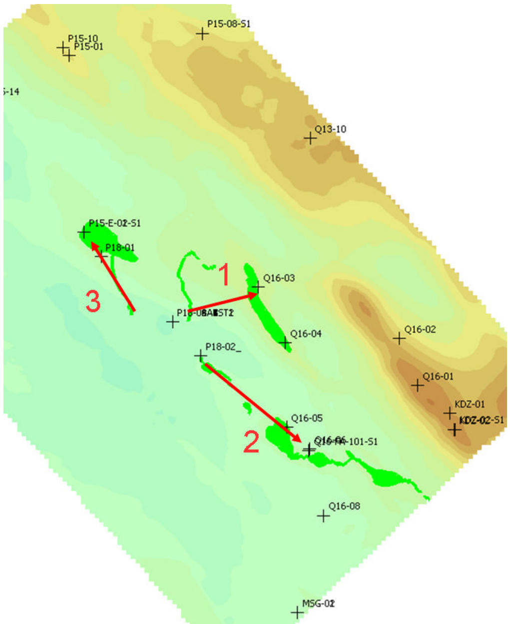

Figure 8.6: Structure map Holland Greensand.

Migration scenario: Texel Greensand

In case of a shortcut via a wellbore, CO_2 can hypothetically migrate into the Texel Greensand aquifer

- Spill originating from P18-A production wells will migrate towards Q16-3 structure and finally Q16-02 (Figure 8.7, arrow 1).
- Spill from P18-02 well will migrate towards Q16-FA structure and finally Q16-01 (Figure 8.7, arrow 2).

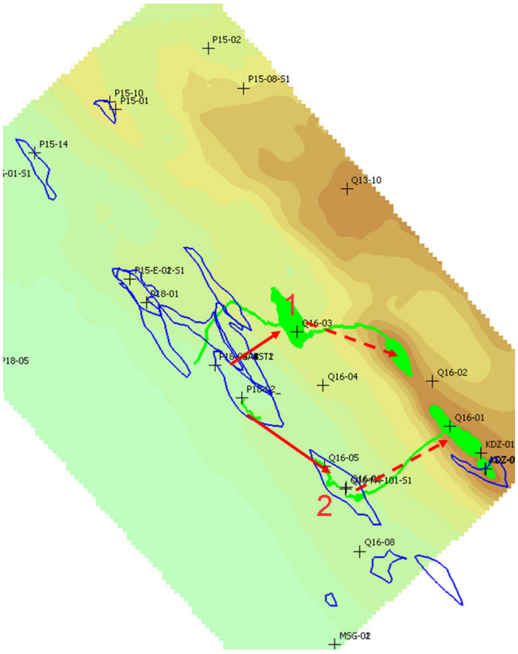

Figure 8.7: Structure map base Chalk Group.

Migration scenario: Dongen sand & Brussel sandstone

In case of shortcut via a wellbore, CO_2 can hypothetically migrate into the North Sea Group aquifer

- Spill originating from P18-A production wells will migrate towards Q13-10 structure (Figure 8.8, arrow 2).
- Spill from P18-02 well will migrate towards Q16-02 structure (Figure 8.8, arrow 2)

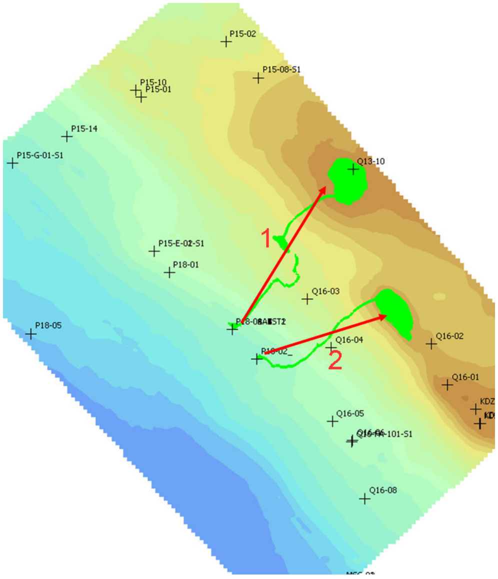

Figure 8.8: Structure map base North Sea Group.

8.5. Present day hydrocarbon migration

Inspection of the overburden revealed the possible existence of shallow gas pockets. (*CATO-2-WP3.1-D01-Geological report P18 (December 2010).* The gas most probably is sourced from Jurassic Posidonia shales (van Baalen, 2000). The Possidonia shales are situated stratigraphically above the Bunter reservoir and seal, so this hydrocarbon migration is no proof of seal failure/leakage of the P18 Bunter reservoir.

Figure 8.9 shows a seismic section of the overburden, to illustrate hydrocarbon migration, and to illustrate a possible migration pathway for CO_2.

Gas is sourced from the Posidonia shale (strong reflector at the base of the lowest arrow), and migrates via a fault into the sands of the North Sea Group. The red ellipses indicate bright spots, which suggest the presence of gas. Migration is also possible within the Brussels sand, indicated by the arrows in Figure 8.9. At the location where the Brussels sand toplaps against the Upper North Sea Group (Mid Miocene Unconformity, orange line), an increase of amplitudes in observed, which suggest migration from the Brussels sand into the Upper North Sea Group.

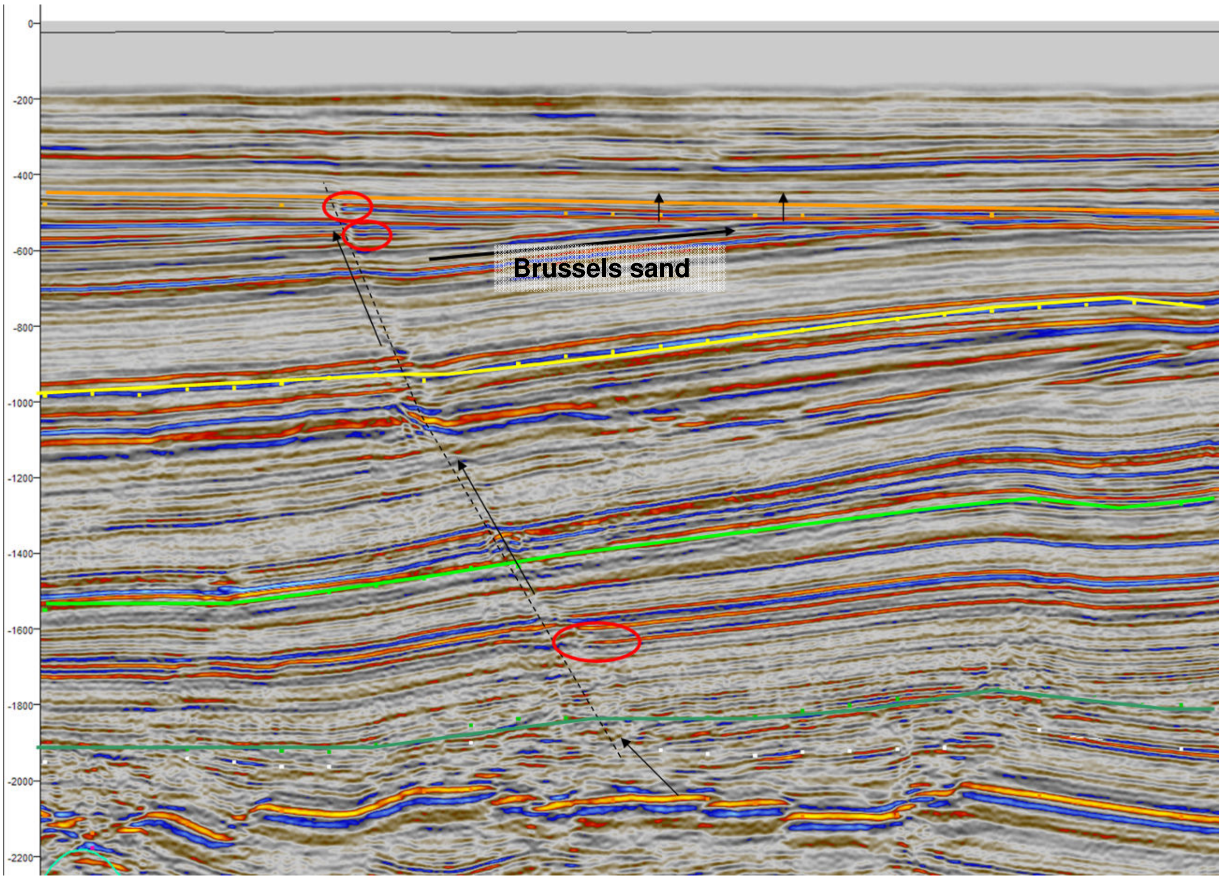

Figure 8.9: Seismic section of the P18 overburden. Arrows indicate hydrocarbon migration along a fault (dashed line). Red elipses mark bright spots on the right side of the fault. Dark green line: base Rijnland (BCU), bright green line: base Chalk, yellow line: base North Sea, orange line: base Upper North Sea (MMU).

8.6. Conclusions

A Petrel model of the overburden has been constructed, which is based on public available data and data provided by TAQA. Based on the geological model and selected hypothetical migration scenarios, a qualitative evaluation of the possible pathways was developed. The main conclusions are that hypothetical migration in the Buntsandstein, caused by overfilling the reservoir, the CO_2 remain trapped within the aquifer and finally will migrate towards the adjacent gas reservoirs. Hypothetical migration of CO_2 in the aquifers of the overburden, caused by a shortcut along the wellbore, will remain trapped within the aquifers. However, migration of CO_2 along faults in the overburden (above the Altena Group) to a shallower aquifer level is not to be excluded.

Overall it can be stated that the most probable pathway to the surface of CO_2 stored in the P18 gasfield is via leaking wells, leaking directly into the atmosphere and not indirectly via pathways originating in deeper parts of the overburden.

8.7. Preliminary monitoring concept

Introduction

This report is meant as input to establish the appropriate final monitoring concept for P18 and is based on the current state of knowledge of the field. This report should not be considered as the final monitoring plan to be submitted for the permit application.

8.7.1. The Eon CCS project

Introduction

Since 1993 high calorific gas has been produced from the P15 and P18 blocks, offshore the Netherlands. This is done from several platforms, among which the P18-A satellite platform, and the P15-ACD processing and accommodation structure, respectively lie 20 and 40 km NW of Rotterdam (Figure 8.10).

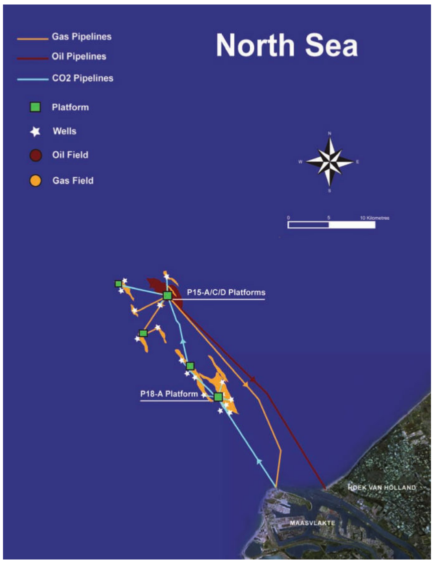

Figure 8.10: Location P15/P18 complex relative to the Dutch shore. Source: CO_2 offshore storage, deep under the Dutch North Sea, (image courtesy TAQA; TAQA, 2009)

The almost depleted gas reservoirs at P15 and P18 are considered suitable for CO_2 storage. They contained large amounts of natural gas under high pressures for millions of years. Furthermore, there is a lot of high quality geological data for these specific structures, to assist in safely storing CO_2. They are relatively close to large CO_2 emitters and are located offshore, which would likely avoid complex permitting procedures.
The CO_2 would be injected into a sandstone formation below impermeable layers of Triassic clay at over 3 km depth.

Infrastructure

The P18 installation consists of a 4 legged steel jacket (Figure 8.11). Its primary function is the production and transfer of wet gas to the P15-D processing platform some 20 km further offshore (Figure 8.12).

Figure 8.11: P18-A Satellite platform. (Courtesy TAQA; TAQA, 2009)

The P15-ACD installation comprises two 6 legged steel jackets and one 4 legged steel jacket (Figure 8.12). Their functions are:

P15- A	Well production
P15-C	Oil processing and accommodation
P15-D	Gas and condensate processing, compression and transporting to shore, metering and control

Figure 8.12: P15-ACD Processing & Accommodation Platforms. (Courtesy TAQA; TAQA, 2009)

Roadmap

Injection of CO_2 in the P18 and P15 fields is planned in several phases:

Phase 1 - From the P18-A platform CO_2 can be injected into several depleted gas reservoirs using multiple injection wells. The combined theoretical storage capacity accessible from this platform amounts to around 41 million tonnes of CO_2. The effective storage capacity will depend on the maximum permitted reservoir pressure.

Phase 2 - After natural gas production ceases from the P18-A platform, the existing pipeline to P15-ACD can be used to transport CO_2 to this central facility from where CO_2 can be distributed to the P15 reservoirs, providing an additional 44 million tonnes of theoretical storage capacity.

Phase 3 - When natural gas throughput ceases completely, the 26 inch pipeline can be turned to CO_2 transport duty. The P15-ACD facility could then be used for many years to boost pressure to transport CO_2 north to other depleted gas reservoirs.

This report is solely related to phase 1 of the CO_2 storage project. For phase 1 the intention is to start injection into the P18-6 field, followed by the P18-4 and finally into the P18-2 field. For the Road project the storage capacity for the envisaged 11 Mtonnes CO_2 can be covered by the combination of P18-6 and P18-4.

8.7.2. The proposed monitoring plan

This proposed monitoring plan is based upon the EU storage directive (2009) and on the EU ETS directive (2009). Since the directives do not provide details on the format of such a monitoring plan, the EU has started to develop guidance documents. The currently proposed monitoring plan is based upon the (draft) guidance document 2 "Implementation of Directive 2009/31/EC on the Geological Storage of Carbon Dioxide" which is available for public consultation currently.
This document has been developed by the European Commission with support from consultants and input from the Information Exchange Group established pursuant to Art. 27(2) of the CCS Directive. It builds on:

- The expertise and experience of the members of the Information Exchange Group, established under the CCS Directive, and the experts involved;
- The results of previous research, methodologies and suggested guidelines.

In the current EU guidance document 2 a global approach is provided for developing a monitoring plan for a storage site. The inventory of monitoring technologies in the document is based on existing literature, essentially the IPCC guidelines for National Greenhouse gas Inventories (2006), the IEA-GHG report (2004), the ASPEN report (2009) and the NSBTF report (2009) as prepared by TNO on behalf of the NSBTF.
The approach adopted in the Aspen report (2009) and the NSBTF report (2009) is inspired on the format for a monitoring plan as produced for the Barendrecht CO_2 storage project by Shell (Shell report, 2008).

Please note, that the proposed format is compliant with the more globally proposed workflow as proposed in the CO_2QUALSTORE guideline (2010) summarized in Table 29.

Table 29: Workflow to prepare a preliminary monitoring plan and to initiate a baseline monitoring program (taken from the CO_2QUALSTORE guideline (2010)).

Preliminary monitoring plan. Initiate baseline monitoring program	
Identify monitoring targets based on identified risks and uncertainties	List of proposed monitoring targets
Identify suitable measurement techniques for monitoring of identified targets	List of suggested measurement techniques
Differentiate between base case monitoring and contingency monitoring triggered by early warning signals	Preliminary base case and contingency monitoring programs
Plan and execute baseline monitoring program	Compilation of results from baseline monitoring activities

8.8. Geological background information

8.8.1. Structure

The reservoir structures comprise multiple compartments bounded by a system of NW-SE oriented faults forming horst and graben structures. The reservoir rocks are of Triassic age, belonging to the Bunter Sandstone ("Main Buntsandstein Subgroup", Van Adrichem Boogaert and Kouwe, 1994, Wong et al., 2007) (Figure 4), and consist of sandstones intercalated with thin layers of shale. The tops of the compartments lie at depths between 3175 m and 3455 m below sea-level (Figure 5).

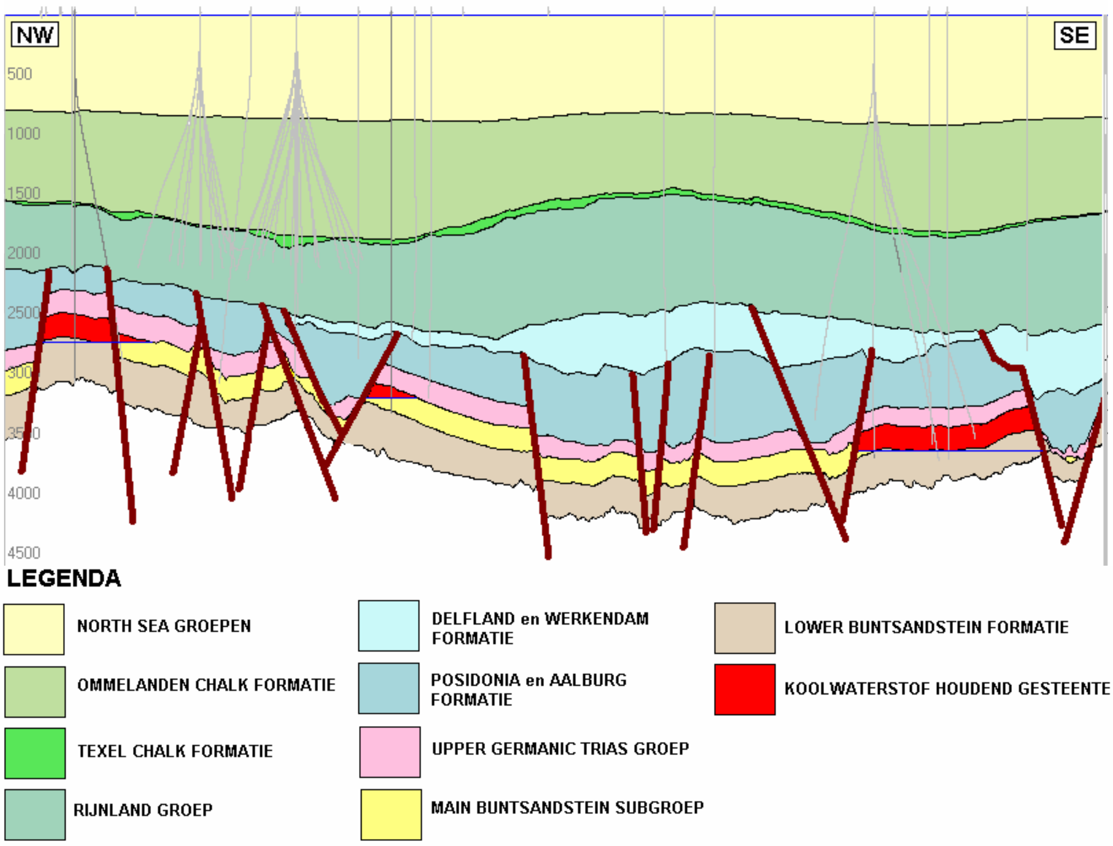

Figure 8.13: Geological crossection of the P15 field, illustrating the stratigraphy and geological setting. Source: Winningsplan P18a, P18c & P15c.

The reservoir rocks were deposited in a typical desert environment with scarce but intense rainfall. The reservoir consists mainly of dune (aeolian) and river (fluvial) sediments. The aeolian sands have the best reservoir properties, comprising clean, well sorted sands with relatively low shale content.

The source rocks for the natural gas, present in the reservoir structures, are the coal layers from the underlying Carboniferous.

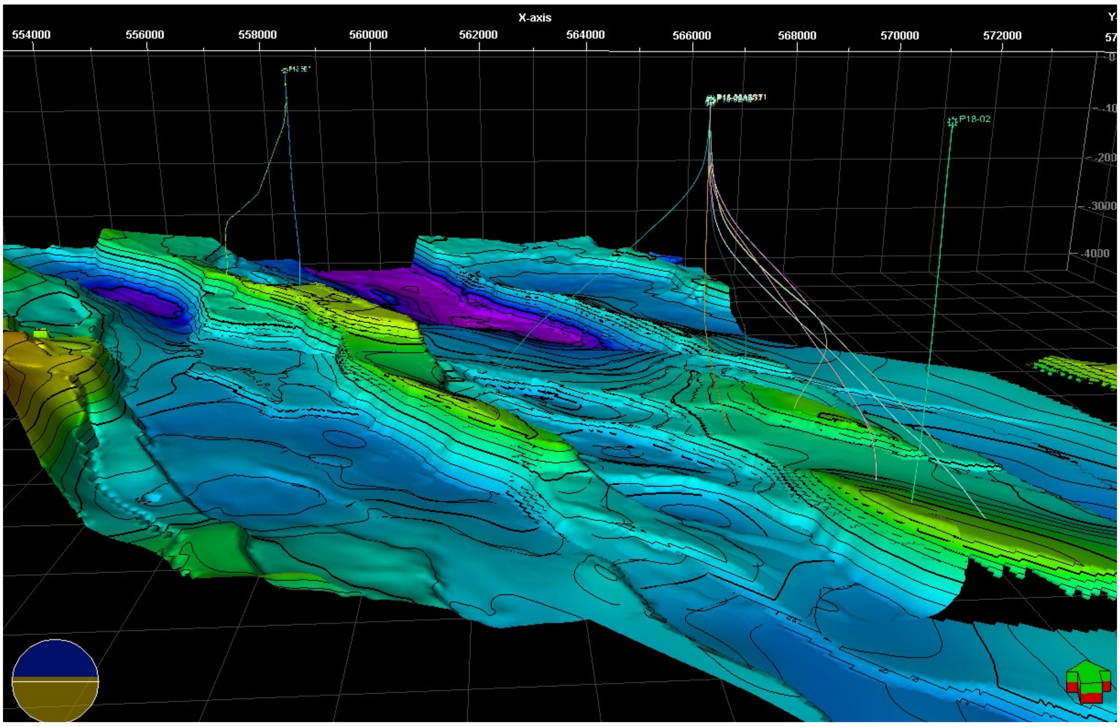

Figure 8.14: 3D view on the top Bunter from a geological model which is still under construction.

8.8.2. Reservoir properties

At P18 the Main Buntsandstein Subgroup consists of several units:

- The Hardegsen Fm.
- The Detfurth Fm.
- The Volpriehausen Fm.

Based on well log data the porosity in the Hardegsen Formation varies around 10-12% and in the Deturth Formation it is slightly lower at about 9-11%. Maximum porosities encountered in the clean sandy parts of both Formations are around 21 %. The combined thickness of both Formations is about 100 m and permeabilities range generally from 0.1 -100 mDarcy. The Volperiehausen has a much lower porosity, around 5%, and also lower permeability. The thickness of the Volperiehausen is around 100 m. Table 30 sums up some general data about these Formations at P18. The irreducible water content is around 15 to 20 % and the abandonment pressures for the compartments are about 20 to 30 bars.

Table 30: General data on Main Buntsandstein Subgroup sandstones at the P18 location.

Formation	Porosity	Thickness
Hardegsen Fm.	10 % – 12 %	100 m (combined thickness)
Detfurth Fm.	9 % - 11 %	
Volpriehausen Fm.	5 %	100 m

For the different reservoir compartments (i.e. P18-2, P18-4 and P18-6) an estimate has been made, based on the gas production history, of the total storage capacity per compartment (Table 31).

Table 31: General data on the compartments at P18.

Compartment	Initial conditions		CO_2 storage capacity (Mt)	Depleted by	wells
	bar	ºC			
P18-2	355	126	32	2017	3
P18-4	340	117	8	2015	1
P18-6	364	117	1	2015	1

Much of the general information of the P18 field also applies to the P15 gas field (Table 32) although depletion dates were not readily available. The geological setting is the same. The platform infrastructure is more complex than that at the P18 location, which is merely a satellite platform.

Table 32: General data on the compartments at P15.

Compartment	Initial conditions		CO_2 storage capacity (Mt)	Depleted by	wells
	bar	ºC			
P15-9	347	117	11	?	2
P15-10	272	104	1	?	1
P15-11	283	102	16	?	2
P15-12	301	112	2	?	1
P15-13	288	107	9	?	1
P15-14	334	107	2	?	1
P15-15	318	120	1	?	1
P15-16	290	109	1	?	1

8.8.3. Overburden properties

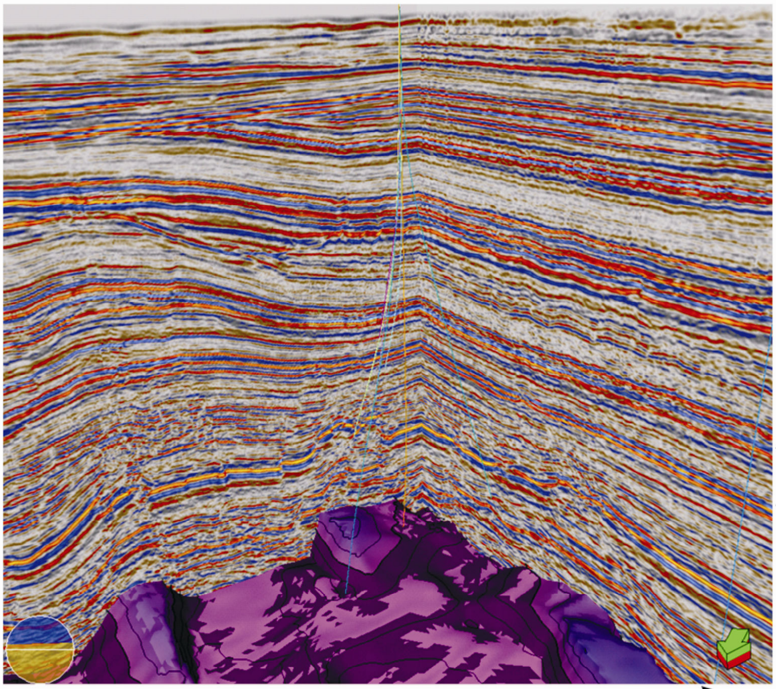

Figure 8.15: Seismic section of the overburden at P18-A. The surface represents the base of the Lower Germanic Trias Group (also base of the reservoir). Note the fractured nature of the Triassic and Jurassic sediments (up to the Posidonia Shale Formation) and the continuity of the Lower Cretaceous and younger sediments.

The overburden at P18-A is formed by several geological formations. The North Sea Supergroup, of Cenozoic age, is the shallowest stratigraphical unit and comprises mostly siliciclastic sediments, from approximately seabed to 1000 m depth. It encompasses the Lower, Middle and Upper North Sea Groups, the bases of which are marked by distinct unconformities. The lower group comprises Paleocene and Eocene strata, predominantly marine deposits, the middle group includes mainly Oligocene marine strata, and the upper group consists of the marine to continental Miocene and younger sediments. The North Sea Supergroup in the area of interest is unfaulted at seismic resolution scale. Clayey sequences are very abundant, especially in the lower parts of the North Sea Supergroup and could very well act as secondary seals. The presence of trap structures has not yet been investigated.
The North Sea Supergroup unconformably overlies the Upper Cretaceous Supergroup, which ranges from approximately 1000 m to 2400 m depth and in this area comprises the Ommelanden Formation, the Texel Formation and the Texel Greensand Member. During the Late Cretaceous, the influx of fine-grained clastics into the marine realm (Lower Cretaceous) diminished. A fairly uniform succession of marls and limestones of the Texel and Ommelanden Formations developed. These sediments have an earthy texture and are commonly known as 'chalk'. The sealing properties of these formations are questionable although this interval is largely unfaulted.
The Lower Cretaceous Supergroup consists of the Holland Formation, the Vlieland Claystone Formation and Vlieland Sandstone Formation and ranges from approximately 2400 m to 3400 m

depth. In locations close to P18-A, some of the sandstone layers present in this interval are gas bearing, demonstrating the sealing capacity of various claystone intervals in this succession.
In the area of interest the Lower Cretaceous is mainly unfaulted (on seismic resolution scale), improving the likelihood that layers in this level could indeed act as secondary seals.
At P18-A the Jurassic Supergroup consists of the Nieuwerkerk Formation, Lower Werkendam Member, Posidonia Shale Formation, Aalburg Formation and the Sleen Formation and ranges in depth from approximately 3400 m to 3900 m. The Nieuwekerk Formation predominantly comprises continental deposits, whereas the other formations consist of marine sediments mainly in the form of clays which could very well act as secondary (or even primary) seals.
The primary seal is formed by clay layers from Triassic and lower Jurassic age (the Upper Germanic Trias and Altena Group). Faults are present in this primary seal, but these do appear to be sealing and in general do not penetrate the caprock further upwards than the Posidonia Shale Formation (Figure 6). Reservoir closure along the bounding faults is obtained by juxtaposition of shale layers of various ages and clay smear. These bounding faults do not continue further upward into the overburden than the shales of the Altena Group (see Chapter 3). Due to the sealing nature of the bounding faults there is no water drive in the compartments.

8.9. Risk assessment of P18

8.9.1. Introduction

For the P18 field a risk assessment has been carried out by Royal-Haskoning dd. July 7, 2010 in the form of a workshop. Below follows a summary of the identified subsurface related risks.

8.9.2. Summary of identified risks

The risks for migration out of the reservoir into the overburden or for leakage at the sea bottom are considered minimal for P18, which is a depleted gasfield with no active aquifer drive. The latter is demonstrated by the straight production P/z curves. Currently the reservoir is well below hydrostatic pressure.
As pointed out in the top seal and fault integrity study (Orlic et al, 2010), geomechanical-related risks of fracturing and fault re-activation are small and can be (partially) reduced by:

- Injecting CO_2 with bottom hole pressures (BHP) which are below fracturing condition.
- Avoid overpressurizing the reservoir above the initial pressure.
- Keeping a safe distance between the injection wells and faults to avoid direct charging of faults by injected CO_2 through natural or induced fractures. Wells closest to faults are wells P18-02A1, P18-02A6, P18-04A2 and P18-06A7ST1. The latter requires most caution, since the injectivity of the P18-06 reservoir is of the least quality.
- Managing thermal effects of injection

During injection, the potential for fault reactivation generally decreases providing that the CO_2 is not injected directly into the fault zone and the thermal effects of injection are negligible. The risk of induced hydro-fracturing increases in the later stage of CO_2 injection when the reservoir is almost re-pressurized to the initial pressure.

Based on the KNMI database of recorded induced seismic events associated with hydrocarbon production in the Netherlands, the P18 field was not seismically active during its production period. The detection limit of the KNMI seismic network was M2.5 until 1995 and M1-1.5 on Richter scale afterwards (Orlic et al., 2010). No major seismic activity is therefore expected.

The caprock has proved to be gas tight based on the production history. However, there are indications on seismic data of natural shallow gas up to the seabottom along and near faults (see Chapter 3). The origin of the shallow gas is unknown. Considering the excellent sealing quality of the primary seal of the P18 reservoir, and the difference in age and dip of the faults in layers above and below the Altena Group, it is unlikely that these potential shallow gas accumulations are related to the P18 reservoirs from which gas is produced. More likely, it originates from either the Posidonia Shale Formation in the overlying Altena Group, which is responsible for charging many Upper Jurassic and lower Cretaceous reservoirs in the vicinity or from shallower layers by biogenic processes.
Furthermore, since the properties of CO_2, especially in combination with connate water, are different from methane, it means that dissolution and precipitation of minerals, respectively creating or blocking migration pathways, needs to be thoroughly investigated (see Chapter 5).

Furthermore the possibility of fault reactivation needs attention, since the reservoir has been depressured (depleted) and CO_2 injection would involve repressuring. On top of that a possible geochemical-geomechanical interaction must be investigated (see Chapter 6). The modeling results show that short-term mineralogical and porosity changes, induced by dissolved CO_2 and corresponding pH decrease, are negligible. On the long-term (thousands of years) mineral reactions will result in a porosity decrease of 0.3 percentage point (pp) for the reservoir and a porosity increase of 0.2 pp for the cap rock. The presence of O_2 as an impurity in the CO_2 stream does not seem to have significant consequences regarding the short-, mid- and long-term geochemical effects of CO_2 storage (see Chapter 5).

The injectivity of the reservoir is considered to be especially an issue in the P18-6 field (see Chapter 4). The main reservoir is heterogeneous with potentially rapid lateral facies changes typical of a fluviatile setting. This may lead to problems during injection such as local pressure build-up. This will be noticed immediately by monitoring the required injection pressure. Apart from geological heterogeneity of the reservoir, near wellbore effects such as salt precipitation or Joule Thompson effects (like freezing) of the CO_2 due to adiabatic expansion do not appear to cause uncontrollable risks (see Chapter 4). The latter may give rise to thermal fraccing. The expectation is, that this will only influence a relatively small part of the reservoir close to the wellbore (see Chapter 4)

In terms of migration of CO_2 into the overburden the main potential pathways considered are along existing or new wellbores A more detailed analysis of the state of the existing wells has been investigated (see Chapter 7). Characterization and proper abandonment of these wells followed by well integrity measurements is necessary. In the worst case this may require a work-over of one or more of the wells.

Laterally the reservoir is constrained by a structural closure and sealing faults (Orlic et al., 2010). Migration within the reservoir is therefore not a crucial parameter to monitor. However, it does provide input for the predictive simulation models demonstrating a proper understanding of the reservoir and associated flow processes.

8.10. Development monitoring plan

8.10.1. Introduction

The starting point for developing the monitoring report is an adequate characterization and risk assessment. The general requirements for both site characterization and risk assessment are given in the EC Storage Directive and its Annexes (2009) with further details in the EU guidance

documents (2010). The monitoring report in its turn must be related to preventive and corrective measures.
Therefore in the adopted template in this report potential risks, monitoring techniques and mitigation measures are linked together.
With respect to timing this report describes a ‘workflow’ for monitoring activities during the pre-injection (site qualification), injection (operation), post-injection (closure and post-closure) phases and after transfer of responsibility (long-term stewardship). However, since monitoring in the different stages of a project is not fundamentally different, they do not play a major role. The philosophy of the monitoring plan is that it must be: complete, transparent, consistent, and verifiable.

Monitoring categories

Monitoring serves several important purposes, which are confirming containment of CO_2, alerting for corrective measures in case of increased leakage risk and gathering evidence for the long-term containment of CO_2.
This can be achieved either by measuring the absence of any leakage through direct detection methods, or by verifying indirectly that the CO_2 is behaving as expected in the reservoir based on static and dynamic modeling and updating thereof corroborated by monitoring data. The main challenge for measuring absence of any leakage consists of spatial and temporal coverage of the monitoring method, i.e. “Where and when do we need to monitor in order to be sure that no leakage occurs”. The strategy should therefore be based on identified risks.

For the indirect model-based monitoring the emphasis is more on scenario confirmation. As long as predictive models are behaving in agreement with monitoring data, the understanding of both the processes occurring and the behavior of the storage complex can be considered sufficient. In case of deviations, one should find the causes of the deviations and where necessary recalibrate the models. If however the deviations fall well beyond the uncertainty ranges of the predictive models , then additional monitoring and possibly contingency measures need to be taken.

In practice often a combination of approaches will be required and the optimal monitoring plan will be guided by the risk assessment and the site characterization.

Following the NSBTF (2009) and the draft EU guidance documents (2010), the following categories for monitoring are identified:

1. Mandatory (in any case for all sites) monitoring: A number of parameters to be monitored is mandatory based on the storage directive.
2. Required (site specific) monitoring: This monitoring group is directed to gathering evidence for containment in the reservoir and to demonstrate integrity of seal, fault and wells in case of regular development.
3. Optional contingency monitoring: The third group refers to a contingency monitoring system which will only be installed if irregularities show up. In the Storage directive a “significant irregularity” is defined as '…any irregularity in the injection or storage operations or in the condition of the storage complex itself, which implies the risk of a leakage or risk to the environment or human health’.

Note, that these three categories as such have not been implemented in Dutch legislation yet, therefore the term mandatory should be read as “mandatory following the EU directive”. Similar for the term required, which is not as such defined in legislation. Required in the context of this report means a preliminary proposal of essentially risk-based monitoring with the current state of knowledge.

The quantification of a leakage at the seabottom for ETS purposes is considered as part of the contingency monitoring. Quantitative monitoring for ETS will only be required, if there is an indication of leakage.
For the North Sea a sound strategy suggested by the NSBTF (2009) would be to detect leakage to the surface by geophysical methods like seismic data (detection of gas chimneys) or sea-bottom echo-sounding (detection of pockmarks) and then sample these leakage areas for direct CO_2 detection repeatedly. Based on the sampling profiles an estimate can be made of leakage rates in time for the area. In case of wellbore leakages an additional monitoring program in and around the well is suggested.

Procedure monitoring plan

A monitoring plan drawn up by the operator should meet the following requirements according to the Storage Directive:

Initial plan

The monitoring plan shall provide details of the monitoring to be deployed at the main stages of the project, including baseline, operational and post-closure monitoring.

The following shall be specified for each phase:

1. Parameters monitored;
2. Monitoring technology employed and justification for technology choice;
3. Monitoring locations and spatial sampling rationale;
4. Frequency of application and temporal sampling rationale.

The parameters to be monitored are identified so as to fulfil the purposes of monitoring. However, the plan shall in any case include continuous or intermittent monitoring of the following items:

1. Fugitive emissions of CO_2 at the injection facility;
2. CO_2 volumetric flow at injection wellheads;
3. CO_2 pressure and temperature at injection wellheads (to determine mass flow);
4. Chemical analysis of the injected material;
5. Reservoir temperature and pressure (to determine CO_2 phase behaviour and state).

The choice of monitoring technology shall be based on best practice available at the time of design.

The following options shall be considered and used as appropriate:

1. Technologies that can detect the presence, location and migration paths of CO_2 in the subsurface and at surface;
2. Technologies that provide information about pressure-volume behaviour and areal/vertical saturation distribution of CO_2-plume to refine numerical 3-D-simulation to the 3-D-geological models of the storage formation established pursuant to Article 4 and Annex I;
3. Technologies that can provide a wide areal spread in order to capture information on any previously undetected potential leakage pathways across the areal dimensions of the complete storage complex and beyond, in the event of significant irregularities or migration of CO_2 out of the storage complex.
4. The yearly report to the competent authorities should encompass the above. If needed comment on site-specific monitoring problems.

Updated plan

The initially installed monitoring system and related procedures need to be updated on the basis of the evaluation and modeling activity, or the verification results. Monitoring plans must be updated, at least every five years, to take into account changes to assessed risk of leakage, changes to assessed risks to environment and human health, new scientific knowledge, and improvements in the best available technology. The national authorities may set a more stringent frequency.

According to Annex II of the Storage Directive one has the following updating requirements:

1. The data collected from the monitoring shall be collated and interpreted. The observed results shall be compared with the behaviour predicted in dynamic simulation of the 3-D-pressure-volume and saturation behaviour undertaken in the context of the security characterisation.
2. Where there is a significant deviation between the observed and the predicted behaviour, the 3-D-model shall be recalibrated to reflect the observed behaviour. The recalibration shall be based on the data observations from the monitoring plan, and where necessary to provide confidence in the recalibration assumptions, additional data shall be obtained.
3. Steps 2 and 3 of Annex I shall be repeated using the recalibrated 3-D model(s) so as to generate new hazard scenarios and flux rates and to revise and update the risk assessment.
4. Where new CO_2 sources, pathways and flux rates or observed significant deviations from previous assessments are identified as a result of history matching and model recalibration, the monitoring plan shall be updated accordingly.
5. Post-closure monitoring shall be based on the information collected and modelled as in a-d. The plan must now also provide information needed for the transfer of responsibilities to the competent authority (long-term stewardship). Especially the site's permanent containment must be indicated, based on all available evidence.

Monitoring at different stages of the project

Pre- injection, Injection and Post-injection monitoring do not differ in intent. Risks may be deemed higher in (parts of) the injection phase, notably the beginning of the injection activities. The monitoring plan reflects higher degrees of risk with more frequent monitoring.

Baseline and repeat measurement acquisition, processing and interpretation will be commented on in the plan. The relation with risk assessment and preventive/corrective measures is described.

In the pre-injection phase the main issue consists of gathering baseline data. At this stage it is of utmost importance to identify all possible baseline data that might be needed later in the injection and post-injection phases both for required monitoring as well as for contingency monitoring. More precisely, the risk assessment and scenario definition is crucial.

The Storage directive requires the operator to provide a provisional plan with corrective measures. This plan must be produced before any operations have begun. The basis therefore depends largely on modelling exercises performed in the context of site characterization and risk assessment. The operator should comment on how models plus forthcoming data lead him to a diagnosis of the problem – if the suspicion of a problem exists and how corrective measures are taken. This will be largely a site-specific exercise, based on the aforementioned risk assessment.

The period required for monitoring after abandonment of the wells and prior to decommisioning of the platform is not defined yet, neither is the period between decommisioning of the platform and transfer of liability to the state authorities. The required lengths of these periods need to be established in agreement with State Supervision of the Mines (SodM).

8.10.2. Proposed monitoring plan

This section describes the actual monitoring plan. The main overview is given by Table 4. The first column describes the parameters to be monitored. These parameters follow both from the mandatory monitoring obligations as stipulated by the storage directive and from the risk assessment.

The second column indicates the proposed technique adopted to measure the parameter. A more detailed description of the technique is provided outside the table.

The third column indicates the category of monitoring (mandatory, required, contingency). The fourth and fifth columns give a description both of the temporal frequencies (column 4) and spatial coverage (column 5) of the data acquisition foreseen in the different phases of the project (pre-injection, injection and post-injection including long-term stewardship after transfer of responsibility). The rationale behind the monitoring strategy related to the identified risks is described in the following section.

Column 6 provides a description of the expected accuracy of the monitoring method and of expected values that indicate normal behavior. Therefore this column is colored green.

The 7th column indicates threshold values, where normal behavior as anticipated stops and where irregularities start. As long as the measured values remain below these threshold values, no actions are required (green column). In case however the values come above the threshold values, one enters the 7th column colored orange with specific actions defined. This stage is considered as an increased alert phase, where behavior starts to deviate from expectations. This could for example lead to recalibration of the models, but when persisting to more stringent measures.

In case the monitor values come above the identified threshold in the 8th column coloured red, the highest alert phase starts and immediate actions (or contingency measures) as defined in the second subcolumn of column 8 are required.

Furthermore the table is divided into different blocks describing the different compartments to be monitored (injection process, injection and monitoring wells, abandoned wells, reservoir integrity, plume tracking, environmental monitoring).

The entire table needs to be updated and submitted to the competent authorities yearly.

Table in Appendix D:Monitoring plan according to the format proposed in the NSBTF (2009) and the draft EU guidance document (2010).

Table in Appendix D:Timeline of the monitoring plan.

Note, that the timing for monitoring of the post injection period including the abandonment of the wells and the decommisioning of the platform and the period to the transfer of liability to the state have not been defined in this plan. The definition of these periods will be subject of discussion with State Supervision of the Mines.

8.10.3. Relation risks – proposed monitoring methods

Introduction

This section provides more detailed background information on the rationale behind the selection of the proposed monitoring techniques. For each section corresponding to an identified risk/purpose the different techniques relevant for monitoring of it are referred to between brackets by their number as appearing in Table 4.

CO_2 Plume imaging (1,8,9,15,16,17,18,19,21,22)

The key tool for plume imaging in general is 3D surface seismic, however this is not deemed suitable for P18. This is because of the considerable depth of the P18 storage reservoir, which renders surface seismic methods less than optimally effective. Additionally, for P18 the presence of (residual) gas within the reservoir makes the feasibility of repeated seismic surveys for plume detection questionable.
Based on the history match of the P18 reservoir the field can be considered as a “tank model” with a good quality straight P/z curve (see Chapter 4) and without an active aquifer drive. Therefore plume migration is expected within the bounds of the original gas reservoir.
The main components for monitoring deviations in expected behavior indicating potential migration out of the reservoir or storage complex consist of pressure (and temperature) monitoring. After proper history matching any deviations from the expected pressure trend (P/z curve) during and after the operational phase is a strong indicator for migration out of the storage complex. As for the K12-B reservoir, pressure monitoring has the potential to be a powerful tool at this site, since there is no strong aquifer drive masking potential deviations. A rough estimation of the threshold of the mass of CO_2 migration out of the reservoir that can be detected is in the order of 100-500 ktonnes of CO_2. The exact value depends heavily on the quality of the P/z curves with proper and reliable pressure measurements. Factors like water influx, communication with neighboring blocks or CO_2 dissolution in water have a negative effect on the detectability.

Proper pressure measurements can be obtained from the injection well after a shut-in, or continuously from a monitoring well. The latter is definitely the preferred option allowing a continuous measurement of the reservoir pressure in equilibrium. In case the reservoir pressure is measured in the injection well after a shut-in care must be taken to take the measurements always at the same time after shut-in or even better, measure the pressure curve over a time interval in the order of days. Based on the curve the equilibrium pressure can be extrapolated (assuming it has not been reached in this period).

Migration in the reservoir can be followed by additional geophysical logs (RST logs) and downhole fluid samples at monitoring wells to detect CO_2 breakthrough. During the injection phase, microseismic monitoring may provide data on the location of the advancing CO_2 temperature front by detecting thermal fraccing. The latter is not considered as an absolutely required measurement for plume tracking, but is recommended.

Top seal integrity (8,9,15,16,17,18,19,20,24,25)

As for the plume imaging, the top seal integrity is assumed intact as long as no abnormal behavior of the pressure is observed. In case significant deviations are observed, contingency monitoring is required including time-lapse seismic data acquisition to detect migration pathways (chimneys) or shallow gas accumulations. 2D surface seismic may be a cost-effective alternative to full 3D, but will not provide full areal coverage of the top seal.

The threshold value of seismically detectable accumulations of CO_2 is in the order of 10's of ktonnes under the condition that CO_2 accumulates as a concentrated gas pocket. The shallower the CO_2 accumulates, the better the chances of picking up the signal.
During the injection phase, microseismic monitoring provides data on whether the topseal is being geomechanically compromised. The feasibility of using wells from neighbouring blocks as monitoring wells for microseismic monitoring has not been explored yet, but is potentially an option.

CO_2 migration in the overburden (19,20,21,23,24,25,26,27)

The key tool for the detection and imaging of CO_2 migration in the overburden is repeated 3D surface seismic. Note, that this is considered as a contingency measurement, only necessary in case of irregular behaviour. Surface 3D seismic can provide full coverage of the overburden volume and utilise its full imaging/resolution potential in the shallower overburden. During the injection phase, microseismic monitoring may provide data on the location of the migrating CO_2 front. As above, during the injection phase, 2D surface seismic may be a cost-effective alternative to full 3D, but will not provide full areal coverage of the overburden. Geophysical logs would not provide reliable indications of generalised CO_2 migration within the overburden except where free CO_2 accumulates in very close proximity to the wellbores. As mentioned above, the threshold value of seismically detectable accumulations of CO_2 is in the order of 10's of ktonnes.
Sampling fluids of shallower aquifers can show traces of leaking CO_2. To detect the absence of migration to the seabed, multi-beam echosounding is recommended identifying pockmarks or bubbles.

Calibration of flow simulations (1,2,3,4,5,8,9,15,16,17,18,21,22)

The calibration of flow simulations combines aspects of several of the above aims, effective plume imaging, accurate pressure and temperature monitoring and insights into fine-scale and geochemical processes. Likely tools are downhole pressure/temperature measurements, RST logs and monitoring breakthrough in monitoring wells. For P18 where seismic imaging of CO_2 in the reservoir is considered difficult if not imposible, downhole pressure/temperature is the key technology. Downhole fluid chemistry also has a role, particularly in constraining amounts of dissolution. As in a number of cases above, microseismic monitoring may be useful in the injection phase.

Well integrity (6,7,8,9,10,11,12,13,14,20,23,24,25,27,28)

The key tool for monitoring well integrity is clearly logging, aimed both directly at the wellbore (cement bond logging etc), but also at the surrounding formations (saturation logging). Pressure-temperature logging and downhole fluid chemistry are also potentially very useful. Non-well-based tools include 2D or 3D surface seismic for volumetric imaging of the overburden around the wellbores and multibeam echosounding to detect surface changes around the wellbore.
During the injection stage, well-based microseismic monitoring can also provide information on flow and degradation processes around the wellbores.

8.10.4. EU Storage Directive / OSPAR

Monitoring requirements of the European Directive and OSPAR are framed around enabling the operator to understand and to demonstrate understanding of current site processes, to predict future site behaviour and to identify any leakage. Further requirements of the monitoring include early identification of deviations from predicted site behaviour, provision of information needed to carry out remediative actions and the ability to progressively reduce uncertainty.

8.10.5. Emissions accounting for ETS

The Monitoring and Reporting Guidelines for CCS under the ETS describe the method for quantifying potential CO_2 emissions from a storage project.

Potential emissions sources for CO_2 emissions from the geological storage of CO_2 include:

- Fuel use at booster stations and other combustion activities such as on-site power plants;
- Venting at injection or at enhanced hydrocarbon recovery operations;
- Fugitive emissions at injection;
- Breakthrough CO_2 from enhanced hydrocarbon recovery operations;
- Leakage from the storage complex.

Quantitative monitoring for ETS will only be required, if there is an indication of leakage. Currently there is no requirement for emission accounting as there is no evidence that the site will leak. However, in case irregularities are observed for example in the downhole pressure and temperature measurements, the need for additional monitoring to detect migration pathways out of the storage complex becomes stringent.

Key question for quantitative monitoring is of course, to what extent does the state-of-the-art technology allow for an accurate quantification. In that perspective the NSBTF (2009) suggests in general choosing a combination of a model-driven approach in combination with a monitoring strategy to best estimate the leakage for ETS purposes.

For P18 a sound strategy would be to detect leakage to the surface by geophysical methods like seismic data (detection of gas chimneys) or sea-bottom sonar techniques (detection of pockmarks) and then carry out in situ gas measurements and/or sample these leakage areas for direct CO_2 detection. Based on these observations an estimate can be made of leakage rates for the area.

In case of wellbore leakages an additional monitoring program in and around the wells is suggested.

8.11. Conclusions

Considering the overall philosophy of the EU Directive enshrined in the three minimum geological criteria for transfer of liability:

- Observed behavior of the injected CO_2 is conformable with the modelled behaviour.
- No detectable leakage.
- Site is evolving towards a situation of long-term stability.

one can say, that the three objectives can be covered by the proposed monitoring programme. The main question will be whether characterization of the caprock in combination with reservoir pressure monitoring provides sufficient confidence to omit seismic monitoring for detecting migration out of the storage complex.

8.12. References

ASPEN report, 2009. Support to the Introduction of the Enabling Legal Framework on Carbon Dioxide Capture and Storage (CCS), Service Request under the atmospheric emissions Framework contract ENV.C.5/FRA/2006/0071.

CO_2QUALSTORE 2010: Guideline for Selection and Qualification of Sites and Projects for Geological Storage of CO_2. DNV Report No.: 2009-1425.

Storage directive, 2009: DIRECTIVE 2009/31/EC OF THE EUROPEAN PARLIAMENT AND OF THE COUNCIL of 23 April 2009 on the geological storage of carbon dioxide and amending Council Directive 85/337/EEC, European Parliament and Council Directives 2000/60/EC, 2001/80/EC, 2004/35/EC, 2006/12/EC, 2008/1/EC and Regulation (EC) No 1013/2006.

ETS directive, 2009: DIRECTIVE 2009/29/EC OF THE EUROPEAN PARLIAMENT AND OF THE COUNCIL of 23 April 2009 amending Directive 2003/87/EC so as to improve and extend the greenhouse gas emission allowance trading scheme of the Community EU Guidance Document 2 (draft 2010): Site Characterisation, CO_2 Stream Composition, Monitoring and Corrective Measures. Draft document for consultation version June 17, 2010.

EU Draft guidance document for consultation (June 17, 2010): Implementation of Directive 2009/31/EC on the Geological Storage of Carbon Dioxide. Draft EU Guidance document 2: Site Characterisation, CO_2 Stream Composition, Monitoring and Corrective Measures.

Intergovernmental Panel on Climate Change (IPCC), 2006, IPCC Guidelines for National Greenhouse Gas inventories, Volume 2 Energy, Chapter 5 Carbon Dioxide, Transport, Injection and Geological Storage.

IEA GHG (Greenhouse Gas Programme), 2004, Overview of Monitoring Requirements for Geologic Storage Project Report PH4/29.

IPCC (2006) Guidelines for National Greenhouse Gas Inventories. Chapter 5: Authors: Sam Holloway (UK), Anhar Karimjee (USA), Makoto Akai (Japan), Riitta Pipatti (Finland), and Kristin Rypdal (Norway) arbon dioxide transport, injection and geological storage.

North Sea Basin Task Force (NSBTF), 2009, Monitoring Verification Accrediting and Reporting (MVAR) Report for CO_2 storage deep under the seabed of the North Sea.

OSPAR (2007). OSPAR Guidelines for Risk Assessment and Management of Storage of CO_2 Streams in Geological Formations (Reference Number: 2007-12), Meeting of the OSPAR Commission, Ostend, 25-29 June 2007.

Shell (2008): Integraal Monitoringsprotocol CO_2-opslag Barendrecht. Shell report EP200812202493 versie: 2 (8 december 2008).

9. Site development plan

9.1. Introduction

This chapter contains an overview of all required steps before CO_2 injection can take place in the P18 field in 2015. This includes information on the key risks at each step along the process and the go / no-go decisions which are involved. The development plan contains three decision gates, where the project is evaluated and has to be approved of in order to enter the following phase in the site development plan. At the end of the chapter, a timeline of the site development plan is included.

9.2. Timeline overview

Table 35 displays a concise overview of the different steps involved in the project; the steps are are further elaborated below. This chapter also provides the projected dates on when certain steps in the process are expected to be finished. It is important to realize that indications of timing are cyclical in nature and very sensitive to changes in for instance commodity prices of oil or metal.

The timing of the activities shown in the table are sketched in Figure 9.1.

.

Table 33: Timeline overview for starting CO_2 storage in P18.

	Activities	Timing
1	P18 feasibility study and high level cost estimate	May 2010 - Jan 2011
2	Evaluate site and engineering concept selection	Dec 2010 - Jan 2011
	Decision gate: Site and engineering concept selection	Jan 2011
3	Environmental Impact Assessment (EIA)	Q4 2010 - Q4 2011
4	Option on initial storage capacity from 2016 in the P18 reservoir blocks	Feb 2011
5	Option on storage capacity from 2018 in the P18 reservoir blocks	Feb 2011
6	Option on transport	Feb 2011
	Decision gate: Go ahead with NER300 funding application	Feb 2011
7	Apply for NER300 funding	Feb - May 2011
8	Obtain licenses	Jan 2011 - Q2 2012
9	FEED (Front-End Engineering and Design)	Q3 - Q4 2011
	Decision gate: Final Investment Decision for EPC	Dec 2011
10	Tendering for detailed Engineering Procurement and Construction	Jan - Feb 2012
11	EPC contract signing	Mar 2012
12	Detailed engineering	Apr - Sep 2012
13	Detailed cost statements (+/- 10%)	Q4 2012
14	Procurement (pipelines, platform installations, equipment and workforce)	Q1 - Q3 2013
15	Construction: wells workovers	Q2 - Q3 2014
16	Construction: equipment of the monitoring well (only possible in compartment P18-2)	Q3 2014
17	Construction: platform modification	Q2 - Q3 2014
18	Construction: pipeline	Q2 - Q3 2014
19	Construction: onshore facilities (compressor, pipeline)	Q1 - Q3 2014
20	Tie-in work and commissioning	Q2 2015
21	Baseline monitoring	Q3 2015
22	Handover	Sep 2015
23	Start injection	Q4 2015

9.3. Detailed timeline overview

Start project

9.3.1. Feasibility study and high-level cost estimate (±40%)

This step is Phase 1 part of the Independent Storage Assessment. During this step, the outline of the project is defined. It also includes setting the scope of the project and defining the requirements, implications, benefits and drawbacks of the project.

Furthermore, the stakeholders and their involvement and commitment should be identified. Stakeholders include various layers of the government, emitters, operators and civil society and research institutes.

In a later part of this step, possible sites for the project are outlined. The requirements of the sites and their suitability should be determined, based on a preliminary survey of the options. An assessment is made of the required data for making a more detailed analysis of the suitable sites and constructing a business case, which is the next step of the project. This data includes geological, seismic and economic parameters of the sites.

The feasibility phase should result in the main risks and limitations of transport and storage at a selection of sites. This should also include limitations on injection rates, requirements of number of wells and well sizes, the possibilities on the transport via shipping or pipelines. The requirements on the injection operation strategies are analyzed in the pre-feed and feed phases. The ideal order of studies is starting with the reservoir injection engineering and well integrity study, followed by the conceptual engineering work.

During this step it has been determined that P18 is a suitable candidate for large scale CCS in the period 2015 – 2020. It has been shown that the reservoirs can handle the injection rate of 1.1 Mt/year and no barriers have been identified.

One of the results from this step is a preliminary cost estimate with a margin of uncertainty of the order of 40%.

Key risk:
Data is difficult to obtain and often incomplete. There are also large uncertainties involved, which should be accounted for.

9.3.2. Concept selection

This step entails the study and selection of the concept from the different options of the feasibility study for a specific field such as P18. This step focuses mainly on the technical aspects of the field, making sure the capacity of the fields is adequate and the seal will not leak.

This step results in the selection of a site and the development of a concept for CO_2 storage at this location. This accounts for all aspects of the project, including capture, transport, injection and storage.

Decision Gate: Site engineering and concept selection
This decision gate follows the first steps of the timeline. This decision gate marks the continuation of the project and allows the other steps to commence. This also means that more funding has to be committed to the project. Criteria in this step:

- ˜ Geological factors: capacity, injectivity, containment
- ˜ Environmental impact indicators, safety
- ˜ Public perception
- ˜ Costs

9.3.3. Environmental Impact Assessment (EIA)

Environmental Impact Assessments play an important part in project development. The EIA is done based in part on the results of a feasibility study (step 1). A successful EIA is one of the requirements to start the process of obtaining various licenses. The duration of obtaining an EIA after the application is typically between 6 and 12 months, but for large projects this can take up to a year and a half.

9.3.4. Option on initial storage capacity from 2016

In this step an option is taken on a field, guaranteeing the availability of the storage site. The current injection plan foresees to start injection in P18-6, after which injection in P18-4 will commence. The capacity with respect to the injection rate is limited in these compartments such that ROAD, which has a priority agreement with TAQA, will need most of the capacity, and only spare capacity is left for third parties. Sufficient additional capacity is available in compartment P18-2 from 2018 onwards when gas production has ceased. For third parties outside ROAD the following options are open, depending on an agreements with TAQA and ROAD, for injection before 2018:

1. Volume-sharing agreement with ROAD for compartments P18-6 and P18-4 for which ROAD has priority in;
2. Agreement with TAQA to use cushion gas N2 during production;
3. Agreement with TAQA to inject in non-producing Block III: requires proper abandonment of the sidetracked well P18-2A6st and re-completion of the parent well P18-2A6.

For the third option it is noted that the CO_2 capacity in Block III is small.

Key risk
Difficulties in negotiations between operators can delay or impede this procedure.

9.3.5. Option on storage capacity from 2018

From 2018 compartment P18-2 would be available, depending on the cessation of production and successful well work-overs. This would give ample storage capacity for third parties.

Key risk
Difficulties in negotiations between the parties can delay or impede this procedure.

9.3.6. Option on transport

The insulated pipeline from the emitters tie-in point to the P18 platform riser is operated by GDFSUEZ. Therefore an agreement with GDFSUEZ must be negotiated in order to get access to the pipeline. For third-parties outside ROAD a tie-in with the ROAD pipeline, including metering and control, must be negotiated.

Decision Gate: Go-ahead with the NER300 application
At this decision gate a decision must be made whether to enter the NER300 application.

9.3.7. Apply for NER300 funding

The NER300, which is a financing instrument from the European Commission for CCS projects, plays an important part in providing funding for the project. The application, for which the details were published in November 2010, should be set in motion as soon as possible, in order to safeguard adequate funding for the project. The deadline for application in the Netherlands is February 9, 2011.

9.3.8. Obtain licenses (national coordination ruling)

During this step, the licenses required for capture, transport, injection and storage of CO_2 should be acquired. There are up to ten legal procedures involved, with a typical duration of around 2 years.

In order to facilitate this process and reduce the amount of time involved in administrative procedures in large scale energy projects, the Dutch government has started an initiative called the “Rijkscoördinatieregeling” or the “National Coordination Ruling”, as it is called in English. Responsibility for the coordination of this process lies with the minister of Economic Affairs (EL&I) because the Mining Act is the foremost applicable law for offshore CO_2 storage. Table 34 shows the different phases involved in this process.

For P18, this process has already been set in motion and the first four phases have been completed. Phase 5, the concept decision, is expected to be finished in January, with the exception of the so called “bestemmingsplan”, which might need an additional couple of months. In July, phase 6, the review period, should be finished. In August, phase 7, the final decision should be finished. Phase 8, the release of the final decision for review, should start at the end of October. All in all, the process should be complete at the end of 2011, with the exception of step 9, which can require and additional 6 months.

Storage license
The underground storage of materials requires an appropriate permit from the Dutch Minister of Economic Affairs, Agriculture and Innovation. The procedure to apply for such a permit is outlined in chapter 3 of the Mining Act. Article 1.3.4, appendix 1 and appendix 2 of the Mining Decree contain a summary of the information that must be provided with a permit application.

Outside the territory of the State, i.e., more than 12 nautical miles from the coast, a MER (Dutch Environmental Impact Assessment) is not needed. Environmental regulations are governed by the Dutch Mining Act, Decree and Regulation, the EU Directive, the London Protocol and OSPAR.

Table 34: Overview of the different phases in the “National Coordination Ruling”.

Phase	
1	The initiating party reveals its plans concerning a large scale energy project to the Minister of Economic Affairs, Agriculture and Innovation. The law determines which projects fall under the national coordination ruling.
2	The ministry determines whether they will provide a “regional” decision and prepare that decision after consultation with both the initiating party and the concerned authorities.
3	“Agentschap NL” investigates in collaboration with the initiating party and the concerning authorities, which licenses and exceptions are required for the project.
4	The initiating party asks for all licenses and exceptions to the concerned authorities. The coordinating minister discusses a common planning with the various parts of government.
5	The concerned authorities collaborate closely and come to their concept decision. The aforementioned minister also (if so decided) arrives at a concept “rijksinpassingsplan”.
6	The concept decisions are bundled and released for public review. During the review period, everybody can object (in writing). One or more information session are organized in which further feedback can be provided.
7	The authorities process the advice and the feedback, after which the decision are made final.
8	The final decisions are again bundled and released for review. Interested parties can object against these decisions, mostly directed to the “Raad van State”.
9	The department administrative justice of “de Raad van State” comes to a verdict on the appeal against one or more of the decisions In case of “rijkscoördinatie” with a “rijksinpassingsplan” this happens in a single ruling, within 6 months after receiving appeal of the concerning authorities.

The time needed to obtaining the required licenses is uncertain. Appendix A contains a preliminary list of the Dutch permits required for CCS projects.

Key risk
The most important risk is a delay in the permitting procedures. Because CCS is a novel topic in legislature, involving long-term effects and international treaties and hence responsibilities, unexpected delays could occur in obtaining the required licenses. This can jeopardize the progress of the project.

9.3.9. FEED

The design phase is generally divided into a FEED (Front End Engineering and Design) phase and the detailed engineering in the EPC (Engineering, Procurement and Construction) phase. The FEED phase concerns the definition of the (transport and storage) system, defining pipeline diameters, transport pressure and compression requirements.

The FEED phase validates the feasibility study, defines the project philosophies and the safety aspects. This phase also includes the full description of injection strategies and procedures such as start-up, shut downs etc. At the end of the phase the system has been designed to a level that allows detailed engineering of the subsystems, such as compressors, pipelines, platform facilities.

The FEED phase is dedicated to the basic engineering and to the cost evaluation (CAPEX and OPEX), as well as the preparation of all technical documents that will constitute the EPC bid package, in order to launch and international tendering for the EPC realization of:

1. CO_2 capture infrastructure at
2. CO_2 transport infrastructure from source to storage site
3. CO_2 injection and storage infrastructure

CO_2 has to be captured and transported from point sources, such as refineries and power plants onshore, to the offshore storage site P18. The CO_2 sources for P18 are located on the industrial area of the Maasvlakte, near Rotterdam. The CO_2 will be transported over a distance of 20 km to the converted CO2 injection platform P18-A. This also requires investments in onshore facilities.

Injection installation:
A single 16” riser is foreseen. The subsea pipeline will be operated by GDF Suez. Taqa will take the CO_2 at the platform. At this moment no choice has been made to meter the injection rates per well or only for the total stream. At the flange a fiscal meter will be set-up. At this point composition measurements are also foreseen. The flowline design rate is 47 kg/s with an expected operating arrival pressure of at least 80 bar. The pipeline is insulated such that the arrival temperature at normal operation is 40^{o}C. The goal is to operate the flowline at all times in the liquid or dense phase. Only during start-up scenario’s the arrival temperature will be lower. For those cases a start-up heater will be used. At this moment no choice for the type of heating (electrical , gas or diesel) is taken. Start-up is foreseen for 12 times per year with a start-up period of 48 hours. Aside the start-up heater, piping and manifold suitable for cold CO_2 will be places on board. For this the test-separator will be removed as this doesn’t lead to changes in the gas production capabilities. These changes will not require additional mechanical modifications to the platform itself. The CO_2 infrastructure will be part of the total current systems as both injection and production from all wells must be possible.

The FEED phase has the following activities:

1. The determination of injection scenarios and procedures consisting of
   a. Planning of the remaining gas production. Currently, P18-4 is foreseen to stop production by 2015, whereas P18-2 may produce until 2018.
   b. Phasing reservoir blocks with respect to start injection. Currently, injection is planned to start in P18-6, then P18-4, and if more capacity is needed, injection could subsequently start in P18-2 from 2018 onwards.
   c. The phasing of the injection wells.
   d. Planning of the injection capacity.
   e. Design of start-up and Emergency Shut-Down (ESD) Procedures.
   f. Phasing of the well work-overs.
2. The design, planning execution and costing of the well workovers.
3. In case a monitoring well is part of the monitoring plan, the design, planning execution and costing of the monitoring well in compartment P18-2.
4. The design, planning execution and costing of the P18 platform modifications includes
   a. Retrofit of the riser connecting the pipeline with the platform.
   b. Installation of a distribution manifold suitable for cold CO_2.
   c. Modification of the monitoring and control system

   d. Modification of the Process Control System and safeguarding, safety facilities, etc.
   e. Revamp of the piping system
   f. Re-engineer wellheads with suitable materials for cold CO_2 injection
   g. Installation of well test and control equipment
   h. Installation of vent and blow down facilities
   i. Installation of the start-up heater
   j. Power generation
   k. Removal of the test separator
5. The design of a monitoring plan
6. The design, planning execution and costing of the insulated pipeline offshore
7. The design, planning execution and costing of the onshore facilities which includes
   a. Dehydration unit
   b. Compression system
   c. Pipeline from capture plant to pipeline
   d. Third-party tie-in to ROAD pipeline including metering and control
8. Test concept design
9. Study for optimal change-over production-injection

The FEED phase concerns the breakdown of the transport and storage system into its building blocks. These building blocks, which are now complete in terms of the requirements and interfaces, can be tendered out to contractors, who will perform the detailed design and construction. It has been estimated that this phase (only for transport and storage) takes approximately 4000 hours.

Decision Gate: Final Investment Decision for FID
At this decision gate, the FEED study is complete and the procedures for obtaining the required licenses have been set in motion. Before FID, the project should be evaluated based on current knowledge before proceeding to the EPC tendering, which consitutes the step to the major investments.

At this decision gate, the majority of the preparatory work is finished. By this time, all risks should be clear and appropriately managed. When this decision gate is passed, the actual implementation of the project is set in motion.

9.3.10. Tendering for detailed Engineering Procurement and Construction

Preparation of all technical documents that will constitute the EPC bid package, in order to launch and internationally tender for the EPC realization.

9.3.11. EPC Contract signing

This step entails acquiring all necessary agreements with the parties in the CCS chain as well as awarding and signing the EPC contracts.

Key risk
The large financial interests involved in the oil and gas business and the insecurities of CCS make it difficult to accurately establish the market value of a (depleted) gas field and its facilities.

This could make negotiation between stakeholders difficult. If no satisfactory agreement is reached, the project can be severely jeopardized.

9.3.12. Detailed engineering

Detailed engineering is performed of:

1. Work-overs six existing wells
2. Modifications to the platform facilities
3. Insulated offshore pipeline
4. Onshore facilities (compressors, pipeline)

9.3.13. Detailed costing

A detailed costing is conducted such that cost estimated are within +/- 10%.

9.3.14. Procurement

This phase involves the procurement of all required elements for the project. The long lead items need to be ordered as soon as possible (potentially in the previous project phase if allowed). This includes materials, such as pipelines and heaters and compressors, and equipment, such as ships and drilling platforms and workforce. Renting a rig is an important part of the procurement phase.

Planning of the well work-overs and laying of the pipeline will require contract singing at least a year before the actual work due to the long procurement periods. This means that contracts need to be signed in the summer of 2012. For timing considerations, it should be kept in mind that constructing pipelines should be done in summer due to the benign weather conditions.

Key risk

Because the procedures are so costly and time consuming, it is not uncommon in the oil and gas industry to have equipment and workforce reserved for years in advance. A key risk is the availability of required materials and workforce for a sustained period, which would significantly delay the project.

9.3.15. Construction: well abandonment and work-over

Deploying a rig in the correct position takes time, depending on the job, and performing a single well work-over it takes between 4 to 10 weeks. During this step, the rig is used for two purposes. First of all, it is used for work-overs on existing wells, which are converted for injection. Secondly, the rig is used to properly abandon wells that are no longer used but which might not have been successfully abandoned.

Required actions of well work-overs at P18:

Required before using P18-2 compartment for CCS

- Rig employment
- Abandonment P18-2 exploration well (current status suspended).
    - Remove cage from seabed.
    - Re-enter well

    - Drill out all but bottom plug
    - Retrieve top uncemented casing
    - Set new cement plugs
- Workover of sidetracked well P18-2A6
    - Abandonment P182-A6st (successful abandonment of this sidetrack would allow for CO_2 storage in the P18-2)
    - Fishing the whip stock in order to get access to parent well and thus compartment III
    - Recompletion of the P18-2A6 parent to enable CO_2 injection in block III

Other injectors in the P18-2 compartment (exception P182-A4) would require:

- new CBL
- Pulling of tubing (using rig)
- In case of bad cement bonding:
    - Perforate casing near poorly cemented area.
    - Perform pressure integrity test
    - Squeeze cement if necessary
    - Isolate created perforation in casing

9.3.16. Construction: equipment of the monitoring well

In case a monitoring well is part of the monitoring plan an existing well needs to be converted, equipped and instrumented. Only in compartment P18-2 would a well be available for monitoring.

9.3.17. Construction: platform modification

The platforms is modified: the test-separator will be removed and new equipment installed. New equipment includes a heaters (used during the first stages of injection and for start-ups), wellhead control and downhole equipment control systems, a retrofit of the riser, a CO_2 manifold, revamp of the piping system and vent and blow down facilities.

9.3.18. Construction: pipeline construction

The pipeline with both onshore and offshore sections is constructed. The pipeline will be insulated such that the CO_2 will have a temperature of 40^{o}C. at the well head at normal operations.

9.3.19. Construction: onshore facilities

Onshore facilities include the compressor and dehydration systems.

9.3.20. Tie-in work and commissioning

This step includes tests to see if everything is working as planned. It results in the handover of the field and the equipment to the new operator.

9.3.21. Baseline monitoring

During this step the baseline for the monitoring of the storage during and after injection is collected. It should take place before injection and ideally a short period after the tie in work and commissioning place.

9.3.22. Handover

This step includes tests to see if the chain is working as planned. It results in the handover of the field and the equipment to the new operator.

9.3.23. Start injection

During this phase, injection is started. Injection is planned to take place in 2015.

It is noted that there is an option to continue production of gas after the start of injection, in which case this would become enhanced gas recovery (EGR). At present, this option is not taken into account. The energy requirements on the platform once CO_2 injection is started are limited, and significant only during the first phase of injection, when a heater is used. Gas produced from one of the wells could be used to this end.

9.4. Schematic overview of project timeline

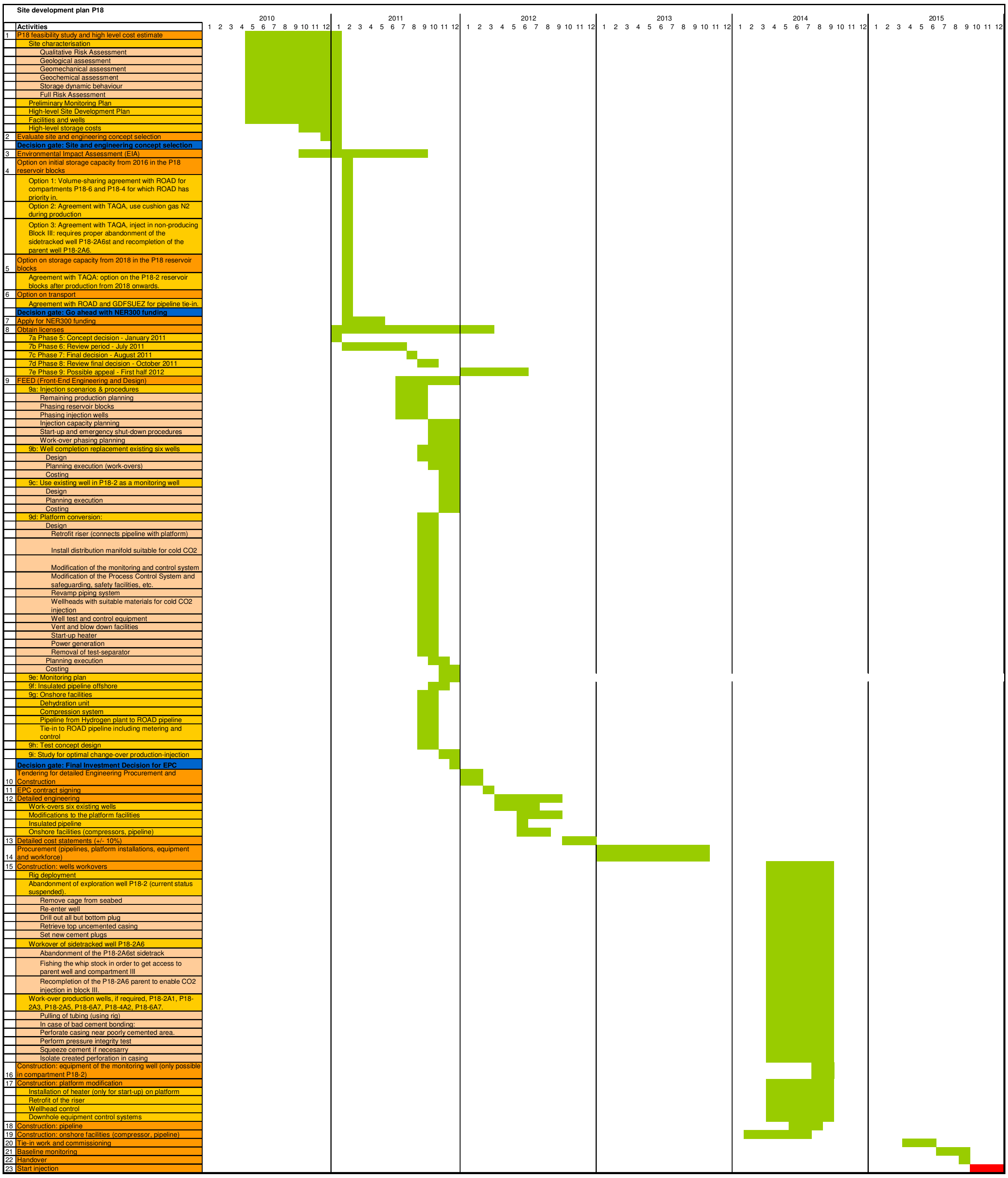

Figure 9.1: Overview of the timeline of activities required to start CO_2 injection at P18, see also Appendix E.

11. Appendix A: Base, top and thickness of formations

Base, top and thickness of the formations (reservoir zones) in the wells

Well ID	Base (m)	Top (m)	Thickness (m)
P18-02 (expl. well)	3441	3326	115
P18-02A1	3665	3553	112
P18-02A3ST2	3575	3465	110
P18-02A5	3464	3350	114
P18-02A6	3683	3575	108
P18-02A6ST1	N.P.	N.P.	-
P18-04A2	3365	3264	101
P18-06A7ST1	N.P.	N.P.	-

Table A1: Data on the base, top and thickness of the Volpriehausen Formation in the P18 wells. N.P. stands for “Not Penetrated”.

Well ID	Base (m)	Top (m)	Thickness (m)
P18-02 (expl. well)	3326	3305	21
P18-02A1	3553	3531	22
P18-02A3ST2	3465	3445	20
P18-02A5	3350	3328	22
P18-02A6	3575	3555	20
P18-02A6ST1	N.P.	N.P.	-
P18-04A2	3264	3245	19
P18-06A7ST1	N.P.	3627	-

Table A2: Data on the base, top and thickness of the Lower Detfurth Sandstone Member in the P18 wells. N.P. stands for “Not Penetrated”.

Well ID	Base (m)	Top (m)	Thickness (m)
P18-02 (expl. well)	3305	3256	49
P18-02A1	3531	3481	50
P18-02A3ST2	3445	3396	49
P18-02A5	3328	3279	49
P18-02A6	3555	3508	47
P18-02A6ST1	N.P.	3288	-
P18-04A2	3245	3198	47
P18-06A7ST1	3627	3578	49

Table A3: Data on the base, top and thickness of the Upper Detfurth Sandstone Member in the P18 wells. N.P. stands for “Not Penetrated”.

Well ID	Base (m)	Top (m)	Thickness (m)
P18-02 (expl. well)	3256	3228	28
P18-02A1	3481	3455	26
P18-02A3ST2	3396	3370	26
P18-02A5	3279	3254	25
P18-02A6	3508	3480	28
P18-02A6ST1	3288	3261	27
P18-04A2	3198	3174	24
P18-06A7ST1	3578	3545	33

Table A4: Data on the base, top and thickness of the Hardegsen Formation in the P18 wells. N.P. stands for "Not Penetrated".

Petrophysical properties of the formations (reservoir zones) in the wells

Well ID	Top	Base	FWL	BPZ	N/G	PHI	S_w	PHI_NPZ
P18-02A1	3553	3665	3680	0.96	0.88	0.034	0.93	0.043
P18-02A3	3465	3575	3680	1.00	0.51	0.034	0.91	0.053
P18-02A5	3350	3464	3680	1.00	0.45	0.056	0.46	0.058
P18-02A6	3575	3683	3680	0.79	0.93	0.033	0.81	0.037
P18-04A2	3264	3365	3377	1.00	0.33	0.034	0.92	0.049

Table A5: Average (arithmetic) petrophysical properties of the Volpriehausen Formation in the P18 wells. Values in columns "Top", "Base" and "FWL" (Free Water Level) are in m TVDSS, with FWL as determined from pressure-depth gradients or mapped spill points, "BPZ" stands for "Bulk Pay Zone", and indicates the part of the formation above the FWL, "N/G" stands for "Net-To-Gross", as calculated by dividing the amount of sand (Vshale cut-off: 0.35, PHI cut-off: 0.02) in m by the total thickness of the formation, "PHI" indicates the porosity (cut-off: 0.02) of the bulk, "S_w" stands for water saturation (Vshale cut-off: 0.35, PHI cut-off: 0.02), and "PHI_NPZ" indicates the average porosity of the pay zone.

Well ID	Top	Base	FWL	BPZ	N/G	PHI	S_w	PHI_NPZ
P18-02A1	3531	3553	3680	1.00	0.88	0.073	0.45	0.075
P18-02A3	3445	3465	3680	1.00	0.67	0.084	0.39	0.096
P18-02A5	3328	3350	3680	1.00	0.82	0.108	0.20	0.108
P18-02A6	3555	3575	3680	1.00	0.80	0.051	0.63	0.051
P18-04A2	3245	3264	3377	1.00	0.81	0.065	0.39	0.065
P18-06A7ST1	N.P.	3627	3680	1.00	0.71	0.059	0.32	0.059

Table A6: Average (arithmetic) petrophysical properties of the Lower Detfurth Sandstone Member in the P18 wells Values in columns "Top", "Base" and "FWL" (Free Water Level) are in m TVDSS, with FWL as determined from pressure-depth gradients or mapped spill points, "BPZ" stands for "Bulk Pay Zone", and indicates the part of the formation above the FWL, "N/G" stands for "Net-To-Gross", as calculated by dividing the amount of sand (Vshale cut-off: 0.35, PHI cut-off: 0.02) in m by the total thickness of the formation, "PHI" indicates the porosity (cut-off: 0.02) of the bulk, "S_w" stands for water saturation (Vshale cut-off: 0.35, PHI cut-off: 0.02), and "PHI_NPZ" indicates the average porosity of the pay zone. N.P. stands for "Not Penetrated".

Well ID	Top	Base	FWL	BPZ	N/G	PHI	S_w	PHI_NPZ
P18-02A1	3481	3531	3680	1.00	0.96	0.074	0.35	0.078
P18-02A3	3396	3445	3680	1.00	0.88	0.089	0.56	0.093
P18-02A5	3279	3328	3680	1.00	0.94	0.117	0.31	0.117
P18-02A6	3508	3555	3660	1.00	0.93	0.061	0.72	0.065
P18-04A2	3198	3245	3377	1.00	0.87	0.091	0.47	0.092
P18-02A6ST1	3288	N.P.	3680	1.00	0.99	0.120	0.20	0.120
P18-06A7ST1	3578	3627	3680	1.00	0.91	0.048	0.57	0.048

Table A7: Average (arithmetic) petrophysical properties of the Upper Detfurth Sandstone Member in the P18 wells. Values in columns “Top”, “Base” and “FWL” (Free Water Level) are in m TVDSS, with FWL as determined from pressure-depth gradients or mapped spill points, “BPZ” stands for “Bulk Pay Zone”, and indicates the part of the formation above the FWL, “N/G” stands for “Net-To-Gross”, as calculated by dividing the amount of sand (Vshale cut-off: 0.35, PHI cut-off: 0.02) in m by the total thickness of the formation, “PHI” indicates the porosity (cut-off: 0.02) of the bulk, “S_w” stands for water saturation (Vshale cut-off: 0.35, PHI cut-off: 0.02), and “PHI_NPZ” indicates the average porosity of the pay zone. N.P. stands for “Not Penetrated”.

Well ID	Top	Base	FWL	BPZ	N/G	PHI	S_w	PHI_NPZ
P18-02A1	3455	3481	3680	1.00	0.97	0.096	0.35	0.096
P18-02A3	3370	3396	3680	1.00	0.97	0.115	0.31	0.116
P18-02A5	3254	3279	3680	1.00	1.00	0.149	0.18	0.149
P18-02A6	3480	3508	3680	1.00	1.00	0.109	0.36	0.110
P18-04A2	3174	3198	3377	1.00	0.99	0.127	0.24	0.131
P18-02A6ST1	3261	3288	3680	1.00	0.95	0.157	0.14	0.157
P18-06A7ST1	3545	3578	3680	1.00	0.81	0.074	0.47	0.074

Table A8: Average (arithmetic) petrophysical properties of the Hardegsen Formation in the P18 wells Values in columns “Top”, “Base” and “FWL” (Free Water Level) are in m TVDSS, with FWL as determined from pressure-depth gradients or mapped spill points, “BPZ” stands for “Bulk Pay Zone”, and indicates the part of the formation above the FWL, “N/G” stands for “Net-To-Gross”, as calculated by dividing the amount of sand (Vshale cut-off: 0.35, PHI cut-off: 0.02) in m by the total thickness of the formation, “PHI” indicates the porosity (cut-off: 0.02) of the bulk, “S_w” stands for water saturation (Vshale cut-off: 0.35, PHI cut-off: 0.02), and “PHI_NPZ” indicates the average porosity of the pay zone.

12. Appendix B: Reservoir emballage

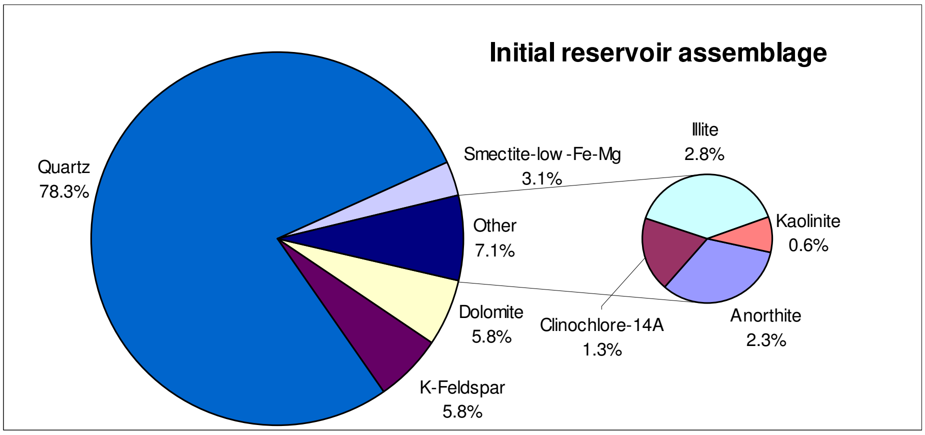

Figure 12.1 Initial, computed reservoir mineralogy (wt%) which deviates slightly from the measured rock composition due to allowance of precipitation of secondary minerals and exclusion of minerals in the diagram with wt% below 0.1 (albite, anhydrite, glauconite, muscovite and pyrite).

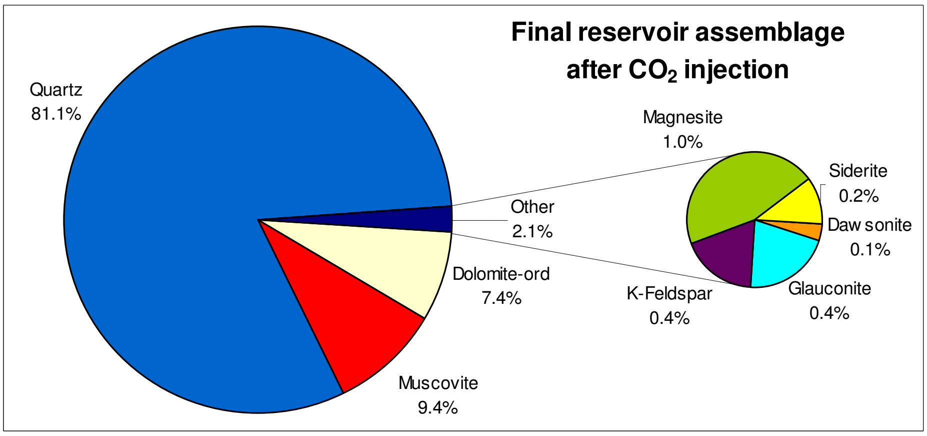

Figure 12.2 Final, computed reservoir assemblage (wt%) after CO_2 injection.

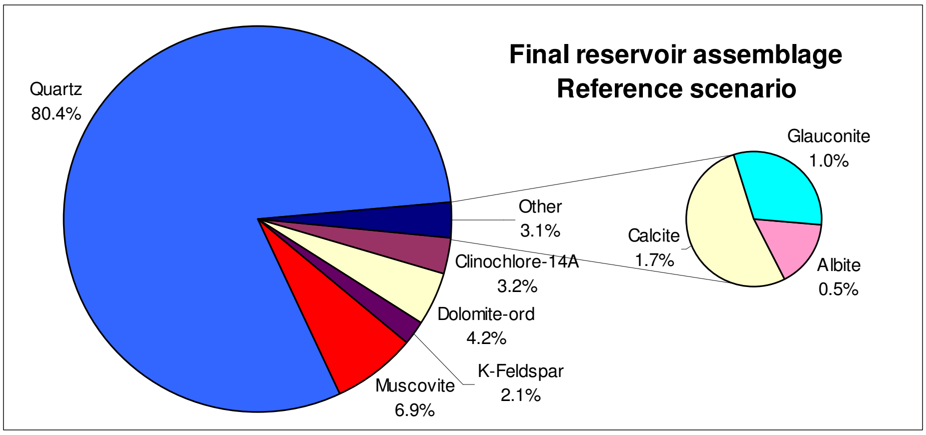

Figure 12.3 Final, computed equilibrium assemblage (wt%) without CO_2 injection.

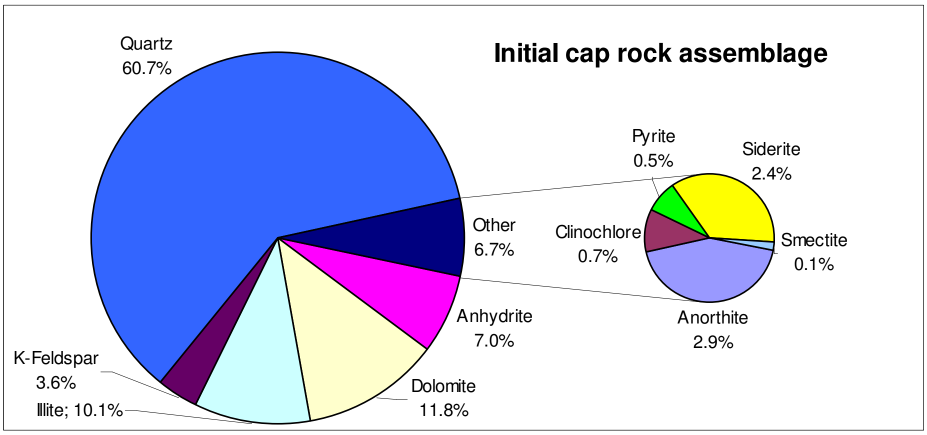

Figure 12.4 Initial cap rock assemblage (wt%). %) which deviates slightly from the measured rock composition due to allowance of precipitation of secondary minerals and exclusion of minerals in the diagram with wt% below 0.1 (albite, diaspore, glauconite and muscovite).

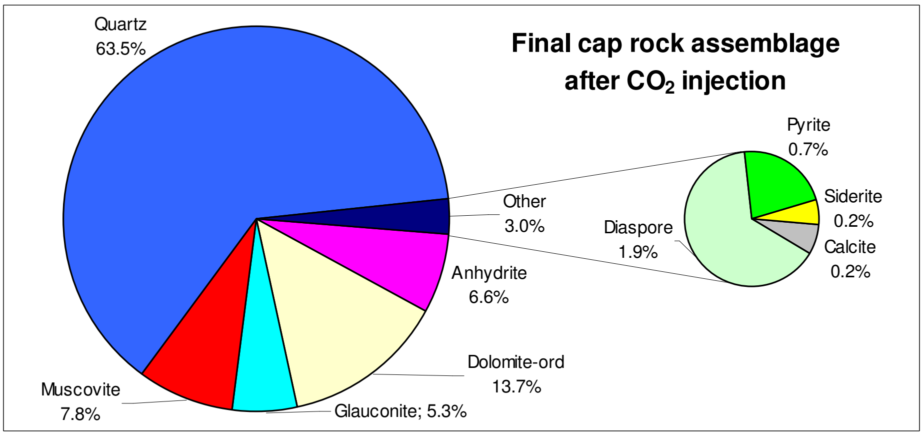

Figure 12.5 Final, computed cap rock assemblage (wt%) after CO_2 injection.

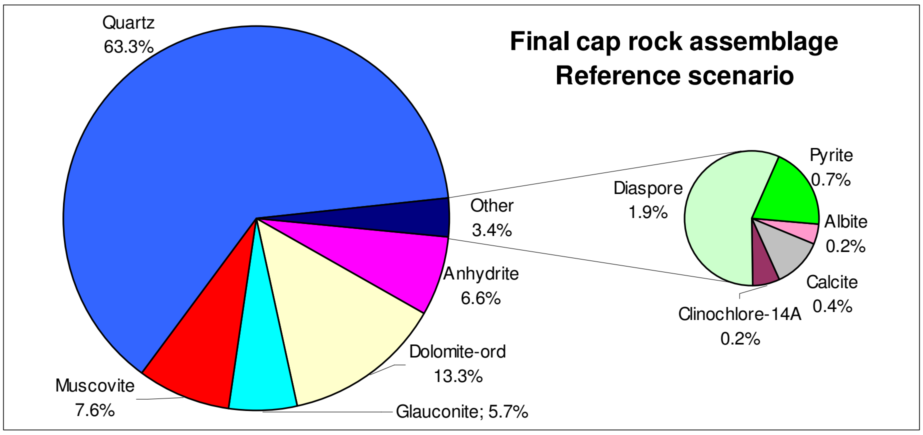

Figure 12.6 Final, computed cap rock assemblage (wt%) without CO_2 injection.

13. Appendix C: Overview of Dutch permits needed for CCS projects

The following list, in alphabetical order, gives a preliminary overview of the Dutch permits which are required for CCS projects. Due to the novelty of the concept, it is not yet sure whether this list is complete.

- Act on Environmental Management
- Act on Management of State Hydraulic Works
- Act on Nature Protection
- Act on Spatial Planning
- Circular on Transport of Hazardous Substances
- Construction permit
- Decision on External Safety of Installations
- Flora and Fauna dispensation
- Mining Law
- National Coordination Regulation

14. Appendix D:

No.	Parameter to be monitored*	Technique adopted	Category of monitoring: Mandatory according to EU	Required (preliminary	Contingency	Project phase and frequency: Pre-inj	Inj	Post-Inj	Post-Inj (abandonment)	Long-term stewardship	Location	Normal situation: Expectation value	Accuracy	Alert value: > Threshold 1	Action**	Contingency value: > Threshold 2	Contingency measures***
	Injection proces																
1	Injection rate	Flow meter	x				Cont				Outflow compressor + at well head	Max rate = 169,2 ton CO2/uur (47 kg/s or 1.48 Mton CO2/year) and no fluctuations at constant pressure, expected value t.b.d.		Fluctuations at constant pressure or value above max. rate	Verify compressor, find cause of increased rate	Fluctuations at constant pressure or value above max. safety margins	Stop injection until flow < threshold 1 value again
2	Injected gas composition	Gas samples & analysis: online system	x				Cont				Compressor station	Defined % for the composition of the gas		Allowed fluctuations reached	Adapt gas composition, reduce injection rate	Above allowed fluctuations	Adapt gas composition, stop injection temporarilly
3	Injected gas composition	Gas samples & analysis: Additional samples for calibration	x				Quarterly				Compressor station	Defined % for the composition of the gas		Allowed fluctuations reached	Adapt gas composition, reduce injection rate	Above allowed fluctuations	Adapt gas composition, stop injection temporarilly
4	Water measurement	Gas measurement	x				Cont				Inlet injection compressor	Specification value		In case specification value is reached	Consultation with the CO2 provider	In case value is above specification value	Stop CO2 delivery, investigate at the CO2 provider the cause, start delivery if value OK again
5	Discontinous emissions through leakage, venting or accidents	Combination of techniques	x				Yearly				Potential leakage points like joints or ventstacks						
	Injection & monitoring wells																
6	Annular pressure	Pressure device		x		Baseline date prior to operations	Monthly	Monthly		-	At the well head of all wells (injection and monitoring) penetrating the reservoir)	Constant pressure		Increase or decrease in pressure within safety margins	Additional measurements like logging or sampling + analysis of fluids to detect CO2	Increase or decrease in pressure above safety margins	Investigate causes (fluid sampling) and options to remediate (in the extreme case well abandonment)
7	Well integrity	Wireline Logging (CBL, PMIT, EMIT, USIT, WAF, optical)		x		Baseline	Every 2 years	Every 2 years			All wells (injection and monitoring) penetrating the reservoir)	Meaurements within the expected range		Measurements above expectation values	Additional measurements (such as repeat) to corroborate observations, potentially seismic contingency measurements in case values large enough to be detected by seismics	Measurements significantly above expectation values	Stop injection, additional measurements and seismic contingency measurements to identify shallow gas accumulations, investigate options to remediate (in the extreme case well abandonment)
8	Well head pressure	Pressure device	x			Baseline	Continuous	Continuous	Continuous		At the well head (injection skid)	No fluctuations expected at constant flow rates		Loss of pressure	Lower the injection flow until normal injection pressure is recovered and investigate fracturing	No recovery of injection pressure after lowering injection flow	Stop injection, investigate the cause (fracturing) and evaluate whether conditions are safe
9	Well head temperature	Temperature device	x			Baseline	Continuous	Continuous	Continuous		At the well head (injection skid)	Determine operational limits for temperature range		In case temperature reaches the determined operational limits (high or low) within 5 to 10 degrees C	Additional measurements to determine the cause	In case temperature reaches the determined operational limits within 5 degrees C	Stop injection until the cause of the temperature change is clarified and safe
	Abandoned wells with pancake plug																
10	Annular pressure	Pressure device		x		Continuous including at least during a month after abandonment					At the well head of all wells (injection and monitoring) penetrating the reservoir)	Constant pressure		Increase or decrease in pressure within safety margins	Additional measurements like logging or sampling + analysis of fluids to detect CO2	Increase or decrease in pressure above safety margins	Investigate causes (fluid sampling) and options to remediate (in the extreme case well abandonment)
11	Monitoring 'pancake' plug	Pressure and gastest	(x)	x		Test after abandonment for wells abandoned at the start of the project			Test after injection period for wells abandoned at the start of the project	Test for wells abandoned after injection period	In the well above the plug	No pressure changes		Minimal pressure changes	Investigate cause with other measurements (e.g. deformation of the wellbore)	Significant pressure changes	Redo the pancake plug
12	Well head pressure	Pressure device	x			Baseline	Continuous	Continuous	Continuous including at least a test during a month after abandonment		At the well head (injection skid)	No fluctuations expected		Increase or decrease in pressure within safety margins	Additional measurements like logging or sampling + analysis of fluids to detect CO2	Increase or decrease in pressure above safety margins	Verify the integrity of the pancake plug (pressure and gas test), in case of leakage redo the pancake plug
13	Well head temperature	Temperature device		x		Baseline	Continuous	Continuous	Continuous including at least a test during a month after abandonment		At the well head (injection skid)	Determine operational limits for temperature range		In case temperature reaches the determined operational limits (high or low) within 5 to 10 degrees C	Additional measurements to determine the cause	In case temperature reaches the determined operational limits within 5 degrees C	Stop injection until the cause of the temperature change is clarified and safe
14	Composition fluids in wellbore above the pancake plug	Fluid measurement			x	In case pressure changes are observed in the wellbore above the plug					Samples at the well head	Max. CO2 concentration content expected		Increased CO2 content	Pressure and gastest of the pancake plug	-	-

	Reservoir integrity															
15	Reservoir (Bottomhole) pressure	pressure device	(x)	x		Baseline data	Cont (monthly with memory gauges)	Cont (monthly with memory gauges)	Cont (monthly with memory gauges)		Downhole permanent sensor or memory gauges	Flowing bottomhole pressure in agreement with simulations		Deviation from expected values	Recalibration of the reservoir simulation model until satisfactory history match	Significant deviation from expected values	Re-evaluate reservoir model, in case no explanation can be provided, stop injection
16	Reservoir (Bottomhole) Temperature	thermometer	x			Baseline data	Cont (monthly with memory gauges)	Cont (monthly with memory gauges)	Cont (monthly with memory gauges)		Downhole permanent sensor or memory gauges	Flowing bottomhole temperature in agreement with well model		Deviation from expected values	Recalibration of the well model until satisfactory history match	Significant deviation from expected values	Re-evaluate well model, in case no explanation can be provided, stop injection
17	Pressure gradient	pressure device (wireline tool or memory gauge) combined with shut-in	(x)	x		Baseline data	6M	6M	6M		Memory gauges combined with shut-in	Pressure date in agreement with expected simulation model and P/z curve		Deviation from expected values	Recalibration of the reservoir simulation model until satisfactory history match	Significant deviation from expected values	Re-evaluate reservoir model, in case no explanation can be provided, stop injection
18	Temperature gradient	thermometer or DTS (wireline tool or memory gauge) combined with shut-in	(x)	x		Baseline data	6M	6M	6M		DTS for permanent installation or memory gauges combined with shut-in	Temperature data in agreement with expected well model		Deviation from expected values	Recalibration of the well model until satisfactory history match	Significant deviation from expected values	Re-evaluate well model, in case no explanation can be provided, stop injection
19	Microseismic activity in the caprock or at faults	Permanent geophones in monitoring well		x	x	Baseline data	Cont	Cont	(Cont)		Monitoring well at caprock and reservoir level	No events in caprock or at faults (re-activation)		Events in the caprock or at faults	Additional measurements like seismic contingency measurements to identify shallow gas accumulations, evaluate whether injection can be continued safely	Large events in the caprock or at faults	Stop injection, additional measurements and seismic contingency measurements to identify shallow gas accumulations, evaluate whether injection can be continued at lower injection rates
20	Suspected leakage	Surface seismic survey			x	Baseline data already available	Only when other monitoring indicates leakage	Only when other monitoring indicates leakage	Only when other monitoring indicates leakage	Survey can be considered for the transfer of liability	Marine vessel (seismic acquisition using streamers)	No changes in the presence of shallow gas pockets or gas chimneys	~10's of ktonnes of CO2	Shallow gas pockets	Determine the origin of the gas		
	Plume tracking															
21	CO2 concentrations around the well(s) in the reservoir	RST logging		x			Every 2 years (for gaining experience every half year to year would be preferable)	Every 2 years (for gaining experience every half year to year would be preferable)			Injection well and potentially at monitoring wells						
22	CO2 breakthrough	Gas measurement		x			Monthly	Monthly			Monitoring well	Breakthrough in agreement with simulations		Breakthrough not in ageement with simulations	Recalibration of the reservoir simulation model until satisfactory history match	N/A	N/A
	Environmental monitoring															
23	Pockmarks at the seabottom	Multi-beam echosounding		x		Basline	after 5 Years	Survey prior to abandonment	Survey prior to decommisioning of the platform	last survey prior to transfer of liability	Acquisition from a ship	No pockmarks		Pockmarks	Additional gas sampling + analysis to identify the origin of potential seepage or leakage. In case of leakage, identify the pathway with time-lapse seismic data.	Detection of bubbles	Additional gas sampling + analysis to identify the origin of potential seepage or leakage. In case of leakage, identify the pathway with time-lapse seismic data. Mitigation to potential leaks
24	Presence of shallow gas or gas chimneys in the subsurface	Baseline seismic data		x	x	Baseline data					Available baseline seismic data	No bright spots or chimneys in the subsurface		Bright spots and/or gas chimneys	Investigate origin of the gas, in case a leakage pathway is suspected, apply time-lapse seismic data	Bright spots and/or gas chimneys to the surface	Additional gas sampling + analysis to identify the origin of potential seepage or leakage. In case of leakage, identify the pathway with time-lapse seismic data. Mitigation to potential leaks
25	Migration pathways for gas in the shallow subsurface	Time-lapse seismic data acquisition (2D or 3D)		x	x		Contingency	Contingency	Contingency	Contingency	Marine acquisition from a vessel	No changes in bright spots or chimneys in the subsurface		Changes in bright spots and/or gas chimneys	Investigate origin of the gas, in case a leakage pathway is suspected, apply time-lapse seismic data	Changes in bright spots and/or gas chimneys to the surface	Additional gas sampling + analysis to identify the origin of potential seepage or leakage. In case of leakage, identify the activeness of the pathway with time-lapse seismic data. Mitigation to potential leaks
26	CO2 in soil	Gas samples using vibrocore + lab analysis			x	Contingency	Contingency	Contingency	Contingency	Contingency	Sampling from a vessel			In case of leakage detection at the seabottom by geophysical methods	Investigate origin of the gas, in case a leakage pathway is suspected, apply time-lapse seismic data	In case of leakage detection at the seabottom by geophysical methods	Investigate origin of the gas, in case a leakage pathway is suspected, apply time-lapse seismic data
27	CO2 in soil	Gas samples using vibrocore + lab analysis		x			Yearly	Yearly	Yearly		Measurements around the wellheads						
28	Bubble detection at wellhead	Acoustic bubble detector			x	Contingency	Contingency	Contingency	Contingency	Contingency	Install at the seabottom	No bubbles		In case of few bubbles	Investigate origin of the gas, in case a leakage pathway is suspected, apply time-lapse seismic data	Significant bubble stream	Well remediation (workover)

*Follows from the risk assessment
** t.b.d. by operator, examples are updating model, additional monitoring, …
*** t.b.d. by operator, examples are stop injection, back-production, well workover, contingency monitoring

P18 CO2 storage base-case monitoring plan

- (cyan) Mandatory monitoring according to Annex II of the EU directive
- (yellow) Preliminary estimation of required monitoring
- (light green) Optional contingency monitoring
- ↔ Period of time t.b.d. with State Supervision of the Mines (SodM)

Decommisioning of the platform

			Pre-injection 2011 2012 2013 2014	Injection 2015 2016 2017 2018 2019 2020	Post-injection ↔	Post-injection (Abandonment) ↔	Post-injection (Transfer of liability) ↔
	Injection proces						
1	Injection rate	Flow meter		Continuous			
2	Injected gas composition	Gas samples & analysis: online system		Continuous			
3	Injected gas composition	Gas samples & analysis: Additional samples for calibration		Quarterly			
4	Water measurement	Gas measurement		Continuous			
5	Discontinuous emissions through leakage, venting or accidents	Combination of techniques		Yearly			
	Injection & monitoring wells						
6	Annular pressure	Pressure device	Baseline	Monthly			
7	Well integrity	Wireline Logging (CBL, PMIT, EMIT, USIT, WAF, optical)	Single baseline before start of the injection				
8	Well head pressure	Pressure device	Continuous				
9	Well head temperature	Temperature device	Continuous				
	Abandoned wells						
10	Annular pressure	Pressure device	Continuous including at least during a month after abandonment				
11	Monitoring 'pancake' plug or other used plug	Pressure and gastest	Single baseline test for wells abandoned at the start of the project		Test after injection period for wells abandoned at the start of the project	Test for wells abandoned after injection period	
12	Well head pressure	Pressure device	Continuous including at least a test during a month after abandonment		Continuous including at least a test during a month after abandonment		
13	Well head temperature	Temperature device	Continuous including at least a test during a month after abandonment		Continuous including at least a test during a month after abandonment		
14	Composition fluids in wellbore above the pancake plug	Fluid measurement	In case pressure changes are observed in the wellbore above the plug		In case pressure changes are observed in the wellbore above the plug		
	Reservoir integrity						
15	Reservoir (Bottomhole) pressure	pressure device	Continuous or monthly with memory gauges (frequency can be adapted according to findings)				
16	Reservoir (Bottomhole) Temperature	thermometer	Continuous or monthly with memory gauges (frequency can be adapted according to findings)				
17	Pressure gradient	pressure device (wireline tool or memory gauge) combined with shut-in	Shut-in pressure measurement every 6 months				
18	Temperature gradient	thermometer or DTS (wireline tool or memory gauge) combined with shut-in	Shut-in temperature measurement every 6 months				
19	Microseismic activity in the caprock or at faults	Permanent geophones in monitoring well	Continuous in available monitoring well (considered contingency monitoring)				
20	Suspected leakage	Surface seismic survey		Survey in case of irregularities			
	Plume tracking						
21	CO2 concentrations around the well(s) in the reservoir	RST logging	Every 2 years (for gaining experience every half year to year would be preferable)				
22	CO2 breakthrough	Gas measurement	Every month				
	Environmental monitoring						
23	Pockmarks at the seabottom	Multi-beam echosounding	(Existing) baseline	survey; survey	survey	survey	
24	Presence of shallow gas or gas chimneys in the subsurface	Baseline seismic data	Baseline: interpretati on existing data				
25	Migration pathways for gas in the shallow subsurface	Time-lapse seismic data acquisition (2D or 3D)		Survey in case of irregularities			
26	CO2 in soil	Gas samples using vibrocore + lab analysis		Survey in case of irregularities			
27	CO2 in soil	Gas samples using vibrocore + lab analysis	Baseline at risk spots	survey; survey	survey	survey	
28	Bubble detection at wellhead	Acoustic bubble detector		Survey in case of irregularities			

15. Appendix E: Project timeline

Site development plan P18

	Activities
1	P18 feasibility study and high level cost estimate
	Site characterisation
	Qualitative Risk Assessment
	Geological assessment
	Geomechanical assessment
	Geochemical assessment
	Storage dynamic behaviour
	Full Risk Assessment
	Preliminary Monitoring Plan
	High-level Site Development Plan
	Facilities and wells
	High-level storage costs
2	Evaluate site and engineering concept selection
	Decision gate: Site and engineering concept selection
3	Environmental Impact Assessment (EIA)
4	Option on initial storage capacity from 2016 in the P18 reservoir blocks
	Option 1: Volume-sharing agreement with ROAD for compartments P18-6 and P18-4 for which ROAD has priority in.
	Option 2: Agreement with TAQA, use cushion gas N2 during production
	Option 3: Agreement with TAQA, inject in non-producing Block III: requires proper abandonment of the sidetracked well P18-2A6st and recompletion of the parent well P18-2A6.
5	Option on storage capacity from 2018 in the P18 reservoir blocks
	Agreement with TAQA: option on the P18-2 reservoir blocks after production from 2018 onwards.
6	Option on transport
	Agreement with ROAD and GDFSUEZ for pipeline tie-in.
	Decision gate: Go ahead with NER300 funding
7	Apply for NER300 funding
8	Obtain licenses
	7a Phase 5: Concept decision - January 2011
	7b Phase 6: Review period - July 2011
	7c Phase 7: Final decision - August 2011
	7d Phase 8: Review final decision - October 2011
	7e Phase 9: Possible appeal - First half 2012
9	FEED (Front-End Engineering and Design)
	9a: Injection scenarios & procedures
	Remaining production planning
	Phasing reservoir blocks
	Phasing injection wells
	Injection capacity planning
	Start-up and emergency shut-down procedures
	Work-over phasing planning
	9b: Well completion replacement existing six wells
	Design
	Planning execution (work-overs)
	Costing
	9c: Use existing well in P18-2 as a monitoring well
	Design
	Planning execution
	Costing
	9d: Platform conversion:
	Design
	Retrofit riser (connects pipeline with platform)
	Install distribution manifold suitable for cold CO2
	Modification of the monitoring and control system
	Modification of the Process Control System and safeguarding, safety facilities, etc.
	Revamp piping system
	Wellheads with suitable materials for cold CO2 injection
	Well test and control equipment
	Vent and blow down facilities
	Start-up heater
	Power generation
	Removal of test-separator
	Planning execution
	Costing
	9e: Monitoring plan
	9f: Insulated pipeline offshore
	9g: Onshore facilities
	Dehydration unit
	Compression system
	Pipeline from Hydrogen plant to ROAD pipeline
	Tie-in to ROAD pipeline including metering and control
	9h: Test concept design
	9i: Study for optimal change-over production-injection
	Decision gate: Final Investment Decision for EPC
10	Tendering for detailed Engineering Procurement and Construction
11	EPC contract signing
12	Detailed engineering
	Work-overs six existing wells
	Modifications to the platform facilities
	Insulated pipeline
	Onshore facilities (compressors, pipeline)
13	Detailed cost statements (+/- 10%)
14	Procurement (pipelines, platform installations, equipment and workforce)
15	Construction: wells workovers
	Rig deployment
	Abandonment of exploration well P18-2 (current status suspended).
	Remove cage from seabed
	Re-enter well
	Drill out all but bottom plug
	Retrieve top uncemented casing
	Set new cement plugs
	Workover of sidetracked well P18-2A6
	Abandonment of the P18-2A6st sidetrack
	Fishing the whip stock in order to get access to parent well and compartment III
	Recompletion of the P18-2A6 parent to enable CO2 injection in block III.
	Work-over production wells, if required, P18-2A1, P18-2A3, P18-2A5, P18-6A7, P18-4A2, P18-6A7.
	Pulling of tubing (using rig)
	In case of bad cement bonding:
	Perforate casing near poorly cemented area.
	Perform pressure integrity test
	Squeeze cement if necesarry
	Isolate created perforation in casing
16	Construction: equipment of the monitoring well (only possible in compartment P18-2)
17	Construction: platform modification
	Installation of heater (only for start-up) on platform
	Retrofit of the riser
	Wellhead control
	Downhole equipment control systems
18	Construction: pipeline
19	Construction: onshore facilities (compressor, pipeline)
20	Tie-in work and commissioning
21	Baseline monitoring
22	Handover
23	Start injection